Drivers and constraints of shape evolution in the vertebral column of felids (Felidae, Carnivora).

Candidate: Marcela Randau da Costa Carvalho

Department of Genetics, Evolution and Environment

UCL

Thesis submitted for the degree of Doctor of Philosophy (PhD)

Declaration

I, Marcela Randau da Costa Carvalho confirm that the work presented in this thesis is my own. Where information has been derived from other sources, I confirm that this has been indicated in the thesis.

Abstract

Morphological studies of the skull and limbs of tetrapods are common in the literature. Nonetheless, the vertebral column has been comparatively neglected, and research shows a bias towards developmental and genetic approaches. Still, these studies have highlighted the unusual uniformity in vertebral count across mammals, unlike the great variation in vertebral numbers observed in other tetrapod clades. This meristic constraint has been suggested to drive higher regionalisation in the mammalian axial skeleton, with adaptation to discrete niches happening primarily through modification of vertebral form rather than changes in numbers.

Living species of the mammalian family Felidae are an ideal group for vertebral studies as all taxa present the same count of 27 presacral vertebrae but vary in ecological specialisations and body mass. In this thesis, I explore the morphological evolution of the presacral vertebral column by, first, investigating ecological and phylogenetic influences on presacral vertebral shape, and then, examining patterns of vertebral trait covariation with an evolutionary developmental perspective.

My results show clear regionalisation of vertebral column shape and function. Specifically, a highly integrated region between the diaphragmatic vertebra and the last lumbar (i.e., T10 – L7) shows the highest levels of ecological

specialization, and potentially higher evolvability, contrasting with a phylogenetically conserved neck region. I found strong support for a widespread two-module model of intravertebral shape based on developmental origins of vertebral components, and this analysis also provided an empirical example of phenotypic integration promoting higher morphological disparity. Exceptions to this model are at boundaries of large vertebral modules and suggest functional overprinting of developmental patterns. Further, I demonstrated the presence of modularity at the organismal level, with decoupling of the vertebral column as a whole from other skeletal structures.

Combined, the work presented in this thesis demonstrates that axial evolution across Felidae reflects both developmental constraints and functional specialisation by concentrating shape change within distinct evolutionary modules. This thesis provides a foundation for further study of vertebral columns combining both functional and developmental perspectives.

Table of contents:

To Colin,

and to the best cats: Bowie, Soxie, Sinatra and Lilica.

Acknowledgements:

First, I would like to greatly thank this PhD examination board, Professor Helen Chatterjee and Doctor Jason Head, for their invaluable contribution and time in evaluating this thesis.

I would also like to thank the people behind The Leverhulme Trust and the SYNTHESYS (Synthesis of Systematic Resources) grant. Their vision and generosity in funding research have allowed me to have the most amazing years working on this project.

Further, I would like to thank many people for their constant professional and personal support during the years taken to finish this work. Between those, there are specific individuals that I must mention and thank directly. The following people have played an important role in my life during the last three years and without them this thesis and its author would be entirely different today and likely still a rough draft.

Colin, thank you. Thank you for being the best and the most supportive person in the world. Life by your side is a dream come true. Nothing makes me happier than being able to share every challenge and accomplishment with you. You have made this major goal feel achievable since the very beginning, when it all was yet too far to believe it. My greatest joy is that I've had you by

my side from the start until this end. Rather, it is even better to know that my every new start will be with you. Eu te amo.

To Professor Anjali Goswami: Anjali, thank you for being nothing short from the best supervisor anyone could ever hope for and a friend in so many situations. I have learnt and grown a lot during the years I have spent under your guidance, and I would like to thank you for believing in me. It has been an immense honour to be your student. You are a true inspiration.

To Professor John Hutchinson: Thank you for your stimulating, generous, and kind supervision. It has been a great pleasure to do research under your direction, and I am very grateful for all you have taught me. I will always be incredibly proud of being part of 'Team Cat'.

To my parents: Aos meus pais, muito obrigada por serem os meus melhores amigos. O apoio de vocês sempre me permitiu ser o meu melhor. Serei eternamente grata pela presença de vocês em todos os aspectos da minha vida. Essa conquista, como todas as anteriores, só foi possível graças a vocês, e não é exagero dizer que sem vocês nada disso teria acontecido. Os tenho sempre comigo, e meu amor e admiração por vocês são sem tamanho.

Henrique, being your younger sister has always been a great responsibility. It is not always easy to follow the steps of someone who is so thoughtful, caring and clever, but your gentle guiding has made growing up by your side the

greatest adventure. Thank you for always inspiring me to be a strong and compassionate person. Thank you even more for always holding my hand.

To my second mother: Tetê, minha segunda mãe, obrigada por tudo. Sua criação é um dos grandes motivos por eu ter chegado até aqui. Grande parte da pessoa que eu sou hoje é inspirada em seus ensinamentos e bondade.

I would like to thank some of the other amazing strong women in my life. Elizabeth Dobson-Jones, Lídia Lins, Lydia Tiller and Anastasia Chamberlein, you have been a guiding light and a harbour in calm and troubling times. Thank you for all of our "coffee and wine" sessions, they have kept me sane. You inspire me to grow every day.

The Goswami Lab team, past and present: thank you for your collegiality and friendship. Our academic discussions have greatly enriched my work, and our less scientific conversations have made it all a lot more enjoyable. Dr Ryan N. Felice, I shall still convince you to permanently stay in the UK so we can work out what a sacrum really is. Thank you for always being so generous with your knowledge, and for being such a great friend. Dr Thomas J. D. Halliday, thank you for our chats, and also for your R knowledge. Dr Andrew R. Cuff, thank you for your professional collegiality, for teaching me how to use Illustrator and allowing me to use your beautiful figures in so many talks, and for always being so helpful and attentive. Also, thank you for secretly loving cats more than dinosaurs. To the three of you, and in addition to Dr Anne-

Claire Fabre, Dr Akinobu Watanabe and Carla Bardua, thank you for being such good friends and for your overwhelming support. It has been an amazing experience to be part of this research group.

I would like to deeply thank the people who made my museum data collection trips possible: M. Lowe and R. Asher at the University Museum of Zoology, Cambridge; R. Portela Miguez and R. Sabin at the Natural History Museum, London; C. Lefèvre at the Muséum National d'Histoire Naturelle, Paris; W. Stanley at the Field Museum of Natural History, Chicago; E. Westwig at the American Museum of Natural History, New York; D. Lunde at the Smithsonian National Museum of Natural History, Washington D.C.; and J. Chupasko at the Harvard Museum of Natural History, Cambridge.

Lastly but not least, I would like to deeply thank the Burgess and Ashleigh-Morris families for taking me in their arms and making me feel so welcome and loved. I am incredibly lucky and happy to have such a warm UK family.

Chapter 1. Introduction

> "Most species do their own evolving, making it up as they go along, which is the way Nature intended. And this is all very natural and organic and in tune with mysterious cycles of the cosmos, which believes that there's nothing like millions of years of really frustrating trial and error to give a species moral fibre and, in some cases, backbone".
>
> *Terry Pratchett (1991)*

The study of morphological trait evolution is a key component of several areas of biological research. From studies of ecological communities to biomechanics to genetic and developmental analyses, the primary steps onto which hypotheses are created involve the characterisation of phenotype and its observed variations (i.e., disparity). Recently, major advances in the analytical tools used to describe shape and its variables have allowed the field of study of morphological evolution to mature, and this greatly expanded the realm of detailed quantitative analyses which compose the discipline of geometric morphometrics (Adams et al. 2004; Zelditch et al. 2012; Adams et al. 2013; Cardini and Loy 2013).

Yet, in the literature concerning morphological studies within vertebrates, there is still a clear bias regarding the traits which are the focus of such analyses. Specifically, analyses of shape evolution and its correlation with ecology have overwhelmingly revolved around cranial and appendicular

elements (e.g., Andersson and Werdelin 2003; Stayton 2005; Goswami 2006b; Pierce et al. 2008; Slater and Van Valkenburgh 2008; Doube et al. 2009; Meachen-Samuels and Van Valkenburgh 2009b; Pierce et al. 2009; Adams and Nistri 2010; Drake and Klingenberg 2010; Figueirido et al. 2010; Goswami and Polly 2010a; Bell et al. 2011; Bennett and Goswami 2011; Ercoli et al. 2012; Foth et al. 2012; Walmsley et al. 2012; Zhang et al. 2012; Alvarez et al. 2013; Fabre et al. 2013a; Piras et al. 2013; Sears et al. 2013; Fabre et al. 2014a; Martín-Serra et al. 2014a); whilst, to date, studies of morphological evolution which focus on the vertebral column are still comparatively fewer in the literature, and research questions focusing on this trait have mostly arisen from a developmental or biomechanical perspective (e.g., Burke et al. 1995; Macpherson and Fung 1998; Macpherson and Ye 1998; Dickinson 2000; Wellik 2007; Müller et al. 2010; Fleming et al. 2015), although recent studies increasingly consider the evolutionary perspective (e.g., Buchholtz et al. 2014; Ward and Mehta 2014; Head and Polly 2015; Jones and Pierce 2015).

In this thesis, I explore the morphological evolution of the vertebral column in living cats (family Felidae, order Carnivora, class Mammalia). First, I take a macroevolutionary perspective to examine body mass and ecological and phylogenetic influences on vertebral shape through the vertebral column. Then, I add an evolutionary developmental perspective and examine patterns of vertebral trait covariation (i.e., morphological integration and modularity,

see below), and how these may have shaped the evolution of the vertebral column by facilitating or constraining morphological change. Combined, these analyses provide a comprehensive understanding of ecological, phylogenetic, and developmental influences on the evolution of felid vertebral column.

The mammalian axial skeleton

Biomechanical analyses of the vertebral column in mammals have shown that it plays a critical role in support and locomotion, respiration, and prey procurement (Pridmore 1992; Gál 1993b; Long et al. 2002; Argot 2003). Consequently, it has been shown that osteological measurements of individual vertebrae (e.g., neural spine lever arm and centrum height) can be used as proxies for inferring muscles' attachment sites and orientation, vertebral musculature mass, and overall range of motion at intervertebral joints, all of which are informative towards vertebral column mobility and overall function (Slijper 1946; Shapiro 1995; Long et al. 1997; Long et al. 2002; Shapiro et al. 2005; Shapiro 2007; Pierce et al. 2011).

Observations of morphological change which correlate to function are especially interesting in mammals due to the high degree of vertebral count uniformity across the clade. Relative to other amniotes, the mammalian axial

skeleton is largely constrained with regards to meristic changes (i.e., changes in vertebral number) (Müller et al. 2010), with exceptions mainly concentrating in the Afrotheria and Xenarthra orders (Narita and Kuratani 2005; Asher et al. 2011). This vertebral count uniformity has been suggested to arise from developmental constraints and to have evolved early in mammalian evolution (Narita and Kuratani 2005; Buchholtz et al. 2012). Further, these observations have led to the hypothesis that the vertebral column is under strong developmental canalisation and stability (Galis 1999; Narita and Kuratani 2005; Wellik 2007; Buchholtz and Stepien 2009; Hautier et al. 2010; Müller et al. 2010; Asher et al. 2011; Varela-Lasheras et al. 2011; Buchholtz et al. 2012; Fleming et al. 2015). This developmental and genetic control has been demonstrated to act on several levels, such as the effect of the sequential expression of *Hox* genes on somite development, and also by spatial relationships between the primaxial (i.e., vertebrae and ribs) and abaxial (i.e., limbs, girdles, and sternum) skeletons (Wellik 2007; Buchholtz and Stepien 2009; Head and Polly 2015). Specifically, Wellik (2007) summarised how the main patterns of vertebral column regionalisation, which partition this structure into four main anatomical regions (i.e., cervicals, anterior thoracics, posterior thoracics, and lumbars) are congruent with the positioning of the anteroposterior expression of *Hox* genes during development of somites (Fig. 1.1). The evolutionary changes in vertebral morphology due to the effects of *Hox* genes can be described as either 'diversifying' or 'skeletogenetic' (Carroll

et al. 2001; Polly et al. 2001), when morphological changes happen at individual vertebrae without changes no vertebral count, both in total and within regional series, or, less frequently, as 'homeotic' changes, when regional count may change due to a trade-off between consecutive series caused by changes in the expression domains of *Hox* genes, but with no change to total vertebral number (Raff 1996; Carroll et al. 2001; Polly et al. 2001; Buchholtz 2007).

Therefore, these constraints in overall and regional vertebral count may result in most variation in axial anatomy and correlated specialisation towards different function across mammalian taxa occurring through changes in vertebral morphology. As mentioned above, and in support of these hypotheses, a few studies have been able to demonstrate that differentiation in locomotor ecology correlate with changes in shape of individual vertebrae, rather than significant changes in vertebral count (Pridmore 1992; Buchholtz 2001b; Shapiro et al. 2005; Pierce et al. 2011; Jones and German 2014; Jones and Pierce 2015).

Hence, it is possible to take, as a starting point, the assumption that regional morphological differences of the vertebral column across mammal species will be both a reflection of shared development and individual specialisation of function. The study of vertebral shape is therefore informative both at the level

of individual vertebrae and at the level of regional functional partitioning of the axial skeleton.

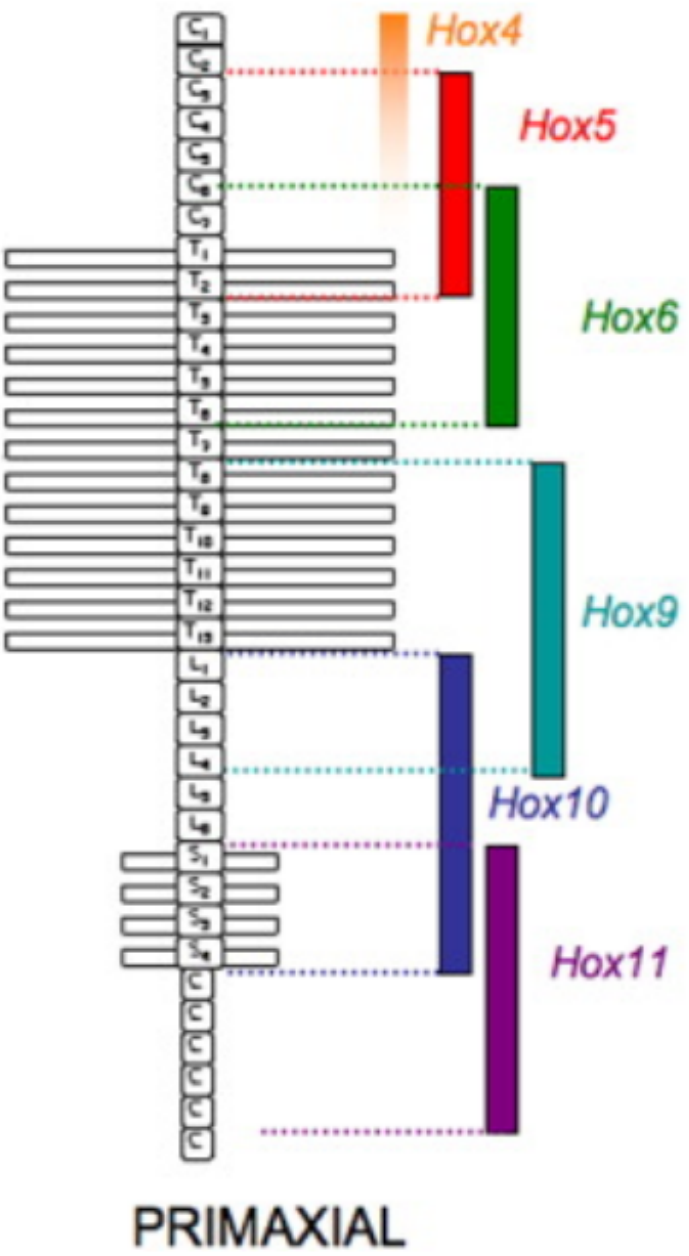

Fig.1.1 Representation of the association between the anterior expression site of *Hox* genes and borders of main regions of vertebral shape across a generalised mammalian vertebral column. Source: modified from Wellik (2007). C/T/L$_{number}$ represent cervical, thoracic, and lumbar vertebrae, respectively, while S$_{number}$ and C stand for sacral and caudal vertebrae.

The study group: Felidae

Within mammals, there has been an uneven distribution of morphological and general evolutionary research attention, with some orders being more studied than others. Specifically, families within the order Carnivora have been the focus of several morphological analyses (e.g., Bertram and Biewener 1990; Antón et al. 2004; Holliday and Steppan 2004; Goswami 2006b; Van Valkenburgh 2007; Goswami et al. 2010; Goswami and Polly 2010b; Meachen-Samuels and Van Valkenburgh 2010; Hudson et al. 2011; Meachen-Samuels 2012; Walmsley et al. 2012; Zhang et al. 2012; Fabre et al. 2013a; Fabre et al. 2014b; Jones 2015; Cuff et al. 2016a, 2016b). Although the role of research funding opportunities and individual researchers' personal affinities might play a significant part in this perhaps unfair division of focus, when it comes to studies of the relationship between form and function of an under-explored trait, it may be preferable to start by having species which have been extensively analysed with regards to ecology, and which are present at museum collections in numbers sufficient to capture biological variation in a relevant degree to evolutionary analyses.

Felidae, the family of living and extinct cats, then becomes a very interesting choice of study group. Due to the charismatic and top predatory qualities of felid species, and their keystone species status, much has been done towards describing their life history and ecological attributes and studying their origin

(e.g., Ewer 1973; Gonyea 1978; Leyhausen 1979; Dayan et al. 1990; Mattern and McLennan 2000; Sunquist and Sunquist 2002; Johnson et al. 2006; Driscoll et al. 2007; MacDonald et al. 2010; Tseng et al. 2014).

The timing and location of felid origins have been placed in the Late Oligocene (33.9 – 23 million years ago; ma hereafter) of Asia by use of both molecular and morphological data (Peigné 1999; Johnson et al. 2006; MacDonald et al. 2010). Traditionally, species have been divided into two sub-families: the extinct Machairodontinae, which includes the sabre-toothed cats (i.e., species possessing enlarged and mediolaterally compressed upper canines, such as *Smilodon fatalis*), and Felinae, the conical-toothed cats (i.e., having an almost completely round cross-section of the canines) which include all living species and other fossil taxa (Ewer 1973; Nowak 1999). Within Felinae, the number of living species ranges from 38 to 41 taxa (Ewer 1973; Wozencraft 2005; Johnson et al. 2006), and these have been divided into eight well-supported major lineages by analysis of nuclear DNA (Johnson and O'Brien 1997; Pecon-Slattery et al. 2004; Johnson et al. 2006): the 'Panthera', 'Bay cat', 'Caracal', 'Ocelot', 'Lynx', 'Puma', 'Leopard cat', and 'Domestic cat' lineages (Fig. 1.2). The radiation of the modern species started with the split of the 'Panthera' lineage in the Miocene at 10.8ma, and subsequent radiation of other lineages and their species was fast, over a period of 6.3 million years, suggesting ecological release (Johnson et al. 2006; MacDonald et al. 2010). Nevertheless,

the relationships between species within each of the above mentioned lineages of Felinae, and the overall fossil history of conical-toothed cats still lack fine resolution due to this rapid recent radiation, an incomplete fossil record, likely due to preservation bias regarding size and habitat, and relative increased similarity in skeletal traits when compared to other clades (Fig. 1.2; Johnson et al. 2006; MacDonald et al. 2010).

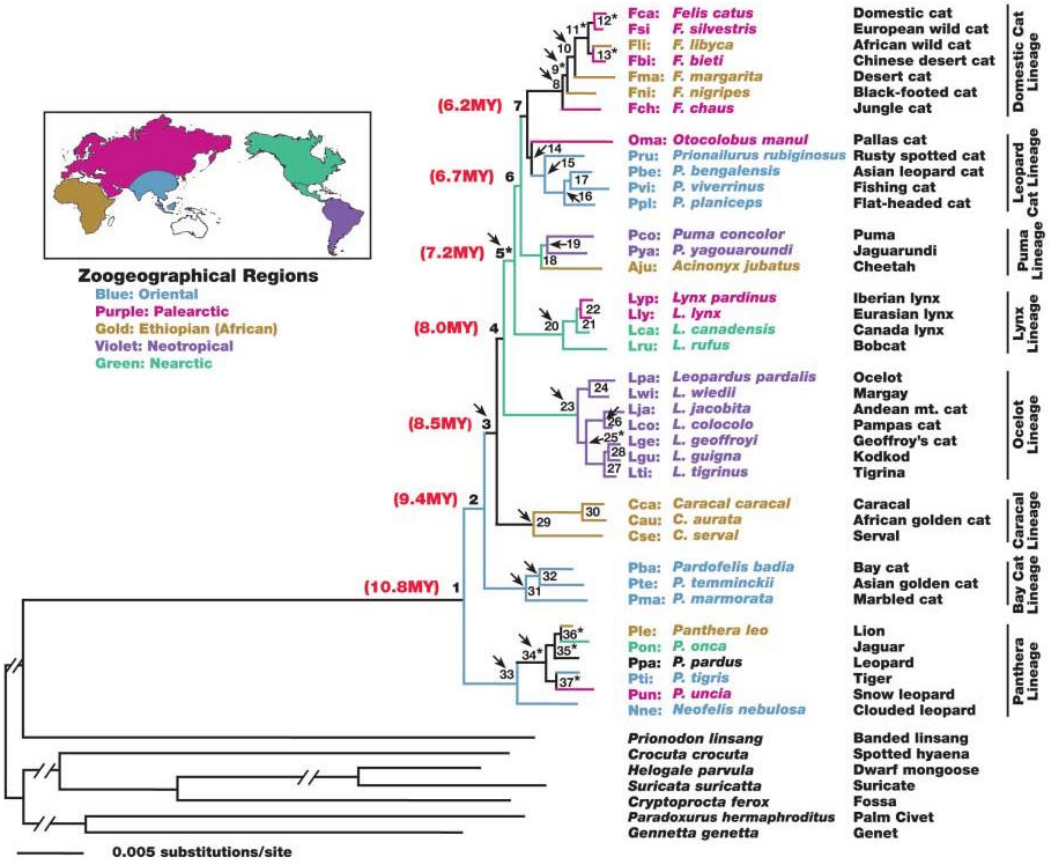

Fig 1.2. Molecular phylogeny of 38 living species of Felidae showing grouping of taxa into eight major lineages. Colours on species labels and map inset describe current and historic species' distributions based on authors' analyses and current and fossil zoogeographic occupation. Asterisks mark nodes with relative low resolution. Source: Johnson et al. (2006).

Within living Felidae there is an impressive range in body size across the species, with the smallest cat at around just 1kg (*Prionailurus rubiginosus*, rusty-spotted cat) and the largest tigers weighing over 300kg (*Panthera tigris*) (Fig. 1.3; Ewer 1973; Sunquist and Sunquist 2002; MacDonald et al. 2010). However, there is a clear division of body sizes across the genera and evolution of body mass in felids may have been driven by two optima. While traditional and qualitative assessment of species have sub-divided felids into 'small' and 'big' cats (Ewer 1973; Sunquist and Sunquist 2002), Cuff et al. (2015) have demonstrated that this division still holds when quantitative and powerful analyses including both fossil and living species are performed. The two body size optima which have driven felid evolution are a small body mass of around 5kg and a large size of over 25kg. Additionally, Cuff et al. (2015) showed that body mass has strong phylogenetic signal in Felidae, and, specifically in living taxa, large body mass of over 25kg is concentrated in the 'Panthera' lineage (specifically in the *Panthera* genus), with the addition of species in the Puma lineage (e.g., *Puma concolor* and *Acinonyx jubatus*), which are phylogenetically closer to smaller cats but convergently show increase in body mass.

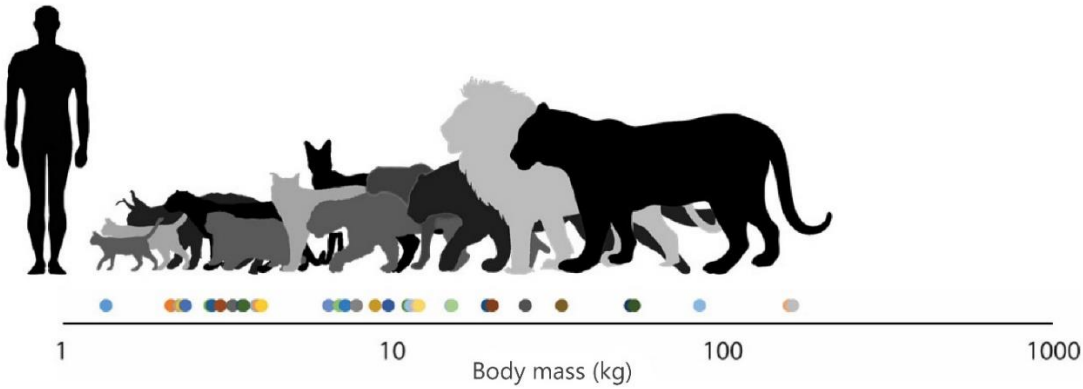

Fig. 1.3 Schematic representation of body mass variation in living Felidae, with human on the left for size comparison. Coloured circles position extant species in the felid body mass (kg) spectrum (Cuff et al. 2015). Source: Figure created by Dr Andrew R Cuff.

Interestingly, however, there is a remarkable gross phenotypic similarity across all species within Felidae, with suggestions that species have not changed much morphologically when compared to the first appearances in the fossil record (i.e., fossils of *Proailurus* sp.; Fig. 1.4) (Turner and Antón 1996; Peigné 1999; Meachen-Samuels and Van Valkenburgh 2009a). Such similarities have also been noted in skull morphology, both across and within species, with little variation in shape and predominant isometry through ontogeny in felids, contrasting with more dramatic changes seen in canids (Wayne 1986; Sears et al. 2007). In addition to similarities in morphology, despite the large body mass range, there is remarkable uniformity of limb posture across felids (Day and Jayne 2007). This homogeneity is contrary to the biomechanical expectations of increases in limb erectness accompanying

increases in body mass in mammals to avoid damage to supporting tissues (Biewener 1989; Bertram and Biewener 1990; Biewener 2005) and suggest that cats may have distinct ways of accounting for such steep increases in body mass without changing posture.

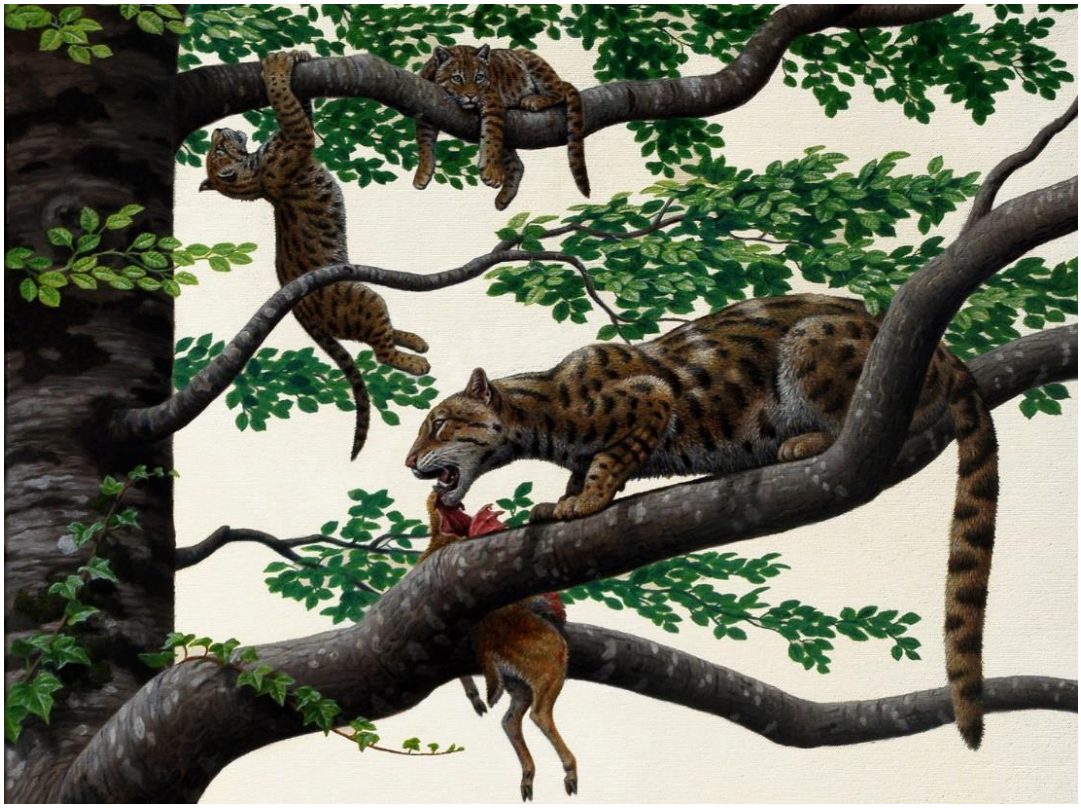

Fig. 1.4 Reconstruction of *Proailurus lemanensis*, the earliest felid (Turner and Antón 1996; Peigné 1999), with size equivalent to a bobcat, based on skeletal remains found at Saint-Gérand-le-Puy, France, by artist Mauricio Antón. Source: modified from the Chasing Sabretooths blog (https://chasingsabretooths.wordpress.com/2014/11/27/the-beginnings-of-catkind-proailurus/).

Continuing with the theme of gross anatomical similarities in cats, with regards to the vertebral column, there is absolutely no meristic variation

across felids, and all species present the same 27 presacral vertebrae (Turner and Antón 1996; De Iuliis and Pulerà 2006; MacDonald et al. 2010). These are divided into seven cervicals, 13 thoracics, and seven lumbars, and all species display an anticlinality switch in the anteroposterior orientation of the neural spine at vertebral position T11 (Figs. 1.5 and 1.6). At T11, this vertebral process is usually very reduced, and sometimes almost perpendicular to centrum length, and after this vertebra, the neural spine changes from caudally oriented to cranially oriented (De Iuliis and Pulerà 2006).

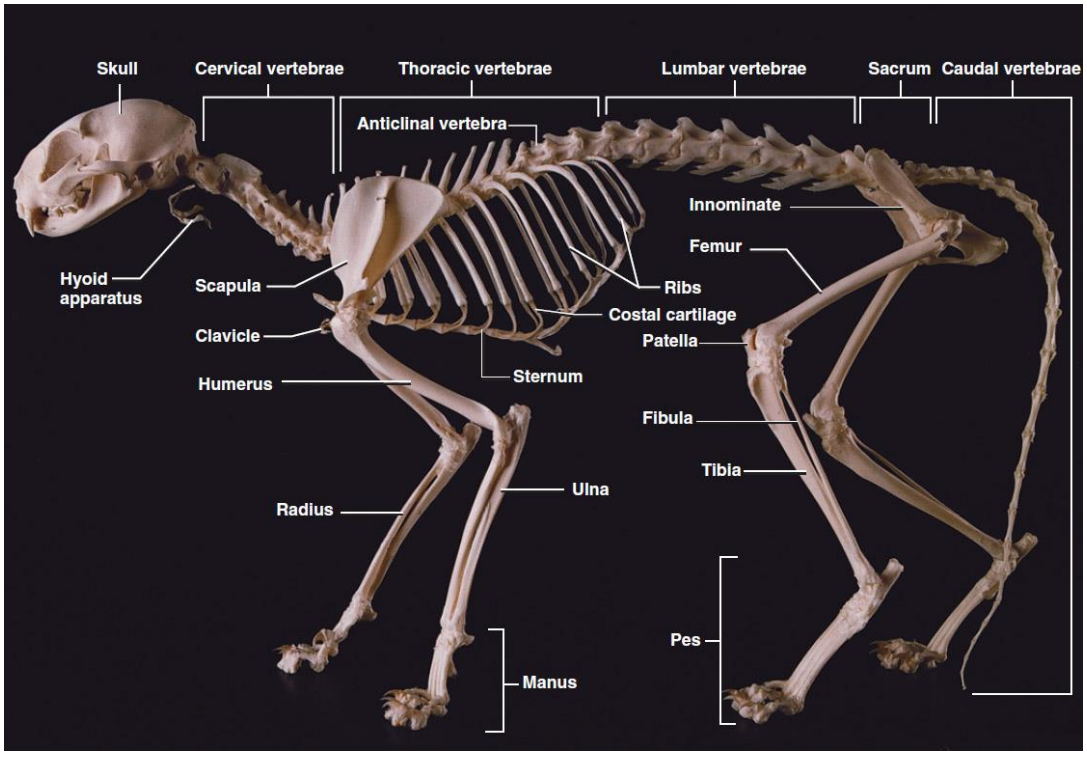

Fig. 1.5 The skeleton of a domestic cat (*Felis catus*) with labelled anatomical elements. Note presence of seven cervicals, 13 thoracics, and seven lumbars, with the anticlinal vertebra at T11 (Source: De Iuliis and Pulerà 2006).

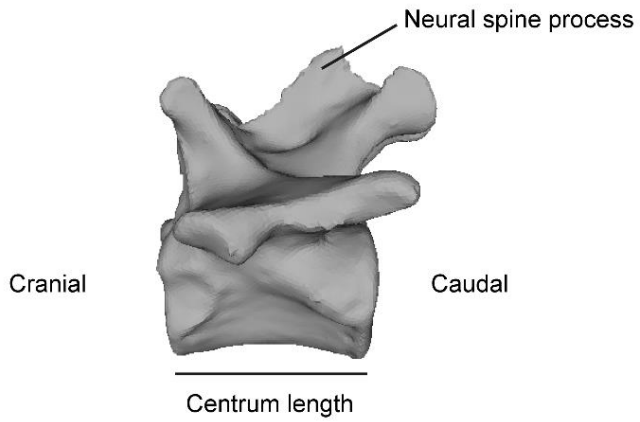

Fig. 1.6 The anticlinal vertebral (T11) of a cheetah (*Acinonyx jubatus*, USNM 520539), in left lateral view, showing a reduced neural spine process.

Although the diet of felids is also fairly uniform, and all cats are classified as hypercarnivores, having a diet composition of at least 70% vertebrate prey (Ewer 1973; Van Valkenburgh 2007), there is substantial specialisation of species towards prey size and, consequently, prey killing techniques (Leyhausen 1979; Dayan et al. 1990; Antón and Galobart 1999; Mattern and McLennan 2000; Sunquist and Sunquist 2002; MacDonald et al. 2010). Further, felids present locomotor specialisations which range from very specialised arboreal species (such as the margay, *Leopardus wiedii*) to the fastest living carnivoran, the cursorial cheetah (*Acinonyx jubatus*) (Hildebrand 1959; Sunquist and Sunquist 2002).

Hence, among the cranial and appendicular studies of shape within mammals, many have used felids as examples of morphology correlating with ecology (e.g., Antón and Galobart 1999; Slater and Van Valkenburgh 2008; Meachen-

Samuels and Van Valkenburgh 2009a, 2009b; Salesa et al. 2010; Meachen-Samuels 2012; Zhang et al. 2012; Meloro et al. 2013; Wroe et al. 2013; Cuff et al. 2016a). However, notwithstanding with the observations of gross similarity, quantitative morphological analyses of this group have shown that some cranial and appendicular traits show differential scaling with body size and shape (i.e., an allometric rather than isometric relationship) which distinguish species with regards to the two major ecological classifications: prey size (i.e., small, mixed and large prey specialists) and locomotor mode (i.e., arboreal, cursorial, scansorial and terrestrial) (Dayan et al. 1990; Sunquist and Sunquist 2002; Doube et al. 2009; Meachen-Samuels and Van Valkenburgh 2009a, 2009b; MacDonald et al. 2010; Meachen-Samuels 2012). This differentiation suggests that the general anatomical similarity of Felidae may obscure more cryptic changes in skeletal shape that reflect ecological specialisation of morphology.

Therefore, two sources of information become available which are key to testing relationships of functional morphology on a new skeletal system: 1. there is sufficient literature on felid taxa ecologies and life history, and 2. there is evidence showing that skeletal elements, both in the skull and postcranium, correlate with these factors. In order to understand how the ecomorphological diversification of cats has affected the postcranium as a whole, and how different traits under potentially different developmental regimes respond to

similar selection pressures, the study of the vertebral column's shape becomes the next necessary step.

Quantifying morphology: A three-dimensional geometric morphometrics approach

As mentioned above, individual vertebral dimensions have been shown to be a good proxy for intervertebral range of motion and to correlate with ecological adaptations in both mammalian and other vertebrate taxa (e.g., Slijper 1946; Long et al. 1997; Shapiro et al. 2005). Nevertheless, the advances in data collection and analytical software have allowed for techniques which greatly improve on the amount and resolution of biological information from complex traits (Mitteroecker and Gunz 2009; Adams et al. 2013; Cardini and Loy 2013; Fabre et al. 2014a). Specifically, landmark-based data is a collection of points which describe the morphology of an anatomical structure. Each landmark point, if three-dimensional, possesses three position variables (i.e., x, y, and z dimensions) which allow for a more accurate description of detailed morphology and can be defined according to three types (Bookstein 1991): type I landmarks define trait aspects related to clear biological structures, such as contact points between distinct bones in one structure (i.e., sutures); type II are landmarks which describe points of maximum curvature or extension

(e.g., anterior-most tip of left nasal bone); and type III landmarks are defined by the location of two preliminary points (e.g., a point which is defined by the middle location between landmark A and B) (Zelditch et al. 2012). With the transition from linear data to landmark-based geometric morphometrics, the quantification of shape has gone through major 'revolutions' regarding the acquiring of data and its treatment (Adams et al. 2004, 2013). Specifically, the concretization of modern morphometrics took place with the implementation of the 'Procrustes paradigm' by which shape variables could be isolated from the objects of interest by removal of non-shape variation (i.e., aspects regarding information on scale, rotation and translation of objects) (Rohlf and Slice 1990; Bookstein 1991; Rohlf 1999). With this, further differentiation between shape and form could be made in which 'form' refers to a combination of both shape and size. The use of the Procrustes analysis involves normalisation by scaling to the unit centroid size (i.e., the squared root of the summed squared distances of each landmark to the centre), followed by the translation of objects to the origin, and ends with object rotation which minimises the sums-of-squares deviations of the landmarks of all specimens compared to the mean shape configuration (Fig. 1.7; Bookstein 1991; Klingenberg 2010; Zelditch et al. 2012; Adams et al. 2013). It is on the Procrustes coordinates (i.e., shape variables) that further analyses are then performed.

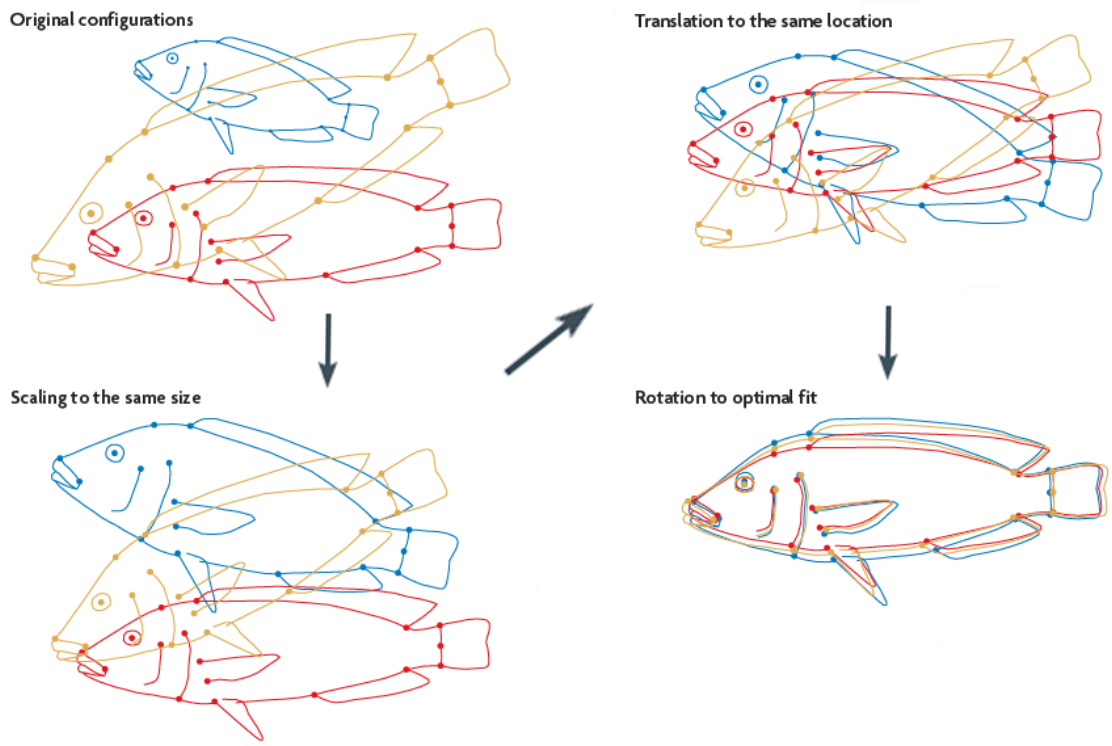

Fig. 1.7 Schematics of the Procrustes superimposition analysis showing the removal of variables concerning scale, translation and rotation from objects in order to maintain only shape variables. Source: modified from Klingenberg (2010).

When compared to linear measurements, three-dimensional landmark-based data offer many benefits, such as an increase in the number of shape variables, and notably, a more detailed ability to accurately locate and describe the areas of shape change and therefore improve the description of changes which are linked to diversification of function (Herrel et al. 2007; Kaliontzopoulou et al. 2007; Cornette et al. 2013b; Fabre et al. 2014a). Additionally, the improved power of landmark-based geometric morphometrics approaches, and the refinement of methods of visualisation of shape differences, may be even more

important when taking into account the gross anatomical similarly observed in cats, as methods which are less sensitive may be insufficient to fully differentiate taxa.

Morphological Integration and Modularity

Organisation is a central characteristic of biological forms. With its opposite, the complete lack of interrelationships among trait units, a chaos incoherent with life itself would set, as some coordination is required for the maintenance of function (Bookstein 2015). The ground onto which the ideas of how traits are organised and display coordinated variation was laid by Olson and Miller (1958) with their work on the concepts of morphological integration and modularity. According to these concepts, traits present an overall pattern of intercorrelation (i.e., integration) which can be measured and varies with regards to strength (Olson and Miller 1958; Goswami and Polly 2010c; Bennett and Goswami 2011; Klingenberg and Marugán-Lobón 2013; Armbruster et al. 2014). When sets of traits are highly covariant, but present lower correlations with traits outside of the set boundaries, such traits are said to form a module (Wagner 1996; Bolker 2000; Marroig et al. 2009; Clune et al. 2013). Regarding how these patterns of trait organisation originate, it has been shown that they can arise due to shared developmental and genetic pathways, embryonic origin, changes in postnatal function, and heterochronic shifts (Zelditch and

Carmichael 1989; Cheverud 1996; Goswami et al. 2009; Zelditch et al. 2009; Bennett and Goswami 2011; Goswami et al. 2014). Moreover, these patterns have been shown to change both through ontogeny and in response to strong selection (Drake and Klingenberg 2010; Goswami et al. 2012).

It is important to consider these organisational patterns when studying trait evolution as, through the strength of covariation between units, morphological integration and modularity may drive or constrain change due to selection by modulating the trait response range (West-Eberhard 1989; Cheverud 1996; Klingenberg and Marugán-Lobón 2013; Goswami et al. 2016). Specifically, high trait integration might mean that, because of the strong covariation between morphological variables and consequent correlations in magnitude and direction of changes in individual traits, only responses along the preferred axes of morphological variation are facilitated, whilst responses along orthogonal axes are deterred (Schluter 1996a; Hansen and Houle 2008; Marroig et al. 2009; Goswami et al. 2014). It follows, therefore, that unhindered optimum ranges of response might only be able to be achieved if these axes of preferred variation are parallel to the selection vector. On the other hand, modularity may balance this by breaking the links among larger sets and forming smaller modules which can respond to sometimes opposing selection drivers more independently and without obstruction (Goswami 2006a; Hansen and Houle 2008; Goswami and Polly 2010b; Clune et al. 2013).

Both morphological integration and modularity have been demonstrated in several taxa and traits (e.g., Hallgrímsson et al. 2002; Bookstein et al. 2003; Goswami 2006a; Young and Badyaev 2006; Meloro and Slater 2012; Klingenberg 2013; Armbruster et al. 2014; Fabre et al. 2014b). The observed regionalisation in vertebral shape, and potentially in function, throughout the vertebral column of mammals directly evokes these concepts of trait organisation. Additionally, the strong developmental canalisation which has been suggested to act on the axial skeleton in terms of vertebral numbers (Narita and Kuratani 2005; Buchholtz 2007; Müller et al. 2010; Buchholtz et al. 2012; Buchholtz 2014) implies that shared developmental origin and timing might affect adult vertebral column morphology and dictate trait unit covariation and the formation of modules.

Research aims and outline

The hypotheses I test and analyses I perform have the following research questions as guidance:

1. As observed in cranial and appendicular traits, can we distinguish between felid ecomorphs by analysing vertebral shape?
2. How does body size affect vertebral morphology, and is the scaling relationship consistent throughout the axial skeleton?

3. Do traditional vertebral regions (i.e., cervical, thoracic, lumbar) accurately reflect morphological regionalisation of the vertebral column in felids?
4. Does developmental origin influence vertebral shape evolution?
5. Is morphological variance distributed equally throughout the presacral vertebral column, or are there regions of increased disparity?
6. What are the evolutionary units or modules of shape change in the axial skeleton, and how has their integration promoted or hindered morphological change across cats?

This work presents a novel scientific contribution focusing on an understudied but important structure. Although an active role in organismal movement and ecological function has been assumed for the vertebral column for over two and a half centuries (e.g., Winslow 1732; Barthez 1798; Slijper 1946), a significant portion of the available literature on vertebral evolution is either qualitative in nature or restricted in scope. Here, I start to fill this knowledge gap with a comprehensive analysis of vertebral diversity and evolution in Felidae.

Thesis overview

Quantifying vertebral shape

In order to robustly quantify shape differentiation across species, two different data collection approaches are applied here: linear measurements in Chapter 3; and three-dimensional landmarks in Chapters 4, 5, 6 and 7. Consequently, two sets of species were involved in each data collection approach due to a trade-off between number of species and number of specimens measured per species for each method: 22 species, with one or two specimens per species, were involved in the linear study, while nine species, with 9 to 19 specimens per species, were the focus of the three-dimensional data collection (Table 1.1, and Chapters 2, 3 and 4). Specimen numbers are detailed in each respective chapter, as well as in the methods chapter (Chapter 2). Ecological data are also described in detail in Chapter 2.

Furthermore, one of the issues of analysing the shape of the vertebral column has been its multiple-element composition. In Chapter 4, I demonstrate a novel application of a technique called the Phenotypic Trajectory Analysis (Adams and Collyer 2007, 2009; Collyer and Adams 2013), which overcomes this issue by linking the mean shape of sequential vertebrae in the morphospace and creating a three-dimensional trajectory across them, serving as a proxy to total or regional vertebral column shape.

Table 1.1 List of species studied in each of the data collection approaches, linear or three-dimensional (3D) landmarks, with their corresponding information on locomotor and prey size categories collated from the literature and detailed in Chapter 2 (Sunquist and Sunquist 2002; Meachen-Samuels and Van Valkenburgh 2009a, 2009b).

Species	Locomotion	Prey size	Linear measurements	3D landmarks
Acinonyx jubatus	Terrestrial/ Cursorial	Large	1	15
Caracal aurata	Terrestrial	Mixed	1	-
Felis catus	Scansorial	Small	-	14
Felis chaus	Terrestrial	Small	1	-
Felis lybica	Scansorial	Small	1	-
Herpailurus yagouarundi	Scansorial	Small	1	-
Leopardus colocolo	Scansorial	Small	1	-
Leopardus geoffroyi	Terrestrial	Small	1	-
Leopardus pardalis	Scansorial	Mixed	1	15
Leopardus wiedii	Arboreal	Small	2	-
Leptailurus serval	Terrestrial	Small	2	11
Lynx canadensis	Scansorial	Mixed	1	-
Lynx lynx	Scansorial	Large	1	-
Neofelis nebulosa	Arboreal	Mixed	1	11
Otocolobus manul	Terrestrial	Small	1	-
Panthera leo	Terrestrial	Large	1	12
Panthera pardus	Scansorial	Large	1	19
Panthera tigris	Terrestrial	Large	1	-
Panthera uncia	Scansorial	Large	1	-
Pardofelis temminckii	Scansorial	Mixed	1	-
Prionailurus bengalensis	Scansorial	Small	1	9
Prionailurus viverrinus	Terrestrial	Small	1	-
Puma concolor	Scansorial	Large	1	14

Testing hypotheses of morphological integration and modularity

Using the landmark-based data, Chapters 5, 6 and 7 explore the patterns of covariation among trait units at different organismal levels while taking the vertebral column as the analyses focal point. I test for the covariation patterns

in vertebral morphology at three main levels of organismal organisation: first, I focus on how trait units of individual vertebrae are correlated (i.e., intravertebral integration and modularity, Chapter 5), taking a developmental approach to modularity testing, and studying the relationship between the degree of integration and morphological disparity; then, I investigate the covariation among different vertebrae across the presacral vertebral column (i.e., intervertebral integration, Chapter 6) in order to verify the formation of regions of high within-covariation and their significance with regards to functional and evolutionary change. Finally, I test for the correlation between vertebrae and elements of the skull, girdles and limbs, in order to investigate the skeletal organisation with a focus on the evolution of the vertebral column (Chapter 7).

Outline

Chapter 2:

This chapter describes both types of morphometric data collection included in this thesis (i.e., linear and three-dimensional landmark-based data), details ecological and phylogenetic data taken from the literature, provides pilot analysis and justification for the sampling approach, and details the analyses performed at each stage.

Chapter 3:

Here I collected linear and angular measurements across all 27 presacral vertebrae of 22 species of cats, and tested for correlations of morphological change with prey size and locomotor specialisations. The quantitative analyses I performed include Principal Component Analysis (PCA), MANOVAs and phylogenetic MANOVAs, vertebral measurements profiles, and scaling regressions of vertebral regions' length and linear measurements of individual vertebrae against body size, while accounting for phylogenetic relationships.

Chapter 4:

In this chapter I collected three-dimensional landmark-based data on 19 out of the 27 presacral vertebrae of nine living species of felids. Analyses of this dataset were performed using geometric morphometrics to investigate the influence of size, locomotion, and prey size specialisation on both individual vertebrae and regional morphology of the vertebral column. Additionally, I demonstrated a novel application of the Phenotypic Trajectory Analysis (PTA) in order to overcome the issue of analysing the shape of a contiguous sequence of vertebrae.

Chapter 5

This chapter focuses on the patterns of covariation within individual vertebrae. Specifically, I tested for a two-module model (i.e., 'centrum' and 'neural spine' modules) based on developmental origins of vertebral components across the 19 three-dimensionally landmarked vertebrae, using two metrics for quantifying modularity: the RV coefficient and the Covariance Ratio. Further, I quantify the level of overall intravertebral integration using relative eigenvalue standard deviation and compare these results with the levels of vertebral morphological disparity calculated as both Procrustes variances and maximum Procrustes distances.

Chapter 6

In this chapter I investigated the patterns of covariation across vertebrae in order to assess if the regionalisation of vertebral column shape matches boundaries of vertebral sets showing higher values of shape change correlations. I achieved this by performing pairwise correlation tests by using Two-block Partial Least Squares analyses (PLS) in a phylogenetic context, under a model of Brownian motion evolution. Following the results from Chapter 5, in addition to analyses involving whole-vertebral shape, I assessed if the same patterns of intervertebral covariation are present when only the

shape coordinates belonging to the 'centrum' or the 'neural spine' modules are considered.

Chapter 7

Here, I tested for covariation between presacral vertebrae and ten other skeletal elements to investigate modularity across the full skeleton in felids. These additional elements were also three-dimensionally landmarked and included the following cranial and appendicular elements: skull, dentary, scapula, humerus, radius, ulna, pelvis, femur, tibia, and sacrum. Pairwise covariation between vertebral and cranial or appendicular traits was quantified using PLS analysis, both with and without phylogenetic correction.

Chapter 8

Here I summarise the conclusions of each chapter and discuss them in light of results from following chapters. Specifically, the findings of the chapters on morphological integration and modularity within and across vertebrae (Chapters 5 and 6), and across the whole skeleton (Chapter 7) shed further light onto the interpretations of the heterogeneity of the phylogenetic and ecological signals on shape (Chapters 3 and 4). Together, these chapters form a cohesive assessment of vertebral column evolution in Felidae.

Chapter 2. Methodology

As discussed in the Introduction chapter, this thesis takes a quantitative approach to studying the morphological evolution and modularity of the vertebral column in felids. In this chapter I explain in detail the methodology used throughout the thesis. Specifically, this chapter is divided into three sections according to the type of data analysed: 1. Linear morphometrics study; 2. Geometric morphometrics pilot study; and 3. Geometric morphometrics full study. For each section, I first describe how the data were selected, both regarding the chosen osteological structures (e.g., vertebrae) and the analytical data (linear and three-dimensional measurements) which were collected from these structures. Next, I discuss the analyses which were applied and how certain aspects of the data (e.g., sample size) were accounted for at each step.

Linear morphometrics study

The first data chapter in this thesis (Chapter 3) analyses vertebral morphology with linear measurements on individual vertebrae across the complete

presacral column. In addition to linear data, angular measurements of vertebral processes are also analysed across the column.

Data collection

Species selection

In this preliminary study, 22 species of felids were analysed. Each species was represented by one adult specimen, with the exception of *Leopardus wiedii* (ocelot) and *Leptailurus serval* (serval) which were each represented by two specimens. This number of species represented ~62% of the total number of living felids, spanning their full phylogenetic breadth, with species representing all of the eight clades which have been identified (Johnson et al. 2006). The measured specimens are held in the zoological collections at the Natural History Museum in London (NHM), the University Museum of Zoology Cambridge (UMZC), and the Muséum National d'Histoire Naturelle in Paris (MNHN) (see Table 3.1 in Chapter 3 for specimen numbers).

Additionally, the 22 chosen species represent the full range of ecological categories regarding prey size and locomotion (see below, and Table 2.1), and of body size (i.e., from 2kg to 325kg, the average body masses for *Leopardus colocolo* and *Panthera tigris*, respectively), represented in extant felids (Sunquist

and Sunquist 2002; Meachen-Samuels and Van Valkenburgh 2009a; Meachen-Samuels 2012).

Ecological categories

As discussed in Chapter 1, although there is a remarkable similarity in gross morphology across all species of felids, two ecological categories have been shown in the literature to differentiate species and to correlate with morphological changes in the skull and mandible, and limbs. These two categories are regarding the 'prey size' choice and the 'locomotory' specialisation across felids (Young and Goldman 1946; Schaller 1972; Ewer 1973; Leyhausen 1979; Kitchener 1991; Sunquist and Sunquist 2002; Hunter 2005; Meachen-Samuels and Van Valkenburgh 2009a, 2009b).

Meachen-Samuels and Van Valkenburgh (2009a) made a compilation of prey size preferences across 31 species of felids (Young and Goldman 1946; Schaller 1972; Ewer 1973; Leyhausen 1979; Kitchener 1991; Sunquist and Sunquist 2002; Hunter 2005), and divided the cat species into three categories: small prey, mixed prey, and large prey. These categories were based on behavioural observations recorded in the literature for these species, and on the work of Carbone et al. (2007) which showed that mammalian carnivores specialise in prey size categories that maximise energy gains, and are limited by the net

difference in energy expenditure and intake in the pursue, kill and consume process (Carbone et al. 1999). These prey size categories are correlated with felids' body mass but do not completely overlap with this variable: small prey specialists are cats that kill prey smaller than themselves and mostly have body masses to 15kg; large prey specialists comprise large body-sized felids of more than 25kg body mass and kill prey much larger than themselves; and mixed prey size specialists are cats that kill prey of a range of different sizes depending on availability, and usually have masses between 15 and 25kg (Meachen-Samuels and Van Valkenburgh 2009a).

Regarding the locomotory specialisation, cats can be divided into four groups based on how much they climb and if they hunt in trees (Meachen-Samuels and Van Valkenburgh 2009a, 2009b): 'arboreal' felids will most frequently climb and spend most of their time on trees, where they will also frequently hunt; 'scansorial' species will often climb, especially when seeking refuge, but will only rarely hunt there; 'terrestrial' felids will almost never climb; and finally, there is the 'cursorial' cheetah (*Acinonyx jubatus*), which is a highly specialised type of terrestrial felid with skeletal and muscular adaptations for high speed and longer pursuits (Young and Goldman 1946; Schaller 1972; Ewer 1973; Leyhausen 1979; Kitchener 1991; Turner and Antón 1996; Sunquist and Sunquist 2002; Hunter 2005; MacDonald et al. 2010). In this chapter, because only one cheetah specimen was included in the analyses, this

specimen was classified as 'terrestrial' with regards to its locomotory specialisation to allow for its inclusion in statistical analyses.

Table 2.1 List of species studied and specimen information, including sex, assigned locomotor group, prey size specialization and clade (Johnson et al. 2006; Meachen-Samuels and Van Valkenburgh 2009a, 2009b), and museum specimen numbers. The asterisk (*) denotes potentially captive-reared specimens. NHM, London Natural History Museum; MNHN, Museum National d'Histoire Naturelle; UMZC, University of Cambridge Museum of Zoology. Letters in the 'Sex' column stand for female (F), male (M), and unidentified (U).

SPECIES	SEX	PREY SIZE	LINEAGE	LOCOMOTOR GROUP	SPECIMEN NUMBER
Acinonyx jubatus	U	Large	'Puma'	Terrestrial	NHM 1940.1.20.17
Caracal aurata	F	Mixed	'Caracal'	Terrestrial	NHM 1965.8.26.3
Felis chaus	F	Small	'Domestic cat'	Terrestrial	NHM 1892.5.22.1
Felis lybica	M	Small	'Domestic cat'	Scansorial	NHM 1940.1.20.12
Herpailurus yagouarundi	M	Small	'Puma'	Scansorial	NHM 1932.2.14.1
Leopardus colocolo	U	Small	'Ocelot'	Scansorial	NHM 1848.6.26.8 - 126.B
Leopardus geoffroyi	M	Small	'Ocelot'	Terrestrial	NHM 32.2.14.1
Leopardus pardalis	U	Mixed	'Ocelot'	Scansorial	UMZC K.6022 (934A)
Leopardus wiedii	U	Small	'Ocelot'	Arboreal	NHM 1846.4.21.8 - 123B
Leopardus wiedii	U	Small	'Ocelot'	Arboreal	NHM 1849.11.7.2 – 933a
Leptailurus serval	U	Small	'Caracal'	Terrestrial	NHM 1845.9.25.23 133c
*Leptailurus serval**	F	Small	'Caracal'	Terrestrial	NHM 2006.550
Lynx canadensis	U	Mixed	'Lynx'	Scansorial	UMZC K.6682 (937 I)
Lynx lynx	M	Large	'Lynx'	Scansorial	MNHN 1973-83
Neofelis nebulosa	F	Mixed	'Panthera'	Arboreal	MNHN 1961-217
*Otocolobus manul**	F	Small	'Leopard cat'	Terrestrial	MNHN 2009-251
Panthera leo	M	Large	'Panthera'	Terrestrial	NHM 1931.1.13.1
Panthera pardus	F	Large	'Panthera'	Scansorial	NHM 1938.4.21.11
Panthera tigris	F	Large	'Panthera'	Terrestrial	NHM 1884.1.22.6
*Panthera uncia**	F	Large	'Panthera'	Scansorial	NHM 1967.6.29.1

Pardofelis temminckii	U	Mixed	'Bay cat'	Scansorial	MNHN 1941-293
Prionailurus bengalensis	U	Small	'Leopard cat'	Scansorial	NHM 1860.4.23.18 1309B
Prionailurus viverrinus	M	Small	'Leopard cat'	Terrestrial	NHM 75.2287
Puma concolor	U	Large	'Puma'	Scansorial	UMZC K.5745 936E

Phylogenetic relationships

In order to represent the phylogenetic relationships of the felid species studied here, a time-calibrated species-level supertree of the order Carnivora (Nyakatura and Bininda-Emonds 2012) was used. The supertree strongly agrees with the relationships found by Johnson et al. (2006) for the Felidae family, and it was cropped in Mesquite version 3.02 (Maddison and Maddison 2014) to only represent the relationships between the 22 species of felids included in this study.

Selection of measurements

All 27 presacral vertebrae (seven cervicals, 13 thoracics, and seven lumbars) were measured with digital callipers (accuracy of 0.01mm) for linear measurements and with a goniometer for angular measurements (to the nearest degree).

Selection of the measurements taken was based on vertebral dimensions which had been shown in the literature to be informative about function and general biomechanics. These measurements correlate with flexibility and range of motion of the vertebral column, muscle and tendon size, and attachment sites (Shapiro 1995; Long et al. 1997; Koob and Long 2000; Shapiro 2007; Pierce et al. 2011).

All measurements were repeated three times and averaged to produce the final dataset used in further analyses. Different sets of measurements were collected for each region of the vertebral column (cervical, thoracic, and lumbar) because of the distinct morphologies observed in these regions, and for specific vertebrae with unique shapes (e.g., C1 and C2) (Fig. 2.1, and Table 3.2 in Chapter 3). A total of 28 measurement categories (i.e., centrum length, neural spine angle) and a total sum of 309 variables across the column constituted this dataset (Chapter 3).

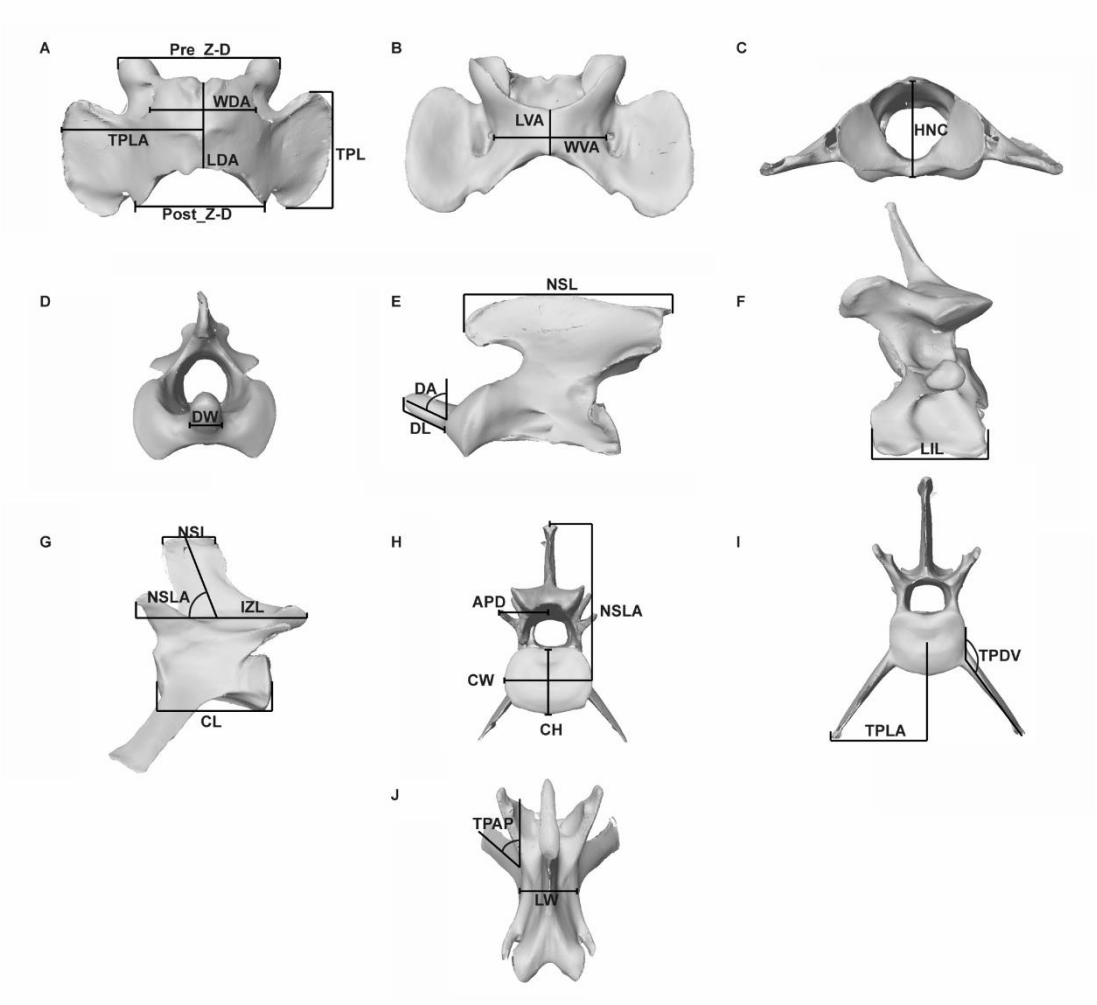

Fig. 2.1: Vertebral measurements: (A-C) atlas, (D-E) axis, (F) C6, and (G-J) L2 Abbreviations. LDA: Length of dorsal arch; Pre_Z-D: Prezygapophyseal distance; Post_Z-D: Postzygapophyseal distance; TPLA: Transverse process lever arm; WDA: Width of dorsal arch. B. LVA: Length of ventral arch; WVA: Width of ventral arch. C. HNC: Height of the neural canal. D. DW: Dens width. E. DA: Dens angle; DL: Dens length; NSL: Neural spine anteroposterior length at tip. F. LIL: Length of inferior lamella. G. CL: Centrum length; IZL: Interzygapophyseal length; NSL: Neural anteroposterior length at tip; NSLA: Neural spine lever arm. H. APD: Accessory process distance; CH: Centrum height; CW: Centrum width; NSLA: Neural spine lever arm. I. TPDV: Transverse process dorsoventral angle; TPLA: Transverse process lever arm. J. LW: Lamina width; TPAP: Transverse process anteroposterior angle. Vertebral images are from of a CT scan of *Acinonyx jubatus* (Cheetah, USNM 520539).

Data analyses

Size correction and log-transformation:

For the analyses included in Chapter 3, linear measurements were first log_{10}-transformed and corrected for differences in body size across the species while also accounting for phylogenetic relationships. Log-transformation of the data prior to further analyses is a helpful procedure. One of the advantages of this procedure is that it accounts for any skew in the data, and normalises the dataset (Sokal and Rohlf 2009; McDonald 2014). The total length of each specimen's vertebral column, which was also log_{10}-transformed, was used as a proxy for body size, following Pierce et al. (2011). The use of other body size proxies, such as basioccipital length, was not performed due to a lack of data in the literature on how both total vertebral column length and individual vertebral dimensions scale with this metric.

Taking evolutionary relatedness into account when correcting for body size in linear measurements is an important step when dealing with species in the Felidae family because a clear phylogenetic signal on body size has been observed in cats (Sunquist and Sunquist 2002; Johnson et al. 2006; Cuff et al. 2015). Phylogenetic size correction removes the effects of body size from the data by using phylogenetic regressions to calculate independent slopes for the clades (Revell 2009).

Principal Component Analysis (PCA):

The phylogenetically size-corrected linear measurements were first analysed with a Principal Component Analysis. This analysis uses the variances and covariances of the variables in the data to create new vectors, which are combinations of these original variables, and describe large proportions of the data variation (Sokal and Rohlf 2009). The new explanatory vectors, now called Principal Component (PC) axes (or eigenvectors), are orthogonal to each other, and are therefore independent of one another. Furthermore, the PC axes are found by centring the data at the origin of a plot, and tracing perpendicular vectors which fit the data in a decreasing manner (i.e., PC1 is the axis that fits the data best, PC2 is the second best fit, and so forth). The amount of the total variance that each PC explains is called the PC eigenvalue, and these values also decrease from the first to the last PC. The combinations of variables which compose each axis are found by the exploration of each PC loadings, which are the contribution of each variable to each PC. The space created by this ordination method applied to morphological data is called the morphospace, which is a representation of the range of morphologies of the studied dataset, and this is usually visualised by plotting two orthogonal PCs at a time (e.g., PC1 x PC2). Finally, the location of specimens according to each PC is demarked by respective PC scores.

Multivariate analysis of variance (MANOVA):

Quantitative analyses for testing for differential morphospace occupation between the ecological and phylogenetic groups investigated here were performed with MANOVAs on PC scores. Specifically, the MANOVA tests for differences in the means of each of the defined populations and considers both the magnitude and the direction of any differences between group means and of within-group variation (Mardia et al. 1979; Goodall 1991).

Correcting for phylogenetic relationships and multiple comparisons:

The use of phylogenetic MANOVAs was done in order to account for the evolutionary relatedness among the species included in this thesis. These analyses were performed under a null hypothesis of a Brownian motion model of evolution. Phylogenetic MANOVAs correct for the overestimation of degrees of freedom in comparative cross-species tests (i.e., for autocorrelation of data), and use the Brownian motion model of trait evolution to simulate the distribution of the relevant dependent variables along a given phylogenetic tree (Garland et al. 1993).

The results of both with and without phylogenetic correction MANOVAs were corrected for the increased chance in obtaining significant results due to multiple comparisons. Specifically, analyses comprising multiple comparisons involving the same units (e.g., multiple comparisons including the same vertebrae) present an increased chance of finding significant results due to chance (i.e., p-value < 0.05). In order to account for this increased chance of finding false positives, a Bonferroni correction was applied to the obtained p-values. With this method of correction, the original p-value threshold (e.g. 0.05) is divided by the number of comparisons performed to obtain a new lower p-value threshold. If, for example, the analysis involved 20 comparisons, the value of 0.05 is divided by 20 to obtain the new threshold point, which in this case would be 0.0025. It is this new value which is used to define if results are significant (i.e., results from the initial analyses are deemed significant if they present p-values equal to or lower than 0.0025) (Simes 1986; McDonald 2014).

Caveats:

Sexual dimorphism is a common characteristic of mammalian species. Most often, the differences between sexes concentrate on distinct ranges of body size, and males tend to be larger than females in general (Nowak 1999; Wozencraft 2005). Regarding the Felidae, this dimorphism has been observed in overall body size, skull length (which is highly correlated with overall size),

and canine length and width (Ewer 1973; Turner and Antón 1996; Gittleman and Van Valkenburgh 1997). Nevertheless, the level of sexual dimorphism is not constant across felid species, and it tends to be more exacerbated in more social species (e.g., lions, *Panthera leo*) (Ewer 1973).

A caveat that should be raised here is that it was not possible to test if specimens' sex was a factor which would explain vertebral shape change. This is due to many specimens lacking this information recorded in the museum labels (e.g., many specimens are listed as 'unidentified' for sex on Table 3.1 in Chapter 3). Ideally, the same number of male and female specimens would have been added to the dataset to account for such possible sexual dimorphism. Rather, the focus was laid on increasing total sample size regarding species number. Nevertheless, although one should be aware of this caveat, two levels of analyses may be used to ascertain that the possible effects sexual dimorphism may have on vertebral morphology are likely minor. Firstly, the analyses performed throughout this work focused on interspecific comparisons, rather than analysing shape change across populations of the same species. Shape differences between species are generally larger than intraspecific variations (Ewer 1973), as seen in Randau and Goswami (2017b). Secondly, the sexual dimorphism that has been observed in osteological traits in felids concerns matters of size rather than presence/absence of structures (Turner and Antón 1996; Gittleman and Van Valkenburgh 1997; Sunquist and

Sunquist 2002). Therefore, the size correction applied to linear measurements prior to all further analysis will have accounted for such differences across specimens. Additionally, the subsequent analyses of allometry (i.e., tests for investigating changes in morphology which are directly driven by size, see below) across species address questions of size influencing shape on an evolutionary (rather than static) level.

Investigating allometry:

Two levels of scaling regressions were performed with the linear vertebral data. First, I examined how the vertebral column length, both regarding the whole presacral column and individual traditional regions, scales with body mass (i.e., average species body mass). Regressions of $\log_{10}$-transformed body mass were made against $\log_{10}$-transformed total presacral vertebral column length (C1-L7) (based on the total sum of centrum lengths, without the intervertebral disc/space). This test was performed with and without phylogenetic correction by performing generalised least squares (GLS) regressions (Martins and Hansen 1996). Analyses to test if vertebral column length could be predicted by body mass in an isometric relationship were made by comparing the obtained slopes to an isometry slope of 0.333 (i.e., length ~ $\sqrt[3]{mass}$). I chose to use average body mass values per species rather

than estimating specimen mass from osteological measurements for the following reasons: 1. Not all specimens included were complete, which would mean a consistent estimation of body mass through measurements of osteological structures could not be performed; 2. More importantly, felid limb proportions and posture do not follow the generalised biomechanical expectations for mammals in general and, instead, display allometric scaling across cross-sections and other dimensions with increases in body size (see Introduction, and Day and Jayne 2007; Doube et al. 2009).

Second, $\log_{10}$-transformed within-vertebra linear dimensions were regressed against $\log_{10}$-transformed total vertebral column length with Reduced Major Axis (RMA) regression (Warton et al. 2006). Analyses to test if these individual linear vertebral measurements scaled isometrically with total vertebral length were made by comparing the obtained slopes to an isometry slope of 1 (i.e., length ~ length^1).

Profiles of linear and angular vertebral dimensions:

To examine in detail how vertebral morphology differs between groups across presacral column, $\log_{10}$-transformed, phylogenetically size-corrected linear measurements, and raw angles were averaged for all species in a corresponding locomotor group, and plotted against vertebral number

following Pierce et al. (2011). The corresponding plots for each of the vertebral dimensions (e.g., centrum length) formed vertebral column profiles that could be qualitatively compared across groups. Each profile was divided into vertebral region bins composed of seven vertebrae each (except bin '3' which was composed of only six vertebrae, from T8 – T13), corresponding to four bins at 25% vertebral intervals: bin '1': atlas – C7; bin '2': T1 – T7; bin '3': T8 – T13; and bin '4': L1 – L7.

In order to also compare groups with a quantitative statistical approach, differences between groups per vertebral profile bins were analysed with ANOVAs. If the ANOVA results showed that groups were statistically different with regards to vertebral profiles, post-hoc pairwise tests between the groups were performed with a Tukey's Honestly Significant Difference (HSD) test (Hammer et al. 2001; Ireland 2010). The results from this analysis were further corrected with a Bonferroni procedure.

Geometric morphometrics (GMM):

All subsequent chapters in this thesis used three-dimensional landmark data and geometric morphometric analyses to characterise vertebral morphology. Three-dimensional landmark data have been shown to describe shape more accurately than linear data due to being a collection of points which constitute

information on variation in three dimensions. Being richer in the description of shape means that using three-dimensional landmark-based data greatly surpasses linear measurements in both the amount and resolution of biological information from complex traits (Mitteroecker and Gunz 2009; Adams et al. 2013; Cardini and Loy 2013; Fabre et al. 2014a). However, 3D data are necessarily more time-consuming to collect, making it unrealistic to gather full 3D datasets from complete presacral vertebral columns for all of the specimens of interest. To determine which subset of vertebrae to include in the full 3D analysis, the results of the linear measurement study, described above and presented in Chapter 3, were augmented with a 3D GMM pilot study, detailed below.

Three-dimensional GMM: Pilot study

To test if the patterns identified in the linear morphometric analysis with regards to vertebral shape clusters were similar with 3D data, a small pilot study was run with three-dimensional data collected across vertebrae comprising the whole presacral vertebral column. This pilot study was conducted with the purpose of: 1. Determining the repeatability of the chosen 3D landmarks; 2. Testing landmark appropriateness for distinguishing vertebrae; and 3. Confirming the subset of vertebrae to include in the full 3D

analysis, as the results of the linear analysis suggested that many vertebrae overlapped largely in shape and thus did not add significant new information. A subset of vertebrae was necessary to identify as time constraints prevented 3D data collection of the full vertebral column without sacrificing specimen numbers, which are more important for statistical accuracy in these sorts of analyses.

1. Landmark repeatability

Selection of measurements:

In light of the results in the literature correlating the above mentioned vertebral proportions (translated as linear and angular measurements) to biomechanical and functional properties of the vertebral column, three-dimensional landmarks were chosen to represent these morphologies. Specifically, landmarks were chosen to maximise vertebral shape description and making sure that the proportion and positions of vertebral centra and processes would be captured. Furthermore, these landmarks were chosen to reflect the vertebral dimensions that have been shown to be functionally informative across a wide range of vertebrates (e.g., centrum dimensions such

as height, length and width; Shapiro 1995; Long et al. 1997; Koob and Long 2000; Shapiro 2007; Pierce et al. 2011).

Due to the lack of natural biological structures forming demarcations on vertebral shape (i.e., sutures), characterising vertebral morphology while still maintaining high accuracy in digitising landmarks was a point of concern. Additionally, the comparative shape analyses across vertebral types performed in this thesis required a set of homologous landmarks over the presacral vertebral column which could be digitised in the maximum number of vertebrae, while still accounting for the changes in morphology across those types. Therefore, sets of Type II landmarks (i.e., which describe points of maximum curvature or extension; Bookstein 1991), which were homologous across Felidae, were chosen to describe vertebral shape.

Whereas distinct sets of landmarks were chosen to characterise different regions which vary in morphology (i.e., C1: 12 landmarks, C2: 14 landmarks, C4: 18 landmarks, C6: 20 landmarks, C7 – T10: 16 landmarks, T11: 16 landmarks, T12 – T13: 17 landmarks, L1 – L4: 19 landmarks, and L6 – L7: 17 landmarks; Table S4.2 in Chapter 4 for landmark description), whenever the vertebral type allowed, each set would include (but not always be entirely comprised of) a minimum number of 16 homologous landmarks that were shared across all vertebrae other than the first two cervicals and the last three thoracics. Vertebrae which possess a more complex morphology, with extra

vertebral processes, were digitised with the same 16 landmarks plus additional points which were also homologous across species (e.g., C6 was digitised with 20 landmarks). The positioning of these landmarks (see Fig. 2.2) reflected major vertebral dimensions which have been shown to be greatly informative about the range of intervertebral movement and overall vertebral column biomechanics. As an example, the landmarks placed along the centrum of each vertebra reflect the height and width of the anterior and posterior articulating surfaces, and the length of the centrum, which have been shown to be correlated with dorsoventral and lateral mobility between vertebrae, and overall flexibility across the vertebral column, respectively (Chapter 3, and Shapiro 1995; Koob and Long 2000; Shapiro 2007; Pierce et al. 2011; Randau et al. 2016b). Furthermore, landmarks placed at the tip of the neural spine, zygapophyses, and transverse processes relate to the length of the lever arm and orientation of these processes, measurements which have also been shown to correlate with intervertebral and overall vertebral column flexibility.

A pilot study was then run to test the repeatability of these selected landmark points. Five vertebrae which represent the range of morphologies and of selected landmarks across the vertebral column were chosen for this study. These were comprised of C1 (atlas, 12 landmarks), C2 (axis, 14 landmarks), C6 (20 landmarks), T1 (16 landmarks) and L1 (19 landmarks) (Fig. 2.2). Three

specimens were used for this pilot study: one domestic cat, *Felis catus*, one serval specimen, *Leptailurus serval*, and one leopard cat, *Prionailurus bengalensis*. Each vertebra per species was measured three times in order to allow for the calculation of landmark repeatability. Here, repeatability was calculated by using a Procrustes ANOVA between the landmark coordinates (i.e., after Procrustes Superimposition) and using the mean squares (MS) term of the result statistics according to the following (Zelditch et al. 2012):

$$\left(\frac{MS(specimens) - MS(residuals)}{3}\right) = Individual\ variation$$

$$\frac{Indivual\ variation}{MS(residuals) + Individual\ variation} = Repeatability$$

Specifically, in the first equation the 'Individual variation' was calculated by dividing the difference between the MS term (i.e., the variance, which is calculated by dividing the total sum of squares by the degrees of freedom) for the specimen and for the residuals by 3 (i.e., the number of replicates per specimen). Repeatability is then calculated as the ratio of the variation per specimen to the total mean squares result (Zelditch et al. 2012). The results shown here (Table 2.2) demonstrate that the range of repeatability of landmarks is between 96% and 99%, comparable to those in other studies (Harris and Smith 2009; Zelditch et al. 2012; Fruciano 2016). According to these

results, the use of these sets of landmarks was ascertained to be appropriate for this study.

Table 2.2 Results from the landmark repeatability tests per each of the five vertebral types tested, showing that the selected landmarks displayed a minimum of 96% reproducibility. Abbreviations stand for: Df. Degrees of freedom; SS. Sums of squares; MS. Mean squares.

Vertebra						
Atlas		Df	SS	MS	R^2	p-value
	Individual	2	0.049	0.025	0.987	0.009
	Residuals	6	0.001	0.000		
	Total	8	0.050			
Repeatability	0.987					
Axis		Df	SS	MS	R^2	p-value
	Individual	2	0.075	0.037	0.986	0.002
	Residuals	6	0.001	0.000		
	Total	8	0.076			
Repeatability	0.986					
C6		Df	SS	MS	R^2	p-value
	Individual	2	0.050	0.025	0.963	0.003
	Residuals	6	0.002	0.000		
	Total	8	0.052			
Repeatability	0.963					
T1		Df	SS	MS	R^2	p-value
	Individual	2	0.046	0.023	0.966	0.009
	Residuals	6	0.002	0.000		
	Total	8	0.047			
Repeatability	0.968					
L1		Df	SS	MS	R^2	p-value
	Individual	2	0.082	0.041	0.963	0.002
	Residuals	6	0.003	0.001		
	Total	8	0.085			
Repeatability	0.963					

2. Assessing landmark sufficiency:

A second test was run to determine the accuracy with which the subsampled set of 16 homologous landmarks could characterise vertebral shape across the vertebral column. Here, the Procrustes coordinates were subjected to a MANOVA with the vertebral types as a factor variable. The MANOVA test (see below for description) is the appropriate test for analysing the patterns of shape across vertebrae rather than a discriminant function analysis because of the assumptions on which the latter method relies. Specifically, a discriminant function analysis (DFA) assumes that the patterns of variation (i.e., direction and amount of variation) within groups (i.e., vertebrae) are the same, and more importantly, DFA assumes that groups share the same covariance matrix, which is inappropriate for morphometric studies of the kind presented here. DFA is also limited to pairwise comparisons. An alternative procedure would have been to use a quadratic discriminant analysis instead; however, both this method and the regular discriminant analysis are highly sensitive to small sample sizes (Mardia et al. 1979; Zelditch et al. 2012; Collyer et al. 2015). As described in the section below, the nonparametric MANOVAs applied throughout this thesis tackle all of these issues consistently.

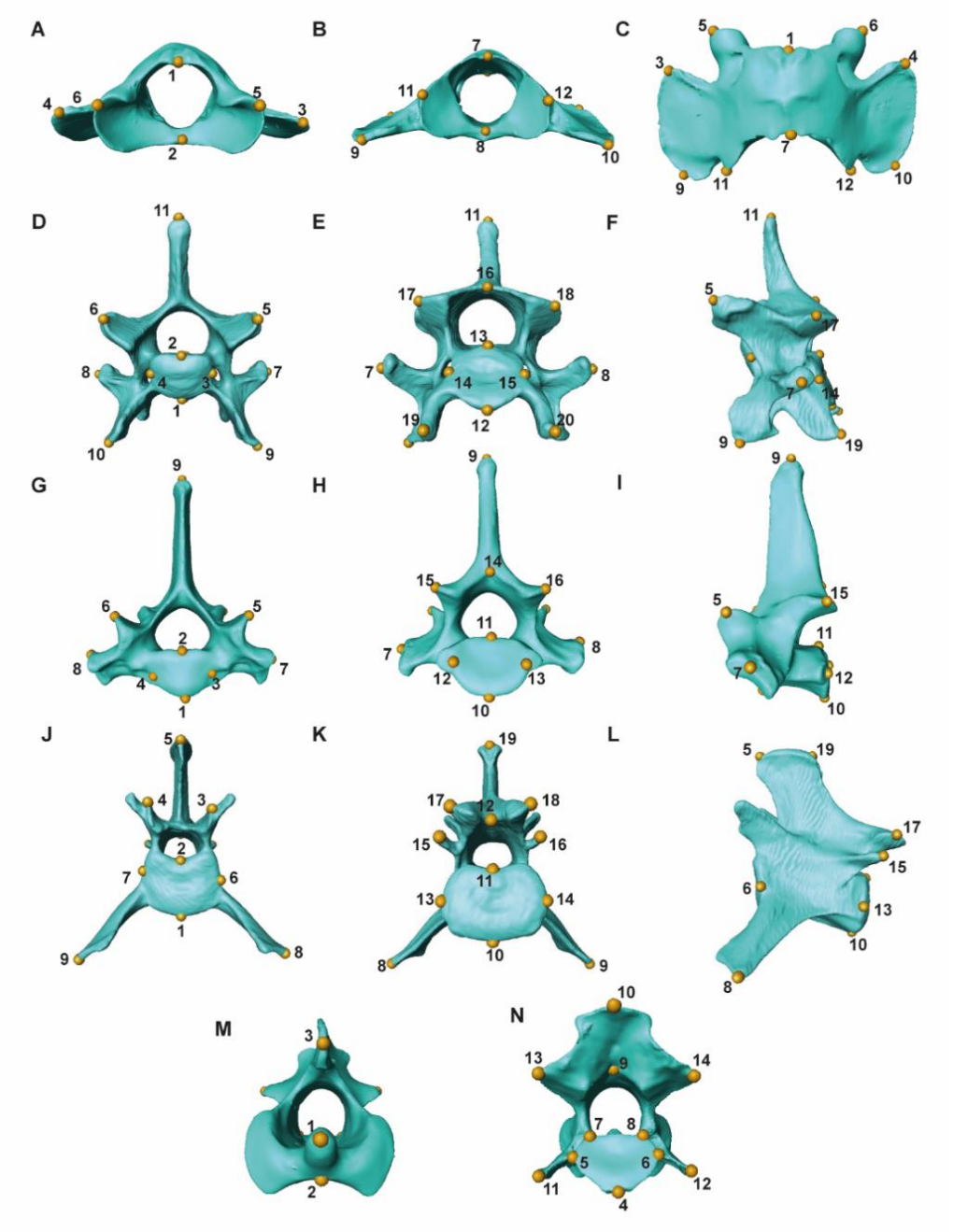

Fig. 2.2. Vertebrae used in the landmark pilot study. Each of the vertebrae shown here is a representative of a unique shape or possesses the maximum number of landmarks per morphology (i.e. the unique C1 and C2, an example of the cervical morphology with C6, T1 demonstrating the thoracic morphology, and L1 showing the lumbar morphology): (A-C) atlas (C1) in anterior, posterior and dorsal view; (D-F) C6 in anterior, posterior and lateral view; (G-I) T1 in anterior, posterior and lateral view; (J-L) L1 in anterior, posterior and lateral view; and (M-N) axis (C2) in anterior and posterior view. Vertebral images are from CT scans of *Acinonyx jubatus* (Cheetah, USNM 520539). Vertebra-specific landmark descriptions can be found in Table S4.2.

Table 2.3 MANOVA results showing accuracy of the set of 16 homologous landmarks in describing vertebral morphology across the vertebral column.

	Df	SS	MS	R^2	p-value
Vertebra	13	146.692	11.284	0.889	0.0002
Residuals	1202	18.298	0.015		
Total	1215	164.99			

Results from the MANOVA show that the 16 homologous landmarks characterise vertebral types at 89% accuracy (p-value = 0.0002; Table 2.3). Whereas this result supports the use of the 16 homologous landmarks with a high level of accuracy, it also supports the observations of the high level of vertebral shape similarity within regions of the vertebral column (see below). This extensive similarity of vertebral shape within certain regions of the vertebral column can be observed by the clustering of vertebral types in the morphospace, showing a high degree of overlap across vertebrae (Figs. 2.3 here, and 4.2 in Chapter 4).

3. Selecting the vertebral subset to include in the full 3D analysis:

The results from the MANOVA of linear morphometric data in Chapter 3 indicated that correlations between vertebral shape and ecological signal were

heterogeneous throughout the vertebral column, and that the gradual change in vertebral morphology within the traditional regions (i.e., cervical, thoracic and lumbar) would allow for subsampling of vertebral units, in exchange for expanded specimen sampling, without significant loss of biological information. Based on the results of the linear morphometric study, the chosen set to be digitised was comprised of the following 19 vertebrae: C1 (atlas), C2 (axis), C4, C6, C7, T1, T2, T4, T6, T8, T10, T11, T12, T13, L1, L2, L4, L6, and L7. Whereas this set assured thorough sampling of each region, it also included all vertebrae with distinct and unique morphology (e.g., C1 and C2), vertebrae which have been suggested to be biomechanically informative (e.g., the diaphragmatic T10 and the anticlinal T11), and vertebrae which were immediately placed at the boundaries between regions and the two vertebrae immediately before and after this pair (e.g., C7 and T1, and C6 and T2, respectively).

In order to ascertain that the exclusion of the eight vertebrae (i.e., C3, C5, T3, T5, T7, T9, L3, and L5) which were not digitised in the main dataset would not compromise the results, a small pilot study was conducted. In this study, all 27 presacral vertebrae from six specimens from three felid species (i.e., three specimens of domestic cat, *Felis catus*, one serval specimen, *Leptailurus serval*, and two specimens of leopard cat, *Prionailurus bengalensis*; Table 2.4 for specimen numbers) held at the mammal collection of the Natural History

Museum (London) were digitised. With the exclusion of vertebrae which possess unique morphology and which have nonetheless been included in the thesis final dataset, vertebrae were digitised with the set of 16 homologous landmarks discussed above and analysed with a PCA to explore how vertebral shape changes across the vertebral column.

The results from this shape analysis have shown that almost all presacral vertebrae cluster in groups of similar morphology, apart from C4 and C7 which plot in separate regions of the morphospace (Fig. 2.3 A-C). Specifically, the following clusters of morphospace occupation are C4, C3 – C6 (with the exception of C4), C7, the thoracic vertebrae, and the lumbar vertebrae. Importantly, this result demonstrates that none of the eight vertebrae which have been excluded from the thesis's three-dimensional dataset form a separate cluster, and therefore the dataset of 19 vertebrae are an accurate representation of presacral vertebral morphology in Felidae.

Table 2.4: Collection numbers from specimens included in the pilot study for vertebral selection. Abbreviation: NHM – Natural History Museum, London.

Species	Collection number
Felis catus	NHM 1988 1
	NHM 1952 10 20 4
	NHM 2002 161
Leptailurus serval	NHM 1845 9 25 23
Prionailurus bengalensis	NHM 1309b 1860 4 23 18
	NHM 77 2896

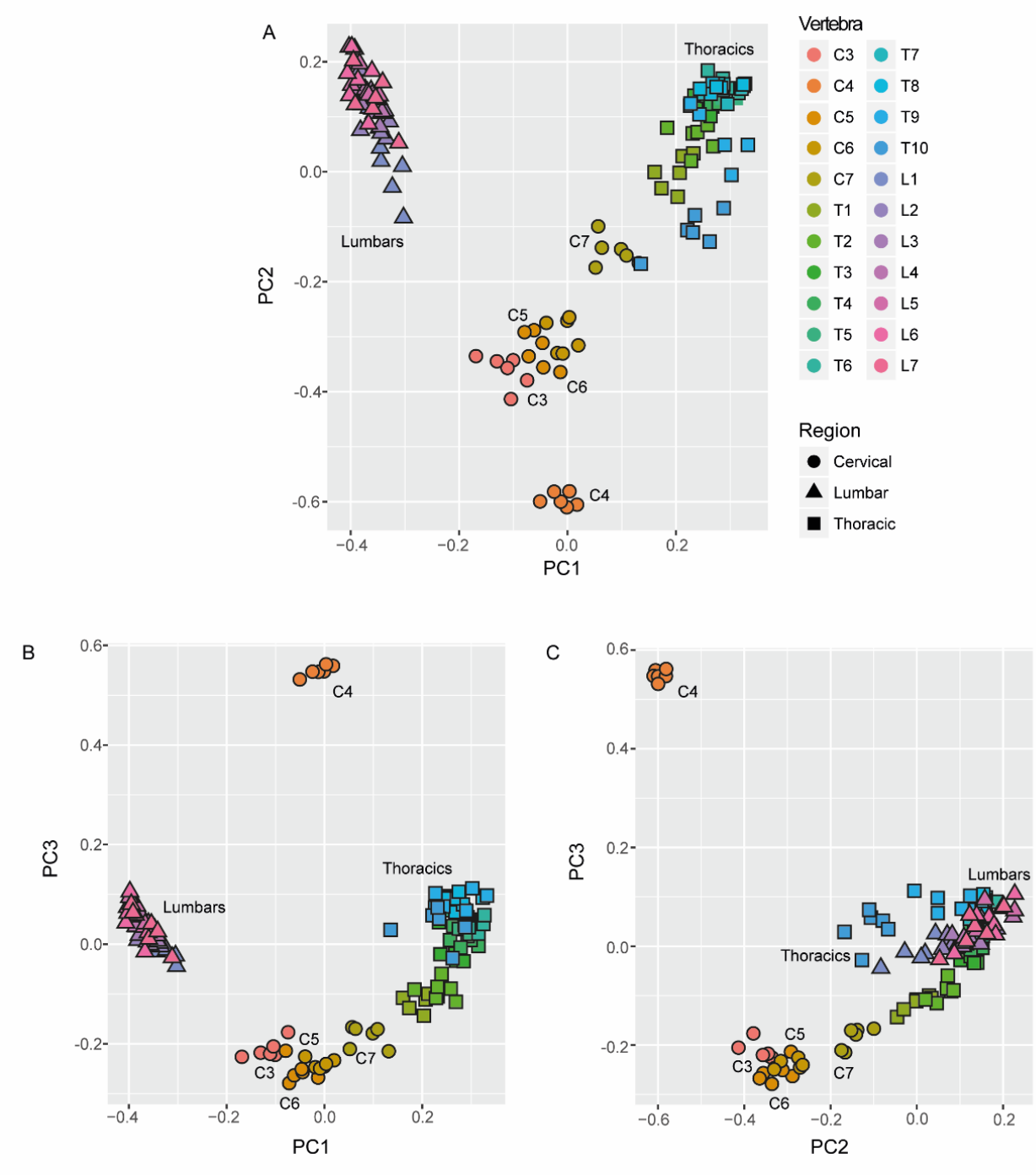

Fig. 2.3: Results from the Principal Component analysis showing clustering of vertebrae. Percentage of shape variation explained per PC: PC1 45%, PC2 27%, and PC3 16%. A. PC1 x PC2; B. PC1 x PC3; C. PC2 x PC3.

Three-dimensional GMM: Full study

Data collection:

Based on the results of the geometric morphometrics pilot study detailed above, three-dimensional landmark data were collected from a group of nine felid species across a sample of vertebrae which accurately represent the range of morphologies in the presacral vertebral column. This subsample of 19 out of the 27 presacral vertebrae (i.e., C1, C2, C4, C6, C7, T1, T2, T4, T6, T8, T10, T11, T12, T13, L1, L2, L4, L6, and L7) were selected to be digitised with an Immersion Microscribe G2X (Solution Technologies, Inc., Oella). Subsampling units across the vertebral column was necessary in order to increase sample size with regards to numbers of specimens per species. This focus regarding sample size was required to assure that a significant portion of the true biological variation was captured. Additionally, having multiple specimens is one of the fundamental assumptions of Geometric Morphometrics: analytical power issues can arise when the ratio between specimens and variables is low, and this ratio can rapidly become smaller due to the fast increase in measurement variables (i.e., the denominator) when three-dimensional landmarks are used (i.e., each individual landmark adds three variables to the denominator of this ratio) (Mitteroecker and Gunz 2009; Adams et al. 2013; Cardini and Loy 2013; Adams 2014b; Collyer et al. 2015). The results of the

three-dimensional pilot study discussed above confirm that subsampling across the vertebral column does not compromise the final conclusions.

Species selection:

Based on online collection databases for seven international museums detailing specimen availability, nine species of felids were selected in order to prioritise species with larger numbers of specimens. Importantly, these species were also selected on the basis of having representatives of each of the categories of the two ecological specialisations observed in felids (i.e., specialisation towards prey size choice and locomotion, as discussed above; Table 2.5), and of comprising the range in body size observed in this family.

Table 2.5 List of species studied in the three-dimensional (3D) study, with their corresponding information on locomotor and prey size categories collated from the literature (Sunquist and Sunquist 2002; Meachen-Samuels and Van Valkenburgh 2009a, 2009b).

Species	Locomotion	Prey size
Acinonyx jubatus	Cursorial	Large
Felis catus	Scansorial	Small
Leopardus pardalis	Scansorial	Mixed
Leptailurus serval	Terrestrial	Small
Neofelis nebulosa	Arboreal	Mixed
Panthera leo	Terrestrial	Large
Panthera pardus	Scansorial	Large
Prionailurus bengalensis	Scansorial	Small
Puma concolor	Scansorial	Large

Phylogenetic relationships

A recent tree of the Felidae family (Piras et al. 2013) was used to depict the phylogenetic structure of the nine species included in the three-dimensional study. The inner relationships of the Felinae part of the tree (i.e., representing the relationships among living felids) also strongly agree with the structure found by Johnson et al. (2006). The original Felidae tree was pruned in R version 3.2.2 (R Core Team 2015b), using the 'geiger' package (Harmon et al. 2014).

Specimen selection:

Specimens were selected on the basis of being in the chosen age stage (i.e., adults) and on completeness. All adult specimens which were available and presented osteological units of the presacral vertebral column were digitised in the visited museum collections. Additionally, this effort to digitise multiple specimens per species was done to capture all available information, and therefore accurately representing the biological variation per species. This likely ascertained that species averages for both shape and size have been included here, especially for the species with the largest sample sizes (see Table 1.1 in Chapter 1).

As noted above, there was limited information on the sex of individuals, preventing consideration of this variable.

Analyses performed:

Procrustes Superimposition:

Prior to each round of geometric morphometric analyses, landmark data were aligned with a Procrustes Superimposition in order to separate shape data (i.e., the Procrustes coordinates) from variables containing information on scaling, rotation and location (see Introduction, pages 31-32, and methodology description on Chapters 4, 5, 6, and 7). It is on the Procrustes coordinates that the analyses described below were applied.

Dealing with small sample sizes

During the data collection phase of this PhD thesis, seven of the museum collections around the world known to hold the largest collections of carnivores were visited. These museums included: the Natural History Museum in London, the University Museum of Zoology, Cambridge, the Muséum National d'Histoire Naturelle, Paris; the Field Museum of Natural History, Chicago; the American Museum of Natural History, New York; the Smithsonian National Museum of Natural History, Washington D.C.; and the Harvard Museum of Natural History, Cambridge.

Due to the nature of museum collections, there is reduced availability of complete skeletal specimens relative to skull-only specimens. For the visited museums, all adult (i.e., presenting fused bone epiphyses) specimens of the nine species studied here which were available were digitised. Visiting those locations allowed me to digitise a total of over 1,700 vertebrae from 109 specimens, which form the main thesis dataset.

The analyses which compose this dissertation have either focused on patterns across the chosen nine species of felids or on ecomorphological subgroups represented by multiple species, rather than focusing on intraspecific variation. Since intraspecific sample sizes were restricted, the broader scope meant that higher sample sizes per group were analysed. Nevertheless, further caution was taken during the analytical procedures:

1. The analyses of variance were non-parametric:

Unlike the parametric analyses used to test for group differences, the non-parametric analyses of variance between groups used here do not require the same assumptions regarding variable distribution and the ratio between variables and observations, instead relying on randomised permutation tests (Anderson 2001a, 2001b). Namely, these non-parametric analyses do not make any assumption on the distribution of the variables in the populations (i.e., they do not require the variables to follow a normal distribution), nor do they

require that populations have equal covariance matrices. The permutation procedure happens through randomly sampling from the original data combined (i.e., pooled from the complete original dataset) to simulate new populations of the same size as the original groups (i.e., observations are relocated to the new populations samples from a single combined dataset). This random permutation procedure was repeated between 5,000 and 10,000 times across the analyses performed in this thesis. For each round of permutation, the new test statistic is compared to the value calculated using the original data. The number of resampling rounds in which the new test statistic was the same or higher than the original value is then divided by the total number of permutations (i.e., the p-value of the test). Finally, it is this ratio that indicates the significance level of the analysis. Furthermore, for the geometric morphometric data, this permutation procedure was expanded to using the 'random residual permutation procedure' (RRPP). This procedure does not rely on the ratio between the number of variables and the number of observations (i.e., specimens). With this method, the values for shape residuals obtained from a reduced model are randomly resampled and used to estimate the effects of the full model (Adams and Collyer 2009; Collyer et al. 2015).

2. Matrix repeatability:

For every osteological element (e.g., vertebral type C7) included in the analyses across the thesis, the stability of the covariance matrices was assessed by performing bootstrap resampling tests with 10,000 permutation rounds with replacement, using random skewers analysis (Goswami and Polly 2010c). The correlation between the original covariance matrix and the resampled matrices varied from 0.91 to 0.96, with a median of 0.94, demonstrating that sample sizes were sufficient for accurately capturing the covariance structure of each vertebra.

Principal component analysis:

The Procrustes coordinates for the 14 vertebrae (i.e., C4, C6, C7, T1, T2, T4, T6, T8, T10, L1, L2, L4, L6, and L7) which were digitised with the same 16 homologous landmarks were analysed with a PCA (see descriptions of PCA method and landmark selection above). In the supplementary information of Chapter 4, three extra thoracic vertebrae (T11 – T13) were digitised, with addition of re-digitisation of lumbars L1, L2 and L4, with two landmarks (i.e., regarding the position of accessory processes) which were analogous to the original transverse process landmarks, and an additional PCA was run.

Multivariate analysis of variance (MANOVA):

In addition to the methodology described above, in the geometric morphometric analyses, factorial MANOVAs (i.e., shape coordinates ~ factor 1 * factor 2) were used to evaluate the effects of centroid size and ecological specialisation (both in terms of locomotion and prey size categories) on vertebral shape. Factorial MANOVAs with this size-ecology interaction accounts for the effect of 'size' (i.e., centroid size) while examining the other factors that describe shape and define the groups. As described above, these MANOVAs were non-parametric and used the RRPP method to evaluate the tests significance (Collyer et al. 2015). Correction for multiple comparisons was performed with a Bonferroni method, as described above.

Investigating allometry:

First, the Procrustes coordinates (i.e., shape data) for individual vertebral types were regressed in a linear model against their unit centroid sizes. Second, this allometric relationship was tested across regions comprised by several vertebrae using the same procedure. Finally, the allometric differences between ecological groups (i.e., locomotion and prey size specialisation) were analysed by calculating allometric trajectories per group (i.e., plotted PC1 of

the predicted values against size) groups (Adams and Nistri 2010). The significance of the differences in the log centroid size ~ shape relationship between groups could be quantified by both the p-value of the comparisons between slope distances, which itself measures differences in amount of shape change per unit of centroid size change, and the slope angle's p-value, which indicates if the directions of these vectors point at different regions of the morphospace (Collyer and Adams 2013; Collyer et al. 2015). As discussed, these tests involved random permutation rounds and use of the RRPP methodology described above. The increased chances of finding false positives in this analysis were accounted for by performing a Bonferroni correction to the p-values.

As for the linear data, it was not possible to test for shape differences due to sex in this sample due to lack of information in museum databases. Rather, all available specimens from the chosen species were digitised with a focus on increasing total sample size, and analyses focus on interspecific comparisons. However, the results of the allometric tests across different-sized species showing that vertebral size explained only a small percentage of vertebral shape (~11%; see Chapter 4) indicated that differences in shape due to the size differences between males and females of the same species would be even smaller.

Testing for phylogenetic signal on centroid size and shape data:

Due to the close evolutionary relatedness between the species included in this thesis, I have tested for phylogenetic signal on both size and shape data (i.e., whether more closely related species were more phenotypically similar; Felsenstein 1985). First, the mean shape was calculated for each vertebra per species, and a value of centroid size for the mean structure was also obtained. The phylogenetic signal on both shape and size was tested with a multivariate version of the Kappa statistic, a method which has been shown to display appropriate Type I error and high statistical power (Blomberg et al. 2003; Adams 2014a). This method used a distance matrices approach, and calculates the signal under a Brownian motion model of trait evolution. The significance level was tested through 10,000 permutation rounds of data across the tips of the phylogenetic tree. Correction for multiple comparisons was performed with a Bonferroni method.

Phylogenetic MANOVA:

When a significant result was found for the test of phylogenetic signal on vertebral shape, phylogenetic MANOVAs were run on the factorial models described above. Specifically for the morphometric data, this phylogenetic

analysis calculates a phylogenetic transformation matrix and the Gower-centred distance matrix from predicted variable values, which are then used to assess significance from comparisons between the values of statistical attributes obtained from those and the observed values (Garland et al. 1993; Adams 2014b; Adams and Collyer 2015). Correction for multiple comparisons was performed again with a Bonferroni method.

Phenotypic trajectory analysis (PTA):

This analysis was used to study the influence of ecological specialisation across the vertebral column in a multi-vertebra approach, rather than analysing vertebrae individually.

PTA is performed according to the following steps: First, the trajectory stages are defined as a factor (i.e., in this thesis, the stages were the vertebral types) and the ecological groups are specified (i.e., if prey size groups: small, mixed and large prey specialists), as per in a factorial MANOVA (see above; e.g., shape ~ vertebra * prey size). Second, the vertebral mean shape for each of the groups is calculated per stage. Finally, a three-dimensional trajectory is traced across the stages for each of the groups. These trajectories are then compared between groups across the morphospace (i.e., all PCs) in the same manner as a cloud of Procrustes coordinates. In order to statistically quantify differences

between trajectories, they are compared regarding three characteristics: the size, the direction in the morphospace, and the shape of the trajectories (Adams and Collyer 2009; Collyer and Adams 2013). As discussed above regarding the allometric trajectories per group, the size of the phenotypic trajectory reflects the amount of shape change across the trajectory stages. The trajectory direction represents differences in the main relative covariations of shape variables between groups. Finally, comparing trajectory shape concerns a combination of size and shape, and the overall three-dimensional morphology of the trajectories. Comparing the structure of phenotypic trajectories across groups allowed me to make inferences about shape convergence (Stayton 2006; Adams et al. 2013). Further, and specifically to the novel application of this method to the study of vertebral column morphology, these comparisons allowed me to examine how shape changes across the vertebral column in a quantitative approach, and to identify in which regions there is greater variation between ecological groups. Again, the significant of the obtained p-values was verified by applying a Bonferroni correction.

Analyses of morphological disparity:

Two measures of morphological disparity were used in this thesis: Procrustes variance, and Procrustes distance (or the maximum range) (Zelditch et al. 2012). Procrustes variances are calculated by dividing the shape residuals from a linear model (i.e., shape ~ group) by the degrees of freedom (i.e., the number of specimens minus 1), whereas the Procrustes distances are calculated from the sum of ranges across the axes in the morphospace. Although Procrustes variance is the most common measure of disparity used in geometric morphometric studies, I decided to also calculate the Procrustes distances as this is the measure of disparity which has been shown to be more highly correlated to levels of integration (Goswami et al. 2014).

Integration analyses:

Measuring overall integration within individual vertebrae:

The degree of intravertebral morphological integration was calculated using the relative eigenvalue standard deviation method developed by Pavlicev et al. (2009), which has been shown to highly correlate to the mean squares correlation coefficient (i.e., r^2, which is a measure of integration) (Marroig et al. 2009; Goswami et al. 2014). This test is derived from the observation that

increased integration leads to concentration of shape variation in fewer dimensions (i.e., axes of the morphospace) due to the augmented covariation between trait variables. This concentration of variation in only a few dimensions therefore causes a great disparity between the eigenvalues. On the other hand, when traits are not highly correlated, the variance tends to be more highly dispersed across the dimensions, and the differences between eigenvalues are smaller (Wagner 1984; Cheverud et al. 1989; Pavlicev et al. 2009).

However, eigenvalue variance depends on the number of eigenvalues (and therefore, the number of traits) per analysed structure (Cheverud et al. 1989; Pavlicev et al. 2009), and therefore should not be directly compared across structures which may differ in number of traits measured. In order to account for this dependency on trait size, and to make results comparable across my dataset and other published studies, I used the relative eigenvalue standard deviation, which is itself independent on eigenvalue number. This value of integration is obtained by dividing the observed eigenvalue variance by the maximum eigenvalue variance for the specific number of traits (i.e., the eigenvalue variance obtained when all trait variables are fully correlated and therefore only one eigenvalue is larger than zero) (Pavlicev et al. 2009). Finally, the relative eigenvalue standard deviation is obtained by calculating the ratio between the square root of the eigenvalue variance and the square root of the

maximum eigenvalue variance, which is done in order to account for building the covariance matrices from limited sample sizes (Wagner 1984; Pavlicev et al. 2009).

Measuring integration between two structures:

The level of integration between two structures (i.e., two vertebrae or between a vertebra and a different osteological structure, such as the skull) was measured with a two-block Partial Least Squares (PLS) analysis (Rohlf and Corti 2000; Bookstein et al. 2003). PLS analyses find the two axes which individually show the greatest predictive power towards the observed shapes, and which have the maximum covariation between structures. These axes are found through the generation of two vectors from the covariance matrix of the two structures which are perpendicular to each other, much like the PC axes generated in a PCA. Importantly, because PLS analyses focus on this pair of axes which account for the most covariation between structures, they do not take into consideration the overall variation throughout the individual parts, nor do these analyses assume any dependency of one variable, or set of variables, over the other (Rohlf and Corti 2000; Goswami and Polly 2010c; Klingenberg 2013). The application of this method in the literature ranges from measuring integration between two highly disparate structures, each

represented by a set of shape coordinates, to measuring covariation between a set of coordinates and a univariate variable, such as diet or locomotion. Specifically, PLS analyses can and have been used to study the covariation between extremely different morphologies which present varying degrees of complexity (e.g., skull and mandible), or between highly descriptive sets of coordinates and ecology, and examples are aplenty (e.g., Rohlf and Corti 2000; Bookstein et al. 2003; Marugán-Lobón and Buscalioni 2006; Laffont et al. 2009; Nogueira et al. 2009; Gómez-Robles and Polly 2012; Hautier et al. 2012; Adams and Felice 2014; Fabre et al. 2014b; Arnold et al. 2016; Fabre et al. 2017).

Species' evolutionary relationships were taken into account when testing for morphological integration between structures with the use of phylogenetic Partial Least Squares (Adams and Felice 2014). This analysis computes the degree of morphological covariation while accounting for phylogeny under a Brownian motion model of trait evolution.

The significance of the PLS analyses performed here was assessed with 5,000 rounds of random permutations of the specimens in one block with regards to those in the second block. Additionally, an alternative method for correction of p-values due to multiple comparisons (i.e., a Benjamini-Hochberg correction) was applied when performing PLS analyses. I have applied this method of correction because the PLS analyses performed here involved a large number of comparisons and using the Bonferroni correction was

considered too conservative; i.e., finding a sizeable number of false negatives (e.g., in analyses involving 200 comparisons, significance would only be achieved if p-values were equal or lower to 0.00025). Instead, the Benjamini-Hochberg correction method uses a ranking technique to account for false positives. First, a false discovery rate (Q) is chosen (e.g., 0.05). Then, the original p-values are ordered in an ascending manner (i.e., from smallest to largest) and ranked from i=1 (lowest) to m= the total number of tests. Benjamini-Hochberg critical values are calculated as $(i/m)Q$ for each of the original p-values. Finally, the largest p-value which is still lower than its assigned Benjamini-Hochberg critical value is determined as the significance threshold. P-values which are equal to or lower than this new significance threshold are classified as significant (Benjamini and Hochberg 1995; McDonald 2014).

Caveats

Allometric effects on vertebral shape change were not corrected for prior to analyses of integration and modularity. The reasoning behind this is as follows: 1. Analyses of allometry on vertebral shape revealed that allometric effects vary across the presacral vertebral column, but only explain up to 11% of vertebral shape differences across felids (mean 11.1%, median 9.9%)

(Chapter 4; Randau et al. 2016a); 2. Studies have shown that body size evolution in felids is highly phylogenetically-dependent (Sunquist and Sunquist 2002; MacDonald et al. 2010; Cuff et al. 2015). Since phylogenetic corrections were applied to covariation analyses, further correction for size could potentially introduce error due to overcorrection; 3. Allometry has been suggested to be a strong driver of morphological integration because its effects tend to affect individual structures uniformly (Klingenberg 2008; Goswami and Polly 2010c; Klingenberg and Marugán-Lobón 2013). In light of one of the main aims of this thesis (i.e., investigating patterns of integration across and within vertebrae), correcting for a factor that may drive integration would potentially obscure real patterns of covariation.

Analyses for testing of modularity models:

Modularity models were tested with two analyses of covariation: The RV coefficient analysis (Escoufier 1973; Klingenberg 2009) and the covariance ratio analysis (CR; Adams 2016). These methods differ in which the RV coefficient analysis includes a measure of within-block variance in the denominator of the ratio along with within-block covariance , whereas the CR does not (i.e., it only includes the covariance within each block in the denominator, which is the necessary information for characterising

modularity and integration) (Adams 2016). Whereas the RV coefficient has traditionally been the method most frequently used to test hypotheses of modularity, it has been recently criticised due to its sensitivity to specimen sample size and landmark number (Fruciano et al. 2013). Conversely, simulation tests using the covariance ratio have shown that this method displays appropriate type I error rates, is consistently robust throughout changes in specimen and landmark sample sizes, and presents higher statistical power relative to the RV coefficient (Adams 2016). Significance of the hypothesis of modularity in both methods is assessed by random permutation of landmarks in 10,000 rounds of alternative models of modularity to generate a distribution of values. The observed signal is then compared to the randomly generated distribution.

Additionally, rather than phylogenetically correcting the vertebral shape data, which, as noted above, could obscure the real patterns of developmental modularity (Polly et al. 2013), I corrected for taxonomic relatedness by calculating a pooled within-species variance-covariance (VCV) matrix for each vertebra tested here individually. This new VCV matrix was then used in a second round of covariance ratio analyses to test for the developmental model of intravertebral modularity. As with the integration analyses, allometric correction was not performed prior to modularity testing due to the reasons described above.

Limitations

Although the above-mentioned caveats should not significantly affect the results of this thesis, one of the main limitations of this work is not being able to conduct intraspecific analyses regarding changes in vertebral shape across adult individuals of different sexes, or across different ontogenetic stages, due to insufficient within-species specimen availability. Questions regarding these topics in future studies would be greatly beneficial for our understanding of vertebral variation and, importantly, for comparisons with the patterns found here for across-species patterns.

Chapter 3. Cryptic complexity in felid vertebral evolution: shape differentiation and allometry of the axial skeleton

Published as: Randau, M., Goswami, A., Hutchinson, J. R., Cuff, A. R., & Pierce, S. E. (2016b). Cryptic complexity in felid vertebral evolution: shape differentiation and allometry of the axial skeleton. *Zoological Journal of the Linnean Society, 178*(1), 183-202.

Abstract

Members of the mammalian family Felidae (extant and extinct cats) are grossly phenotypically similar, but display a 300-fold range in body size, from less than 1 kg to more than 300 kg. In addition to differences in body mass, felid species show dietary and locomotor specializations that correlate to skull and limb osteological measurements, such as shape or cross-sectional area.

However, ecological correlates to the axial skeleton are yet untested. Here, we build on previous studies of the biomechanical and morphological evolution of the felid appendicular skeleton by conducting a quantitative analysis of morphology and allometry in the presacral vertebral column across extant cats.

Our results demonstrate that vertebral columns of arboreal, scansorial and terrestrial felids significantly differ in morphology, specifically in the lumbar region, while no distinction based on dietary specialization was found. Body

size significantly influences vertebral morphology, with clear regionalization of allometry along the vertebral column, suggesting that anterior (cervicals and thoracics) and posterior (lumbar) vertebrae may be independently subjected to distinct selection pressures.

Introduction

The carnivoran family Felidae (Mammalia, Placentalia) includes *ca.* 38 living species of grossly morphologically similar animals (Ewer 1973; Turner and Antón 1996; Sunquist and Sunquist 2002; Johnson et al. 2006; MacDonald et al. 2010). With the exception of fur patterning, body size is the greatest gross anatomical difference observed between species, with the Felidae displaying a considerable body mass range from 1kg in the rusty-spotted cat (*Prionailurus rubiginosus*) to over 300kg in the tiger (*Panthera tigris*). In addition to their overall phenotypic similarity, felids are an exception to the general mammalian biomechanical trend of size-correlated limb posture. According to this trend, increases in body size drive increased limb erectness (i.e., joint extension) in order to maintain safe levels of peak functional stresses acting on supportive tissues (Biewener 1989; Bertram and Biewener 1990; Biewener 2005). However, despite the 300-fold range in body mass in felids, limb posture is remarkably uniform throughout the clade and, instead, some bone

allometry is observed in limb long bones' cross-sections (Day and Jayne 2007; Doube et al. 2009; Zhang et al. 2012). Indeed, it has been hypothesized that the lack of correlation between body size and limb posture in felids may reflect a large-bodied ancestral condition for the clade (Mattern and McLennan 2000; Johnson et al. 2006; Day and Jayne 2007; but see Cuff et al. 2015).

Felids are also remarkably conservative in behavioural and ecological attributes, such as diet: all felids are hypercarnivores specialised in vertebrate prey, with species differing mainly in terms of prey size and prey-killing techniques (Ewer 1973; Carbone et al. 1999; Sunquist and Sunquist 2002). Felid species are known to show different killing strategies in relation to prey size, with bigger cats usually applying a sustained bite to the prey's muzzle or neck, and smaller felids killing by faster nape or head bites (Ewer 1973; Leyhausen 1979; MacDonald et al. 2010). Interestingly, unlike other carnivorans such as canids, the forelimbs of felids present a duality in function between locomotion and prey-killing behaviour (Ewer 1973; Gonyea 1978; Leyhausen 1979), and therefore, along with differences in skull, mandible and dental shape, the shape of the forelimbs also reflect diversification in prey size choice (Slater and Van Valkenburgh 2008; Meachen-Samuels and Van Valkenburgh 2009a, 2009b; Slater and Van Valkenburgh 2009; Meachen-Samuels 2012).

Several recent studies have examined the shape, function, and evolution of mammalian limbs, especially those of carnivorans (Meachen-Samuels 2010)

(Meachen-Samuels and Van Valkenburgh 2009b; Walmsley et al. 2012; Alvarez et al. 2013; Samuels et al. 2013). These studies have demonstrated that osteological measurements of the entire limbs, and of their individual segments, are informative about locomotor habits, such that qualitative reconstructions of the ecology of fossil species are possible by comparing their morphology to better known living species. Within Felidae, these studies have additionally shown that the limb morphology is informative about prey size specialisation and, furthermore, that limb shape is related to hunting strategies in extant and, by inference, extinct species (Meachen-Samuels and Van Valkenburgh 2009b, 2010; Meachen-Samuels 2012). However, to date, the vertebral column has been underrepresented in the morphological and biomechanical literature on felids and other species, and is often treated as one functional segment, with few functional studies considering the complexity and regionalisation of this structure in detail (but see Halpert et al. 1987; Macpherson and Ye 1998; and Jones 2015).

The vertebral column has a critical role in body support against gravity, is connected to the limbs by means of bony, ligamentous and muscular components, and is composed of many consecutive articulations that take active participation in locomotion and prey procurement (Pridmore 1992; Macpherson and Fung 1998; Macpherson and Ye 1998; Long et al. 2002; Schilling 2011). Different degrees of torsion, flexion-extension, and bending

capacities of the vertebral column are important components of movement at different locomotor speeds and postures, and in the control of body deformations and manoeuvres (Carlson et al. 1979; Pridmore 1992; Gál 1993b; Long et al. 1997; Smit 2002; Molnar et al. 2014). Changes in the size and angle of vertebral processes reflect differences in the size of muscles, tendons and ligaments inserting on those elements, and the relative length of centra is associated with the degree of movement between two consecutive vertebrae (Long et al. 1997; Koob and Long 2000; Pierce et al. 2011). Thus, morphological specialisations of vertebrae translate into functional modifications in the flexibility and range of motion of the whole spine, as well as its role in body support and general locomotor performance.

The vertebral column of placental mammals is largely constrained to a fixed number of presacral segments, relative to other amniotes (Müller et al. 2010), with a few exceptions in "southern" placental clades, Afrotheria and Xenarthra (Narita and Kuratani 2005). Potentially due to this constraint in vertebral numbers, specialisation into discrete niches has been accompanied by a diversification of vertebral shapes across placentals (Narita and Kuratani 2005; Müller et al. 2010; Pierce et al. 2011; Buchholtz et al. 2012; Buchholtz 2014). Although studies are limited, identification of correlated changes between vertebral shape and various ecological attributes have extended our understanding of the behaviour of living animals and aided in reconstructing

the behaviour and ecology of extinct species (Antón and Galobart 1999; Argot 2003; Shapiro et al. 2005; Pierce et al. 2011; Pierce et al. 2013). Moreover, morphological specialisations of vertebrae have been associated with body size changes across mammalian clades: for example, Smeathers (1981) suggested that small and large animals differ in the total length and flexibility of the lumbar column due to different metabolic costs required to maintain stability and posture, with larger animals having comparatively shorter, stiffer, and therefore more stable lumbar columns (Gál 1993b).

In order to understand how extant felid ecomorphology and body mass have impacted the size and shape of the postcranium as a whole, detailed data from the vertebral column are required. Here, we investigate whether differences in ecological niche among felid species are reflected in their vertebral shape. Specifically, we test if differences in the whole vertebral column, or in discrete regions of the spine (i.e., cervical, thoracic and lumbar regions), discriminate the different locomotor styles and/or prey-size specializations observed in extant cats. We also examine the effect of body size on felid vertebral evolution through an analysis of scaling across a large suite of biomechanically relevant measurements. In accordance with Smeathers (1981), Gál (1993b) and most recently Jones (2015), we predict that increases in felid body size are correlated with a decrease in the flexibility of the vertebral column. Furthermore, based on these studies, we predict that this effect will be regionally heterogeneous,

with increased robustness and decreased flexibility focused primarily at the posterior portion of the spine of larger species, while flexibility will be maintained more anteriorly, providing a wider range of motion to the neck and thorax associated with tackling prey. Combined, these analyses will allow us to assess the importance of the vertebral column in the evolution of felid size, ecology, and locomotion.

Material and methods

1. Data composition:

Species and specimens. – The data set is composed of 24 specimens representing 22 extant felid species, which is ~62% of total number of species in the family (Fig. 3.1). The chosen species embody the full phylogenetic breadth of extant felids, with each of the eight identified clades (Johnson et al. 2006) represented by at least one species. The sample also encompasses the full range of body sizes (e.g., *Leopardus colocolo* and *Leopardus wiedii*, both at the small body mass end at 2 – 4kg, and *Panthera tigris* at the large body mass extreme of up to 325kg) and ecologies (e.g., arboreal, scansorial, and terrestrial) displayed by living felids (Table 3.1) (Sunquist and Sunquist 2002; Meachen-Samuels and Van Valkenburgh 2009b). Specimens were chosen based on completeness, being disarticulated (which allows a greater number

of anatomical features to be observed and measured) and, whenever possible, being wild caught (known captive-raised specimens are identified in Table 3.1). The specimens sampled are held in the zoological collections at the Natural History Museum in London (NHM), the University Museum of Zoology Cambridge (UMZC), and the Muséum National d'Histoire Naturelle in Paris (MNHN) (Table 3.1).

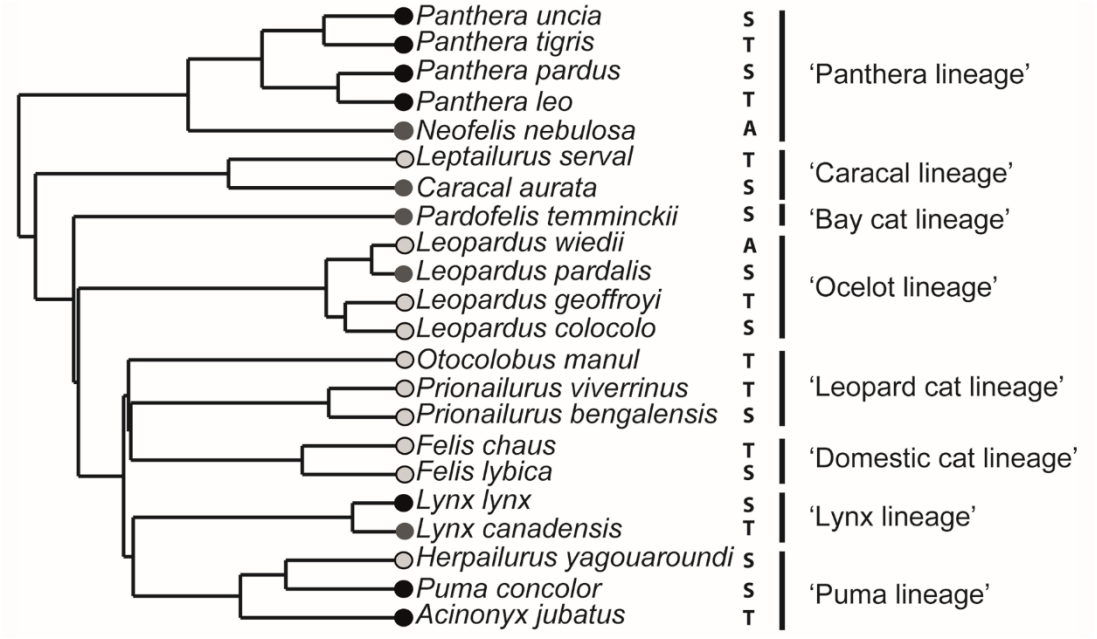

Fig. 3.1. Felid phylogeny showing studied species, from a subset of Nyakatura & Bininda-Emonds (2012), with felid lineage designation according to Johnson et al. (2006), and locomotory (A, S, and T) and prey size specialization (circles at tip of phylogeny) according to Meachen-Samuels & Van Valkenburgh (2009b). Abbreviations: arboreal (A), scansorial (S) and terrestrial (T). Prey size symbols: black circles – large prey specialist; dark grey circles – mixed prey specialist; and light grey with black rim circles – small prey specialist.

Anatomical measurements. – All 27 presacral vertebrae (seven cervicals, 13 thoracics, and seven lumbars) of one to two specimens per species were measured with digital callipers (accuracy of 0.01mm) for linear measurements and with a goniometer for angular measurements (to the nearest degree). The measurements were particular to each of the three regions of the vertebral

Table 3.1 List of species studied and specimen information, including sex, assigned locomotor group, prey size specialization, clade (Johnson et al. 2006; Meachen-Samuels and Van Valkenburgh 2009a, 2009b), total presacral vertebral column length (total length, calculated as the sum of the individual centrum lengths of all presacral vertebrae), and museum specimen numbers. The asterisk (*) demarks potentially captive-reared specimens. NHM, London Natural History Museum; MNHN, Museum National d'Histoire Naturelle; UMZC, University of Cambridge Museum of Zoology. Letters in the 'Sex' column stand for female (F), male (M), and unidentified (U).

SPECIES	SEX	PREY SIZE	LINEAGE	LOCOMOTOR GROUP	TOTAL LENGTH (mm)	SPECIMEN NUMBER
Acinonyx jubatus	U	Large	'Puma'	Terrestrial	750.9	NHM 1940.1.20.17
Caracal aurata	F	Mixed	'Caracal'	Terrestrial	428.1	NHM 1965.8.26.3
Felis chaus	F	Small	'Domestic cat'	Terrestrial	451	NHM 1892.5.22.1
Felis lybica	M	Small	'Domestic cat'	Scansorial	401.5	NHM 1940.1.20.12
Herpailurus yagouarundi	M	Small	'Puma'	Scansorial	420.4	NHM 1932.2.14.1
Leopardus colocolo	U	Small	'Ocelot'	Scansorial	343.1	NHM 1848.6.26.8 - 126.B
Leopardus geoffroyi	M	Small	'Ocelot'	Terrestrial	343.2	NHM 32.2.14.1
Leopardus pardalis	U	Mixed	'Ocelot'	Scansorial	465	UMZC K.6022 (934A)

Leopardus wiedii	U	Small	'Ocelot'	Arboreal	376.2	NHM 1846.4.21.8 - 123B
Leopardus wiedii	U	Small	'Ocelot'	Arboreal	406.7	NHM 1849.11.7.2 – 933a
Leptailurus serval	U	Small	'Caracal'	Terrestrial	522.6	NHM 1845.9.25.23 133c
*Leptailurus serval**	F	Small	'Caracal'	Terrestrial	500.2	NHM 2006.550
Lynx canadensis	U	Mixed	'Lynx'	Scansorial	529.4	UMZC K.6682 (937 I)
Lynx lynx	M	Large	'Lynx'	Scansorial	599.4	MNHN 1973-83
Neofelis nebulosa	F	Mixed	'Panthera'	Arboreal	497.1	MNHN 1961-217
*Otocolobus manul**	F	Small	'Leopard cat'	Terrestrial	322.7	MNHN 2009-251
Panthera leo	M	Large	'Panthera'	Terrestrial	1118.5	NHM 1931.1.13.1
Panthera pardus	F	Large	'Panthera'	Scansorial	586.8	NHM 1938.4.21.11
Panthera tigris	F	Large	'Panthera'	Terrestrial	1057	NHM 1884.1.22.6
*Panthera uncia**	F	Large	'Panthera'	Scansorial	614	NHM 1967.6.29.1
Pardofelis temminckii	U	Mixed	'Bay cat'	Scansorial	519.2	MNHN 1941-293
Prionailurus bengalensis	U	Small	'Leopard cat'	Scansorial	343.4	NHM 1860.4.23.18 1309B
Prionailurus viverrinus	M	Small	'Leopard cat'	Terrestrial	462.2	NHM 75.2287
Puma concolor	U	Large	'Puma'	Scansorial	852.6	UMZC K.5745 936E

column (cervical, thoracic, and lumbar) and only features present in all species were used in statistical analyses. Because different regions have unique vertebral features, different combinations of measurements were taken on separate sets of morphologically similar vertebrae (Fig. 3.2). In total, there were 28 measurement categories (i.e., centrum length, neural spine angle)

with a sum total of 309 variables across the column, and an overall total of 6798 measurement values in the dataset. Missing values (e.g., where vertebrae were broken) were randomly imputed in R version 3.1.3 (2015b) by basing the new values on observed instances for each specific variable. This method also calculates regression values for the missing data and imputation is continued until convergence (German and Hill 2006; Ilin and Raiko 2010). Approximately 2% of the total measurement values were imputed in the dataset. While the linear measurements were used in the statistical analyses presented here, all measurement, both linear and angular, were explored through visualization of vertebral profiles (see below).

Measurements were selected based on their relevance for the flexibility and range of motion of the vertebral column, their identification as important muscle attachment sites, and their potential relevance for understanding how the spine responds to differences in body size (e.g., presence of allometry). The measurements were grounded primarily on those by Pierce et al. (2011), and supplemented with additional measures to capture morphological attributes relevant for felids (Table 3.2). All measurements were taken by one observer (MR), repeated three times, and averaged to produce the final dataset used in further analyses. Measurements of the angles between the pre-zygapophyses and the accessory processes were removed from the original dataset due to high error.

1. Data analyses:

Principal Component Analyses (PCA). – All linear measurements were $\log_{10}$ transformed prior to analysis. Measurements were then phylogenetically size-corrected using $\log_{10}$ total vertebral column length as a proxy for body size in R with the phytools package (Revell 2009). This procedure removes the effects of body size from the data by using phylogenetic regressions to calculate independent slopes for the clades. This is an important step when analysing families such as Felidae where a clear phylogenetic bias is found for body size, and larger-bodied species are concentrated in a few closely related genera (e.g., the *Panthera* clade) (Sunquist and Sunquist 2002; Johnson et al. 2006; Cuff et al. 2015). Phylogenetic relationships were based on a recent supertree analysis of carnivorans (Nyakatura and Bininda-Emonds 2012), which was cropped in Mesquite version 3.02 (Maddison and Maddison 2014) to only include species represented in this study (Fig. 3.1). These measurements were analysed with a Principal Components Analysis (PCA) in PAST version 2.17c (Hammer et al. 2001) for five subsets of the original dataset: all vertebrae (i.e., all 27 vertebrae), cervicals only (i.e., only the seven vertebrae of the cervical region), thoracics only (i.e., only the 13 vertebrae of the thoracic region), lumbars only (i.e., only the seven vertebrae of the lumbar region), and thoracics + lumbars combined (i.e., the 20 vertebrae composing the thoracic and lumbar regions, from T1 to L7).

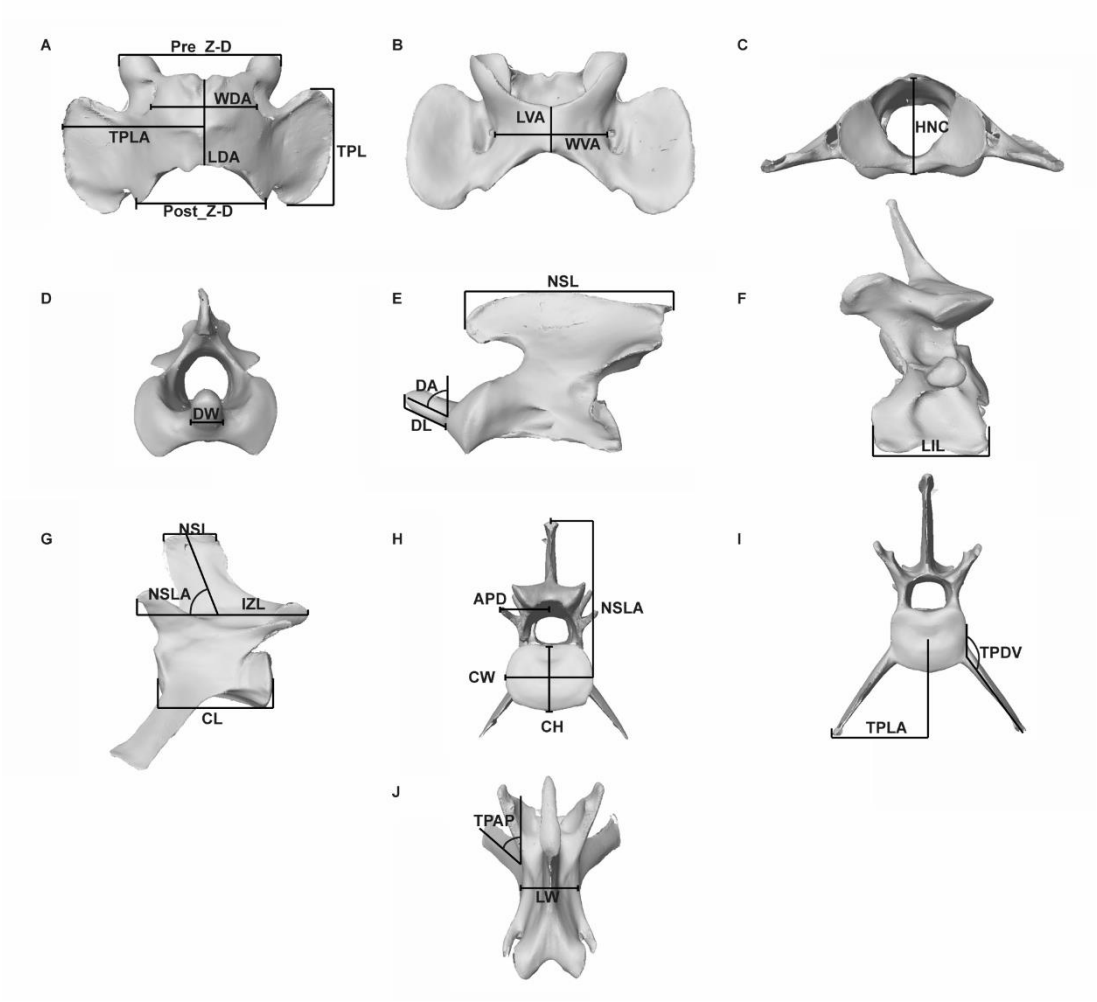

Fig. 3.2: Vertebral measurements: (A-C) atlas, (D-E) axis, (F) C6, and (G-J) L2 Abbreviations. LDA: Length of dorsal arch; Pre_Z-D: Prezygapophyseal distance; Post_Z-D: Postzygapophyseal distance; TPLA: Transverse process lever arm; WDA: Width of dorsal arch. B. LVA: Length of ventral arch; WVA: Width of ventral arch. C. HNC: Height of the neural canal. D. DW: Dens width. E. DA: Dens angle; DL: Dens length; NSL: Neural spine anteroposterior length at tip. F. LIL: Length of inferior lamella. G. CL: Centrum length; IZL: Interzygapophyseal length; NSL: Neural anteroposterior length at tip; NSLA: Neural spine lever arm. H. APD: Accessory process distance; CH: Centrum height; CW: Centrum width; NSLA: Neural spine lever arm. I. TPDV: Transverse process dorsoventral angle; TPLA: Transverse process lever arm. J. LW: Lamina width; TPAP: Transverse process anteroposterior angle. Vertebral images are from of a CT scan of *Acinonyx jubatus* (Cheetah, USNM 520539).

Table 3.2 List of all measurements taken on each vertebra. C, cervical vertebra; T, thoracic vertebra; L, lumbar vertebra. Measurements in italics were not included in subsequent statistical analyses due to higher measurement error.

VERTEBRA	MEASUREMENT	ABBREVIATION
ATLAS	Length of ventral arch	LVA
	Width of ventral arch	WVA
	Length of dorsal arch	LDA
	Width of dorsal arch	WDA
	Transverse process lever arm	TPLA
	Interzygapophyseal length	IZL
	Pre-zygapophyseal distance	Pre-Z_D
	Post-zygapophyseal distance	Post-Z_D
	Height of neural canal	HNC
AXIS	Length of centrum	CL
	Height of centrum	CH
	Width of centrum	CW
	Neural spine lever arm	NSLA
	Interzygapophyseal length	IZL
	Dens length	DL
	Dens width	DW
	Dens angle	DA
	Transverse process anteroposterior angle	TPAP
C3 – C7	Length of centrum	CL
	Height of centrum	CH
	Width of centrum	CW
	Neural spine lever arm	NSLA
	Transverse process lever arm	TPLA
	Neural spine anteroposterior length at tip	NSL
C3-C6 ONLY	Length of inferior lamella	LIL
	Interzygapophyseal length	IZL
	Width of lamina	LW
	Neural spine angle	NSA
C3-L7 ONLY	*Pre-zygapophyseal angle*	*Pre-ZA*

C3-C6 ONLY	Inferior lamella dorsoventral angle	ILDV
C3-C6 ONLY	Inferior lamella anteroposterior angle	ILAP
C5-C7 ONLY	Transverse process dorsoventral angle	TPDV
C5-C7 ONLY	Transverse process anteroposterior angle	TPAP
T1 – T13	Length of centrum	CL
	Height of centrum	CH
	Width of centrum	CW
	Neural spine lever arm	NSLA
	Transverse process lever arm	TPLA
	Interzygapophyseal length	IZL
	Width of lamina	LW
	Neural spine angle	NSA
	Neural spine anteroposterior length at tip	NSL
T1 – T10 ONLY	Transverse process dorsoventral angle	TPDV
T1 – T10 ONLY	Transverse process anteroposterior angle	TPAP
T12 – T13 ONLY	Accessory process distance	APD
T12 – T13 ONLY	*Accessory process dorsoventral angle*	APDV
T12 – T13 ONLY	*Accessory process anteroposterior angle*	APAP
L1-L7	Length of centrum	CL
	Height of centrum	CH
	Width of centrum	CW
	Neural spine lever arm	NSLA
	Transverse process lever arm	TPLA
	Interzygapophyseal length	IZL
	Width of lamina	LW
	Neural spine angle	NSA
	Transverse process dorsoventral angle	TPDV
	Transverse process anteroposterior angle	TPAP
	Neural spine anteroposterior length at tip	NSL
L1-L5 ONLY	Accessory process distance	APD
L1-L5 ONLY	*Accessory process dorsoventral angle*	APDV
L1-L5 ONLY	*Accessory process anteroposterior angle*	APAP

In order to ensure that size had been removed prior to our PCA, and therefore that PCs were uncorrelated with size, PC scores from significant PC axes (i.e., those with eigenvalues higher than the Jollife cut-off) in the 'all vertebrae' PCA were regressed against $\log_{10}$ total vertebral column length (Table 3.1) as a proxy for body size. The scores were regressed both across the full 'all vertebrae' sample and per locomotor group (as this was the main trait influencing morphospace occupation; see Results). This same procedure was repeated for the full 'all vertebrae' sample while controlling for phylogeny, with independent contrasts (Felsenstein 1985) calculated for the PC scores from significant axes and for total vertebral length using the R package 'ape' (Paradis et al. 2004). This further step was performed in order to ensure that size had been removed from our data even when phylogeny was taken into account. Independent contrasts (for scores of each PC axis against vertebral column length) were then subjected to Reduced Major Axis (RMA) regression in R using the 'smatr' package (Warton et al. 2012).

To test how locomotor specialization affects vertebral shape, species were categorised by three primary locomotor modes - arboreal, scansorial, and terrestrial - and qualitatively evaluated in PCA morphospace (the full linear dataset and four regional linear subsets) using convex hulls. Species assignment to locomotor categories are detailed in Fig. 3.1 and Table 3.1 and were based on the studies of Meachen-Samuels and Van Valkenburgh (2009b)

and Sunquist and Sunquist (2002). Further, to explore the impact of prey specialization on vertebral shape, the 'cervicals only' and the 'all vertebrae' subsets were qualitatively examined in PCA morphospace by grouping species by prey size (i.e., small, mixed, and large) according to the study by Meachen-Samuels and Van Valkenburgh (2009a). Finally, to assess the effect of phylogenetic relatedness on vertebral morphology, species were also categorised according to clade ('Panthera', 'Bay cat', 'Caracal', 'Ocelot', 'Lynx', 'Puma', 'Leopard cat', and 'Domestic cat' lineages based on Johnson et al. (2006; Fig. 3.1) in the resulting PCA morphospace. All qualitative assessments using PCA were followed by the confirmatory analyses detailed below.

MANOVA and Phylogenetic MANOVA. – Differences in the area of morphospace occupied by each of the locomotor, prey size, and clade groupings were further assessed quantitatively using MANOVA. Locomotor and prey size groupings were also analysed with phylogenetic MANOVAs (pMANOVAs) to account for the potentially confounding effect of phylogeny. These pMANOVAs address the issue of non-independence due to relatedness in species' phenotypes by correcting the overestimation of degrees of freedom in comparative cross-species tests (Garland et al. 1993). Specifically, the significance of the standard test statistic is assessed using a Brownian motion model to simulate the distribution of the relevant dependent variables along a given phylogenetic tree. MANOVAs and pMANOVAs were performed on

the PC scores of all axes that presented an eigenvalue equal to or higher than the Jolliffe cut-off (i.e., the first nine PCs for the 'all vertebrae' analysis, which were all higher than the cut-off value of 0.04595). The phylogenetic relationships used were identical to those used to conduct the phylogenetic size-correction (see above). All standard and phylogenetic MANOVA analyses were performed in R software (R Core Team 2015b) using the 'geiger' and 'stats' packages (Harmon et al. 2014).

Vertebral profiles - To further examine variation along the vertebral column and identify aspects of individual vertebrae and vertebral regions associated with niche specialisation, vertebral profiles were plotted for a subset of 12 measurements: centrum length, height and width, width of centrum lamina, lever arm and angle of the neural spine, anteroposterior length of the tip of neural spine, lever arm and angles (anteroposterior and dorsoventral projections) of the transverse process, length of interzygapophyseal distance, and accessory process distance. In addition, variation in centrum shape was examined by calculating the change in relative centrum length [2*centrum length/(centrum height + centrum width)] throughout the vertebral column (Pierce et al. 2011). This measure of centrum shape provides clearer information in regards to the flexibility and range of motion of intervertebral joints (Buchholtz 2001b, 2001a).

To generate niche-specific vertebral profiles, $\log_{10}$ transformed, phylogenetically size-corrected linear measurements, and raw angles were averaged for all species in a corresponding group, and plotted against vertebral number. Only measurement variables that were found either on all vertebrae or on at least three or more consecutive vertebrae (e.g., accessory processes, from T12 to L5) were plotted and no imputed variables were used in this analysis. Statistical significance of the differences between vertebral profiles was evaluated by performing ANOVAs on vertebral bins composed of seven vertebrae each (except bin '3' which was composed of only six vertebrae, from T8 – T13), corresponding to four bins at 25% vertebral intervals: bin '1': atlas – C7; bin '2': T1 – T7; bin '3': T8 – T13; and bin '4': L1 – L7.

Scaling regressions. –

a) *Vertebral column length and body mass* – To test if vertebral column length is a robust predictor of specimen body size (see below), and to examine how the whole column scaled with body mass, generalised least squares (GLS) regressions of $\log_{10}$ body mass (based on average species body mass (based on average species body mass from Cuff et al. 2015) were made against $\log_{10}$ total presacral vertebral column length (C1-L7) (based on the sum total of centrum lengths, without the intervertebral disc/space). The generalised least squares regressions were carried out with and without

phylogenetic correction under a Brownian motion model of evolution using the 'pGLS' package (Martins and Hansen 1997; Mao and Ryan 2013) within R. We also investigated regional scaling by performing phylogenetically-corrected GLS regressions of $\log_{10}$ body mass against each of the separate $\log_{10}$ total lengths of the cervical, thoracic and lumbar regions. Analyses to test if vertebral column length scaled isometrically with body mass were made by comparing the obtained slopes to an isometry slope of 0.333 (i.e., length ~ $\sqrt[3]{mass}$). Averaged body mass per species was used here, rather than directly estimating mass from each specimen, due to a few methodological concerns. Firstly, not all measured specimens presented a complete postcranial skeleton from which measurements could be taken from the same bones across species. Secondly, and most importantly, shape and biomechanical studies focusing on the posture and cross-section of felid limbs have shown that they do not follow biomechanical expectations for mammals based on their body size (Day and Jayne 2007; Doube et al. 2009) and, therefore, body mass estimations on their limb proportions could skew our results. Further, body mass averages for the species shown here have been used in the literature to test for correlations between body size and cranial and limb morphologies (Meachen-Samuels and Van Valkenburgh 2009a, 2009b). Finally, our results based on these analyses closely match the results of others who used direct estimations of mass from chosen

specimens, only differing when phylogeny is taken into account (see below). As noted above and seen in Table 3.1, data on individuals' sexes are rarely available for museum specimens and thus sexual dimorphism could not be considered. However, dimorphic differences within species are far smaller than differences across the species in this sample and shape was corrected for a specimen-specific size estimate (total presacral vertebral column length). Thus dimorphism is unlikely to affect analyses of phylogenetic and ecological signal in vertebral column shape.

b) *Individual vertebrae and total length* – In addition, we also tested for allometric changes within individual vertebrae. To control for phylogeny, independent contrasts of $\log_{10}$ raw linear measurements and $\log_{10}$ total vertebral column length were calculated using the same procedure cited above. Those independent contrasts (for scores of each individual linear vertebral measurement against vertebral column length) were then subjected to Reduced Major Axis (RMA) regression in R using the 'smatr' package (Warton et al. 2012). Analyses to test if these individual linear vertebral measurements scaled isometrically with total vertebral length were made by comparing the obtained slopes to an isometry slope of 1 (i.e., length ~ length^1).

Results

Principal Component Analysis, MANOVA and Phylogenetic MANOVA. – The 'all vertebrae' PCA revealed nine PCs which were significant according to the Jolliffe cut-off value of 0.04595 (Table 3.3), and the sum of the variance explained by those reached almost 80% (i.e., 79.166%) of the total variance. Regressions of all significant PC scores from the 'all vertebrae' PCA on $\log_{10}$ total vertebral column length, before and after phylogenetic correction and between locomotory groups, demonstrated that shape variables were statistically uncorrelated with size ($r^2 << 0.4$, and p-value $>> 0.05$) and that the effects of size variation were removed prior to PCA.

PC1xPC2 showed a large area of overlap between the terrestrial and scansorial groups, but a clear clustering of arboreal species in a distinct area of morphospace (Fig. 3.3A). There was a much better separation of all three locomotory groups in PC1xPC3 (Fig. 3.3B), with only a very small overlap between the terrestrial and scansorial groups. The vertebral features which were most relevant to contributing to this result in terms of high correlation coefficients (i.e., $r > 0.6$, following Pierce et al. 2011) are detailed in Table 3.4. While most variables exhibited high PC1 loading correlation values, PC3 was only highly correlated with measurements of neural spine anteroposterior length at tip in the thoracic and lumbar regions, and centrum height in the lumbar region.

Table 3.3: PCA results from the 'all vertebrae' analysis. PCs with an eigenvalue higher than the Jolliffe cut-off of 0.046 are marked in bold.

PC	EIGENVALUE	% VARIANCE EXPLAINED
1	**0.341**	**24.747**
2	**0.160**	**11.610**
3	**0.138**	**9.974**
4	**0.106**	**7.656**
5	**0.088**	**6.384**
6	**0.074**	**5.393**
7	**0.073**	**5.265**
8	**0.058**	**4.241**
9	**0.054**	**3.896**
10	0.044	3.218
11	0.041	2.993
12	0.037	2.691
13	0.036	2.620
14	0.032	2.317
15	0.026	1.883
16	0.022	1.574
17	0.017	1.214
18	0.012	0.885
19	0.012	0.864
20	0.008	0.575
21	0.000	0.000

Clade groupings in the 'all vertebrae PCA' were significant as a clustering factor when analysed with MANOVA, showing that among the species studied here, closely related taxa tended to be more similar in their axial skeletal morphology. The 'all vertebrae PCA' revealed that the clustering of species by their locomotor groups was indeed statistically significant, both with (phylogenetic p-value $<< 0.05$) and without (p-value $<< 0.05$) phylogenetic

correction. Prey size groups in the 'all vertebrae' morphospace were non-significant (p-value >> 0.05, and phylogenetic p-value >> 0.05; Table 3.5).

The 'thoracics only', 'lumbars only', and the 'thoracics + lumbars' subset analyses revealed clustering similar to the 'all vertebrae' PCA (not shown). MANOVA results calculated from the 'lumbars only' subset showed that locomotory groups occupied different areas of morphospace, both with and without phylogenetic correction (p-value < 0.05). However, for both the 'thoracics only' and 'thoracics + lumbars' subsets, significant statistical difference between locomotory groups was only achieved when phylogeny was taken into account. However, comparison of all significant results with a Bonferroni corrected p-value = 0.0065 resulted in only the 'all vertebrae' and 'lumbars only' subsets exhibiting significant separation between locomotory clusters.

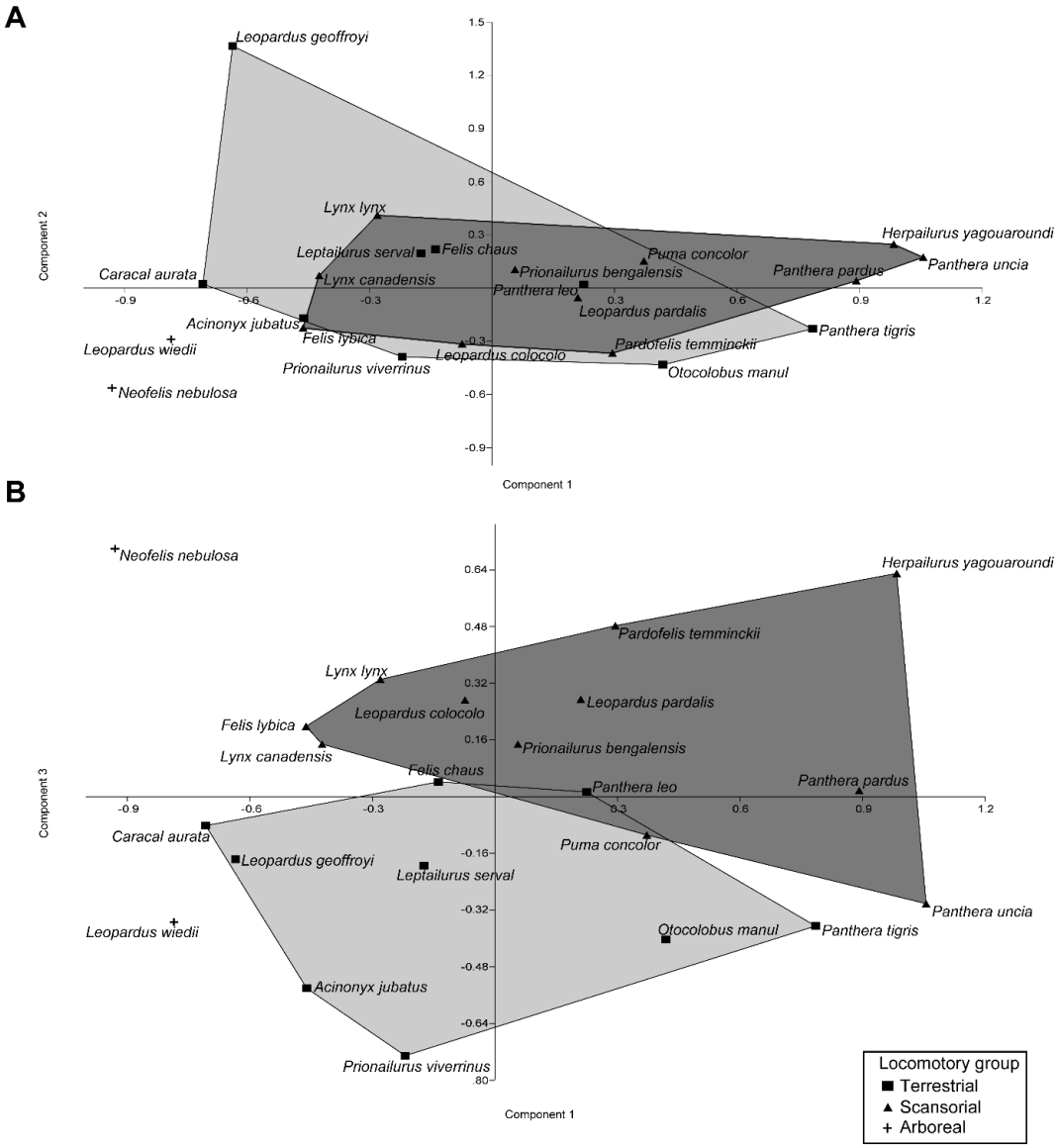

Fig. 3.3: PCA plots of PC1 x PC2 (A) and PC1 x PC3 (B) showing species distribution in vertebral morphospace. Species are grouped according to their locomotory mode (i.e., cross: arboreal species; triangle: scansorial species, and squares: terrestrial species).

Table 3.4: Vertebral measurements that display high (i.e., >0.6) correlations on PC axes for the 'all vertebrae' PCA

VERTEBRA	MEASUREMENT WITH HIGH PC LOADINGS (i.e., CORRELATION >0.6)	PC AXES WITH HIGH LOADINGS CORRELATIONS
ATLAS	Length of ventral arch	PC1
	Length of dorsal arch	PC1
	Length of transverse process	PC1
AXIS	Length of centrum	PC4
	Width of centrum	PC1
	Interzygapophyseal length	PC6
C3 - C7	Height of centrum	PC1
	Width of centrum	PC1
	Transverse process lever arm	PC1
	Width of lamina	PC1
	Neural spine length at tip	PC1
T1 – T13	Height of centrum	PC1, PC2
	Width of centrum	PC1, PC2
	Neural spine lever arm	PC1, PC4, PC5
	Transverse process lever arm	PC1, PC2, PC7
	Interzygapophyseal length	PC1, PC4
	Width of lamina	PC1, PC2
	Neural spine length at tip	PC1, PC2, PC3, PC4, PC5
L1-L7	Length of centrum	PC4
	Height of centrum	PC1, PC3
	Width of centrum	PC1
	Transverse process lever arm	PC1
	Width of lamina	PC1
	Neural spine length at tip	PC1, PC3
L1-L5 ONLY	Accessory process distance	PC1

Table 3.5: Results of the MANOVA and phylogenetic MANOVA tests on PC scores from significant PCs as determined by the Jolliffe cut-off. Significance at p-value < 0.05 is indicated in italics, while significance after Bonferroni correction (i.e., p-value < 0.00625) is shown in bold.

GROUPS TESTED	MANOVA (p-value)	PHYLOGENETIC MANOVA (p-value)
PC1-9 ('ALL VERTEBRAE', LOCOMOTORY GROUPS)	*0.03043*	***0.006***
PC1-9 ('ALL VERTEBRAE', PREY SIZE GROUPS)	0.2811	0.6454
PC1-9 ('ALL VERTEBRAE', CLADES: 'PANTHERA' X 'OCELOT' LINEAGES)	***0.0000***	N.A.
PC1-9 ('THORACICS ONLY', LOCOMOTORY GROUPS)	0.0648	*0.0120*
PC1-9 ('THORACICS + LUMBARS', LOCOMOTORY GROUPS)	*0.0662*	*0.0120*
PC1-9 ('LUMBARS ONLY', LOCOMOTORY GROUPS)	*0.0083*	***0.002***
PC1-9 ('CERVICALS ONLY, LOCOMOTORY GROUPS')	0.4293	0.2547
PC1-9 ('CERVICALS ONLY', PREY SIZE GROUPS)	0.3	0.6693

The 'cervicals only' analyses did not reveal any clear association of taxa by locomotor or prey size groupings, and the respective phylogenetic MANOVA again confirmed the non-significance of these groups (locomotor groups: p-value and phylogenetic p-value >> 0.05; prey-size groups: p-value and phylogenetic p-value > 0.05). Results for all MANOVAs and pMANOVAs are shown in Table 3.5.

Vertebral profiles. – As locomotor mode was the only examined ecological trait found to have a significant influence on morphospace

occupation, average vertebral profiles were created for species designated arboreal, scansorial, or terrestrial. The profiles revealed similar overall trends along the vertebral column, with some localised differences in the shape of individual vertebral features (Fig. 3.4A-M). After Bonferroni correction, only the ANOVAs of four pairwise comparisons between group profiles were statistically significant (Table 3.6): centrum width (CW) between arboreal and terrestrial species at bin '2', with terrestrial species having lower values for CW or more narrow vertebrae; centrum shape (CS) between arboreal and scansorial groups at bin '3', with the scansorial group displaying smaller values for CS and, therefore, shorter and wider vertebrae; inter-zygapophyseal length (IZL) between arboreal and terrestrial groups at bin '2', for which the terrestrial group presented the shortest IZL; and the transverse process dorsoventral projection (TPDV) between arboreal and scansorial categories at bin '3', where the scansorial species had the lowest TPDV angle values (i.e., the least ventrally directed).

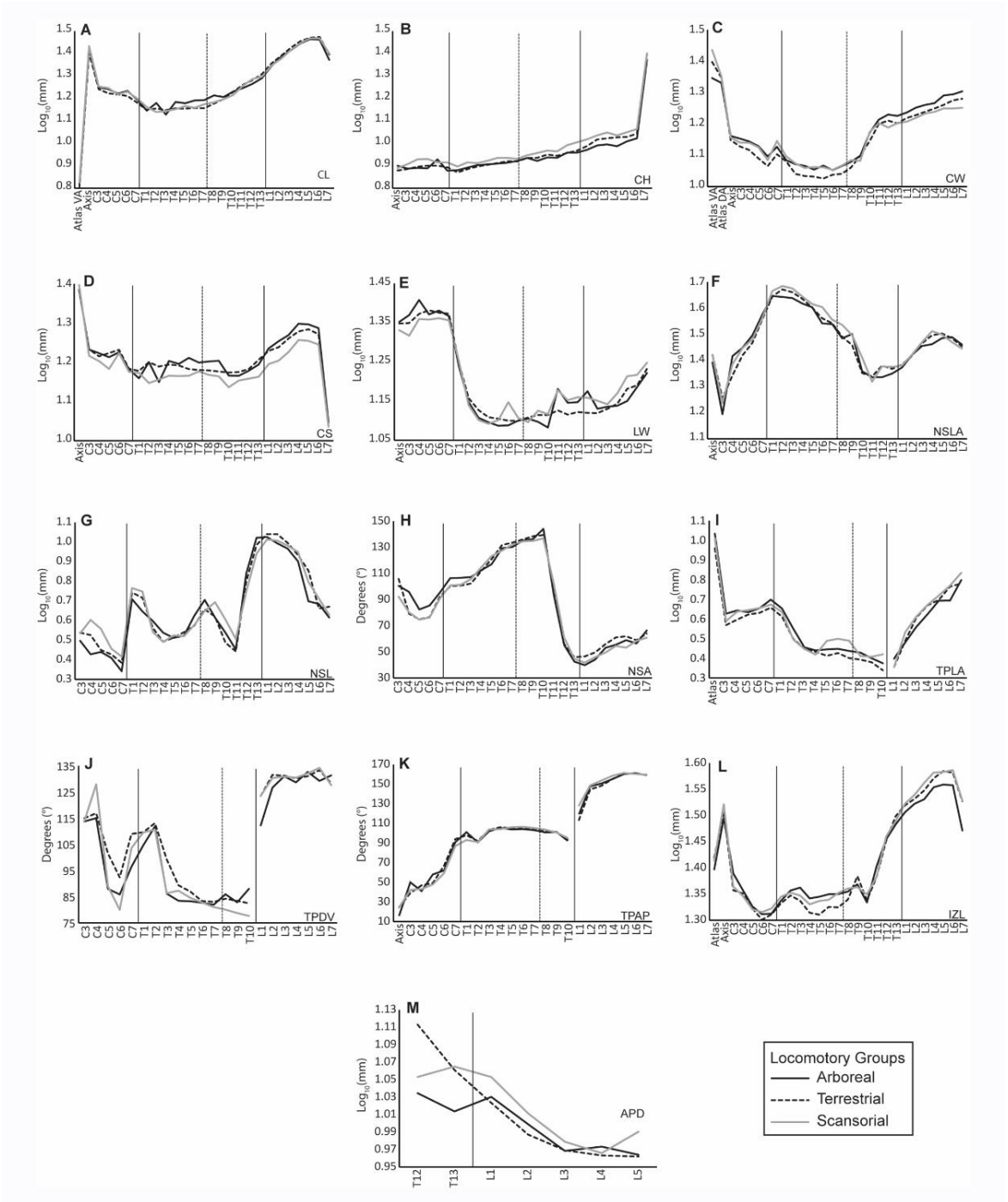

Fig. 3.4: Vertebral profile plots of locomotor groups (i.e., arboreal, terrestrial, and scansorial species) showing variation in vertebral measurements along the vertebral column number. A. Centrum length (CL); B. Centrum height (CH); C. Centrum width (CW); D. Centrum shape (CS); E. Lamina width (LW); F. Neural spine lever arm (NSLA); J. Transverse process dorsoventral angle (TPDV); K. Transverse process anteroposterior angle (TPAP); L. Interzygapophyseal length (IZL); (Cont.)

Fig. 3.4: (Cont.) M. Accessory process distance (APD). Regular vertical bars mark the boundaries between vertebral regions (i.e., cervical, thoracic, and lumbar regions) and the corresponding analytical bins, while dotted vertical lines mark boundaries only related to vertebral bins.

Table 3.6: Results from the ANOVAs and Turkey pairwise tests on vertebral profile bins. Vertebrae were divided into four bins of seven vertebrae each, with the exception of 'bin 3' with only six vertebrae, representing 25% intervals (i.e., cervical, anterior thoracic, posterior thoracic and lumbar vertebrae). Significance at p-value < 0.05 is indicated in italics, while significance after Bonferroni correction (i.e., p-value < 0.0125) is shown in bold.

	ANOVA	**TUKEY'S PAIRWISE COMPARISON P-VALUE**		
	F TEST p-value	**ARBOREAL x SCANSORIAL**	**ARBOREAL x TERRESTRIAL**	**SCANSORIAL x TERRESTRIAL**
CH				
BIN 1	0.0346	0.0840	0.928	*0.0423*
BIN 2	0.0573			
BIN 3	0.0162	*0.0167*	0.7482	0.0681
BIN 4	0.8472			
CL				
BIN 1	0.9747			
BIN 2	0.1148			
BIN 3	0.9901			
BIN 4	0.8993			
CW				
BIN 1	0.9258			
BIN 2	0.0051	0.9675	***0.0086***	*0.0146*
BIN 3	0.883			
BIN 4	0.0199	*0.0159*	0.4386	0.1798
CS				
BIN 1	0.9544			
BIN 2	0.01341	*0.0246*	0.999	*0.027*
BIN 3	0.0063	***0.0096***	0.941	*0.01851*
BIN 4	0.6848			
IZL				
BIN 1	0.9924			
BIN 2	0.00248	0.5606	***0.0025***	*0.0228*
BIN 3	0.9985			
BIN 4	0.1712			

NSLA				
BIN 1	0.9821			
BIN 2	0.4854			
BIN 3	0.8225			
BIN 4	0.9231			
NSL				
BIN 1	0.139			
BIN 2	0.9971			
BIN 3	0.9572			
BIN 4	0.8664			
TPLA				
BIN 1	0.8853			
BIN 2	0.6615			
BIN 3	0.1421			
BIN 4	0.9081			
LW				
BIN 1	0.0403	*0.0372*	0.7032	0.1606
BIN 2	0.9099			
BIN 3	0.4424			
BIN 4	0.41			
APD				
ALL AS 1 BIN	0.7078			
BIN 3	0.1575			
BIN 4	0.5943			
NSA				
BIN 1	0.3712			
BIN 2	0.9856			
BIN 3	0.9981			
BIN 4	0.4832			
TPAP				
BIN 1	0.9749			
BIN 2	0.9759			
BIN 3	0.9142			
BIN 4	0.8732			
TPDV				
BIN 1	0.753			
BIN 2	0.7959			
BIN 3	0.0081	***0.0073***	0.3255	*0.0416*
BIN 4	0.559			

Scaling:

a) *Vertebral column length and body mass –*

The GLS for $\log_{10}$ total presacral vertebral column length against $\log_{10}$ body mass showed a relationship significantly different from isometry (slope=0.267; $r^2 = 0.815$, p-value $\ll 0.05$), but after phylogenetic correction, the relationship was weaker ($r^2 = 0.483$) and the regression slope was not significantly differently from isometry (Table 3.7). All individual vertebral column regional regressions (i.e., cervical, thoracic and lumbar lengths) had similarly weak correlation values ($r^2 = 0.483$) and possessed slopes that were not significantly different from an isometric relationship (Table 3.7).

Table 3.7: Results from scaling analysis for vertebral column length against average body mass, with lower and upper confidence limits from the slope value. Bold indicates the only correlation significantly different from isometry (i.e., a slope of 0.333), while the prefix '(phyl.)' marks GLS regressions with phylogenetic correction.

VERTEBRAL COLUMN LENGTH	SLOPE	LOWER LIMIT	UPPER LIMIT	COEFFICIENT OF DETERMINATION (R^2)	P-VALUE
Total length	**0.267**	**0.225**	**0.308**	**0.815**	**<0.001**
(phyl.) Total length	0.286	0.220	0.353	0.483	<0.001
(phyl.) Cervical length	0.321	0.240	0.401	0.483	<0.001
(phyl.) Thoracic length	0.286	0.222	0.350	0.483	<0.001
(phyl.) Lumbar length	0.263	0.192	0.335	0.483	<0.001

b) *Within individual vertebrae –*

Phylogenetically-corrected scaling analyses of individual linear vertebral measurements revealed 64 cases of significant allometric scaling, i.e., with a

regression slope different from 1 (Table 3.8; and complete table in Appendix 3.1): 61 positive and three negative. There was clear regionalisation of vertebral allometry: out of 64 instances, 19 (18 positive and one negative) were in the cervical region, 34 (33 positive and one negative) in the thoracic region, and only 11 (ten positive and one negative) in the lumbar region. These allometric measurements could be further divided into five categories: centrum-related (30 instances), neural spine-related (25 instances), zygapophyseal-related (six instances), inferior lamella-related (two instances), and transverse process-related (one instance).

Out of the 19 allometric instances in the cervical region, 16 were found in the five similarly-shaped post-axis vertebrae (i.e., C3 – C7). All of the post-axis cervical vertebrae exhibit a positive allometric relationship in terms of centrum length and height. Whereas C4 and C5 displayed the exact same instances of allometric change (centrum length, centrum height, length of the inferior lamella, and interzygapophyseal length), C6 showed the lowest number of instances (centrum length and centrum height only). The atlas had a unique combination of allometric changes, while the axis only presented positive allometric change in centrum height.

Within the thoracic region, allometry was observed in almost all vertebrae for two primary features: centrum height, which was positively allometric from T1-T12; and neural spine lever arm, which was positively allometric from T5-

T13 (although absent on T8). Although a positively allometric relationship was also found for the neural spine anteroposterior length at its tip for most thoracic vertebrae, six of these had weak correlation values between the variables (i.e., $r^2 < 0.45$). Within the thoracic region, there appears to be two sub-groups of vertebrae that showed the same combination of allometric features: T2 – T3 (centrum length and centrum height, both showing positive allometry), and T10 – T12 (centrum height, and neural spine lever arm, both also showing positive allometry).

The presence of allometry was weakest in the lumbar region. Although all seven lumbar vertebrae presented instances of allometry, these were restricted to only one measurement in most cases: the neural spine lever arm, always demonstrating positive allometry with total vertebral column length. In addition to this, L5 and L7 also showed positive allometry on the length at the tip of the neural spine, L4 presented negative allometry on its lamina width, and L7 shows positive allometry with respect to centrum height.

Table 3.8: Results from the phylogenetic scaling analyses showing the slope for the relationship between the variables on the first column and body size (i.e., total vertebral length), with lower and upper confidence limits from the slope value, and P-value for the null hypothesis of the slope being different from 1 (i.e., isometry). Variables from thoracic vertebrae are shown in bold, while variables from lumbar vertebrae are shown in italics. Variables that have an apparent allometric relationship with body size are shown here; scaling results for all variables are show in Appendix 2.1.

VARIABLE	SLOPE	SLOPE LOWER LIMIT	SLOPE UPPER LIMIT	SLOPE P-VALUE	REGRESSION P-VALUE	CORRELATION (R^2)
Atlas_LVA	1.249	1.013	1.540	0.039	0.000	0.806
Atlas_PRE.Z_D	0.729	0.599	0.888	0.003	0.000	0.830
Axis_CH	1.292	1.096	1.522	0.004	0.000	0.882
C3_CL	1.162	1.019	1.326	0.028	0.000	0.924
C3_CH	1.215	1.037	1.422	0.018	0.000	0.891
C3_IZL	1.165	1.002	1.356	0.048	0.000	0.900
C4_CL	1.153	1.021	1.301	0.024	0.000	0.936
C4_CH	1.279	1.081	1.513	0.006	0.000	0.876
C4_LIL	1.312	1.068	1.612	0.012	0.000	0.813
C4_IZL	1.178	1.036	1.340	0.015	0.000	0.928
C5_CL	1.307	1.143	1.495	0.000	0.000	0.921
C5_CH	1.256	1.044	1.512	0.018	0.000	0.849
C5_LIL	1.548	1.054	2.272	0.027	0.007	0.328
C5_IZL	1.221	1.046	1.425	0.014	0.000	0.896
C6_CL	1.250	1.059	1.475	0.011	0.000	0.880
C6_CH	1.216	1.052	1.405	0.011	0.000	0.909

C7_CL	1.133	1.020	1.258	0.022	0.000	0.952
C7_CH	1.339	1.161	1.544	0.000	0.000	0.911
C7_DW	1.228	1.021	1.476	0.031	0.000	0.851
C7_IZL	1.158	1.064	1.261	0.002	0.000	0.969
T1_CH	**1.274**	**1.107**	**1.466**	**0.002**	**0.000**	**0.914**
T1_NSL	**1.596**	**1.074**	**2.371**	**0.022**	**0.013**	**0.284**
T2_CL	**1.105**	**1.001**	**1.220**	**0.047**	**0.000**	**0.957**
T2_CH	**1.269**	**1.116**	**1.442**	**0.001**	**0.000**	**0.928**
T2_NSL	**1.555**	**1.084**	**2.231**	**0.018**	**0.002**	**0.410**
T3_CL	**1.119**	**1.003**	**1.250**	**0.045**	**0.000**	**0.947**
T3_CH	**1.308**	**1.141**	**1.500**	**0.001**	**0.000**	**0.918**
T3_NSL	**1.817**	**1.219**	**2.708**	**0.004**	**0.015**	**0.272**
T4_CL	**1.083**	**1.003**	**1.170**	**0.044**	**0.000**	**0.974**
T4_CH	**1.236**	**1.093**	**1.397**	**0.002**	**0.000**	**0.934**
T4_NSL	**1.338**	**1.022**	**1.752**	**0.035**	**0.000**	**0.677**
T5_CH	**1.209**	**1.061**	**1.378**	**0.007**	**0.000**	**0.925**
T5_Calculated_NSLA	**1.234**	**1.029**	**1.480**	**0.025**	**0.000**	**0.856**
T6_CH	**1.212**	**1.095**	**1.341**	**0.001**	**0.000**	**0.955**
T6_Calculated_NSLA	**1.292**	**1.078**	**1.548**	**0.008**	**0.000**	**0.857**
T6_NSL	**1.470**	**1.031**	**2.095**	**0.034**	**0.001**	**0.431**
T7_CH	**1.288**	**1.148**	**1.446**	**0.000**	**0.000**	**0.942**
T7_Calculated_NSLA	**1.221**	**1.078**	**1.383**	**0.003**	**0.000**	**0.933**
T7_IZL	**0.869**	**0.763**	**0.989**	**0.035**	**0.000**	**0.926**
T7_NSL	**1.492**	**1.007**	**2.209**	**0.046**	**0.011**	**0.297**
T8_CH	**1.240**	**1.123**	**1.369**	**0.000**	**0.000**	**0.957**
T8_NSL	**1.635**	**1.148**	**2.329**	**0.008**	**0.001**	**0.435**
T9_CH	**1.262**	**1.161**	**1.371**	**0.000**	**0.000**	**0.970**

T9_Calculated_NSLA	**1.249**	**1.035**	**1.508**	**0.023**	**0.000**	**0.844**
T9_Calculated_TPLA	**1.562**	**1.076**	**2.265**	**0.020**	**0.003**	**0.371**
T10_CH	**1.461**	**1.002**	**2.130**	**0.049**	**0.004**	**0.354**
T10_Calculated_NSLA	**1.574**	**1.095**	**2.263**	**0.016**	**0.002**	**0.403**
T11_CH	**1.167**	**1.050**	**1.296**	**0.006**	**0.000**	**0.952**
T11_Calculated_NSLA	**1.301**	**1.104**	**1.532**	**0.003**	**0.000**	**0.882**
T12_CH	**1.288**	**1.042**	**1.592**	**0.021**	**0.000**	**0.803**
T12_Calculated_NSLA	**1.491**	**1.095**	**2.031**	**0.013**	**0.000**	**0.573**
T13_Calculated_NSLA	**1.310**	**1.068**	**1.608**	**0.012**	**0.000**	**0.816**
T13_NSL	**1.463**	**1.027**	**2.084**	**0.036**	**0.001**	**0.434**
L1_Calculated_NSLA	*1.294*	*1.141*	*1.469*	*0.000*	*0.000*	*0.930*
L2_Calculated_NSLA	*1.336*	*1.172*	*1.523*	*0.000*	*0.000*	*0.925*
L3_Calculated_NSLA	*1.253*	*1.092*	*1.438*	*0.003*	*0.000*	*0.917*
L4_Calculated_NSLA	*1.241*	*1.079*	*1.428*	*0.004*	*0.000*	*0.914*
L4_WL	*0.839*	*0.708*	*0.995*	*0.044*	*0.000*	*0.873*
L5_Calculated_NSLA	*1.220*	*1.004*	*1.484*	*0.046*	*0.000*	*0.832*
L5_NSL	*1.962*	*1.397*	*2.755*	*0.000*	*0.000*	*0.480*
L6_Calculated_NSLA	*1.277*	*1.099*	*1.483*	*0.003*	*0.000*	*0.902*
L7_CH	*1.195*	*1.043*	*1.369*	*0.013*	*0.000*	*0.919*
L7_Calculated_NSLA	*1.281*	*1.102*	*1.491*	*0.003*	*0.000*	*0.900*
L7_NSL	*1.664*	*1.275*	*2.172*	*0.001*	*0.000*	*0.685*

Discussion

Shape and ecology.–

Here, we quantitatively analysed the morphology of the entire presacral vertebral column in felids to test whether morphological differentiation of the vertebral column across species is driven by body size and/or ecologically derived traits, such as locomotor mode and prey-hunting specialization, as has been previously demonstrated for felid limbs (Gonyea 1978; Meachen-Samuels and Van Valkenburgh 2009b; Meachen-Samuels 2012). Our study shows that linear shape variation in the felid vertebral column significantly discriminated terrestrial, arboreal, and scansorial species, demonstrating that locomotory specialization, but not prey size, has fashioned vertebral column evolution within felids. Locomotor differentiation was statistically significant only when phylogenetic relationships were taken into account, and only when either 'all vertebrae' were analysed together or when the analysis was restricted to the lumbar vertebrae. In a study comparing the relative lengths of limbs and axial skeletons of species of large-bodied felids, Gonyea (1976) suggested that locomotor specialisation was reflected by changes in the length of the lumbar region (but see scaling results below). This result indicates that, although size-independent changes in shape are somewhat dispersed

throughout the whole vertebral column, wide-spread changes in the lumbar vertebra are particularly important for locomotor specialization.

Although there was significant differentiation of locomotor groups across all principal components, there was also clear overlap between scansorial and terrestrial species on most PCs (Fig. 3.3). Such morphological similarities between these locomotor groups may reflect a hypothesized scansorial ancestral condition for felids, as has been reconstructed for *Proailurus*, the earliest fossil felid (Turner and Antón 1996; Peigné 1999), or that all living species have the ability to climb (Ewer 1973; Sunquist and Sunquist 2002; MacDonald et al. 2010). Only a few conspicuous locomotor specialisations are observed in living cats, such as the cheetah, *Acinonyx jubatus*, which is more cursorial than other felids (Ewer 1973; Sunquist and Sunquist 2002; MacDonald et al. 2010), and the highly arboreal margay, marbled cat, and clouded leopard; *Leopardus wiedii, Pardofelis marmorata*, and *Neofelis nebulosa*, respectively; with their broad feet and very flexible ankles (Sunquist and Sunquist 2002; MacDonald et al. 2010).

This relative similarity in the felid axial skeleton was also demonstrated by our vertebral column profile analyses (Fig. 3.4). The profile plots revealed a strong general resemblance between locomotor groups, with a few instances of significant statistical difference between them (Table 3.6), and primarily in the thoracic region. These instances were found in comparisons between the

arboreal group's profile and the other two locomotor groups, suggesting that arboreality may require distinct morphological specialisation of the axial skeleton. Our results indicate that arboreal species present greater passive stiffness in the thoracic region due to larger values of centrum width and shape (Fig. 3.4C-D) (Long et al. 1997; Koob and Long 2000; Shapiro 2007; Pierce et al. 2011). This may, however, be counterbalanced by a greater propensity for intervertebral mobility (i.e., *sensu* range of motion) granted by a larger interzygapophyseal length (IZL) in the anterior thoracic region (Fig. 3.4L) (Jenkins 1974; Pierce et al. 2011). Contrary to the profile plots, our PC analyses recovered the lumbar region as holding the majority of the locomotory signal. This discrepancy may indicate that unlike similar analyses (e.g., Pierce et al. 2011; Jones and German 2014; Molnar et al. 2014), univariate measures are not sufficient to discriminate between felid locomotor specialisations, and that such distinction is best achieved with more complex, multidimensional shape analyses.

Prey-killing techniques, which if reflective of prey size choice, can subdivide species based on the morphological signal of the forelimbs and cranium (Leyhausen 1979; Slater and Van Valkenburgh 2008; Meachen-Samuels and Van Valkenburgh 2009a, 2009b, 2010). However, prey size was not significantly associated with vertebral shape in this study, counter to our expectations for the cervical vertebrae. This result may be a reflection of the

measurements chosen in this study, which were based on biomechanical traits relevant for locomotor modes (Pierce et al. 2011) or that variation in vertebral shape across felid evolution is not closely tied to variations in prey-killing techniques. To more fully understand the effect of prey specialization on the vertebral column of felids, most specifically on the cervical vertebrae, further investigation of vertebral shape using more sophisticated analytical techniques (e.g., geometric morphometrics) would be advantageous.

Shape and body size.–

Our analyses revealed widespread allometry in the vertebral column of extant felids, a pattern consistent with Doube et al. (2009), who found similar scaling in the appendicular skeleton. Therefore, body size, which is often the most conspicuous difference when grossly comparing the skeletons of distantly related felid species, has a great influence on the overall morphology of the vertebral column. In light of the suggestions of shorter and stiffer lumbar regions in larger mammals (Smeathers 1981; Gál 1993b; and recently Jones 2015), and also taking into account the postural uniformity in felids through increases in body size (Day and Jayne 2007; Doube et al. 2009; Zhang et al. 2012), we had initially hypothesized that, as felid species increase in size, there would be an increase in vertebral column stiffness. Further, we hypothesized that this increase in stiffness would be particularly evident in the posterior column due to the necessity to support greater body mass. In keeping with

this, the total length of the vertebral column in living felid species was shown to be highly correlated with body mass (Table 3.7), and there was a negatively allometric relationship between the two variables (i.e., the vertebral column is relatively shorter in larger species). This result agrees with the recent findings of allometric shortening of the thoracolumbar region in felids by Jones (2015). However, the relationship found here was not maintained after phylogenetic correction, and the length of the whole vertebral column, or of discrete vertebral column regions, displayed a relationship with body mass that was not significantly different from what is expected from isometry. In contrast, Jones (2015) found that her evolutionary negatively allometric patterns were consistent prior to and after phylogenetic correction, both for total thoracolumbar length and for the individual thoracic and lumbar regions. The cause of this disagreement between analyses is unclear, but may lie in the different phylogenetic methods used (i.e., independent contrasts in Jones 2015 vs. phylogenetic GLS here), or because here we use average species body mass rather than an estimate of body mass based on a regression equation from limb dimensions. As discussed in the methodology chapter (Chapter 2), it was not possible to test for the possible effect of sexual dimorphism on vertebral shape due to the lack of information regarding the sex of many specimens (Table 3.1). Therefore, it was not possible to test if allometric effects on shape differ between sexes. Nevertheless, because the linear measurements used in the scaling test were previously size-corrected, therefore accounting for

differences in size across specimens, and because the analyses performed were focused on differences across species (rather than across populations of the same species), sexual dimorphism effects would not significantly alter the results presented here.

Compared to our whole vertebral column results, analyses of individual vertebral measurements showed extensive intravertebral allometry, with most vertebral dimensions being positively allometric when corrected for phylogeny (i.e., relatively larger in larger species), particularly in the thoracic region (Table 3.7). The most prevalent allometry was centrum height, being present in over 2/3 of the vertebral column (19 out of 27 vertebrae), from the atlas to T12 and L7. Increased height of the centrum in larger felid species suggests greater stability in the dorsoventral plane in the cervical and thoracic region. Jones (2015) also found centrum height to be positively allometric in the thoracic region; however, she also found this measurement to be positively allometric in the mid-lumbar region. Our analyses found no support for allometric scaling of centrum dimensions in the lumbar region, except for L7. The most prevalent allometry in the lumbar vertebrae was the neural spine lever arm; longer neural spines in larger animals will increase passive stiffness due to the presence of larger epaxial musculature (and ligaments), but it will also increase the leverage for dorsoventral bending capacity of the lumbar region (Long et al. 1997; Pierce et al. 2011), which may contribute to stride

length. Therefore, our data imply that larger felid species increase passive stiffness in the lumbar region via acquisition of greater muscle mass and ligament leverage, rather than changes in centrum dimensions.

The three main groups of allometric variables - centrum-related, neural spine-related, and zygapophyseal-related - appear to dominate in different regions of the column (i.e., before and after the anticlinal vertebra T11): whereas the neural spine-related allometries were almost equally spread throughout the vertebral column, the centrum and zygapophyseal-related allometries were concentrated in the cervical and thoracic regions, with few instances in the lumbar vertebrae. Allometry has been suggested to be a strong factor contributing to morphological integration (Klingenberg 2008; Klingenberg and Marugán-Lobón 2013), and the pattern of regionalization of specific allometric trends would be consistent with the presence of modularity in the vertebral column (i.e., existence of sets of characters that covary more strongly between themselves due to shared function or proximity, and present some evolutionary independence from other traits; Olson and Miller 1958). Morphological, developmental, and functional modularity has been studied in the mammalian skeleton, with many examples focusing on the skull (e.g., Goswami 2006a; Goswami et al. 2012; Meloro and Slater 2012; Piras et al. 2013) but also on the vertebral column and limbs (Polly et al. 2001; Goswami et al. 2009; Buchholtz et al. 2012; Buchholtz 2014; Fabre et al. 2014b).

Based on the distribution of allometries recovered here, we propose the hypothesis of the presence of two major functional modules in the felid vertebral column: an anterior module composed of the cervical and thoracic vertebrae, and a posterior or lumbar module. Moreover, our findings of similar allometric trends in cervicals C4 and C5 match the previously suggested diaphragmatic module for the mammalian column (Buchholtz 2014), and we additionally propose a functional 'anticlinality module' composed of the anticlinal vertebra (T11) and the immediate surrounding vertebrae (T10 and T12). These hypothesized modules within the felid vertebral column are an interesting starting point for further analysis of morphological integration and morphological/functional regionalization of the felid vertebral column using more appropriate methodologies (e.g., Goswami and Polly 2010c; Klingenberg and Marugán-Lobón 2013; Fabre et al. 2014b; Head and Polly 2015).

Comparative functional studies on animals with similar musculoskeletal anatomy are important to understand the form-function relationship (e.g., Irschick 2002; and Nyakatura and Fischer 2010), and such studies allow researchers to better understand the behaviour of living organisms and infer the habits of extinct species (Moon 1999; Hutchinson 2012). The work we present here provides a new perspective on how extant felids have adapted

their postcranial skeleton to deal with ecological specialisations over a wide range of body mass, irrespective of having a relatively conservative morphology. Specifically, our results show evidence for hitherto-underappreciated differentiation in vertebral shape in Felidae, which reflects specialisation for locomotion mode (arboreal, scansorial, and terrestrial). Furthermore, there is evidence for extensive allometric scaling within individual vertebrae. In particular, evolutionary increases in body size have driven stabilisation of the anterior axial skeleton (cervical and thoracic vertebrae) through widespread modification of vertebral form. In contrast, size-correlated stabilisation of the lumbar region seems to be primarily accomplished by means of increases in epaxial muscle mass in felids. The heterogeneous effects of axial allometry within the felid vertebral column suggest the presence of modularity beyond traditional regionalisation boundaries, which will be tested in future studies.

Appendix 3.1

Table S3.1: Results from the phylogenetic scaling analysis showing the slope of the relationship between the variables in the first column and body size (i.e., total vertebral length), with lower and upper 95% confidence limits from the slope value, and p-value for the null hypothesis of the slope being different from 1 (i.e., isometry). Variables that have an apparent allometric relationship with body size are shown in bold. Regression p-values which are not significant and show variables are uncorrelated are underlined.

VARIABLE	SLOPE	SLOPE LOWER LIMIT	SLOPE UPPER LIMIT	SLOPE P-VALUE	REGRESSION P-VALUE	CORRELATION (R^2)
Atlas_LVA	**1.249**	**1.013**	**1.540**	**0.039**	**0.000**	**0.806**
Atlas_WVA	1.188	0.905	1.559	0.204	0.000	0.671
Atlas_LDA	1.071	0.883	1.299	0.470	0.000	0.836
Atlas_WDA	1.006	0.734	1.378	0.971	0.000	0.556
Atlas_LTP	0.994	0.829	1.193	0.948	0.000	0.854
Atlas_calculated_TLA	1.386	0.933	2.059	0.103	0.013	0.285
Atlas_IZL	1.110	0.903	1.365	0.305	0.000	0.812
Atlas_PRE.Z_D	**0.729**	**0.599**	**0.888**	**0.003**	**0.000**	**0.830**
Atlas_POS.Z_D	0.993	0.851	1.158	0.925	0.000	0.896
Atlas_HNC	0.978	0.803	1.193	0.822	0.000	0.827
Axis_CL	1.084	0.871	1.348	0.453	0.000	0.790
Axis_CH	**1.292**	**1.096**	**1.522**	**0.004**	**0.000**	**0.882**

Axis_CW	1.049	0.909	1.210	0.497	0.000	0.911
Axis_calculated_NSLA	1.122	0.933	1.349	0.209	0.000	0.851
Axis_NSL	1.002	0.828	1.213	0.982	0.000	0.840
Axis_IZL	1.040	0.929	1.163	0.478	0.000	0.945
Axis_DL	0.980	0.845	1.138	0.783	0.000	0.903
Axis_DW	1.092	0.834	1.429	0.509	0.000	0.677
C3_CL	**1.162**	**1.019**	**1.326**	**0.028**	**0.000**	**0.924**
C3_CH	**1.215**	**1.037**	**1.422**	**0.018**	**0.000**	**0.891**
C3_CW	1.026	0.878	1.200	0.731	0.000	0.894
C3_Calculated_NSLA	1.222	0.967	1.544	0.090	0.000	0.758
C3_Calculated_TPLA	1.042	0.883	1.231	0.611	0.000	0.879
C3_LIL	1.164	0.954	1.419	0.128	0.000	0.827
C3_IZL	**1.165**	**1.002**	**1.356**	**0.048**	**0.000**	**0.900**
C3_LW	1.274	0.850	1.910	0.233	0.021	0.250
C3_NSL	2.510	1.583	3.978	0.000	0.627	0.013
C4_CL	**1.153**	**1.021**	**1.301**	**0.024**	**0.000**	**0.936**
C4_CH	**1.279**	**1.081**	**1.513**	**0.006**	**0.000**	**0.876**
C4_CW	1.042	0.896	1.211	0.576	0.000	0.901
C4_Calculated_NSLA	1.192	0.949	1.497	0.126	0.000	0.770
C4_Calculated_TPLA	1.038	0.878	1.226	0.651	0.000	0.878
C4_LIL	**1.312**	**1.068**	**1.612**	**0.012**	**0.000**	**0.813**
C4_IZL	**1.178**	**1.036**	**1.340**	**0.015**	**0.000**	**0.928**
C4_LW	0.948	0.702	1.279	0.716	0.000	0.598
C4_NSL	1.579	1.028	2.426	0.038	0.084	0.149
C5_CL	**1.307**	**1.143**	**1.495**	**0.000**	**0.000**	**0.921**
C5_CH	**1.256**	**1.044**	**1.512**	**0.018**	**0.000**	**0.849**
C5_CW	1.027	0.831	1.268	0.798	0.000	0.804

C5_Calculated_NSLA	1.077	0.884	1.313	0.441	0.000	0.828
C5_Calculated_TPLA	1.018	0.857	1.209	0.831	0.000	0.870
C5_LIL	**1.548**	**1.054**	**2.272**	**0.027**	**0.007**	**0.328**
C5_IZL	**1.221**	**1.046**	**1.425**	**0.014**	**0.000**	**0.896**
C5_LW	0.970	0.713	1.321	0.842	0.000	0.574
C5_NSL	1.983	1.283	3.064	0.003	0.116	0.125
C6_CL	**1.250**	**1.059**	**1.475**	**0.011**	**0.000**	**0.880**
C6_CH	**1.216**	**1.052**	**1.405**	**0.011**	**0.000**	**0.909**
C6_CW	1.033	0.878	1.214	0.683	0.000	0.885
C6_Calculated_NSLA	1.073	0.898	1.283	0.419	0.000	0.861
C6_Calculated_TPLA	1.173	0.949	1.450	0.133	0.000	0.802
C6_LIL	1.251	0.985	1.589	0.065	0.000	0.747
C6_IZL	1.164	0.998	1.358	0.052	0.000	0.897
C6_LW	0.931	0.695	1.247	0.619	0.000	0.620
C6_NSL	1.044	0.745	1.463	0.797	0.000	0.486
C7_CL	**1.133**	**1.020**	**1.258**	**0.022**	**0.000**	**0.952**
C7_CH	**1.339**	**1.161**	**1.544**	**0.000**	**0.000**	**0.911**
C7_CW	**1.228**	**1.021**	**1.476**	**0.031**	**0.000**	**0.851**
C7_Calculated_NSLA	1.128	0.890	1.431	0.305	0.000	0.750
C7_Calculated_TPLA	1.014	0.892	1.152	0.822	0.000	0.929
C7_IZL	**1.158**	**1.064**	**1.261**	**0.002**	**0.000**	**0.969**
C7_LW	0.910	0.685	1.209	0.501	0.000	0.641
C7_NSL	0.975	0.729	1.304	0.860	0.000	0.623
T1_CL	1.044	0.933	1.168	0.431	0.000	0.945
T1_CH	**1.274**	**1.107**	**1.466**	**0.002**	**0.000**	**0.914**
T1_CW	1.069	0.839	1.362	0.573	0.000	0.741
T1_Calculated_NSLA	1.040	0.871	1.242	0.648	0.000	0.862

T1_Calculated_TPLA	0.934	0.834	1.046	0.223	0.000	0.944
T1_IZL	1.023	0.886	1.181	0.746	0.000	0.910
T1_LW	0.911	0.756	1.097	0.307	0.000	0.849
T1_NSL	1.596	1.074	2.371	0.022	0.013	0.284
T2_CL	**1.105**	**1.001**	**1.220**	**0.047**	**0.000**	**0.957**
T2_CH	**1.269**	**1.116**	**1.442**	**0.001**	**0.000**	**0.928**
T2_CW	1.046	0.921	1.187	0.471	0.000	0.930
T2_Calculated_NSLA	1.227	0.914	1.648	0.165	0.000	0.612
T2_Calculated_TPLA	0.914	0.792	1.055	0.206	0.000	0.910
T2_IZL	1.161	0.824	1.638	0.381	0.001	0.468
T2_LW	0.878	0.682	1.131	0.300	0.000	0.716
T2_NSL	**1.555**	**1.084**	**2.231**	**0.018**	**0.002**	**0.410**
T3_CL	**1.119**	**1.003**	**1.250**	**0.045**	**0.000**	**0.947**
T3_CH	**1.308**	**1.141**	**1.500**	**0.001**	**0.000**	**0.918**
T3_CW	0.966	0.840	1.110	0.608	0.000	0.915
T3_Calculated_NSLA	1.141	0.968	1.345	0.110	0.000	0.882
T3_Calculated_TPLA	0.934	0.849	1.027	0.150	0.000	0.961
T3_IZL	0.926	0.800	1.071	0.284	0.000	0.907
T3_LW	0.940	0.784	1.128	0.490	0.000	0.855
T3_NSL	**1.817**	**1.219**	**2.708**	**0.004**	**0.015**	**0.272**
T4_CL	**1.083**	**1.003**	**1.170**	**0.044**	**0.000**	**0.974**
T4_CH	**1.236**	**1.093**	**1.397**	**0.002**	**0.000**	**0.934**
T4_CW	1.005	0.886	1.139	0.939	0.000	0.931
T4_Calculated_NSLA	1.157	0.967	1.384	0.105	0.000	0.860
T4_Calculated_TPLA	0.946	0.820	1.090	0.422	0.000	0.912
T4_IZL	0.898	0.775	1.041	0.145	0.000	0.905
T4_LW	0.960	0.794	1.161	0.662	0.000	0.842

T4_NSL	**1.338**	**1.022**	**1.752**	**0.035**	**0.000**	**0.677**
T5_CL	1.058	0.966	1.158	0.210	0.000	0.964
T5_CH	**1.209**	**1.061**	**1.378**	**0.007**	**0.000**	**0.925**
T5_CW	0.972	0.809	1.168	0.750	0.000	0.852
T5_Calculated_NSLA	**1.234**	**1.029**	**1.480**	**0.025**	**0.000**	**0.856**
T5_Calculated_TPLA	0.956	0.718	1.271	0.746	0.000	0.637
T5_IZL	0.954	0.822	1.108	0.520	0.000	0.903
T5_LW	0.903	0.778	1.047	0.167	0.000	0.904
T5_NSL	1.118	0.771	1.621	0.544	0.003	0.373
T6_CL	1.046	0.971	1.127	0.225	0.000	0.976
T6_CH	**1.212**	**1.095**	**1.341**	**0.001**	**0.000**	**0.955**
T6_CW	0.957	0.848	1.080	0.460	0.000	0.936
T6_Calculated_NSLA	**1.292**	**1.078**	**1.548**	**0.008**	**0.000**	**0.857**
T6_Calculated_TPLA	0.933	0.711	1.225	0.605	0.000	0.670
T6_IZL	0.914	0.785	1.064	0.233	0.000	0.899
T6_LW	1.093	0.766	1.560	0.612	0.001	0.428
T6_NSL	**1.470**	**1.031**	**2.095**	**0.034**	**0.001**	**0.431**
T7_CL	1.006	0.912	1.109	0.902	0.000	0.959
T7_CH	**1.288**	**1.148**	**1.446**	**0.000**	**0.000**	**0.942**
T7_CW	0.984	0.856	1.131	0.807	0.000	0.915
T7_Calculated_NSLA	**1.221**	**1.078**	**1.383**	**0.003**	**0.000**	**0.933**
T7_Calculated_TPLA	0.916	0.692	1.212	0.526	0.000	0.651
T7_IZL	**0.869**	**0.763**	**0.989**	**0.035**	**0.000**	**0.926**
T7_LW	0.922	0.806	1.054	0.219	0.000	0.921
T7_NSL	**1.492**	**1.007**	**2.209**	**0.046**	**0.011**	**0.297**
T8_CL	1.003	0.923	1.091	0.931	0.000	0.970
T8_CH	**1.240**	**1.123**	**1.369**	**0.000**	**0.000**	**0.957**

T8_CW	1.017	0.867	1.194	0.825	0.000	0.888
T8_Calculated_NSLA	1.133	0.972	1.321	0.105	0.000	0.897
T8_Calculated_TPLA	1.012	0.813	1.258	0.913	0.000	0.790
T8_IZL	0.939	0.820	1.076	0.348	0.000	0.919
T8_LW	0.931	0.808	1.073	0.307	0.000	0.912
T8_NSL	**1.635**	**1.148**	**2.329**	**0.008**	**0.001**	**0.435**
T9_CL	1.027	0.969	1.090	0.349	0.000	0.985
T9_CH	**1.262**	**1.161**	**1.371**	**0.000**	**0.000**	**0.970**
T9_CW	1.122	0.900	1.400	0.291	0.000	0.785
T9_Calculated_NSLA	**1.249**	**1.035**	**1.508**	**0.023**	**0.000**	**0.844**
T9_Calculated_TPLA	**1.562**	**1.076**	**2.265**	**0.020**	**0.003**	**0.371**
T9_IZL	1.155	0.915	1.458	0.212	0.000	0.760
T9_LW	0.914	0.824	1.014	0.086	0.000	0.953
T9_NSL	1.799	1.174	2.759	0.008	0.074	0.158
T10_CL	0.986	0.905	1.073	0.725	0.000	0.969
T10_CH	**1.461**	**1.002**	**2.130**	**0.049**	**0.004**	**0.354**
T10_CW	1.207	0.904	1.612	0.193	0.000	0.626
T10_Calculated_NSLA	**1.574**	**1.095**	**2.263**	**0.016**	**0.002**	**0.403**
T10_Calculated_TPLA	1.033	0.749	1.424	0.838	0.000	0.538
T10_IZL	0.995	0.832	1.189	0.950	0.000	0.861
T10_LW	0.990	0.706	1.389	0.953	0.000	0.483
T10_NSL	2.426	1.546	3.808	0.000	0.296	0.057
T11_CL	0.919	0.841	1.004	0.061	0.000	0.966
T11_CH	**1.167**	**1.050**	**1.296**	**0.006**	**0.000**	**0.952**
T11_CW	1.049	0.930	1.182	0.418	0.000	0.937
T11_Calculated_NSLA	**1.301**	**1.104**	**1.532**	**0.003**	**0.000**	**0.882**
T11_IZL	0.978	0.832	1.150	0.781	0.000	0.886

T11_LW	1.063	0.711	1.591	0.760	0.019	0.256
T11_NSL	1.689	2.683	1.063	0.027	0.869	0.001
T12_CL	0.950	0.897	1.006	0.074	0.000	0.986
T12_CH	**1.288**	**1.042**	**1.592**	**0.021**	**0.000**	**0.803**
T12_CW	1.042	0.903	1.202	0.555	0.000	0.911
T12_Calculated_NSLA	**1.491**	**1.095**	**2.031**	**0.013**	**0.000**	**0.573**
T12_IZL	0.983	0.849	1.138	0.808	0.000	0.906
T12_LW	1.087	0.883	1.337	0.415	0.000	0.810
T12_Calculated_APL	1.399	0.912	2.145	0.121	0.075	0.157
T12_NSL	2.447	1.574	3.806	0.000	0.167	0.098
T13_CL	0.921	0.820	1.033	0.151	0.000	0.942
T13_CH	1.138	0.973	1.330	0.100	0.000	0.893
T13_CW	1.083	0.937	1.253	0.264	0.000	0.908
T13_Calculated_NSLA	**1.310**	**1.068**	**1.608**	**0.012**	**0.000**	**0.816**
T13_IZL	0.916	0.779	1.077	0.273	0.000	0.885
T13_LW	0.867	0.707	1.064	0.162	0.000	0.816
T13_Calculated_APL	1.305	0.843	2.021	0.226	0.127	0.118
T13_NSL	**1.463**	**1.027**	**2.084**	**0.036**	**0.001**	**0.434**
L1_CL	0.975	0.882	1.078	0.605	0.000	0.957
L1_CH	1.140	0.976	1.330	0.093	0.000	0.896
L1_CW	1.085	0.939	1.255	0.252	0.000	0.908
L1_Calculated_NSLA	**1.294**	**1.141**	**1.469**	**0.000**	**0.000**	**0.930**
L1_Calculated_TPLA	1.308	0.928	1.843	0.120	0.001	0.470
L1_IZL	1.039	0.918	1.175	0.525	0.000	0.934
L1_LW	0.854	0.707	1.032	0.098	0.000	0.843
L1_Calculated_APL	0.990	0.800	1.225	0.922	0.000	0.800
L1_NSL	1.280	0.982	1.668	0.067	0.000	0.688

L2_CL	0.976	0.883	1.080	0.624	0.000	0.956
L2_CH	1.111	0.963	1.283	0.141	0.000	0.910
L2_CW	1.033	0.884	1.206	0.672	0.000	0.894
L2_Calculated_NSLA	**1.336**	**1.172**	**1.523**	**0.000**	**0.000**	**0.925**
L2_Calculated_TPLA	1.128	0.913	1.394	0.251	0.000	0.802
L2_IZL	0.982	0.870	1.110	0.764	0.000	0.935
L2_LW	0.935	0.758	1.153	0.513	0.000	0.807
L2_Calculated_APL	0.933	0.776	1.122	0.442	0.000	0.851
L2_NSL	1.272	0.986	1.642	0.063	0.000	0.712
L3_CL	0.996	0.902	1.100	0.940	0.000	0.957
L3_CH	1.157	0.981	1.364	0.080	0.000	0.881
L3_CW	1.035	0.885	1.211	0.652	0.000	0.892
L3_Calculated_NSLA	**1.253**	**1.092**	**1.438**	**0.003**	**0.000**	**0.917**
L3_Calculated_TPLA	1.160	0.940	1.431	0.158	0.000	0.806
L3_IZL	0.945	0.837	1.067	0.345	0.000	0.936
L3_LW	0.911	0.768	1.080	0.266	0.000	0.873
L3_Calculated_APL	0.954	0.776	1.172	0.640	0.000	0.814
L3_NSL	1.166	0.860	1.579	0.310	0.000	0.587
L4_CL	0.940	0.842	1.051	0.262	0.000	0.946
L4_CH	1.143	0.992	1.316	0.063	0.000	0.913
L4_CW	1.016	0.878	1.175	0.826	0.000	0.908
L4_Calculated_NSLA	**1.241**	**1.079**	**1.428**	**0.004**	**0.000**	**0.914**
L4_Calculated_TPLA	1.189	0.969	1.460	0.093	0.000	0.815
L4_IZL	0.947	0.834	1.074	0.375	0.000	0.930
L4_LW	**0.839**	**0.708**	**0.995**	**0.044**	**0.000**	**0.873**
L4_Calculated_APL	0.923	0.743	1.146	0.449	0.000	0.793
L4_NSL	1.246	0.906	1.713	0.168	0.000	0.545

L5_CL	0.921	0.838	1.011	0.080	0.000	0.962
L5_CH	1.102	0.932	1.303	0.240	0.000	0.877
L5_CW	1.036	0.828	1.297	0.744	0.000	0.778
L5_Calculated_NSLA	**1.220**	**1.004**	**1.484**	**0.046**	**0.000**	**0.832**
L5_Calculated_TPLA	1.142	0.973	1.339	0.099	0.000	0.888
L5_IZL	1.202	0.814	1.774	0.344	0.009	0.309
L5_LW	0.912	0.692	1.204	0.502	0.000	0.658
L5_Calculated_APL	1.182	0.860	1.625	0.290	0.000	0.547
L5_NSL	**1.962**	**1.397**	**2.755**	**0.000**	0.000	0.480
L6_CL	0.980	0.893	1.076	0.661	0.000	0.962
L6_CH	1.116	0.964	1.293	0.135	0.000	0.905
L6_CW	1.033	0.859	1.242	0.720	0.000	0.850
L6_Calculated_NSLA	**1.277**	**1.099**	**1.483**	**0.003**	**0.000**	**0.902**
L6_Calculated_TPLA	1.150	0.980	1.350	0.083	0.000	0.888
L6_IZL	0.933	0.836	1.041	0.200	0.000	0.948
L6_LW	0.920	0.763	1.108	0.360	0.000	0.847
L6_NSL	1.306	0.900	1.894	0.154	0.003	0.372
L7_CL	1.011	0.881	1.160	0.871	0.000	0.917
L7_CH	**1.195**	**1.043**	**1.369**	**0.013**	**0.000**	**0.919**
L7_CW	1.055	0.891	1.249	0.518	0.000	0.875
L7_Calculated_NSLA	**1.281**	**1.102**	**1.491**	**0.003**	**0.000**	**0.900**
L7_Calculated_TPLA	1.106	0.954	1.282	0.171	0.000	0.905
L7_IZL	1.028	0.867	1.219	0.738	0.000	0.873
L7_LW	0.908	0.781	1.056	0.198	0.000	0.901
L7_NSL	**1.664**	**1.275**	**2.172**	**0.001**	**0.000**	**0.685**

Chapter 4. Regional differentiation of felid vertebral column evolution: a study of 3D shape trajectories

Published as: Randau, M., Cuff, A. R., Hutchinson, J. R., Pierce, S. E., & Goswami, A. (2016a). Regional differentiation of felid vertebral column evolution: a study of 3D shape trajectories. *Organisms Diversity and Evolution, 17*(1), 305-319.

Abstract:

Recent advances in geometric morphometrics provide improved techniques for extraction of biological information from shape and have greatly contributed to the study of ecomorphology and morphological evolution. However, the vertebral column remains an under-studied structure due in part to a concentration on skull and limb research, but most importantly because of the difficulties in analysing the shape of a structure composed of multiple articulating discrete units (i.e., vertebrae).

Here, we have applied a variety of geometric morphometric analyses to three-dimensional landmarks collected on 19 presacral vertebrae to investigate the influence of potential ecological and functional drivers, such as size, locomotion, and prey size specialisation, on regional morphology of the vertebral column in the mammalian family Felidae. In particular, we have here provided a novel application of a method – Phenotypic Trajectory

Analysis (PTA) – that allows for shape analysis of a contiguous sequence of vertebrae as functionally linked osteological structures.

Our results showed that ecological factors influence the shape of the vertebral column heterogeneously and that distinct vertebral sections may be under different selection pressures. While anterior presacral vertebrae may either have evolved under stronger phylogenetic constraints or are ecologically conservative, posterior presacral vertebrae, specifically in the post-T10 region, show significant differentiation among ecomorphs. Additionally, our PTA results demonstrated that functional vertebral regions differ among felid ecomorphs mainly in the relative covariation of vertebral shape variables (i.e., direction of trajectories, rather than in trajectory size) and, therefore, that ecological divergence among felid species is reflected by morphological changes in vertebral column shape.

Introduction

From species description to detailed studies of ecomorphology, analyses of form have long been used by researchers examining ecological and evolutionary trends in both living and fossil organisms (e.g., Gould 1966; Gonyea 1978; Lauder 1995; Boszczyk et al. 2001; Rudwick 2005; Davies et al. 2007; Benoit 2010; Goswami et al. 2012; Goswami et al. 2014; Dumont et al.

2015). The geometric morphometrics revolution has greatly improved the scientific capacity to extract detailed information from biological structures. Yet it has also been hindered by computation issues with statistical tests used and the constraints involved in analysing data that are dense (e.g., large numbers of landmarks) and multidimensional, with specimen:landmark ratios decreasing as a result of these new advances (Mitteroecker and Gunz 2009; Adams et al. 2013; Cardini and Loy 2013; Adams 2014b; Collyer et al. 2015). Newly developed software and methods are rapidly tackling these analytical power issues, with a plethora of recent papers describing and applying these approaches to diverse morphometric datasets (e.g., Adams and Collyer 2009; Mitteroecker and Gunz 2009; Klingenberg and Marugán-Lobón 2013; Mitteroecker et al. 2013; Monteiro 2013; Polly et al. 2013; Sheets and Zelditch 2013; Adams 2014a, 2014b; Adams et al. 2015; Collyer et al. 2015).

Among morphological studies in the vertebrate literature, both those using geometric morphometrics (GMM) and studies using linear or cross-sectional measurements, there is a clear bias towards the morphology of the skull (e.g., Stayton 2005; Goswami 2006b; Pierce et al. 2008; Slater and Van Valkenburgh 2008; Meachen-Samuels and Van Valkenburgh 2009a; Pierce et al. 2009; Drake and Klingenberg 2010; Figueirido et al. 2010; Goswami and Polly 2010a; Foth et al. 2012; Piras et al. 2013; Fabre et al. 2014a; Meachen et al. 2014), followed by studies of the limbs (e.g., Andersson and Werdelin 2003; Doube et al. 2009;

Meachen-Samuels and Van Valkenburgh 2009b; Adams and Nistri 2010; Bell et al. 2011; Bennett and Goswami 2011; Ercoli et al. 2012; Walmsley et al. 2012; Zhang et al. 2012; Alvarez et al. 2013; Fabre et al. 2013a; Sears et al. 2013; Martín-Serra et al. 2014a). The axial skeleton, in contrast, is comparatively underrepresented in the morphological literature, with the majority of work on this structure taking a biomechanical or developmental perspective (e.g., Smeathers 1981; Gál 1993a; Long et al. 1997; Macpherson and Fung 1998; Boszczyk et al. 2001; Breit and Künzel 2004; Chen et al. 2005; Narita and Kuratani 2005; Wellik 2007; Chatzigianni and Halazonetis 2009; Müller et al. 2010; Buchholtz et al. 2012; Buchholtz et al. 2014; Galis et al. 2014; Schilling and Long 2014; Molnar et al. 2015). Additionally, due to the difficulties in studying a structure that is composed of discrete units, research on axial skeletal morphology has frequently focused on separate analyses of individual vertebrae, with a few studies presenting intervertebral comparisons of individual measurements or differential morphospace occupation of vertebral types, rather than combined analysis of the full column (e.g., Manfreda et al. 2006; Alvarez et al. 2013; Buchholtz et al. 2014; Jones 2015; Arnold et al. 2016). Nevertheless, the limited morphometric studies of vertebral form have demonstrated that ecological specialisations and developmental patterning are reflected in the morphology of individual vertebrae, as well as along the entire spine (Johnson et al. 1999; Chen et al. 2005; Shapiro 2007; Pierce et al. 2011; e.g., Jones and German 2014; Ward and Mehta 2014; Böhmer et al. 2015;

Head and Polly 2015; Jones and Pierce 2015; Werneburg et al. 2015; Chapter 2; Randau et al. 2016b). Indeed, many large clades, including the vast majority of placental mammals, do not display significant meristic changes (i.e., variation in number) in the axial skeleton; therefore, adaptation of this structure must happen through modifications of its shape (Narita and Kuratani 2005; Müller et al. 2010; Buchholtz et al. 2012; Buchholtz 2014).

Recently, we conducted a large-scale linear morphometric analysis of the felid (cats) presacral vertebral column and found that this method was unable to strongly differentiate taxa based on either prey size specialization or locomotor mode (Chapter 2; Randau et al. 2016b). For instance, there were few statistical differences in vertebral profile plots (i.e., variation in linear and angular measures along the column), and a principal components analysis found a locomotory signal only in the lumbar region. These results were surprising considering felid prey size specialization has been shown to correlate with osteological measures of the skull and appendicular skeleton (Slater and Van Valkenburgh 2008; Meachen-Samuels and Van Valkenburgh 2009a, 2009b) and similar linear morphometric studies on other mammalian groups (e.g., pinnipeds, whales) have found the vertebral column to hold a strong ecological signal (e.g., Finch and Freedman 1986; Buchholtz 2001a, 2001b; Hua 2003; Pierce et al. 2011). As felids are a morphologically conservative group, with little variation in musculoskeletal anatomy across

the clade (Day and Jayne 2007; Doube et al. 2009; Cuff et al. 2016b, 2016a), it remains uncertain whether the felid vertebral column holds little ecological signal or if linear morphometric techniques are not powerful enough to discriminate more subtle variation in vertebral form. To investigate this further, we extend our work by quantifying vertebral morphology in felids using three-dimensional landmarks-based GMM, and include a novel application of phenotypic trajectory analysis (Adams and Collyer 2009; Collyer and Adams 2013) to identify ecological signal in serial structures. Three-dimensional (3D) landmarks are expected to provide greater detail and biological information than linear data (e.g., Cardini and Loy 2013; Fabre et al. 2014a), and thus this work expands and improves upon existing linear studies considering this clade (Jones 2015; Randau et al. 2016b). To our knowledge, two previous uses of 3D GMM to study the shape of a complete vertebral region have been reported in the literature (e.g., the cervical region, Böhmer et al. 2015; Werneburg 2015). While Böhmer et al. (2015) analysed individually landmarked cervical vertebrae by plotting them together with a Principal Component Analyses, which described main shape variation among those and allows for qualitative analyses of shape change across taxa, Werneburg (2015) described a complex methodology that may not be broadly applicable. Specifically, that method relied on finding landmarks on three-dimensional reconstructions which had been matched to photographs of either manually articulated cervical vertebrae to approximate *in vivo* orientations, or on model

reconstructions of CT scans obtained from living animals. Those conditions are not readily available for many taxa, and thus we believe that the approach described here will be useful for a broader range of future studies. Additionally, Head and Polly (2015) used two-dimensional landmarks to characterise the precoaclal axial skeleton of squamates; however, the methodology described was applied to investigate patterns of regionalisation in the axial skeleton instead of testing correlations between shape and ecology.

We first analyse the individual shape of selected vertebrae and test for the influence of factors known to affect the shape of skull and limbs, including size, locomotion and prey size specialisation (Carbone et al. 1999; Meachen-Samuels and Van Valkenburgh 2009a, 2009b). We then conduct separate analyses of each region of the vertebral column (cervical, thoracic, and lumbar regions, and hypothesized functional regions composed of different combinations of these regions), and assess shape differences and differential allometry associated with ecological groupings. Finally, we apply phenotypic trajectory analysis to the main dataset, a combined analysis of cervical, thoracic, and lumbar vertebrae, and also to individual regions with significant ecological signal, to analyse the shape of the vertebral column as a succession of contiguous units, thus overcoming the long-standing issue of analysing vertebrae as independent objects in geometric morphometric studies. We use these approaches to test the following hypotheses: 1) ecology is a significant

influence on the morphology of felid vertebral column; and 2) vertebral regions display different levels of ecological and phylogenetic signal due to the regionalisation of shape in the mammalian vertebral column.

Material and Methods

Data collection

As discussed in Chapter 2, in order to compose our 3D dataset, landmarks were collected from 19 presacral vertebrae from nine species of extant cats using an Immersion Microscribe G2X (Solution Technologies, Inc., Oella). This dataset included the following vertebrae: atlas, axis, C4, C6, C7, T1, T2, T4, T6, T8, T10, T11, T12, T13, L1, L2, L4, L6, and L7. As time constraints hindered the ability to collect dense data for every vertebra, but sufficient data were needed to describe the full presacral vertebral column morphology, the selection of these vertebrae was based on the following criteria: vertebrae with measurements that accounted for the highest principal component loadings in a previous linear study (Chapter 3; Randau et al. 2016b); vertebrae comprising the boundaries between vertebral regions and immediately preceding and succeeding vertebrae (e.g., C7 and T1, and C6 and T2, respectively); and vertebrae which are thought to be of particular biomechanical importance (e.g., T11, the anticlinal vertebra). As discussed in Chapter 2, the selected

vertebrae are an accurate representation of the vertebral morphologies of the presacral column of felids. Landmarks were collected from 109 specimens, ranging from seven to 17 specimens per species, with the final dataset including a total of 1712 individual vertebrae (see Table S4.1 for specimen numbers). Analyses grouped this dataset in various ways, ranging from treating all vertebrae individually to pooling vertebrae in the most inclusive grouping (C4 – L7, excluding T11 –T13), as described further below. Vertebrae were also grouped into the following five regions for some analyses, including: C4 – T10, T1 – T10, T1 – L7, T10 – L7, and L1 – L7. These regions were selected because they correspond to or group clear anatomical regions (e.g., T1 – T10, L1 – L7, and T1 – L7) or more inclusive regions demarked by anatomical transitions (i.e., anterior or posterior vertebral column defined by the dorsal limit of the diaphragm, e.g., C4 –T10 and T10 – L7, respectively; Gray et al. 2005; Buchholtz et al. 2012; Jones 2015).

Sixteen homologous landmarks were identified on 14 of these vertebrae (i.e., the post-atlanto-axial and presacral C4 – L7 except for the T11 – T13). 12 landmarks were gathered on C1 (atlas), and 14 on C2 (axis), due to their unique morphologies (Fig. 4.1, and Table S4.2 of landmarks). Vertebrae T11 to T13 lack transverse processes and thus two out of the 16 selected landmarks (i.e., the right and left transverse process tips) could not be identified on those elements. Comparative analyses across all sampled vertebrae require all

observations to have the same landmarks. For this reason, the majority of the following analyses, unless otherwise stated, only used the 14 vertebral types that contained the same 16 landmarks (Fig. 4.1D-I, i.e., not including the axis and atlas, shown on Fig. 4.1 A-B, and J-K respectively, due to their unique shape, or vertebrae T11 to T13). The pilot study described in Chapter 2 demonstrated that both the homologous landmarks and the vertebra-specific landmarks included in the analyses presented here show very high repeatability (i.e., from 96.3% to 98.7% reproducibility) and accurately describe vertebral shape (~89%; Chapter 2).

In order to still include the T11-T13 vertebrae in our tests of ecological correlates of axial skeleton morphology, we conducted a second analysis using two alternative landmarks that represent the locations of the right and left accessory processes of these vertebrae (Fig. S4.1, landmarks 7 and 8). Accessory processes are slender processes that originate on the pedicle and extend posteriorly, laterally to each postzygapophyses, and reinforce the interzygapophyseal joint (De Iuliis and Pulerà 2006). Additionally, accessory processes were also present on vertebrae L1, L2 and L4 of all species analysed here. Therefore, the second analysis used the two accessory process landmarks instead of transverse process landmarks for the vertebrae T11 – L4, while the remaining vertebrae (C4- T10 and L6 - L7) continued to use the transverse processes landmarks. In this manner, a dataset of 16 landmarks was

constructed for 17 vertebrae, although two of these landmarks are not homologous in all of the vertebrae.

As only the 14-vertebrae dataset (excluding C1-C2 and T11-T13) was composed of homologous landmarks, we focus on the 'multi-vertebrae' analyses of that dataset, hereafter referred to as the "homologous dataset" (or C4 – L7 for shortening, although not containing T11 – T13, as stated). The results from the alternative dataset that includes T11-T13 by using two non-homologous landmarks (accessory processes landmarks instead of transverse process landmarks for T11-L4), hereafter referred to as the "alternative dataset", were remarkably consistent and are presented in the supplementary information (Appendix 4.1, Supplementary information).

Ecological data for all analyses were collated from the literature (Sunquist and Sunquist 2002; Meachen-Samuels and Van Valkenburgh 2009a, 2009b). As detailed in Chapter 2, prey size groupings include: small, mixed and large prey specialists. Locomotor groupings include: arboreal, cursorial, scansorial and terrestrial. Phylogenetic comparative analyses used the composite tree of Piras et al. (2013) pruned to the species sampled here.

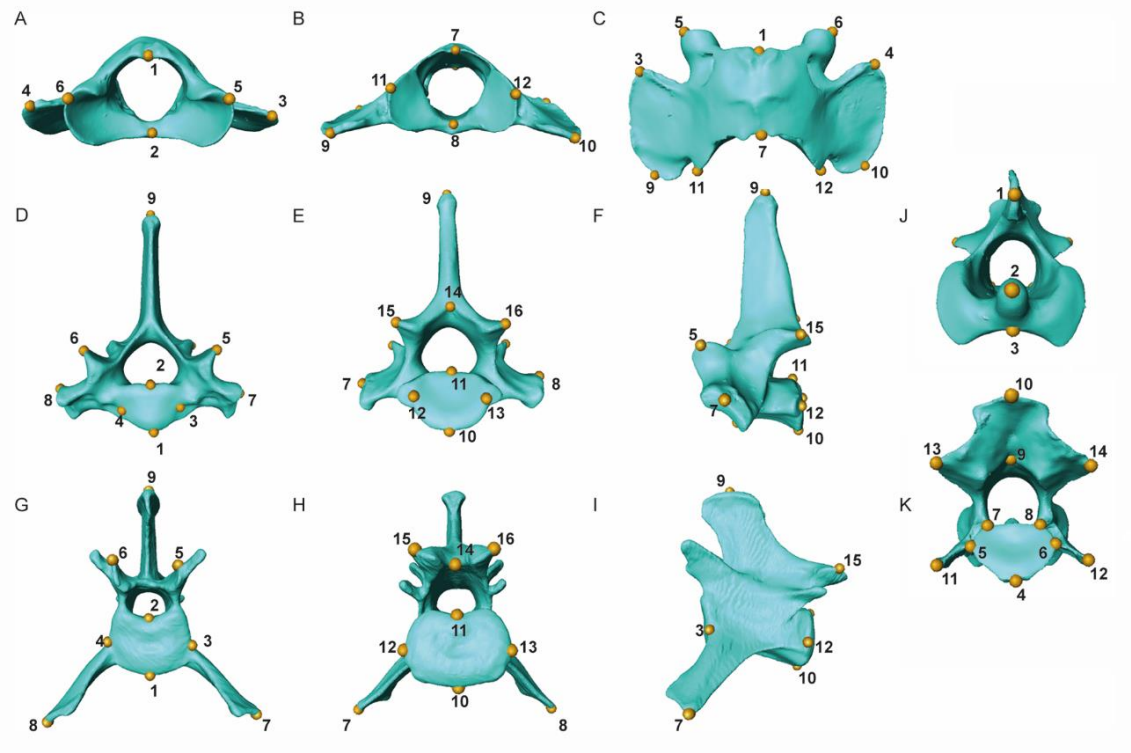

Fig. 4.1: Different vertebral morphologies and their respective three-dimensional landmarks: (A-C) atlas in anterior, posterior and dorsal view; (D-F) T1 in anterior, posterior and lateral view; (G-I) L1 in anterior, posterior and lateral view; and (J-K) axis in anterior and posterior view. Vertebral images are from CT scans of *Acinonyx jubatus* (Cheetah, USNM 520539). Landmark descriptions can be found in Table S4.2.

Caveats

Due to information on sex not being recorded for a great majority of museum specimens (Chapter 2), it was not possible to test if there was a significant signal of sexual dimorphism on three-dimensional vertebral shape. Nevertheless, as previously discussed on Chapter 2, sexual dimorphism in carnivorans, and specifically in felids, has been shown to be mainly characterised by differences in body size, and not by presence/absence of

morphological structures, and to vary according to the degree of sociality observed in the species (Ewer 1973; Wozencraft 2005). Therefore, the scaling process of all specimens involved in the Procrustes Superimposition (see methodology in Chapter 2, and below), and the analysis of the influence of size on shape performed here address this issue accordingly. Additionally, as all available specimens in museum collections per this thesis' selected species were digitised, and the focus of the analyses performed was either on the familial or ecological group levels (i.e., involving multiple species, and not concentrating on intraspecific results), any potential differences across specimens due to sexual dimorphism should not alter the results discussed throughout this thesis.

Furthermore, the effort to digitise multiple specimens per species is likely to ascertain that species averages for both shape and size have been included here, even if this is impossible to control for as it is dependent on specimen availability.

Data analysis

All analyses were carried out in R version 3.2.2 (R Core Team 2015b), using the 'geomorph' (Adams and Otarola-Castillo 2013; Adams et al. 2015), 'ape' (Paradis et al. 2004), and 'geiger' (Harmon et al. 2014) packages.

Prior to all subsequent analyses, missing landmarks due to broken specimens were imputed using the multivariate regression ("Reg") method in the 'estimate.missing' function of 'geomorph'. This approach predicts the missing landmarks by using a multivariate regression of the specimen with missing values on all other landmarks in the set of complete specimens (Gunz et al. 2009). A total of 126 out of 30695 (0.41%) landmarks were imputed. All vertebrae were then subjected to Procrustes Superimposition within the relevant sample (i.e., either within same vertebral type sample, or specific vertebral region analysed depending on the analysis level) to remove any effects due to scale, rotation, and translation.

Phylogenetic and ecological signal of individual and regional vertebral shape

Preliminary analysis of vertebral column shape was performed with a combined Principal Component Analysis (PCA) of all of the vertebrae in the homologous landmark dataset (C4 – L7, excluding T11-T13). A second PCA was performed on the region encompassing vertebrae T10 – L7 in the homologous landmark dataset. Scans of individual cheetah (*Acinonyx jubatus*, USNM 520539) vertebrae were used to create an average reference mesh with the 'warpRefMesh' function in geomorph, and this mesh was used to warp the PC1 and PC2 minimum and maximum shapes in order to display vertebral shape changes across the main eigenvectors.

The effects of centroid size and ecological specialisation (both in terms of locomotion and prey size categories) on vertebral shape were evaluated with factorial MANOVAs of the vertebral Procrustes coordinates (i.e., shape ~ centroid size * ecology). Factorial MANOVAs with this size-ecology interaction accounts for the effect of 'size' while examining the other factors that describe shape and define the groups. Additionally, these non-parametric MANOVAs with 'RRPP' (residual randomization permutation procedure) allowed for significance tests with multidimensional data that have fewer observations than dimensions (Collyer et al. 2015). These analyses were performed separately on each vertebra from C1-L7, with each set composed of an across species pool (i.e., C1 dataset contained all C1 vertebrae measured, across all nine species) as well as on the complete homologous dataset (see supplementary information for further details on analyses of the alternative dataset, Appendix 4.1). Additionally, factorial MANOVAs were applied to the five vertebral regions as described above, using the homologous dataset. Each described region contained all vertebrae of the named types, including all species listed here.

In order to assess the influence of phylogenetic relatedness on vertebral shape and centroid size (i.e., whether more closely related species were more phenotypically similar; Felsenstein 1985), we first constructed the mean shape for each individual vertebra (C1 to L7) per species and calculated the

phylogenetic signal with the 'Kmult' method (i.e., a multivariate version of the K-statistic; Adams 2014a) with the 'physignal' function in 'geomorph'. As L1-L4 have both transverse processes and accessory processes and thus are the only elements with different landmarks in the homologous and alternative datasets, this analysis was performed for both datasets for those elements. For individual vertebrae that presented a significant phylogenetic signal in their shape across the studied species, we also performed phylogenetic MANOVAs to assess the relationship between shape, centroid size and ecological factors. Phylogenetic MANOVAs use a phylogeny-informed context under a Brownian motion model of evolution to calculate a phylogenetic transformation matrix and the Gower-centred distance matrix from predicted variable values, which are then used to assess significance from comparisons between the values of statistical attributes obtained from those and the observed values (Garland et al. 1993; Adams 2014b; Adams and Collyer 2015). Phylogenetic MANOVAs were done using the 'procD.pgls' function in 'geomorph'.

The interaction of allometry and ecology in vertebral regions

Considering that previous studies of felid vertebral morphology have demonstrated the widespread influence of allometry in vertebral linear dimensions (see below, and Chapter 3; Jones 2015; Jones and Pierce 2015;

Randau et al. 2016b), we investigated whether prey size or locomotory ecomorphs presented different allometries in their vertebral shape. Based on the MANOVA results (see below), the vertebral region with the highest absolute variance explained by the two ecological variables (i.e., T10 – L7) was selected to examine differences in vertebral allometry with respect to ecological specialisation.

Using the "PredLine" method of the 'plotAllometry' function in 'geomorph', the predicted allometric scores for these regions were calculated for each ecological group from the shape against centroid size regression. The method used produced allometric trajectories (i.e., plotted PC1 of the predicted values against size) which clearly exhibited allometric differences between ecological groups (Adams and Nistri 2010). The significance of the differences in the log centroid size ~ shape relationship between groups could be quantified by both the p-value of the comparisons between slope distances, which itself measures differences in amount of shape change per unit of centroid size change, and the slope angle's p-value, which indicates if the directions of these vectors point at different regions of the morphospace (Collyer and Adams 2013; Collyer et al. 2015). This last step was performed using the 'advanced.procD.lm' function in 'geomorph'.

Ecological signal across the vertebral column

Shape for the proxy of an entire vertebral column (i.e., C4 – L7, excluding T11 – T13), as well as for individual regions, was quantified using a novel application of Phenotypic Trajectory Analysis (PTA). PTA identifies a shape trajectory among associated data points (vertebrae, in this case) and then compares this trajectory among vertebra within each predetermined group (e.g., mean shape of C7 for all arboreal taxa), and then traces the trajectory between these means (e.g., C6 to C7, C7 to T1, etc.) (Adams and Collyer 2007, 2009; Collyer and Adams 2013). The trajectories can then be visualised in morphospace for a qualitative comparison between groupings, and differences in size, direction, and shape of the trajectories for each group can also be quantitatively compared. As above, taxa were grouped by prey size and locomotory categories for analysis of ecological signal in phenotypic trajectories.

Results

Phylogenetic and ecological signal in individual and regional vertebral shape

The majority of the variance (90%) was summarised by the first four PCs in both the homologous and alternative datasets (Table 4.1, and Tables S4.3 and S4.4). PCA plots show three general morphological groupings: a C4 cluster, an

'end-cervicals' to T10 cluster (i.e., C6, C7, T1, T2, T4, T6, T8, and T10) and a lumbar cluster (i.e., L1, L2, L4, L6, and L7) (Fig. 4.2A-B, and Fig. S4.2 in Appendix 4.1).

Table 4.1: Principal component results from the 'C4 – L7' analyses showing PCs 1 – 8 which together explain over 95% of total variation.

PRINCIPAL COMPONENT	EIGENVALUE	PROPORTION OF VARIANCE	CUMULATIVE PROPORTION
PC1	0.244	0.439	0.439
PC2	0.185	0.251	0.691
PC3	0.142	0.148	0.839
PC4	0.093	0.064	0.903
PC5	0.062	0.028	0.931
PC6	0.041	0.012	0.943
PC7	0.033	0.008	0.951
PC8	0.031	0.007	0.958

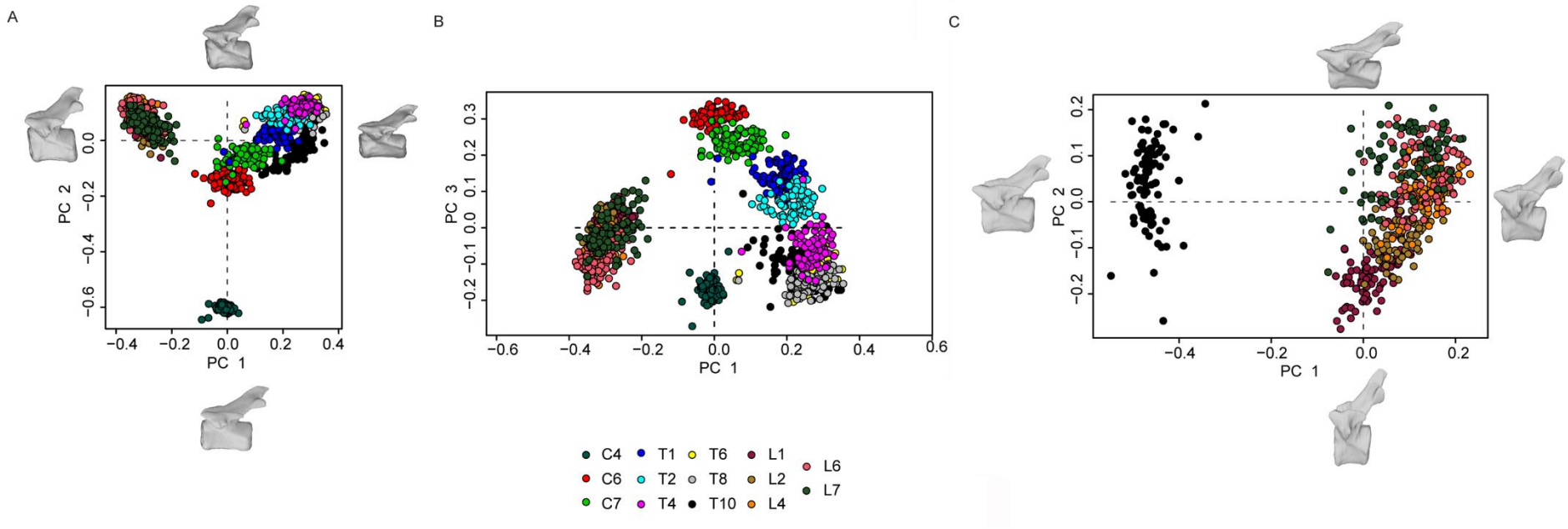

Fig. 4.2: Plots of Principal Component Analyses. (A-B): C4 – L7 PCA plots showing distribution of vertebral elements on PC1xPC2 (A), with respective warps showing extremes of morphology explained by each eigenvector (i.e., PC), and on PC1xPC3 (B). (C): T10 – L7 PCA plot showing distribution of vertebral elements on PC1xPC2, and also displaying eigenvector extremes of vertebral shape. Vertebral types are identified by same colour in all plots.

As noted in Methods, all of the following results refer to the homologous dataset unless otherwise indicated. The PC1 minimum shape was generally mediolaterally and anteroposteriorly compressed and dorsoventrally elongated, with smaller centrum width and centrum length, smaller distances between transverse processes, pre-zygapophyses, and post-zygapophyses, and larger heights for the centrum, neural canal, and neural spine. The PC1 maximum shape showed larger centrum width and centrum length, larger distances between transverse processes and intra-zygapophyses, but shorter heights for the centrum, neural canal, and neural spine. PC2, which separated the C4 cluster from the other two vertebral clusters, presented similar shape differences, with the PC2 minimum shape displaying even more exaggerated features related to mediolateral compression, but, in contrast, also exhibiting some anteroposterior elongation. The main feature of PC2's maximum shape was the relative augmentation of the distances in the mediolateral dimension, with larger centrum width and intra-zygapophyseal distances. Results from the PCA applied to the 'T10-L7' region (Table 4.2 and Table S4.3, see below) showed that the majority of the variation (>90%) was explained by the first five PCs, with PC1 explaining >60% of total variance.

When individual vertebral datasets were subjected to factorial MANOVAs of shape against centroid size, locomotion and prey size groups (Table 4.3), all vertebrae displayed significant correlations of shape with all three factors (p-

value < 0.001 – 0.05), with the exception of the T8 x prey size (p-value > 0.05). After Bonferroni correction, only three correlations ceased from being significant (i.e., p-value > 0.003): C6 and T10 vs. prey size, and L7 vs. centroid size. The three examined factors explained a range between 3% and 23.77% of vertebral shape (highlighted on Table 4.3). Further, estimating the influence of evolutionary relatedness on vertebral shape recovered a significant (i.e., p-value < 0.05) phylogenetic signal for the mean shape (i.e., Procrustes coordinates) of only five vertebrae: atlas, axis, C6, T1 and T2 (Table 4.4), however, after Bonferroni correction this signal was only significant for the atlas and axis (i.e., p-value < 0.003). Conservatively, all of these five vertebrae were further subjected to a second round of MANOVAs using the same factors as above, while controlling for this phylogenetic signal. After this correction, none of ecological correlations were significant (p-value >> 0.05, Table 3.5). No phylogenetic signal was recovered for centroid size of any of the analysed vertebrae.

Table 4.2: Principal component results from the 'T10-L7' analyses showing PCs 1 – 10 which together explain *circa* 95% of total variation.

PRINCIPAL COMPONENT	EIGENVALUE	PROPORTION OF VARIANCE	CUMULATIVE PROPORTION
PC1	0.216	0.639	0.639
PC2	0.103	0.145	0.784
PC3	0.065	0.058	0.842
PC4	0.052	0.037	0.879
PC5	0.041	0.023	0.902
PC6	0.035	0.017	0.919
PC7	0.031	0.013	0.932
PC8	0.025	0.009	0.941
PC9	0.025	0.008	0.949
PC10	0.021	0.006	0.955

Table 4.3: Factorial MANOVA results for analyses of individual vertebrae. For each factor (i.e., centroid size, locomotion, and prey size), the highest coefficient of determination (R^2) value is shown in bold, and the lowest value is displayed in italics. The sole test which was not statistically significant (i.e., p-value > 0.05) is underlined. Tests which are not significant after Bonferroni correction (i.e., p-value > 0.003) are marked with an asterisk.

VERTEBRA	**CENTROID SIZE**		**LOCOMOTION**		**PREY SIZE**	
	P-VALUE	R^2	P-VALUE	R^2	P-VALUE	R^2
atlas	0.001	**0.187**	0.001	*0.074*	0.001	0.080
axis	0.001	0.155	0.001	0.117	0.001	0.081
HOMOLOGOUS DATASET						
C4	0.001	0.080	0.001	0.208	0.001	0.042
C6	0.001	0.083	0.001	0.147	0.007*	0.034
C7	0.001	0.089	0.001	0.142	0.003	0.037
T1	0.001	0.083	0.001	0.121	0.001	0.046
T2	0.001	0.063	0.001	0.161	0.001	0.089
T4	0.001	0.095	0.001	0.122	0.001	0.062
T6	0.001	0.099	0.001	0.146	0.001	0.042
T8	0.001	0.059	0.001	0.145	<u>0.062</u>	
T10	0.001	0.183	0.001	0.169	0.016*	*0.030*
L1	0.001	0.154	0.001	**0.238**	0.001	0.041
L2	0.001	0.176	0.001	0.185	0.001	0.061
L4	0.001	0.137	0.001	0.130	0.001	0.059
L6	0.001	0.110	0.001	0.105	0.001	0.077
L7	0.006*	*0.043*	0.001	0.121	0.001	**0.118**

Table 4.4: Phylogenetic signal results for mean shape and centroid size per individual vertebrae. Vertebrae displaying significant (p-value > 0.05) phylogenetic signal are shown in bold. Results which are not significant after Bonferroni correction (i.e., p-value > 0.003) are marked with an asterisk.

vertebra	**Mean shape**		**Mean Centroid size**	
	K	**p-value**	**K**	**p-value**
Atlas	1.023	**0.002**	0.685	0.545
Axis	0.977	**0.002**	0.832	0.271
Homologous dataset				
C4	0.587	0.731	0.801	0.34
C6	0.875	**0.026***	0.749	0.405
C7	0.494	0.904	0.494	0.917
T1	0.94	**0.006***	0.762	0.373
T2	0.847	**0.027***	0.512	0.89
T4	0.738	0.301	0.747	0.37
T6	0.817	0.105	0.615	0.712
T8	0.743	0.221	0.686	0.602
T10	0.901	0.135	0.929	0.149
L1	0.709	0.541	0.62	0.7
L2	0.888	0.056	0.59	0.752
L4	0.9	0.241	0.74	0.445
L6	0.902	0.238	0.913	0.185
L7	0.813	0.124	0.496	0.904

Table 4.5: Phylogenetic factorial MANOVA results for analyses of individual vertebrae which showed significant phylogenetic signal.

	CENTROID SIZE	LOCOMOTION	PREY SIZE
VERTEBRA	**P-VALUE**	**P-VALUE**	**P-VALUE**
ATLAS	0.23976	0.98501	0.096903
AXIS	0.1968	0.9021	0.14486
C6	0.35265	0.78122	0.071928
T1	0.51149	0.81019	0.064935
T2	0.70529	0.62438	0.26873

Table 4.6: Factorial MANOVA results for analyses of vertebral regions. The highest coefficient of determination (R^2) values for both prey size and locomotion were found in the T10 – L7 region and are shown in bold. The tests which were not statistically significant (i.e., p-value > 0.05) are underlined. All significant tests were still significant after Bonferroni correction (i.e., p-value < 0.008).

	CENTROID SIZE		PREY SIZE		LOCOMOTION	
REGION	**P-VALUE**	**R^2**	**P-VALUE**	**R^2**	**P-VALUE**	**R^2**
C4 - L7	0.001	0.036	0.001	0.070	<u>0.101</u>	
C4 - T10	0.005	0.007	0.001	0.016	<u>0.164</u>	
T1 - T10	0.001	0.023	0.001	0.042	0.002	0.020
T1 - L7	0.001	0.057	0.001	0.126	0.001	0.119
T10 - L7	0.001	0.078	0.001	**0.176**	0.001	**0.122**
L1 - L7	0.001	0.081	0.001	0.109	0.001	0.100

Factorial MANOVAs were also applied to five regions composed of multiple vertebrae for quantification of the influence of ecological factors on vertebral regions. The highest ecological signal in vertebral shape was observed in the region from T10 to L7, with ~17.55% and ~12.2% of overall shape explained by prey size and locomotor categories, respectively (see MANOVAs in Table 4.6 for all results). This region also displayed the second highest values for the influence of centroid size on shape (~7.8%, Table 4.6). No significant correlation with locomotor categories was found for the complete homologous dataset (C4 – L7) or for the C4-T10 region, while significant (i.e., both prior and after Bonferroni correction) correlations with both locomotor and prey size groups were found for the other regions but those ranged between 2.0 – 11.9% for locomotion and 1.6 – 12.6% for prey size (Table 4.6).

The interaction of allometry and ecology in vertebral regions

As stated above, the interaction factor between ecological groups and centroid size was significant and exhibited its highest values (Table 4.6) for the T10-L7 region, demonstrating that species belonging to different ecological groups displayed distinct shape versus size relationships in the posterior presacral vertebrae. Plots of the predicted allometric trajectories for each ecological factor on both datasets are presented (Fig. 4.3A and B). The analysis using prey size groups for categorisation showed that, while 'small' and 'big' prey size groups possessed allometric trajectories that were very similar in slope

distance (p-value > 0.1, Table 4.7), the 'mixed' prey size group's trajectory exhibited a slope distance that was significantly different from both the large and small prey size groups (p-value << 0.05). However, differences in the slope distance of the allometric trajectories between 'large' and 'mixed' prey size groups were not significant after Bonferroni correction (i.e., p-value > 0.006).

Table 4.7: Pairwise comparisons between allometric trajectories of locomotion and prey size categories showing the p-value for the comparisons between the distances and angles of their slopes. Statistically significant values (i.e., p-value < 0.05) are shown in bold. Correlation which are not significant after Bonferroni correction (i.e., p-value > 0.006) are marked with an asterisk.

	ALLOMETRIC TRAJECTORY	
	SLOPE DISTANCE	**SLOPE ANGLE**
	P-VALUE	**P-VALUE**
LOCOMOTION		
ARBOREAL X CURSORIAL	0.558	0.997
ARBOREAL X SCANSORIAL	**0.002**	0.839
ARBOREAL X TERRESTRIAL	**0.001**	0.212
CURSORIAL X SCANSORIAL	**0.002**	0.864
CURSORIAL X TERRESTRIAL	**0.002**	0.103
SCANSORIAL X TERRESTRIAL	**0.003**	**0.003**
PREY SIZE		
LARGE X MIXED	**0.007***	0.137
LARGE X SMALL	0.107	**0.008***
MIXED X SMALL	**0.002**	0.091

Slope angles were significantly different between the 'large' and 'small prey' categories, but not after Bonferroni correction.

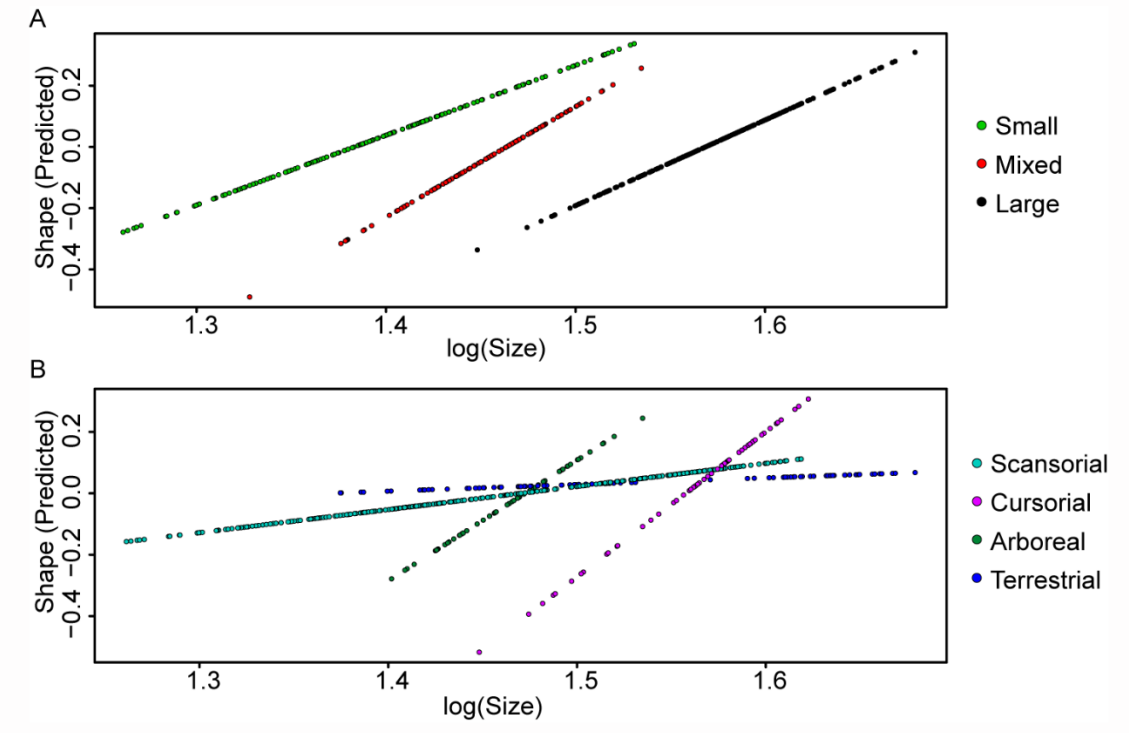

Fig. 4.3: Allometric trajectories displaying the differences in the predicted shape:size relationship between ecological groups. (A): Species groups by their prey size, (B): species grouped by locomotory category.

Grouping species by their locomotory modes resulted in allometric trajectories that were similar in slope distance between 'arboreal' and 'cursorial' groups (p-value >> 0.05), but both differed in all other pairwise comparisons between locomotory groups (p-value << 0.05). Slope angles were only significantly different between the 'terrestrial' and 'scansorial' subsets (p-value << 0.05).

Ecological signal across the vertebral column

Phenotypic trajectory analysis was first performed using the most inclusive homologous dataset (i.e., C4 – L7) to quantify the shape of the post-atlantoaxial presacral vertebral column (Table 4.8, and Fig. 4.4), followed by analysis of the T10 – L7 region. When species were grouped by prey size specialisation, phenotypic trajectories for the full dataset were significantly different in in shape. The 'small' prey size trajectory was also different from both the 'mixed' and 'big' prey size groups in terms of trajectory size. Grouping species by locomotor mode with the complete dataset was not performed because the MANOVA results for this region exhibited a non-significant correlation with locomotor groups (p-value >> 0.05, Table 4.6).

Analysis of the T10-L7 vertebrae resulted in significant differences in phenotypic trajectories for both ecological factors (Table 4.9, and Fig. 4.5A and B). With prey size categorisation, the phenotypic trajectories were all significantly different in direction. The 'small' prey size trajectory was also different from both the 'mixed' and 'big' prey size groups in terms of shape. Locomotor group trajectories were different in direction for all pairwise comparisons, except between the 'scansorial' and 'terrestrial' groups. In terms of shape, the 'cursorial' phenotypic trajectory was statistically different from the 'arboreal' and 'scansorial' trajectories, but only before Bonferroni correction and not after (p-value < 0.05 but > 0.006, respectively).

Table 4.8: Pairwise comparisons between phenotypic trajectories of 'C4-L7' of prey size categories. Statistically significant values (i.e., p-value < 0.05) are shown in bold. All significant correlations remained significant after Bonferroni correction (i.e., p-value < 0.02).

	Phenotypic Trajectory		
	Size p-value	**Direction p-value**	**Shape p-value**
Prey size			
Large x Mixed	0.639	0.233	**0.001**
Large x Small	**0.001**	0.123	**0.001**
Mixed x Small	**0.001**	0.237	**0.001**

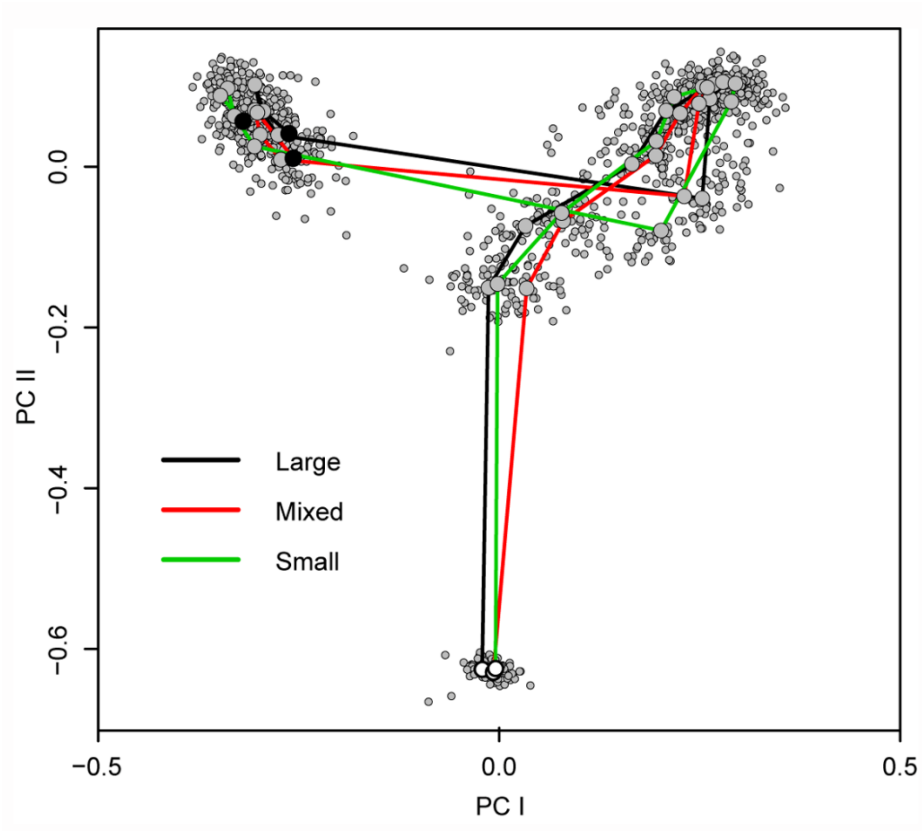

Fig. 4.4: Phenotypic trajectory analysis (PTA) of post-atlantoaxial presacral vertebrae (i.e., C4 – L7) grouped by prey size categories. Larger-sized circles show the average shape location of each individual group per stage. White-filled circles represent the first stage of the trajectory, grey-filled circles represent all intermediate stages, and black-filled circles mark the final stage of each trajectory.

Table 4.9: Pairwise comparisons between phenotypic trajectories of the 'T10-L7' region of prey size and locomotory categories. Statistically significant values (i.e., p-value < 0.05) are shown in bold. Pairwise comparisons which were not significant after Bonferroni correction (i.e., p-value > 0.006) are marked with an asterisk.

	PHENOTYPIC TRAJECTORY		
	SIZE	**DIRECTION**	**SHAPE**
	P-VALUE	**P-VALUE**	**P-VALUE**
LOCOMOTION			
ARBOREAL X CURSORIAL	0.829	**0.001**	**0.012***
ARBOREAL X SCANSORIAL	0.759	**0.001**	0.211
ARBOREAL X TERRESTRIAL	0.933	**0.001**	0.208
CURSORIAL X TERRESTRIAL	0.744	**0.001**	0.180
CURSORIAL X SCANSORIAL	0.890	**0.001**	**0.010***
SCANSORIAL X TERRESTRIAL	0.548	0.144	0.997
PREY SIZE			
LARGE X MIXED	0.203	**0.001**	0.072
LARGE X SMALL	0.955	**0.001**	**0.004**
MIXED X SMALL	0.228	**0.001**	**0.002**

Discussion

When combined, analyses of the relationship among 3D vertebral shape, size, ecology, and phylogeny provide a more complete understanding of the forces shaping the evolution of the felid vertebral column. The results reported here have confirmed our initial hypotheses on ecological drivers in the vertebral column shape differentiation in felids, and we have detailed how

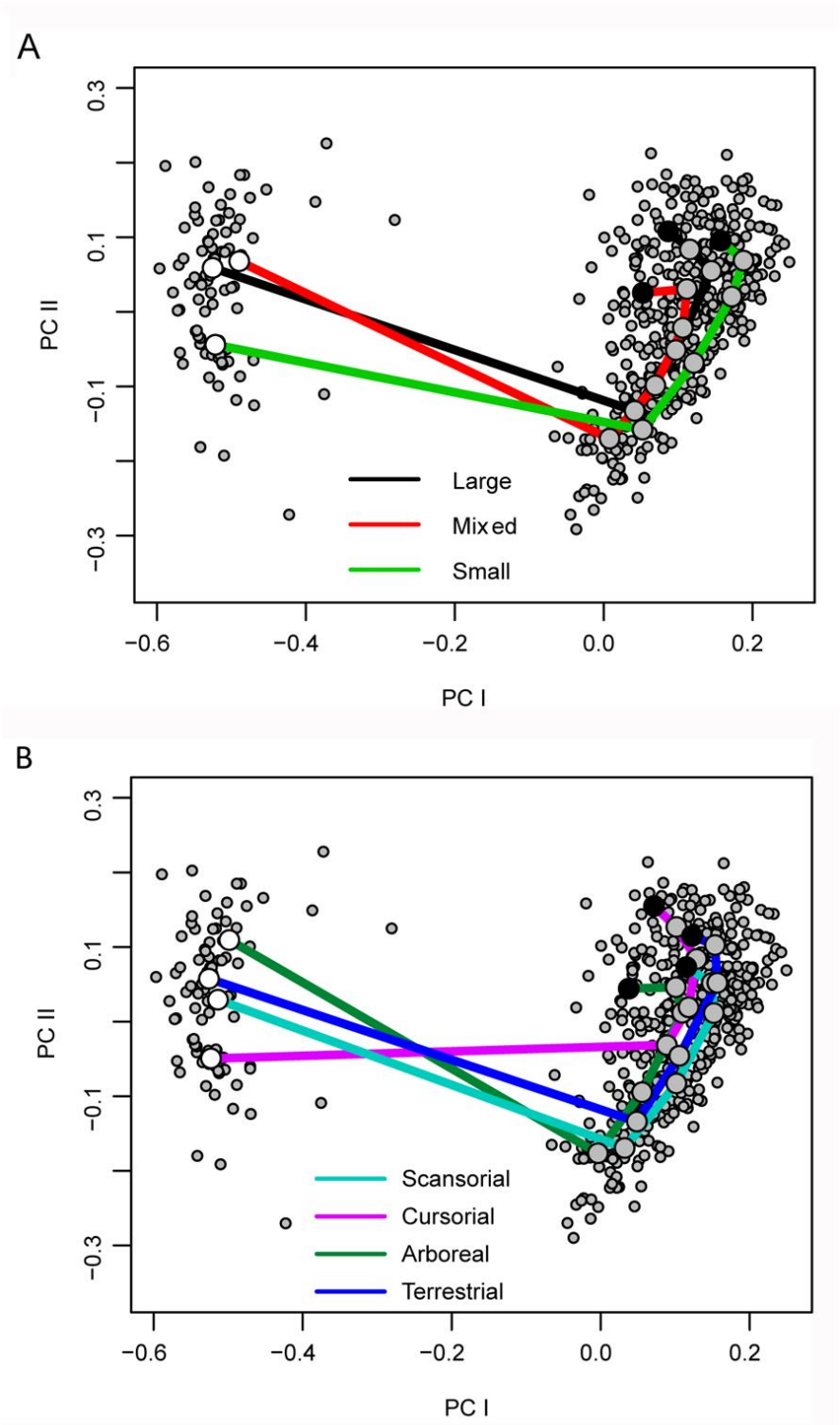

Fig. 4.5: Phenotypic trajectory analysis (PTA) of vertebrae in the T10 – L7 region grouped by prey size (A) and locomotory (B) categories. Larger-sized circles show the average shape location of each individual group per stage. White-filled circles represent the first stage of the trajectory, grey-filled circles represent all intermediate stages, and black-filled circles mark the final stage of each trajectory.

specialisation towards the observed ecologies correlates with regionalisation of the presacral axial skeleton. While vertebrae in the anterior-most region of the felids' vertebral columns (i.e., atlas and axis, but also C6, T1, and T2) were more phylogenetically conservative in shape, the posterior regions of the vertebral column showed a stronger influence of ecological specialisations. That the strongest size and ecology correlations are observed in this more caudal region of the presacral vertebral column (i.e., T10 – L7; see Appendix 4: Supplementary information for similar results on the dataset using the accessory processes landmarks) supports the inference that this region may be subjected to stronger selection, or equally to weaker evolutionary constraints, and might present greater evolutionary respondability across felids, or even more broadly. This observation agrees with the work by Jones and German (2014), in which they found that, in mammals, centrum length varied the most in the lumbar region both through ontogeny and interspecifically. As an osteological measurement that is informative towards the degree of passive robustness at intervertebral joints (Shapiro 1995; Koob and Long 2000; Shapiro 2007; Pierce et al. 2011), centrum length can be used to make inferential comparisons of resistance to intervertebral bending and general biomechanical properties between species or ecological groups. An additional PCA limited to the T10 – L7 vertebrae (post-diaphragmatic homologous dataset) (Fig. 4.2C) shows that the anteroposterior vertebral axis, which

primarily represents centrum length, is one of the main contributors to variation in this dataset.

When compared to our previous work on the linear morphological change in the felid axial skeleton (Chapter 3; Randau et al. 2016b), our present study supports our general conclusions of regionalisation of ecological signal in the vertebral column, with stronger locomotor signal present in the posterior region. However, contrary to results from linear data (Chapter 3; Randau et al. 2016b), the 3D analyses described here also found a significant correlation between vertebral morphology and prey size specialisation. Previous studies of individual vertebral attributes (e.g., centrum length) and different proxies for body size (e.g., total vertebral length, body mass) using length measurements have also identified significant allometry across felids (Chapter 3; Jones 2015; Randau et al. 2016b). Here, we were interested in investigating whether the influence of size (i.e., centroid size) on vertebral multidimensional shape was also regionalised, and most importantly, whether such scaling relationships differed with ecology. As discussed previously (Chapters 2 and 3, and in Material and Methods here), it was not possible to isolate any possible effects that sexual dimorphism may have on vertebral size or shape due to this information being absent from most specimen labels. Nevertheless, as also previously explained, these effects (if present) are understood to be very reduced when compared to the differences across species or ecological

groups explored here, and are indirectly taken into account through the process of scaling (included in the Procrustes Superimposition; Chapter 2) and by the efforts to include all available specimens per species.

Our results reinforce the conclusion that size influences vertebral shape throughout the axial skeleton (i.e., C4 and post-T2 vertebrae), but that these size effects are strongest in T10 and the lumbars (Tables 4.3 and 4.6, and in the last thoracics in Table S3.6). Additionally, we have demonstrated that ecological specialists, especially in terms of locomotory specialisation, indeed exhibit a distinct scaling relationship between shape and centroid size (Table 4.7). Observed differences between prey size subsets were very consistent with both measures of differentiation (slope angle and distance). 'Small' and 'mixed' prey size groups were shown to have distinct allometric vertebral shapes. Although 'large' and 'small' prey groups were not significantly different in terms of the intensity of their allometries (i.e., the Procrustes distances between slopes), they displayed distinct angles in their slope vector, showing that the covariances between the variables are different in these ecological categories (Adams and Collyer 2009; Collyer and Adams 2013). However, these differences between 'large' and 'small' categories, or regarding the intensity of the allometry between 'large' and 'mixed' categories, were not significant after correction, suggesting differences in allometry between prey size specialist groups might be subtle. This could

therefore be one of the factors which caused linear measurements were not to be successful in finding correlations between felid vertebral morphology and specialisation towards prey size (Chapter 3; Randau et al. 2016b). With regards to locomotory specialisation, the two statistical attributes presented different patterns. A better separation between the groups was found in terms of the intensity of their allometries than in their directions. Additionally, it is clear from the observation of regression slopes (Fig. 4.3B) that allometric shape changes are much greater in 'arboreal' and 'cursorial' species and, although significant, size-related changes in the posterior vertebral morphology are less demarked in 'scansorial' and 'terrestrial' felids. Although all but one pairwise comparisons were significantly different with regards to slope distance, the only significant difference in the direction of the allometric trajectories was found between the 'terrestrial' and 'scansorial' categories. Hence, although these two more generalist locomotory groups show a comparatively smaller degree of vertebral allometric scaling, they are still distinct in the relative way size influence vertebral shape variables.

As nearly all individual vertebrae showed some significant correlation between shape and ecology (i.e., Table 4.3), individual analyses alone provide little clarity in terms of regionalisation of ecological and phylogenetic signals. Such differentiation was only possible when sets of vertebrae were analysed together through PTA. With this method, we were able to quantitatively

differentiate the vertebral shape gradient changes between locomotor and prey size specialist felid species, therefore extracting the subtle morphological changes between the recognised ecomorphs in this phenotypically-conserved clade.

Of the two ecological factors examined in this study, only prey size specialisation as an isolated factor exhibited a significant correlation with total vertebral column shape, contrary to the results of linear analyses (Chapter 3; Randau et al. 2016b). This result once again supports the regionalisation of locomotor specialisation in the vertebral column, which was instead found to significantly correlate only to more posterior regions, while also highlighting the increased resolution provided by 3D data. However, because prey size specialisation is directly correlated to the species' body mass (Carbone et al. 1999; Carbone et al. 2007), a significant correlation between this factor and vertebral shape is possibly an indirect reflection of overall body size influence on vertebral 3-dimensional shape.

When we focused our analyses on the vertebral regions with highest correlations between shape and the factors examined, the T10 – L7 trajectories were best able to separate among ecological groups, both for the locomotion and prey size categories (Fig. 4.5A-B). All significant differences between trajectories were found in comparisons of the shape and direction of those trajectories (Table 4.9). This result suggests that no differences in the amount

of shape variation (i.e., trajectory size) were found in the species of felids studied here. Additionally, this differentiation in trajectory direction implies that the differences found were primarily based on the distinct relative covariations of vertebral shape variables between ecological groups throughout the vertebral column (Adams and Collyer 2009; Collyer and Adams 2013). More interestingly put, these differences in trajectory direction between groups are evidence of ecological divergence between those groups (Stayton 2006; Adams et al. 2013). As it follows, the only two groups that did not differ significantly in trajectory direction (the 'scansorial' and 'terrestrial' groups) show ecological convergence in the shape of the posterior vertebral column.

Combining the PTA and posterior region PCA results (Fig. 4.2C) provides additional information on the changes in vertebral morphology correlated with cursoriality in felids. Cheetahs (*Acinonyx jubatus*), as the species represented by the 'cursorial' locomotory group, presented an average lumbar morphology that exhibited longer centra, and overall less shortening of the centrum from L1 to L7, which could be visualised by the trajectory lumbar points presenting lower values on PC1, and higher values on PC2 (Fig. 4.5B). The relative length of centra has been shown to be associated with the degree of flexibility between two consecutive vertebrae (Koob & Long, 2000; Long et al., 1997; Pierce, Clack & Hutchinson, 2011), and results from a study by Jones

(2015) on linear vertebral dimensions revealed allometric shortening of the lumbar region in felids (but see Chapter 3, Randau et al. 2016b, for alternative results showing isometric scaling of the lumbar region in this family, albeit with a different sample). Ergo, having lumbar vertebrae that are relatively longer might indeed contribute to greater sagittal bending, and contribute to having the longer stride lengths observed in this highly specialised felid (Hildebrand 1959).

The vertebral column has been underrepresented in the functional morphology and morphometric literature, but recent studies have shown that vertebral form carries rich developmental and ecomorphological signals. Here, through multivariate statistical analyses, we have demonstrated that the use of geometric morphometrics to study the axial skeleton can offer even more detailed ecomorphological information than what has been reported by linear studies. Additionally, we have here provided the first application of a method that allows for the shape analysis of a contiguous sequence of vertebrae as functionally linked osteological structures.

We have shown that ecological correlates influence the shape of the vertebral column heterogeneously, specifically with discrete regions such as the posterior axial skeleton presenting higher correlation with both locomotory and prey size specialisation. Furthermore, we suggest that the post-T10

vertebrae may be the most ecologically adaptable region among felid species. While anterior vertebrae may either have evolved under stronger phylogenetic constraints or are more ecologically conservative, posterior vertebrate show clearer differentiation between ecomorphs in Felidae.

Future studies, which may benefit from focusing on a more restricted species range, or on smaller vertebral regions, would gain from including vertebrae that were not analysed here in order to compare the general patterns found to specific complete regional trends.

Appendix 4.1

Table S4.1: Museum numbers for specimens used in the analyses. Museum abbreviations are as follows: NHM: Natural History Museum, London; UMCZ: University Museum of Zoology, Cambridge; MNHN: Muséum National d'Histoire Naturelle, Paris; MCZ: Harvard Museum of Natural History, Cambridge; AMNH: American Museum of Natural History, New York; FMNH: Museum of Natural History, Chicago; USNM: Smithsonian National Museum of Natural History, Washington D.C.

SPECIES	**SPECIMEN NUMBER**
Acinonyx jubatus	AMNH119654
	AMNH119655
	AMNH119656
	AMNH119657
	AMNH36426
	FMNH127834
	FMNH34589
	FMNH57826
	FMNH60447
	FMNH60535
	MNHN1933 442
	NHM 1940-1-20-17
	USNM520539
	USNM521037
Felis catus	AMNH 248700
	MCZ 58665
	NHM 1936 2 5 20
	NHM 1952 10 20 4
	NHM 1988 1
	NHM 2002 161
	USNM 396268
	USNM 396271
	USNM 396392
	USNM 397631
	USNM 398871
	USNM 398991
	USNM A21665
Leopardus pardalis	AMNH 14022
	AMNH 214744

	AMNH 248728
	FMNH 68895
	FMNH 93174
	MNHN 1998 1866
	MNHN 2005 282
	MNHN A3456
	USNM 271094
	USNM A14182
Leptailurus serval	AMNH 34767
	FMNH 104800
	FMNH 127843
	FMNH 44438
	FMNH 60491
	NHM 1845 9 25 23
	NHM 1855 6 30 2
	NHM 1966 7 11 1
	NHM 2006 550
	USNM 521039
	USNM 548666
Neofelis nebulosa	AMNH 35273
	FMNH 104730
	FMNH 183653
	FMNH 54304
	MNHN 1961 217
	MNHN 1980 16
	NHM 1854 6 14 2
	NHM 1965 1 18 1
	USNM 399291
	USNM 545387
Panthera leo	AMNH 6260
	AMNH 85147
	AMNH 85149
	FMNH 127839
	FMNH 49340
	MCZ 13273
	MCZ 20976
	MCZ 62919
	MCZ 9487
	USNM 172677
	USNM A22705
Panthera pardus	AMNH 186944
	AMNH 54462
	AMNH 54854
	MNHN 1876 711
	MNHN 1892 1079
	MNHN 1898 100

	MNHN 1906 454
	MNHN 1945 70
	MNHN A13045 1844
	MNHN A7932
	MNHN BII 4
	MNHN CG1998 582
	NHM 1880 2 16 1
	NHM 1940.1.20.18
	USNM 15684
	USNM 258660
	USNM 270126
	USNM 303320
Prionailurus bengalensis	FMNH 121228
	FMNH 99363
	NHM 1309b 1858
	NHM 1979 2895
	NHM 77 2896
	USNM 317282
	USNM 317283
	USNM 330710
Puma concolor	AMNH10259
	AMNH135341
	AMNH181997
	AMNH90213
	FMNH129338
	FMNH129339
	FMNH206424
	MNHN1937 4
	MNHNCG1883 56
	NHM 1855-12-2-6
	USNM A21526
	USNM A21528
	USNM264166
	UMCZK5745

Table S4.2: Landmark descriptions.

VERTEBRA	LANDMARK	DESCRIPTION
ATLAS	1	Anterior mid-point of dorsal arch
	2	Anterior mid-point of ventral arch
	3	Anterior lateral-most tip of left transverse process
	4	Anterior lateral-most tip of right transverse process
	5	Dorso-anterior-most tip of left pre-zygapophysis
	6	Dorso-anterior-most tip of right pre-zygapophysis
	7	Posterior mid-point of dorsal arch
	8	Posterior mid-point of ventral arch
	9	Posterior lateral-most tip of left transverse process
	10	Posterior lateral-most tip of right transverse process
	11	Posterior-most tip of left post-zygapophysis
	12	Posterior-most tip of right post-zygapophysis
AXIS	1	Anterior-most point at tip of dens
	2	Ventral mid-point at base of dens
	3	Anterior-most point of neural spine
	4	Posterior ventral mid-point of centrum
	5	Posterior left lateral-most point of width of centrum
	6	Posterior right lateral-most point of width of centrum
	7	Posterior left dorso-lateral point of centrum
	8	Posterior right dorso-lateral point of centrum
	9	Posterior dorsal mid-point of the neural canal.
	10	Dorsal posterior-most point at tip of neural spine

	11	Left lateral-most posterior tip of transverse process
	12	Right lateral-most posterior tip of transverse process
	13	Posterior-most dorsal point of left post-zygapophysis
	14	Posterior-most dorsal point of right post-zygapophysis
HOMOLOGOUS DATASET		
C4 - L7	1	Anterior ventral mid-point of centrum
	2	Anterior dorsal mid-point of centrum
	3	Anterior left lateral-most point of centrum
	4	Anterior left lateral-most point of centrum
	5	Anterior dorsal-most point of left pre-zygapophysis
	6	Anterior dorsal-most point of right pre-zygapophysis
	7	Lateral-most point of left transverse process
	8	Lateral-most point of right transverse process
	9	Dorsal-most point at tip of neural spine
	10	Posterior ventral mid-point of centrum
	11	Posterior dorsal mid-point of centrum
	12	Posterior Left lateral-most point of centrum
	13	Posterior right lateral-most point of centrum
	14	Posterior dorsal mid-point of the neural canal
	15	Posterior-most point of left post-zygapophysis
	16	Posterior-most point of right post-zygapophysis
ACCESSORY PROCESS DATASET		
T11 - L4	1	Anterior ventral mid-point of centrum
	2	Anterior dorsal mid-point of centrum

3	Anterior left lateral-most point of centrum
4	Anterior left lateral-most point of centrum
5	Anterior dorsal-most point of left pre-zygapophysis
6	Anterior dorsal-most point of right pre-zygapophysis
7	Posterior-most point of tip of left accessory process
8	Posterior-most point of tip of right accessory process
9	Dorsal-most point at tip of neural spine
10	Posterior ventral mid-point of centrum
11	Posterior dorsal mid-point of centrum
12	Posterior Left lateral-most point of centrum
13	Posterior right lateral-most point of centrum
14	Posterior dorsal mid-point of the neural canal
15	Posterior-most point of left post-zygapophysis
16	Posterior-most point of right post-zygapophysis

Table S4.3: Principal component results from the 'C4-L7' analyses, showing results for all PCs.

PRINCIPAL COMPONENT	EIGENVALUE	PROPORTION OF VARIANCE	CUMULATIVE PROPORTION
PC1	0.244	0.439	0.439
PC2	0.185	0.251	0.691
PC3	0.142	0.148	0.839
PC4	0.093	0.064	0.903
PC5	0.062	0.028	0.931
PC6	0.041	0.012	0.943
PC7	0.033	0.008	0.951
PC8	0.031	0.007	0.958
PC9	0.025	0.005	0.963
PC10	0.024	0.004	0.967
PC11	0.022	0.004	0.971
PC12	0.020	0.003	0.973
PC13	0.019	0.003	0.976
PC14	0.019	0.003	0.979
PC15	0.018	0.002	0.981
PC16	0.017	0.002	0.983
PC17	0.015	0.002	0.985
PC18	0.014	0.002	0.986
PC19	0.014	0.001	0.988
PC20	0.013	0.001	0.989
PC21	0.012	0.001	0.990
PC22	0.011	0.001	0.991
PC23	0.011	0.001	0.992
PC24	0.010	0.001	0.992
PC25	0.010	0.001	0.993
PC26	0.010	0.001	0.994
PC27	0.009	0.001	0.995
PC28	0.009	0.001	0.995
PC29	0.009	0.001	0.996
PC30	0.008	0.001	0.996
PC31	0.008	0.000	0.997
PC32	0.008	0.000	0.997

PC33	0.007	0.000	0.997
PC34	0.007	0.000	0.998
PC35	0.007	0.000	0.998
PC36	0.007	0.000	0.998
PC37	0.006	0.000	0.999
PC38	0.006	0.000	0.999
PC39	0.006	0.000	0.999
PC40	0.006	0.000	0.999
PC41	0.005	0.000	1.000
PC42	0.005	0.000	1.000
PC43	0.004	0.000	1.000
PC44	0.001	0.000	1.000
PC45	1.20E-16	0.00E+00	1.00E+00
PC46	6.50E-17	0.00E+00	1.00E+00
PC47	5.54E-17	0.00E+00	1.00E+00
PC48	3.94E-17	0.00E+00	1.00E+00

Table S4.4: Principal component results from the 'T10-L7' analyses, showing all PCs:

PRINCIPAL COMPONENT	EIGENVALUE	PROPORTION OF VARIANCE	CUMULATIVE PROPORTION
PC1	0.216	0.639	0.639
PC2	0.103	0.145	0.784
PC3	0.065	0.058	0.842
PC4	0.052	0.037	0.879
PC5	0.041	0.023	0.902
PC6	0.035	0.017	0.919
PC7	0.031	0.013	0.932
PC8	0.025	0.009	0.941
PC9	0.025	0.008	0.949
PC10	0.021	0.006	0.955
PC11	0.020	0.005	0.960
PC12	0.018	0.005	0.965

PC13	0.017	0.004	0.969
PC14	0.016	0.003	0.972
PC15	0.015	0.003	0.975
PC16	0.014	0.003	0.978
PC17	0.013	0.002	0.980
PC18	0.012	0.002	0.982
PC19	0.011	0.002	0.984
PC20	0.011	0.002	0.986
PC21	0.010	0.001	0.987
PC22	0.009	0.001	0.988
PC23	0.009	0.001	0.989
PC24	0.009	0.001	0.990
PC25	0.009	0.001	0.991
PC26	0.008	0.001	0.992
PC27	0.008	0.001	0.993
PC28	0.008	0.001	0.994
PC29	0.008	0.001	0.995
PC30	0.007	0.001	0.995
PC31	0.007	0.001	0.996
PC32	0.006	0.001	0.997
PC33	0.006	0.001	0.997
PC34	0.006	0.000	0.998
PC35	0.006	0.000	0.998
PC36	0.006	0.000	0.998
PC37	0.005	0.000	0.999
PC38	0.005	0.000	0.999
PC39	0.005	0.000	0.999
PC40	0.005	0.000	1.000
PC41	0.004	0.000	1.000
PC42	0.000	0.000	1.000
PC43	0.000	0.000	1.000
PC44	0.000	0.000	1.000
PC45	0.000	0.000	1.000
PC46	0.000	0.000	1.000
PC47	0.000	0.000	1.000
PC48	0.000	0.000	1.000

Supplementary Information:

In order to include the analyses regarding the morphology of vertebrae T11, T12 and T13, which lack transverse processes, we selected two alternative landmarks to represent the locations of the right and left accessory processes of these vertebrae (Fig. S4.1 A and B, landmarks 7 and 8). Accessory processes are slender processes that originate on the pedicle and extend posteriorly, laterally to each postzygapophyses, and reinforce the interzygapophyseal joint (De Iuliis and Pulerà 2006). As accessory processes are also present in vertebrae L1, L2 and L4, we have also analysed these vertebrae with the accessory processes landmarks. The landmarks for vertebrae C4 – T10 were not changed.

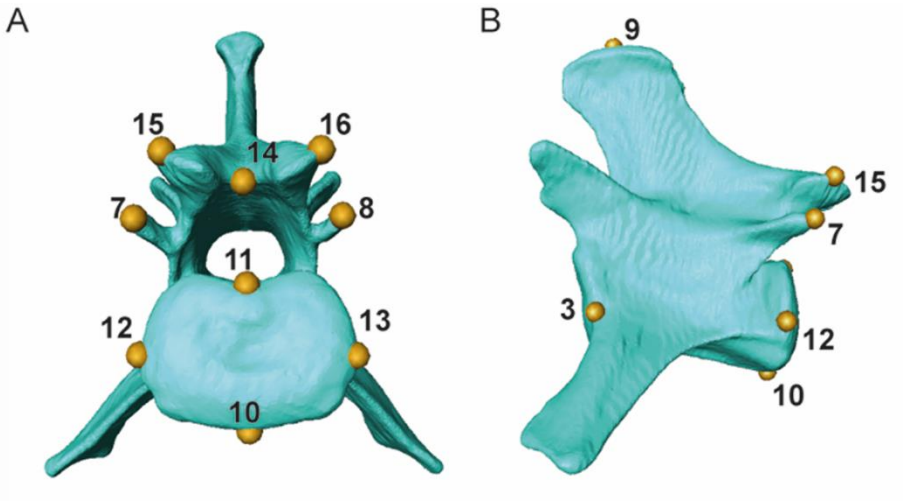

Fig. S4.1: L1 morphology in posterior (A) and lateral (B) views, showing the location of three-dimensional landmarks. Landmarks '7' and '8' represent the accessory processes. Vertebral images are from CT scans of *Acinonyx jubatus* (Cheetah). Landmark descriptions can be found in Table S4.2.

Here we report the results of the Principal Component analysis, and analyses of phylogenetic and ecological signal (detailed in the main text), but using this dataset that differed in the identity of vertebrae and landmarks post-T10. In addition to analyses being performed on individual vertebrae (e.g., T11), they were also performed on the complete 'accessory process' (C4 – L4) dataset, and groups of vertebrae composing distinct vertebral regions within those (i.e., C4 – T13, T1 – T13, T1 – L4, T10 – T13, T10 – L4, L1 – L4).

Supplementary results

Phylogenetic and ecological signal in individual and regional vertebral shape

PC axes 1 – 4 explained >90% of the variance (Table S4.5), and the three general groups on PC1 x PC2 were the 'C4 and T11' cluster, the 'end-cervicals to T10' cluster (i.e., C6, C7, T1, T2, T4, T6, T8, and T10) and the 'end-thoracics + lumbars' cluster (i.e., T12, T13, L1, L2, and L4). Again, the extreme shapes at the ends of the PC1 and PC2 spectrums showed general deformations on the three dimensions. The PC1 minimum and maximum shape values differed in general anteroposterior, mediolateral and dorsoventral dimensions, but also in overall size. In this case, due to a different distribution of the vertebrae on the morphospace, compared to PC1 maximum shape, the PC1 minimum shape described elongation of the anteroposterior axis, with larger centrum

Table S4.5: Principal component results from the 'C4-L4' analyses.

PRINCIPAL COMPONENT	EIGENVALUE	PROPORTION OF VARIANCE	CUMULATIVE PROPORTION
PC1	0.278	0.474	0.474
PC2	0.216	0.288	0.761
PC3	0.143	0.125	0.886
PC4	0.068	0.028	0.914
PC5	0.059	0.022	0.936
PC6	0.039	0.009	0.945
PC7	0.038	0.009	0.954
PC8	0.029	0.005	0.959
PC9	0.026	0.004	0.964
PC10	0.024	0.004	0.967
PC11	0.023	0.003	0.970
PC12	0.023	0.003	0.974
PC13	0.020	0.002	0.976
PC14	0.019	0.002	0.978
PC15	0.018	0.002	0.980
PC16	0.017	0.002	0.982
PC17	0.016	0.002	0.983
PC18	0.016	0.002	0.985
PC19	0.016	0.002	0.987
PC20	0.014	0.001	0.988
PC21	0.014	0.001	0.989
PC22	0.013	0.001	0.990
PC23	0.012	0.001	0.991

PC24	0.012	0.001	0.992
PC25	0.011	0.001	0.993
PC26	0.011	0.001	0.993
PC27	0.010	0.001	0.994
PC28	0.010	0.001	0.995
PC29	0.010	0.001	0.995
PC30	0.010	0.001	0.996
PC31	0.009	0.001	0.996
PC32	0.009	0.001	0.997
PC33	0.009	0.000	0.997
PC34	0.008	0.000	0.998
PC35	0.008	0.000	0.998
PC36	0.008	0.000	0.998
PC37	0.008	0.000	0.999
PC38	0.007	0.000	0.999
PC39	0.007	0.000	0.999
PC40	0.006	0.000	1.000
PC41	0.006	0.000	1.000
PC42	0.003	0.000	1.000
PC43	0.002	0.000	1.000
PC44	0.001	0.000	1.000
PC45	0.000	0.000	1.000
PC46	0.000	0.000	1.000
PC47	0.000	0.000	1.000
PC48	0.000	0.000	1.000

length and inter-zygapophyseal distance. This extreme shape also showed augmentation of the mediolateral dimension, with larger centrum width and intra-zygapophyseal distances, and larger distances between the transverse/accessory processes. However, this PC1 minimum shape exhibited compression along the dorsoventral axis, with shorter centrum, neural canal and neural spine heights. The main feature change described by the extremes of the PC2 axis concerned the elongation of the anteroposterior axis in the minimum end of the spectrum, with larger centrum lengths and inter-zygapophyseal distances, but this side of the spectrum also exhibited some compression in the dorsoventral axis and a slightly smaller overall size.

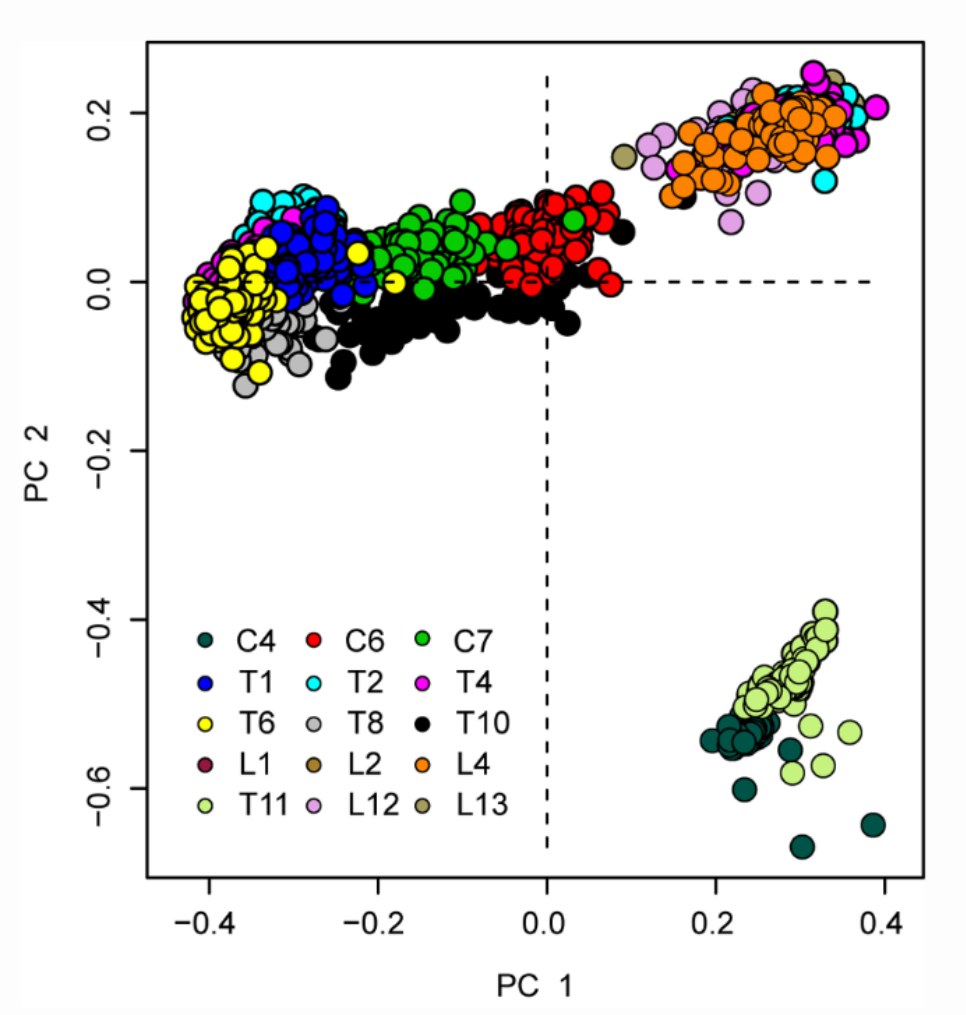

Fig. S4.1: Principal Component Analysis plot using the 'C4 – L4' dataset, with accessory processes landmarks for vertebrae T11 – L4. Vertebral types are identified by colour.

MANOVA results for the correlation tests between vertebral shape and centroid size and ecology are displayed in Table S4.6. No phylogenetic signal was found on shape or centroid size for the vertebrae analysed here (Table S4.7). Interestingly, as in the homologous landmarks-dataset, the strongest ecological signal was found in the posterior region of the vertebral column, and here when the lumbars (L1 – L4) were analysed separately (Table S4.8).

Quantification of the influence of those factors on shape showed that locomotory groups and centroid size significantly explained ~16.4% and 13.6% of shape variance, respectively. Prey size influenced shape at ~3.6%.

Table S4.6: Factorial MANOVA results for analyses of individual vertebrae with accessory processes' landmarks. Correlations which are not significant after Bonferroni correction (i.e., p-value > 0.008) are marked with an asterisk.

VERTEBRA	**CENTROID SIZE**		**LOCOMOTION**		**PREY SIZE**	
	P-VALUE	**R^2**	**P-VALUE**	**R^2**	**P-VALUE**	**R^2**
T11	0.001	0.150	0.001	0.114	0.005	0.046
T12	0.001	0.125	0.003	0.048	0.012*	0.038
T13	0.001	0.109	0.001	0.091	0.002	0.044
L1	0.001	0.108	0.001	0.113	0.018*	0.035
L2	0.001	0.150	0.001	0.136	0.001	0.074
L4	0.001	0.161	0.001	0.130	0.001	0.065

Ecological signal across the vertebral column

Similarly to the results of the complete homologous dataset, results of PTA for the complete analogous dataset were significant when using prey size as a factor (p-value < 0.05), but not with locomotory categories. Prey size phenotypic trajectories were significantly different between the three groups

in all trajectory attributes (p-value < 0.001), with the exception of the pairwise comparison in trajectory size between 'large' and 'mixed' prey specialists (p-value > 0.05).

Table S4.7: Phylogenetic signal results for mean shape and centroid size per individual vertebrae with accessory processes' landmarks.

VERTEBRA	K	MEAN SHAPE	K	MEAN CENTROID SIZE
	VALUE	P-VALUE	VALUE	P-VALUE
T11	0.616	0.685	0.668	0.561
T12	0.842	0.065	0.544	0.842
T13	0.784	0.167	0.951	0.144
L1	0.641	0.572	0.706	0.494
L2	0.749	0.360	0.537	0.880
L4	0.714	0.541	0.709	0.945

Table S4.8: Factorial MANOVA results for analyses of vertebral regions with accessory processes' landmarks for vertebrae in the T11 – L4 region. The highest correlation (R^2) values for both prey size and locomotion were found in the L1 – L4 region and are shown in bold. The correlations which were not statistically significant (i.e., p-value > 0.05) are underlined. Correlations which are not significant after Bonferroni correction (i.e., > 0.007) are marked with an asterisk.

	CENTROID SIZE		PREY SIZE		LOCOMOTION	
REGION	P-VALUE	R^2	P-VALUE	R^2	P-VALUE	R^2
C4 - L4	0.001	0.009	0.038*	0.003	<u>0.169</u>	
C4 - T13	0.001	0.008	<u>0.149</u>		<u>0.551</u>	
T1 - T13	0.001	0.012	<u>0.103</u>		<u>0.402</u>	
T1 - L4	0.001	0.009	0.001	0.016	0.001	0.026
T10 - T13	0.008*	0.013	0.001	0.035	0.001	0.062
T10 - L4	0.001	0.027	0.001	**0.058**	0.001	0.054
L1 - L4	0.001	**0.136**	0.001	0.036	0.001	**0.164**

Chapter 5. Unravelling intravertebral integration, modularity and disparity in Felidae (Mammalia).

Published as: Randau, M., & Goswami, A. (2017). Unravelling intravertebral integration, modularity and disparity in Felidae (Mammalia). *Evolution and Development*, *19*, 85-95.

Abstract

Morphological integration and modularity, which describe the relationships among morphological attributes and reflect genetic, developmental, and functional interactions, have been hypothesized to be major influences on trait responses to selection and thus morphological evolution.

The mammalian presacral vertebral column shows little variation in vertebral count and therefore specialisation for function occurs primarily through modification of vertebral shape. However, vertebral shape has been suggested to be under strong control from developmental canalisation, although this has never been explicitly tested. Here we assess hypotheses of developmental modules in the vertebrae of felids to determine whether developmental interactions are a primary influence on vertebral modularity. Additionally, we analyse the magnitudes of both intravertebral integration and disparity to evaluate if level of integration varies along the vertebral column and, if so, whether integration and disparity are associated.

Our results confirm the hypothesis of vertebral developmental modularity, with most presacral vertebrae displaying two modules. Exceptions are concentrated in the boundaries among traditional and functional regions, suggesting that intravertebral modularity may reflect larger-scale modularity of the felid vertebral column. We further demonstrate that overall integration and disparity are highest in posterior vertebrae, thus providing an empirical example of integration potentially promoting greater morphological responses to selection.

Introduction

The dichotomy between maximum individual trait adaptation and cohesion between functioning parts is one that directly affects phenotypic response to selection (Klingenberg et al. 2003; Badyaev et al. 2005; Hansen and Houle 2008; Porto et al. 2009; Goswami and Polly 2010b; Goswami et al. 2014). The basis for understanding how organisms are organised was laid by the seminal work by Olson and Miller (1958) in which they described the fundamental concepts of phenotypic integration and modularity as can be ascertained through quantification of patterns of trait covariation. In line with these, modules are a set of traits that show higher covariation among them than with other parts of the organism due to shared genetic or developmental origins or function,

while integration is the overall pattern of intercorrelation (e.g., Hansen and Houle 2008; Klingenberg 2008; Goswami and Polly 2010a; Klingenberg and Marugán-Lobón 2013). Interestingly, however, those two definitions are not contradictory and complex traits may present overall high integration and still be modular (Bookstein 2015), such as the mammalian skull (Goswami 2006a, 2006b; Goswami and Polly 2010b). Specifically, trait units might present significant covariation among the whole structure (i.e., integration), while still showing higher organisation into smaller sets which present consistently higher within-set covariation than across the whole phenotype. Moreover, trait integration has been shown to reflect shared developmental pathways in early ontogeny, postnatal function, and heterochronic shifts (Zelditch and Carmichael 1989; Goswami et al. 2009; Zelditch et al. 2009; Bennett and Goswami 2011; Goswami et al. 2012; Goswami et al. 2014), and to be susceptible to reorganisation by extreme changes in selection (Drake and Klingenberg 2010).

Intravertebral Developmental Modularity

Morphological traits in fully grown organisms may present correlations due to developmental modularity, by which variation in a set of traits is dependent on a common embryonic origin or other shared developmental history (Cheverud 1996; Arthur 1997; Raff and Sly 2000; Arthur 2002; Klingenberg 2003; Buchholtz et al. 2012). However, trying to infer developmental

modularity through the organisation of adult morphology can be problematic due to repatterning of integration through ontogeny (Hallgrímsson et al. 2009). Nevertheless, knowledge of trait developmental origin can be used in confirmatory analyses to test hypotheses of developmental modularity (Klingenberg et al. 2003; West-Eberhard 2003; Klingenberg 2013). Here we test the hypothesis that developmental origins of vertebral components (i.e., centrum *versus* neural spine attributes) dictate adult vertebral morphology in cats (i.e., Felidae, Mammalia).

Mammalian vertebral column development has been suggested to be under strong canalisation and developmental stability (Galis 1999; Narita and Kuratani 2005; Wellik 2007; Buchholtz and Stepien 2009; Hautier et al. 2010; Müller et al. 2010; Asher et al. 2011; Varela-Lasheras et al. 2011; Buchholtz et al. 2012; Fleming et al. 2015), and the derivation of somitic segments into the tissues involved into limb and vertebral column formation has been described in great detail (Christ et al. 2007).

For mammals, in which presacral vertebral count shows very little variation when compared to other vertebrate clades (Narita and Kuratani 2005; Müller et al. 2010; Buchholtz et al. 2012; Buchholtz 2014), changes in the axial skeleton are typically manifested in changes in vertebral shape. Buchholtz (2007) summarised the types of evolutionary change that have been observed in vertebral column morphology; those concerning changes in the mammalian

axial skeletal morphology may reflect 'diversifying' or 'skeletogenetic' changes (caused by effects of *Hox* genes and growth factors) or be due to changes in 'module association' of these vertebrae (Raff 1996; Polly et al. 2001; Buchholtz 2007).

Additionally, Christ et al. (2007) have described how vertebral components are derived from distinct somitic origins through segmentation of the sclerotome. The vertebral body (centrum) originates from the ventral and, to a lesser degree, central regions of the sclerotome, while the neural arch, spinous process, pedicles and transverse processes originate from the dorsal and posterior central regions of the sclerotome and integrated somitocoel cells (Fig. 4.1). The condensation of these two vertebral parts has also been shown to be distinct, with the centrum-related sclerotome condensing around the notochord, whilst the same is not true and not yet fully understood for the development of the other vertebral elements (Hall 1977; Christ et al. 2000; Christ et al. 2007). Additionally, Boyd (1976) has confirmed that all presacral vertebrae in cats originate from two ossification centres, the only exception being C2 (axis) with a third ossification centre for the dens.

Trait integration can direct responses to selection

Research in the last few decades has built on the work on integration and modularity by demonstrating how trait relationships can both shape responses to selection and be affected by extrinsic perturbations such as

environmental stress (West-Eberhard 1989; Badyaev and Foresman 2004; Hansen and Houle 2008; Badyaev 2010; Goswami and Polly 2010a; Buchholtz et al. 2012; Cardini and Polly 2013; Clune et al. 2013; Klingenberg and Marugán-Lobón 2013; Goswami et al. 2014; Goswami et al. 2015). Some of the direct ways integration and modularity have been suggested to affect trait evolution are by either constraining or promoting the spectrum of responses to selection (Cheverud 1996; Hansen and Houle 2008; Marroig et al. 2009; Klingenberg and Marugán-Lobón 2013; Sears et al. 2013). Integration has been traditionally hypothesized to constrain these responses to a smaller portion of the morphospace because high correlation among traits means that any change in the trait directly affected by selection can be hindered by stabilising selection on other covarying traits. Similarly, modularity has been hypothesized to counter this effect, by breaking larger sets of correlated traits into smaller modules, allowing newly independent modules to respond more freely (i.e., potentially promoting larger phenotypic variation). However, Goswami et al. (2014) demonstrated through the use of simulation analyses that integration may promote both lower and higher degrees of morphological disparity, and that range in disparity can be considerably larger in correlated traits than in uncorrelated ones, confirming previous hypotheses on the possible effects of integration (Schluter 1996a; Klingenberg 2005). By directing variation along particular axes of the total possible morphospace, the

maximum range of variation can be increased (Schluter 1996a; Goswami et al. 2014).

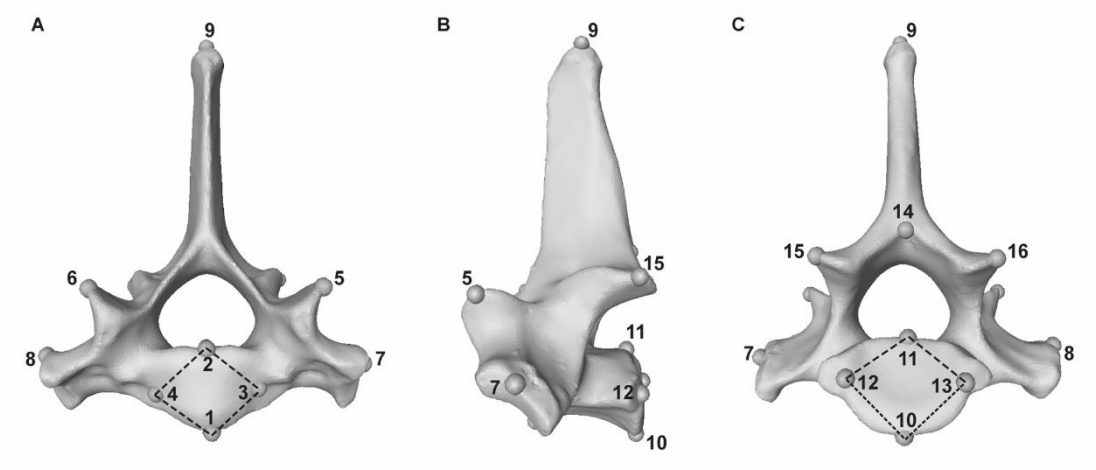

Fig. 5.1: Three-dimensional model of CT scan of T1 vertebrae of *Acinonyx jubatus* (Cheetah, USNM 520539) showing 16 landmarks in anterior (A), lateral (B), and posterior (C) views. Landmarks inside dashed boxes composed the suggested 'centrum' developmental module, while landmarks outside these lines compose the 'neural spine' developmental module. See Table S5.1 for landmark definitions.

Here we first test the hypothesis that developmental origin drives intravertebral modularity, resulting in two intravertebral modules in adult morphology: the centrum and the neural spine. We subsequently quantify the magnitude of overall integration in individual vertebrae of felids by measuring relative eigenvalue standard deviation (Pavlicev et al. 2009) and compare these results to vertebral morphological disparity to determine whether higher integration is associated with higher or lower disparity. We conduct these analyses in the presacral vertebral column of felids and discuss

our results in relation to previous analyses of ecological specialisation in felid vertebral morphology (Randau et al. 2016b) and previous studies of the evolutionary significance of phenotypic integration and modularity.

Material and Methods

Three-dimensional (3D) landmarks were collected on 19 out of the 27 presacral vertebral from nine felid species (*Acinonyx jubatus, Felis catus, Leopardus pardalis, Leptailurus serval, Neofelis nebulosa, Panthera leo, Panthera pardus, Prionailurus bengalensis* and *Puma concolor*; Table S5.1 for specimen numbers) using an Immersion Microscribe G2X (Solution Technologies, Inc., Oella, Maryland). This dataset included the following vertebrae: atlas, axis, C4, C6, C7, T1, T2, T4, T6, T8, T10, T11, T12, T13, L1, L2, L4, L6, and L7 (see Chapter 2 for vertebral selection). These vertebrae cover the extent of presacral vertebral morphology and comprise the boundaries between vertebral regions and immediately preceding and succeeding vertebrae (e.g., C7 and T1, and C6 and T2, respectively). Further selection of vertebrae was based on vertebrae with high-scoring measurements for the Principal Component loadings in a study using linear measurements to characterise the whole presacral column of 22 species of felids (Chapter 3; Randau et al. 2016b). Landmarks were collected

from 108 specimens, ranging from seven to 17 specimens per species, with the final dataset including a total of 1712 individual vertebrae.

In order to capture the most detail in vertebral morphology, and due to morphological differences throughout the vertebral column, different sets of landmarks were collected in some vertebral regions: 12 landmarks were gathered on C1 (atlas), 14 on C2 (axis), 18 on C4, 20 on C6, 16 on C7 – T10, 16 on T11, 17 on T12 – T13, 19 on L1 – L4, and 17 on L6 – L7 (see Table S5.2 for landmarks identity). Additionally, in order to facilitate direct comparisons across as many vertebrae as possible, 16 landmarks are homologous in C4 – T10 and L1-L7, and thus only these landmarks and vertebrae were used in analyses of disparity and an additional analysis of integration for direct comparison to the disparity results (described below in the data analysis section). Vertebrae C1, C2, and T11 – T13 were not included in the disparity analysis due to their unique morphology (e.g., vertebrae T11 – T13 lack transverse processes but present accessory processes).

Data analysis

All analyses were carried out in R version 3.2.3 (R Core Team 2015a), using the 'geomorph' (Adams and Otarola-Castillo 2013; Adams et al. 2015), and 'FactoMineR' (Husson et al. 2016) packages.

Intravertebral modularity

Vertebra-specific landmark coordinates for C1 – L7 were assigned to modules based on models of developmental origins and ossification centres (Table 5.1). All vertebrae were hypothesized to be composed of two developmental modules: 'centrum' and 'neural spine' (Christ et al. 2007) as depicted in Fig. 5.1. Additionally, a three-module hypothesis was also tested for C2 (axis) as the dens has been shown to originate from an additional ossification centre that fuses with the centrum early in vertebral development (Boyd 1976).

Table 5.1: Hypothesized associations of vertebral landmarks in developmental modules. Asterisk (*) demarks the C7 – T10 landmarks which were used as homologous landmarks for the C4 – L7 intervertebral analyses.

	CENTRUM MODULE	**NEURAL-SPINE MODULE**	**DENS MODULE**
ATLAS	2; 8	1; 3 – 7; 9 - 12	
AXIS (2 MODULES)	1; 2; 4 - 8	3; 9 -12	
AXIS (3 MODULES)	4 - 8	3; 9 – 14	1; 2
C4	1 – 4; 10 – 13	5 – 9; 14 – 18	
C6	1 – 4; 12 – 15	5 – 11; 16 – 20	
C7 – T10*	1 – 4; 10 – 13	5 – 9; 14 – 16	
T11	1 – 4; 8 – 11	5 – 7; 12 – 16	
T12 – T13	1 – 4; 9 – 12	5 – 8; 13 – 17	
L1 – L4	1; 2; 6; 7; 10; 11; 13; 14	3 – 5; 8; 9; 12; 15 – 19	
L6 – L7	1; 2; 6; 7; 10; 11; 13; 14	3 – 5; 8; 9; 12; 15 – 17	

The degree of modularity and the significance of these models were evaluated by using two alternative methods: RV coefficient analysis (Escoufier 1973; Klingenberg 2009) and Covariance Ratio analysis (CR; Adams 2016). Both methods are similar in their outputs, but differ in that CR disregards within-trait variation and uses only the covariation between and among traits for its calculations, while RV accounts for both measures. We have chosen to present both results because, while RV has been one of the most used confirmatory analyses of modularity in recent years (Klingenberg 2009; Goswami and Polly 2010c), it has recently been shown to be sensitive to sample size and landmark number (Fruciano et al. 2013; Adams 2016). Significance of the hypothesis of modularity in both methods is obtained by randomly assigning landmarks to 10,000 alternative models of modularity to generate a distribution of values. Significant results are indicated if the observed signal is small (here, p-value < 0.05) relative to the randomly generated distribution.

Accounting for phylogenetic relationships

Modularity results prior to any phylogenetic correction to vertebral shape or analyses are displayed due to the following reasons: 1. the mammalian vertebral column has been suggested to be under strong developmental control and, especially with the Felidae family being very constrained in count, there is no reason to assume that individual felid species should present

distinct developmental pathways to vertebral formation (Narita and Kuratani 2005; Müller et al. 2010; Buchholtz et al. 2012); 2. removal of any potential phylogenetic signal on shape may conceal real patterns of morphological modularity or integration driven by genetic or developmental origins (Polly et al. 2013); 3. tests for phylogenetic signal in shape were significant for only two anterior vertebrae in felids, the atlas and the axis (Chapter 4; Randau et al. 2016a), while tests for phylogenetic signal in both shape and centroid size of all other studied vertebrae were not significant.

Instead, we corrected for grouping multiple species into a single analysis by first calculating a pooled within-species variance-covariance matrix (VCV) for each vertebrae and then used this VCV matrix in CR analysis of vertebral modularity. This pooled within-species VCV matrix was calculated using the 'covW' function in the 'Morpho' package (Schlager 2016) in R. It is important to raise the caveat that this is a new implementation of the CR method, one which has not yet been tested through the use of simulations, and therefore caution should be kept in mind when applying this methodology to other studies. Nevertheless, modularity results both with and without using the pooled within-species VCV matrix were similar and therefore there is no obvious reason to think that the properties of the CR method would not hold in this case.

Overall vertebral integration and disparity

Vertebrae C4 – L7 (excluding T11 – T13) containing the 16 homologous landmarks were individually subjected to a General Procrustes Superimposition for extraction of shape coordinates (i.e., excluding information on size, rotation and translation). The correlation matrix was obtained from these shape coordinates, and this was subsequently used to calculate the singular-value decomposition to generate matrix eigenvalues.

The overall morphological integration per vertebra was calculated using relative eigenvalue standard deviation (i.e., eigenvalue dispersion) as detailed by Pavlicev et al. (2009). High numbers of eigenvalue dispersion indicate strong integration, as variance is concentrated on fewer eigenvectors due to high covariance of traits, at the cost of low variance explained by higher eigenvectors. This measure of integration has been shown to be highly correlated with r^2 (mean squared correlation coefficient, not to be confused with the coefficient of determination R^2) (Marroig et al. 2009; Goswami et al. 2014), and to be independent of trait number, and thus can be readily used for comparison across datasets. Therefore, we also calculated this measure using the specific vertebral landmark datasets for C1, C2, C4, C6, T11, T12 – T13, L1 – L4, and L6 – L7 for maximum shape information, after subjecting individual vertebrae to General Procrustes Superimposition.

Morphological disparity per vertebra (e.g., T1) was calculated on the C4 – L7 shape coordinates (homologous landmarks) both as Procrustes variances and as maximum Procrustes distance between specimens (Zelditch et al. 2012). The Procrustes variance analysis was performed both with and without centroid size as a covariate, as vertebral size has been shown to correlate with shape throughout the spine (Chapters 3 and 4; Randau et al. 2016a; Randau et al. 2016b). Both measures of disparity were calculated first per individual species per vertebra, and then across taxa per vertebra, using the species mean shapes.

Results

Intravertebral modularity

Results from both RV and CR analyses of modularity were consistent in all but one case, and strongly supported the two-module model (p-value < 0.01) for all but six (C2, C7, T1, T8, L6 and L7) of the 19 analysed vertebrae. They differed only with regards to T13, which was marginally significant for the tested modules with RV analysis, but significant when analysed with CR (p-value = 0.051 and 0.011, respectively; Table 5.2). The three-module model tested for C2 was not supported (p-value >> 0.05). When testing the modularity model using the pooled within-species VCV matrix, three vertebrae presented different results: the three-module model was supported

for the axis, and the two-module model was significantly supported for C7 but not for C4. As these are the most conservative results, and similar to the raw RV and CR results, our discussion focuses on them.

Overall vertebral integration and disparity

Results from the eigenvalue dispersion analysis using the homologous only landmarks for C4 – L7 (and therefore not sampling C1, C2, and T10-T13) or the vertebra-specific landmark coordinates were extremely similar for the vertebrae analysed with both datasets (Table 5.3). Values for eigenvalue dispersion ranged from 0.226 to 0.307 in the C4 – L7 homologous dataset (mean 0.267; median 0.263), and from 0.215 to 0.300 in the vertebra-specific C1 – L7 dataset (mean 0.261; median 0.253). Although these values can be considered moderate in the integration spectrum (Pavlicev et al. 2009), in both datasets, vertebrae T10 and L1 – L7 presented the highest values of eigenvalue dispersion (> 0.27), with the addition of C2 and T11 for the vertebra-specific landmarks analysis.

Procrustes variances across species for the C4 – L7 homologous coordinates were the same both before and after accounting for centroid size, and ranged from 0.002 to 0.012, with a mean and a median of 0.005 (Table 5.3). However, only six vertebrae displayed values of Procrustes variance higher than the mean: C4, T10, L1, L2, L4 and L6, with Procrustes variances of 0.006 for all of

Table 5.2: Results from the intravertebral modularity tests for RV and CR analyses and their respective p-values. CR* pooled WG VCV stands for the modified CR test calculated with the pooled within-group variance-covariance matrix. Significant results (p-value < 0.05) are shown in bold.

VERTEBRA	RV	P-VALUE	CR	P-VALUE	CR* (POOLED WG VCV)	P-VALUE
ATLAS	0.267	**0.044**	0.728	**0.032**	**0.727**	**0.016**
AXIS (3 MODULES)	0.490	0.825	1.406	0.781	**0.983**	**0.012**
AXIS (2 MODULES)	0.569	0.642	0.999	0.435	1.034	0.089
C4	0.382	**0.009**	0.772	**0.010**	1.023	0.470
C6	0.438	**0.026**	0.843	**0.008**	**0.843**	**0.000**
C7	0.470	0.174	0.854	0.105	**0.855**	**0.020**
T1	0.510	0.156	0.898	0.102	0.899	0.110
T2	0.508	**0.029**	0.866	**0.009**	**0.866**	**0.000**
T4	0.521	**0.007**	0.895	**0.001**	**0.895**	**0.000**
T6	0.563	**0.037**	0.945	**0.013**	**0.945**	**0.001**
T8	0.454	0.144	0.880	0.053	0.880	0.061
T10	0.512	**0.009**	0.858	**0.003**	**0.859**	**0.000**
T11	0.265	**0.001**	0.649	**0.001**	**0.651**	**0.001**
T12	0.476	**0.007**	0.873	**0.004**	**0.873**	**0.046**
T13	0.506	0.051	0.888	**0.011**	**0.888**	**0.016**
L1	0.507	**0.002**	0.829	**0.000**	**0.831**	**0.000**
L2	0.553	**0.007**	0.870	**0.004**	**0.870**	**0.022**
L4	0.550	**0.021**	0.869	**0.013**	**0.869**	**0.011**
L6	0.701	0.613	1.030	0.282	1.030	0.268
L7	0.749	0.477	1.066	0.452	1.066	0.102

these, except T10 with a variance value of 0.012 (Table 5.3, and Fig. 5.2). Similarly, the maximum Procrustes distance across specimens per vertebra ranged from 0.109 to 0.296, and only five vertebrae (T10, L1, L2, L4 and L6) presented values higher than the mean and median (0.181 and 0.159, respectively). With both measures of disparity, L7 showed values very close to the mean and higher than the disparity values observed for the anterior vertebrae (with the exception of variance in the atlas).

Table 5.3: Overall vertebral integration, quantified by eigenvalue dispersion, and morphological disparity, quantified by Procrustes variance (with and without centroid size as a covariate) and maximum Procrustes distance, across felid species. The 'eigenvalue dispersion-16' column shows the results for the C4 – L7 16 homologous landmarks, while the 'eigenvalue dispersion' values are regarding the C1 – L7 vertebra-specific landmarks. Bold results mark results higher than the mean and median for the eigenvalue dispersion analyses.

VERTEBRA	EIGENVALUE DISPERSION	EIGENVALUE DISPERSION-16	VARIANCE	VARIANCE (WITH SIZE)	MAXIMUM DISTANCE
ATLAS	0.243				
AXIS	**0.278**				
C4	0.253	0.261	**0.006**	**0.006**	0.160
C6	0.215	0.234	0.004	0.004	0.142
C7	0.242	0.242	0.004	0.004	0.146
T1	0.242	0.242	0.003	0.003	0.152
T2	0.251	0.251	0.003	0.003	0.157
T4	*0.265*	0.265	0.003	0.003	0.124
T6	0.248	0.248	0.003	0.003	0.130
T8	0.226	0.226	0.002	0.002	0.109
T10	**0.291**	**0.291**	**0.012**	**0.012**	**0.296**
T11	**0.272**				
T12	0.247				
T13	0.243				
L1	**0.288**	**0.294**	**0.006**	**0.006**	**0.260**
L2	**0.300**	**0.297**	**0.006**	**0.006**	**0.233**
L4	**0.279**	**0.284**	**0.006**	**0.006**	**0.223**
L6	**0.286**	**0.294**	**0.006**	**0.006**	**0.223**
L7	**0.289**	**0.307**	0.005	0.005	0.179
MEAN	0.261	0.267	0.005	0.005	0.181
MEDIAN	0.253	0.263	0.005	0.005	0.159

Table 5.4: Within-species vertebral disparity, measured as Procrustes variance with and without (~Csize) centroid size. Results in bold show values higher or equal to the mean vertebral disparity for each species.

PROCUSTES VARIANCE SPECIES	**C4**	**C6**	**C7**	**T1**	**T2**	**T4**	**T6**	**T8**	**T10**	**L1**	**L2**	**L4**	**L6**	**L7**	**MEAN**
Acinonyx jubatus	**0.019**	0.017	0.015	0.013	0.013	0.012	0.009	0.016	**0.022**	**0.038**	**0.028**	**0.022**	**0.024**	0.015	0.019
Felis catus	**0.015**	0.013	0.013	0.011	0.011	0.012	0.011	0.011	**0.028**	**0.014**	**0.01**	**0.008**	**0.019**	**0.017**	0.014
Leopardus pardalis	0.013	0.009	0.009	0.01	0.01	0.015	0.01	0.01	**0.021**	**0.013**	**0.02**	**0.02**	**0.021**	**0.032**	0.015
Leptailurus serval	**0.017**	**0.022**	0.015	0.011	0.011	0.007	0.01	0.011	**0.046**	**0.016**	**0.016**	0.01	**0.019**	**0.019**	0.016
Neofelis nebulosa	**0.015**	0.011	0.01	0.012	0.012	0.011	0.013	0.013	**0.02**	**0.02**	0.014	0.011	**0.017**	**0.027**	0.015
Panthera leo	0.01	0.012	0.013	0.01	0.01	0.009	0.01	0.008	**0.037**	0.014	0.014	**0.019**	**0.031**	**0.023**	0.016
Panthera pardus	**0.015**	**0.016**	**0.014**	0.011	0.011	0.008	0.009	0.009	**0.02**	0.012	0.011	0.009	**0.018**	**0.022**	0.013
Prionailurus bengalensis	0.015	0.015	0.014	0.015	0.015	0.013	0.013	0.014	**0.049**	0.017	**0.02**	0.017	**0.022**	**0.02**	0.019
Puma concolor	**0.013**	0.011	0.009	0.011	0.011	0.008	0.007	0.008	**0.017**	**0.014**	**0.012**	**0.014**	**0.018**	**0.014**	0.012
PROCUSTES VARIANCE (~Csize) SPECIES	**C4**	**C6**	**C7**	**T1**	**T2**	**T4**	**T6**	**T8**	**T10**	**L1**	**L2**	**L4**	**L6**	**L7**	**MEAN**
Acinonyx jubatus	**0.018**	**0.017**	0.013	0.012	0.015	0.011	0.009	**0.016**	**0.028**	**0.022**	**0.016**	0.013	**0.018**	0.013	0.016
Felis catus	**0.012**	0.011	**0.012**	0.009	0.009	0.01	0.01	0.01	**0.019**	**0.012**	0.009	0.007	**0.018**	**0.016**	0.012

Leopardus pardalis	**0.013**	0.01	0.009	0.01	0.009	0.015	0.01	0.01	**0.022**	0.011	**0.018**	**0.016**	**0.02**	**0.032**	0.015
Leptailurus serval	**0.016**	**0.02**	0.014	0.01	0.011	0.007	0.009	0.011	**0.041**	**0.017**	**0.015**	0.01	**0.018**	**0.02**	0.016
Neofelis nebulosa	**0.015**	0.011	0.011	0.012	0.009	0.011	0.013	0.013	**0.022**	**0.018**	0.012	0.011	**0.017**	**0.028**	0.015
Panthera leo	0.009	**0.011**	**0.011**	0.01	0.009	0.005	0.005	0.007	**0.015**	**0.015**	**0.011**	0.007	**0.016**	**0.018**	0.011
Panthera pardus	**0.013**	**0.014**	**0.013**	0.01	0.009	0.007	0.007	0.008	**0.013**	**0.014**	0.011	0.009	**0.019**	**0.022**	0.012
Prionailurus bengalensis	0.013	0.011	0.011	0.011	0.012	0.01	0.011	0.012	**0.034**	0.012	0.013	0.01	**0.015**	**0.018**	0.014
Puma concolor	**0.013**	0.01	0.008	**0.011**	0.008	0.008	0.006	0.007	**0.012**	0.01	**0.011**	**0.015**	0.02	**0.015**	0.011

Table 5.5: Within species vertebral disparity, measured as maximum Procrustes distance. Results in bold show values higher or equal to the species disparity mean.

PROCUSTES DISTANCE SPECIES	C4	C6	C7	T1	T2	T4	T6	T8	T10	L1	L2	L4	L6	L7	MEAN
Acinonyx jubatus	0.189	**0.267**	0.161	**0.204**	0.153	**0.204**	0.166	**0.32**	0.172	0.155	0.135	0.153	**0.277**	**0.24**	0.200
Felis catus	**0.255**	**0.223**	0.197	0.205	0.181	0.132	0.155	0.189	**0.229**	**0.24**	**0.212**	**0.214**	**0.272**	**0.225**	0.209
Leopardus pardalis	0.185	0.192	0.184	0.187	0.178	0.158	0.186	**0.217**	**0.373**	0.207	**0.217**	0.143	**0.228**	**0.258**	0.208
Leptailurus serval	0.161	0.184	0.171	0.18	0.147	0.171	0.146	0.14	**0.302**	0.143	0.128	0.156	**0.240**	**0.319**	0.185
Neofelis nebulosa	0.185	0.176	0.179	**0.226**	0.152	0.161	0.157	0.171	**0.283**	**0.221**	0.161	0.176	**0.246**	**0.393**	0.206
Panthera leo	0.179	0.260	0.208	0.222	0.221	0.211	**0.263**	0.251	**0.499**	**0.285**	0.248	0.242	**0.296**	**0.278**	0.262
Panthera pardus	0.208	0.236	0.198	0.188	0.182	**0.319**	0.225	0.251	**0.264**	0.223	0.31	0.232	**0.322**	**0.446**	0.257
Prionailurus bengalensis	0.214	**0.263**	0.224	0.216	0.194	0.185	**0.248**	0.188	**0.399**	0.207	0.218	0.226	**0.324**	**0.311**	0.244
Puma concolor	0.221	0.213	0.227	0.217	0.221	0.188	0.187	**0.263**	**0.322**	**0.276**	0.175	0.146	**0.270**	**0.296**	0.230

Regarding the disparity results per vertebra and per individual species, more species presented disparity values that were higher than the mean and median for all vertebrae, both as Procrustes variance and as maximum Procrustes distance, in the general region of T10 – L7, and consistently on vertebrae T10, L6 and L7 (Fig. 5.3, Tables 5.4 and 5.5).

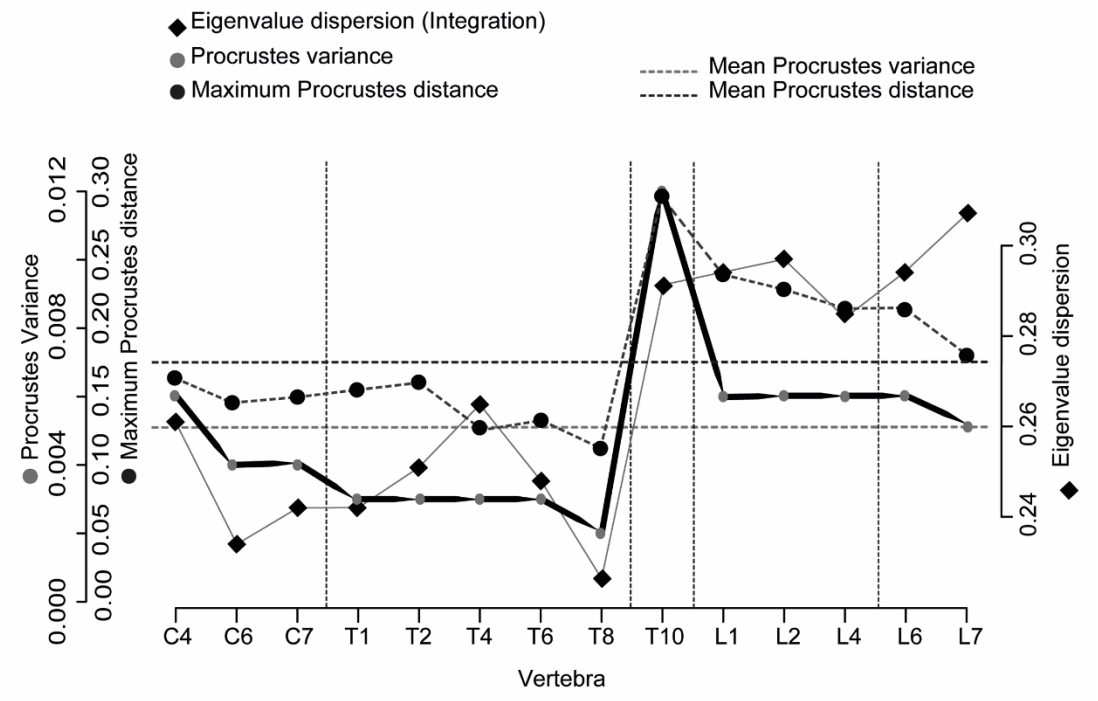

Figure 5.2: Plot showing distribution of morphological disparity across species (as Procrustes variance and maximum Procrustes distance) and eigenvalue dispersion (i.e., morphological integration) throughout the C4 – L7 vertebrae, calculated using 16 homologous landmarks (see text). Dashed vertical lines illustrate morphological and functional boundaries in the presacral vertebral column, while horizontal dashed lines depict the mean Procrustes variance (grey) and mean Procrustes distance (black).

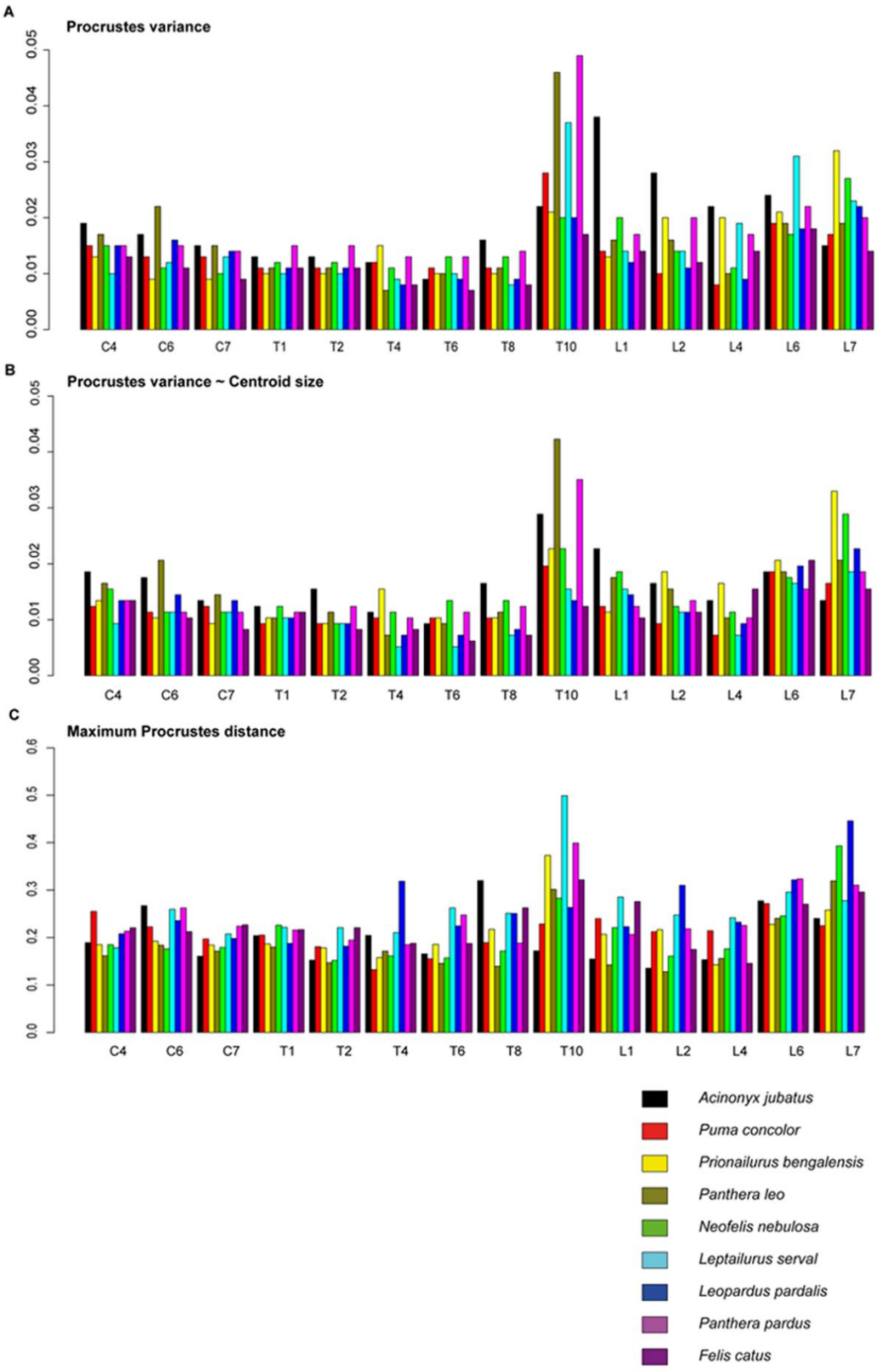

Figure 5.3: Bar plots showing distribution of morphological disparity values per individual species per vertebra as measures of Procrustes variance (A), Procrustes variances while taking size into account (B), and maximum Procrustes distance (C).

Discussion

Here we have analysed the patterns of intravertebral modularity and integration throughout the presacral vertebral column and evaluated these patterns in the combination with data on function and morphological disparity. Combined, this work provides a novel view of the evolutionary and developmental forces contributing to vertebral shape differentiation.

The results from our modularity analyses are consistent with the hypothesis that distinct somitic contributions and separate ossification centres in vertebral development result in similar modules in adult vertebral morphology throughout the presacral vertebral column. Only five out of the 19 analysed vertebrae failed to show support for the two hypothesized modules (centrum and neural spine) based on somitic origins. However, these five vertebrae (C4, T1, T8, L6 and L7) all either form, or are adjacent to, boundaries of traditional vertebral morphological regions, as discussed in detail below.

C4 is part of a previously suggested mammalian developmental module composed of mid-cervicals C3 – C5 (Buchholtz et al. 2012). Buchholtz et al. (2012) argued that the commitment of migratory muscle precursor cells from the C3 – C5 somites to the formation of the muscularised diaphragm resulted in modular organisation of this cervical region, which secondarily contributed to the fixation of cervical number in mammals. Additionally, the cervical

region has previously been shown to present its own regionalisation, with vertebrae divided into 'upper' cervicals (i.e., atlas and axis) responsible for skull articulation, intermediate cervicals (i.e., C3 – C5), and 'lower' cervicals (i.e., C6 and C7) responsible for neck movement and with morphologies more similar to those seen in the anterior thoracic region (Vidal et al. 1986; Graf et al. 1995; De Iuliis and Pulerà 2006; Buchholtz 2014; Arnold et al. 2016). Interestingly, the modular results for felid neck vertebrae expand on the conclusions of a recent study of integration in dog vertebrae (Arnold et al. 2016), in which they found high integration in the cervical (C3 – C7) morphology of domestic dogs and suggested that this result can be expanded to a general mammalian pattern. Our results of eigenvalue dispersion support a hypothesis of moderate integration in the cervical region, although we emphasize that this does not contradict support for developmental modularity within cervical vertebrae. Modularity and integration should not be interpreted as the opposing ends of a spectrum, as modules are typically highly integrated within themselves (Porto et al. 2009; Klingenberg 2013; Bookstein 2015). As the method used by Arnold et al. (2016) (i.e., PLS, Partial Least Squares; Rohlf and Corti 2000) is mostly suited for testing hypotheses of integration, rather than providing an output value that can discriminate between whole integration and modularity, we suggest that the pattern observed here of developmental modularity for 14 out of 19 vertebrae,

including C1, C2, C6 and C7, may also represent a broader mammalian pattern.

Continuing with vertebrae that failed to support the developmental two-module model, the first thoracic vertebra (T1) is at the boundary between the cervical and thoracic regions, with the highly conserved number of seven vertebrae in the mammalian neck (Buchholtz et al. 2012; Buchholtz 2014), and appearance of ribs and consequent reduced mobility in T1. T8 may also be involved in the boundary between two large and more inclusive vertebral regions, although the lack of T9 in our dataset hinders further testing of this hypothesis. Nevertheless, T8 is only two vertebrae away from another previously defined boundary which divides the vertebral column into pre- and postdiaphragmatic regions, T10. This boundary marks the transition between rib-bearing vertebrae, which are restricted by the diaphragm and surround vital organs such as heart and lungs, and the end-thoracics and lumbar region, which undergo more pronounced sagittal bending (Polly et al. 2001; Narita and Kuratani 2005; Buchholtz 2014; Jones 2015). Our previous analyses also suggest that the posterior region, especially the T10 – L7 region, may be more evolutionarily responsive as it shows stronger ecological signal than the anterior column and greater distinction in shape between species showing distinct locomotory specialisation (Chapters 3 and 4; Randau et al. 2016a; Randau et al. 2016b). This vertebral boundary hypothesis can also be

adopted towards interpreting the results from L6 and L7, which are the last vertebrae of the presacral region of felids and display higher overall integration.

Given the identities and locations of these five vertebrae that do not show a modular structure related to somite origin, we therefore suggest that a functional overprinting of developmental vertebral patterning may occur in these structures in order to maintain larger modular organisation of the whole vertebral column (Polly et al. 2001; Buchholtz 2007). However, further analyses in other datasets are needed to confirm this hypothesis.

One unexpected exception to this pattern is T10, which forms one of the most significant boundaries in the vertebral column, but shows significant support for the model of developmental modularity. Based on our hypothesis of vertebral regional boundaries, as well as the results for vertebral disparity and integration, we expected this vertebra to also be an exception to the developmental signal pattern, but it is instead a good example of a structure presenting both a modular organisation and an elevated overall integration index. T11 (i.e., the anticlinal vertebra, which marks the change in anteroposterior orientation of the neural spine from caudally to cranially oriented processes) also exhibited high overall integration, and most importantly, the lowest RV and CR values, suggesting the strongest modular organisation of the vertebral shape. The consecutive T12 also displayed

similarly low and significant RV and CR values. These results suggest that T10-T12 are under strong developmental control (West-Eberhard 1989; Arthur 2002; West-Eberhard 2003; Badyaev et al. 2005), which is maintained even when subjected to varied selection pressures that likely drive the high disparity observed for T10 (and presumably for T11 and T12, although they were not directly compared in disparity due to the lack of homologous landmarks).

The results presented here support the hypothesis that phenotypic integration may promote morphological disparity (Goswami et al. 2014), as observed in the association between higher vertebral overall integration and higher values of morphological disparity (Fig. 5.2 and 5.3, Tables 5.3, 5.4 and 5.5). Posterior vertebrae (T10 – L7) exhibited the highest degree of overall vertebral integration, as demonstrated by eigenvalue dispersion values higher than both the observed mean and median throughout the vertebral column. These results are particularly interesting when considered with the observation that those vertebrae presented markedly higher values of morphological disparity (both as Procrustes variance and maximum distance) than other vertebrae. We have previously shown that the posterior region is the vertebral section that presented the highest shape differentiation and correlation with ecological specialisation in felids, in terms of locomotor mode and prey size, and also allometry (Chapters 3 and 4; Randau et al. 2016a; Randau et al. 2016b), and

this may suggest that this region might display the greatest evolutionary respondability (i.e., raw magnitude of response in any direction to selection, Hansen and Houle 2008) across felids, or even more broadly. Goswami et al. (2014) demonstrated through the use of simulations that integration might increase disparity by coordinating the evolution of traits within functional units and directing this response through paths of higher trait covariance (Klingenberg 2010), although this association has only rarely been supported by empirical data. They have additionally shown that eigenvalue dispersion was highly and significantly positively correlated with respondability. By concentrating variance within determined evolutionary paths the range of morphological diversity is increased, meaning more disparate morphologies may occur than if traits are uncorrelated (Goswami et al. 2014).

Here we have conducted analyses of vertebral morphological integration and disparity throughout the presacral column of felids, and demonstrated that both measures present their highest values in the posterior axial skeleton, linking these measures to previously demonstrated high levels of ecological diversification (Chapters 3 and 4; Randau et al. 2016a; Randau et al. 2016b). With this, we add an empirical example of positive association between high integration and disparity to the existing discussion of the role of covariation in promoting versus constraining evolution (Klingenberg 2010; Goswami et al. 2014). Finally, we provided confirmation for the hypothesis that a two-

module intravertebral organisation is driven by somatic origins dominates in the presacral vertebral column in felids, but that this pattern is disrupted, or overprinted, at the boundaries of vertebral regions.

Appendix 5.1

Table S5.1: Species and specimen number information for specimens used in the analyses. Museum abbreviations are as follows: NHM: Natural History Museum, London; UMCZ: University Museum of Zoology, Cambridge; MNHN: Muséum National d'Histoire Naturelle, Paris; MCZ: Harvard Museum of Natural History, Cambridge; AMNH: American Museum of Natural History, New York; FMNH: Museum of Natural History, Chicago; USNM: Smithsonian National Museum of Natural History, Washington D.C.

Species	Specimen Number
Acinonyx jubatus	AMNH 119654
	AMNH 119655
	AMNH 119656
	AMNH 119657
	AMNH 36426
	FMNH 127834
	FMNH 34589
	FMNH 57826
	FMNH 60447
	FMNH 60535
	MNHN 1933 442
	NHM 1940-1-20-17
	USNM 520539
	USNM 521037
Felis catus	AMNH 248700
	MCZ 58665
	NHM 1936 2 5 20
	NHM 1952 10 20 4
	NHM 1988 1
	NHM 2002 161
	USNM 396268
	USNM 396271
	USNM 396392
	USNM 397631
	USNM 398871
	USNM 398991
	USNM A21665
Leopardus pardalis	AMNH 14022
	AMNH 214744
	AMNH 248728
	FMNH 68895

	FMNH 93174
	MNHN 1998 1866
	MNHN 2005 282
	MNHN A3456
	USNM 271094
	USNM A14182
Leptailurus serval	AMNH 34767
	FMNH 104800
	FMNH 127843
	FMNH 44438
	FMNH 60491
	NHM 1845 9 25 23
	NHM 1855 6 30 2
	NHM 1966 7 11 1
	NHM 2006 550
	USNM 521039
	USNM 548666
Neofelis nebulosa	AMNH 35273
	FMNH 104730
	FMNH 183653
	FMNH 54304
	MNHN 1961 217
	MNHN 1980 16
	NHM 1854 6 14 2
	NHM 1965 1 18 1
	USNM 399291
	USNM 545387
Panthera leo	AMNH 6260
	AMNH 85147
	AMNH 85149
	FMNH 127839
	FMNH 49340
	MCZ 13273
	MCZ 20976
	MCZ 62919
	MCZ 9487
	USNM 172677
	USNM A22705
Panthera pardus	AMNH 186944
	AMNH 54462
	AMNH 54854
	MNHN 1876 711
	MNHN 1892 1079
	MNHN 1898 100
	MNHN 1906 454
	MNHN 1945 70

	MNHN A13045 1844
	MNHN A7932
	MNHN BII 4
	MNHN CG1998 582
	NHM 1880 2 16 1
	NHM 1940.1.20.18
	USNM 15684
	USNM 258660
	USNM 270126
	USNM 303320
Prionailurus bengalensis	FMNH 121228
	FMNH 99363
	NHM 1309b 1858
	NHM 1979 2895
	NHM 77 2896
	USNM 317282
	USNM 317283
	USNM 330710
Puma concolor	AMNH 10259
	AMNH 135341
	AMNH 181997
	AMNH 90213
	FMNH 129338
	FMNH 129339
	FMNH 206424
	MNHN 1937 4
	MNHN CG1883 56
	NHM 1855-12-2-6
	USNM A21526
	USNM A21528
	USNM 264166
	UMCZ K5745

Table S5.1: Landmark number and definition per vertebrae.

VERTEBRA	LANDMARK	DESCRIPTION
ATLAS	1	Anterior mid-point of dorsal arch
	2	Anterior mid-point of ventral arch
	3	Anterior lateral-most tip of left transverse process
	4	Anterior lateral-most tip of right transverse process
	5	Dorso-anterior-most tip of left pre-zygapophysis
	6	Dorso-anterior-most tip of right pre-zygapophysis
	7	Posterior mid-point of dorsal arch
	8	Posterior mid-point of ventral arch
	9	Posterior lateral-most tip of left transverse process
	10	Posterior lateral-most tip of right transverse process
	11	Posterior-most tip of left post-zygapophysis
	12	Posterior-most tip of right post-zygapophysis
AXIS	1	Anterior-most point at tip of den
	2	Ventral mid-point at base of den
	3	Anterior-most point of neural spine
	4	Posterior ventral mid-point of centrum
	5	Posterior left lateral-most point of width of centrum
	6	Posterior right lateral-most point of width of centrum
	7	Posterior left dorso-lateral point of centrum
	8	Posterior right dorso-lateral point of centrum
	9	Posterior dorsal mid-point of the neural canal
	10	Dorsal posterior-most point at tip of neural spine
	11	Left lateral-most posterior tip of transverse process
	12	Right lateral-most posterior tip of transverse process
	13	Posterior-most dorsal point of left post-zygapophysis
	14	Posterior-most dorsal point of right post-zygapophysis
C4	1	Anterior ventral mid-point of centrum
	2	Anterior dorsal mid-point of centrum
	3	Anterior left lateral-most point of centrum
	4	Anterior left lateral-most point of centrum

	5	Anterior dorsal-most point of left pre-zygapophyses
	6	Anterior dorsal-most point of right pre-zygapophyses
	7	Anterior-most point of left lamina
	8	Anterior-most point of right lamina
	9	Dorsal-most point at tip of neural spine
	10	Posterior ventral mid-point of centrum
	11	Posterior dorsal mid-point of centrum
	12	Posterior Left lateral-most point of centrum
	13	Posterior right lateral-most point of centrum
	14	Posterior dorsal mid-point of the neural canal
	15	Posterior-most point of left post-zygapophyses
	16	Posterior-most point of right post-zygapophyses
	17	Lateral-most point of left transverse process
	18	Lateral-most point of right transverse process
C6	1	Anterior ventral mid-point of centrum
	2	Anterior dorsal mid-point of centrum
	3	Anterior left lateral-most point of centrum
	4	Anterior left lateral-most point of centrum
	5	Anterior dorsal-most point of left pre-zygapophyses
	6	Anterior dorsal-most point of right pre-zygapophyses
	7	Lateral-most point of left transverse process
	8	Lateral-most point of right transverse process
	9	Anterior-most point of left lamina
	10	Anterior-most point of right lamina
	11	Dorsal-most point at tip of neural spine
	12	Posterior ventral mid-point of centrum
	13	Posterior dorsal mid-point of centrum
	14	Posterior Left lateral-most point of centrum
	15	Posterior right lateral-most point of centrum
	16	Posterior dorsal mid-point of the neural canal
	17	Posterior-most point of left post-zygapophyses
	18	Posterior-most point of right post-zygapophyses
	19	Posterior-most point of left lamina
	20	Posterior-most point of right lamina
C7 - T10*	1	Anterior ventral mid-point of centrum
	2	Anterior dorsal mid-point of centrum

	3	Anterior left lateral-most point of centrum
	4	Anterior left lateral-most point of centrum
	5	Anterior dorsal-most point of left pre-zygapophysis
	6	Anterior dorsal-most point of right pre-zygapophysis
	7	Lateral-most point of left transverse process
	8	Lateral-most point of right transverse process
	9	Dorsal-most point at tip of neural spine
	10	Posterior ventral mid-point of centrum
	11	Posterior dorsal mid-point of centrum
	12	Posterior Left lateral-most point of centrum
	13	Posterior right lateral-most point of centrum
	14	Posterior dorsal mid-point of the neural canal
	15	Posterior-most point of left post-zygapophysis
	16	Posterior-most point of right post-zygapophysis
T11	1	Anterior ventral mid-point of centrum
	2	Anterior dorsal mid-point of centrum
	3	Anterior left lateral-most point of centrum
	4	Anterior left lateral-most point of centrum
	5	Anterior dorsal-most point of left pre-zygapophysis
	6	Anterior dorsal-most point of right pre-zygapophysis
	7	Posterior-most point of tip of left accessory process
	8	Posterior-most point of tip of right accessory process
	9	Dorsal-most point at tip of neural spine
	10	Posterior ventral mid-point of centrum
	11	Posterior dorsal mid-point of centrum
	12	Posterior Left lateral-most point of centrum
	13	Posterior right lateral-most point of centrum
	14	Posterior dorsal mid-point of the neural canal
	15	Posterior-most point of left post-zygapophysis
	16	Posterior-most point of right post-zygapophysis
T12 - T13	1	Anterior ventral mid-point of centrum
	2	Anterior dorsal mid-point of centrum
	3	Anterior left lateral-most point of centrum
	4	Anterior left lateral-most point of centrum

	5	Anterior dorsal-most point of left pre-zygapophyses
	6	Anterior dorsal-most point of right pre-zygapophyses
	7	Anterior Dorsal-most point at tip of neural spine
	8	Posterior Dorsal-most point at tip of neural spine
	9	Posterior ventral mid-point of centrum
	10	Posterior dorsal mid-point of centrum
	11	Posterior Left lateral-most point of centrum
	12	Posterior right lateral-most point of centrum
	13	Posterior dorsal mid-point of the neural canal
	14	Posterior-most point of left post-zygapophyses
	15	Posterior-most point of right post-zygapophyses
	16	Posterior-most point of tip of left accessory process
	17	Posterior-most point of tip of right accessory process
L1 - L4	1	Anterior ventral mid-point of centrum
	2	Anterior dorsal mid-point of centrum
	3	Anterior dorsal-most point of left pre-zygapophyses
	4	Anterior dorsal-most point of right pre-zygapophyses
	5	Dorsal anterior-most point at tip of neural spine
	6	Anterior left lateral-most point of centrum
	7	Anterior left lateral-most point of centrum
	8	Lateral-most point of left transverse process
	9	Lateral-most point of right transverse process
	10	Posterior ventral mid-point of centrum
	11	Posterior dorsal mid-point of centrum
	12	Posterior dorsal mid-point of the neural canal
	13	Posterior Left lateral-most point of centrum
	14	Posterior right lateral-most point of centrum
	15	Posterior-most point of tip of left accessory process
	16	Posterior-most point of tip of right accessory process
	17	Posterior-most point of left post-zygapophyses
	18	Posterior-most point of right post-zygapophyses
	19	Dorsal posterior-most point at tip of neural spine
L6 - L7	1	Anterior ventral mid-point of centrum
	2	Anterior dorsal mid-point of centrum

3	Anterior dorsal-most point of left pre-zygapophyses
4	Anterior dorsal-most point of right pre-zygapophyses
5	Dorsal anterior-most point at tip of neural spine
6	Anterior left lateral-most point of centrum
7	Anterior left lateral-most point of centrum
8	Lateral-most point of left transverse process
9	Lateral-most point of right transverse process
10	Posterior ventral mid-point of centrum
11	Posterior dorsal mid-point of centrum
12	Posterior dorsal mid-point of the neural canal
13	Posterior Left lateral-most point of centrum
14	Posterior right lateral-most point of centrum
15	Posterior-most point of left post-zygapophyses
16	Posterior-most point of right post-zygapophyses
17	Dorsal posterior-most point at tip of neural spine

Chapter 6: Morphological modularity in the vertebral column of Felidae (Mammalia, Carnivora)

Published as: Randau, M., & Goswami, A. (2017). Morphological modularity in the vertebral column of Felidae (Mammalia, Carnivora). *BMC Evolutionary Biology*, *17*, 133-144.

Abstract

Previous studies have demonstrated that the clear morphological differences among vertebrae across the presacral vertebral column are accompanied by heterogeneous functional signals in vertebral shape. Further, several lines of evidence suggest that the mammalian axial skeleton is a highly modular structure. These include its composition of serial units, a trade-off between high shape variance and strong conservation of vertebral count, and direct association of regions with anterior expression sites of *Hox* genes. Here we investigate the modular organisation of the presacral vertebral column of modern cats (Felidae, Carnivora, Mammalia) with pairwise comparisons of vertebral shape covariation (i.e., integration) across the presacral axial skeleton and evaluate our results against hypotheses of developmental and functional modularity. We used three-dimensional geometric morphometrics to quantify vertebral shape and then assessed integration between pairs of vertebrae with phylogenetic two-block partial least square analysis (PLS).

Six modules were identified in the pairwise analyses: an anterior module (C1 to T1); a transitional module situated between the last cervicals and first thoracics (C6 to T2); an anterior to middle thoracic set (T4 to T8); an anticlinal module (T10 and T11); a posterior set composed of the last two thoracics and lumbars (T12 to L7); and a module showing covariation between the cervicals and the posterior set (T12 to L7). These modules reflect shared developmental pathways, ossification timing, and observed ecological shape diversification in living species of felids.

We show here that patterns of shape integration reflect modular organisation of the vertebral column of felids. While this pattern corresponds with hypotheses of developmental and functional regionalisation in the axial skeleton, it does not simply reflect major vertebral regions. This modularity may also have permitted vertebral partitions, specifically in the posterior vertebral column, to be more responsive to selection and achieve higher morphological disparity than other vertebral regions.

Introduction

Numerous studies have demonstrated that organisms can be partitioned into sets of phenotypic traits or structures that show coordinated patterns of variation or evolution. These sets of traits, termed phenotypic modules, can be

defined as units composed of multiple traits that display high levels of covariation with other traits within that unit, but relatively weak covariation with traits outside of the unit. The related concept of integration refers to the overall magnitude of covariation of phenotypic traits, and can refer to a single module, which would be expected to display relatively high within-module integration, or may span multiple modules or structures (Terentjev 1931; Olson and Miller 1958; Goswami and Polly 2010c). The integration of traits, and their organisation into discrete phenotypic modules, has been hypothesised to arise and/or evolve as a product of shared developmental origin or pathways, genetic pleiotropy, or common function (Olson and Miller 1958; Bolker 2000; Buchholtz 2007; Goswami and Polly 2010c). Strong integration within modules, and reduced integration between modules, is further hypothesised to promote coordination among functionally-related traits, while allowing independence and differential specialization of distinct modules (Olson and Miller 1958; Cheverud 1996; Klingenberg 2008; Clune et al. 2013; Buchholtz 2014). In such, modules are characterised by displaying hierarchical structure and may present nested patterns. As an example, mammalian skulls have been shown to have a 'face' *versus* 'neurocranium' modular structure (Drake and Klingenberg 2010), but a greater number of modules has also been demonstrated to exist when smaller partitions regarding specific functional groups are defined within each of the two blocks (e.g,. oral-nasal, molar, orbit, and zygomatic-pterygoid within the 'face'

module, and the cranial vault and basicranium with the 'neurocranium' module) (Cheverud 1982, 1995; Goswami 2006a; Goswami and Finarelli 2016).

Functional and developmental hypotheses of modularity can be difficult to untangle in many structures, as hypothesized developmental and functional models may largely overlap (Goswami 2006a). For this reason, theoretical correlation matrix analysis often fails to select one or the other driver of modularity. Testing hypotheses directly derived from functional and biomechanical observations may aid in distinguishing between these two drivers of modularity (O'Higgins et al. 2010). Ultimately, the combination of the results presented throughout this thesis to biomechanical and functional analyses of the vertebral column may elucidate the drivers of morphological modularity in this structure. However, the validity of phenotypic modules is not contingent on being able to discriminate the underlying causes of that modularity, which may, in many cases, be impossible due to the organisation of modularity changing with the repatterning of integration through ontogeny (Hallgrímsson et al. 2009).

With its serial organisation and composition of vertebral units, distinguishable morphological differences among regions (cervical, thoracic, and lumbar), and direct association of those regions with expression sites of genes in the *Hox* family, the presacral axial skeleton would appear to encapsulate the concepts of regionalisation and modularity (Burke et al. 1995;

Polly et al. 2001; Buchholtz 2007; Wellik 2007; Guinard and Marchand 2010; Head and Polly 2015).

Although regionalisation of the vertebral column can be observed in amniotes in general (Head and Polly 2015), the mammalian axial skeleton shows the greatest differentiation in regional vertebral shape (Boszczyk et al. 2001; Buchholtz 2001b; Shapiro 2007; Buchholtz and Stepien 2009; Pierce et al. 2011; Jones and German 2014; Head and Polly 2015). This increased divergence is accompanied by strict constraints in regional vertebral number, particularly in the cervical region with seven vertebrae present in almost all of the ~5,000 mammalian species. Total presacral vertebral count is also highly conserved (Narita and Kuratani 2005; Müller et al. 2010; Buchholtz et al. 2012), although some restricted variation does occur (Asher et al. 2011). This invariability with regards to vertebral count has been suggested to signal strong canalisation (i.e., limitation of variation between individuals due to the tendency of organisms to "follow predetermined developmental pathways in spite of environmental and genetic perturbations" (and also see Waddington 1942; Lazić et al. 2015, page 44) and developmental stability in the axial skeleton, and is thought to have evolved early in mammalian history (Müller et al. 2010; Buchholtz et al. 2012). Additionally, rather than being the target of selection on the traits themselves, highly fixed vertebral numbers in mammals may reflect developmental constraints related to the muscularisation of the

diaphragm and the advantages of involving the lumbar region in abdomen expansion during inspiration and in sagittal bending during locomotion (Buchholtz et al. 2012; Buchholtz 2014).

In addition to the almost universally fixed count of seven vertebrae in the cervical region in mammals, species of the order Carnivora also show little variation in thoracolumbar count, generally between 19 and 20 vertebrae (Narita and Kuratani 2005). Moreover, some families, such as Felidae (i.e., cats), display absolutely no variation in vertebral numbers between taxa: all felid species present 27 presacral vertebrae which are traditionally divided into the three main vertebral column regions (i.e., cervical, thoracic, and lumbar) by clear morphological differences (Boyd 1976; Boszczyk et al. 2001; De Iuliis and Pulerà 2006; Galis et al. 2014; Randau et al. 2016b). In accordance with the observed trade-off between vertebral count invariability and high morphological disparity, both linear and landmark-based analyses of vertebral shape have shown evident functional regionalisation in the axial skeleton of felids. These analyses revealed regions which differ in magnitude of phylogenetic and ecological signal (e.g., specialisation related to locomotor mode) and both ontogenetic and evolutionary allometric scaling (Chapters 3 and 4; Jones 2015; Randau et al. 2016a; Randau et al. 2016b). Specifically, the highest covariation between vertebral shape and prey size choice or locomotory mode (i.e., the two main ecological categories that have been used

to describe felid ecology in the literature (Ewer 1973; Leyhausen 1979; Sunquist and Sunquist 2002; Meachen-Samuels and Van Valkenburgh 2009a, 2009b; MacDonald et al. 2010; Cuff et al. 2015) were found in the posterior region of the vertebral column, composed of the vertebrae caudal to the posterior attachment of the diaphragm, from T10 to L7; conversely, vertebrae in the cervical region displayed high phylogenetic signal and little significant ecological signal (Chapters 3 and 4; Randau et al. 2016a; Randau et al. 2016b).

These examples of conspicuous morphological and functional regionalisation are strong indicators of modularity in the vertebral column, and not surprisingly, modularity has indeed already been described, or at least suggested, at different levels within the mammalian axial skeleton (e.g., Buchholtz 2007; Chapters 3 and 4; Randau et al. 2016b; Randau and Goswami 2017b). One example of a hypothesised vertebral module is composed of the mid-cervicals C3 to C5. These vertebrae, whose somites have migratory muscle precursor cells which are committed to diaphragm transformation, have been suggested to be involved in the muscularisation of the septum and consequent fixed cervical number across almost all mammals (Buchholtz et al. 2012).

A larger hypothesised module stems from the relatively fixed count of total thoracolumbar vertebrae has been suggested to arise from close association of these two regions, with any changes in regional vertebral number being

counteracted by the inverse change in the opposite series, and thus no change to the total count (i.e., homeotic changes) (Raff 1996; Polly et al. 2001; Narita and Kuratani 2005; Buchholtz 2007; Müller et al. 2010; Chapter 4; Randau and Goswami 2017b).

Our previous studies of vertebral shape evolution in felids have already suggested some hypotheses of modularity specific to this study system. The observation of regionalised patterns of allometric scaling in a linear morphometric study both supported the mid-cervical vertebral module and suggested the presence of three additional modules: an anterior cervicothoracic module, a lumbar module, and a functional 'anticlinality module' composed of the T10-T12 vertebrae (Chapter 3; Randau et al. 2016b). Additionally, we have previously demonstrated that presacral vertebral shape in felids is driven by the developmental origins of vertebral components, with two morphological modules found in adult vertebral shape: the 'centrum' and the 'neural spine-related' modules (Boyd 1976; Christ et al. 2007; Chapter 4; Randau and Goswami 2017b). Interestingly, this model of modularity, although widespread through most of the presacral column, was not supported in vertebrae which are positioned immediately at or adjacent to the borders of morphological vertebral column regions: specifically, C4, T1, T8, L6 and L7. This observation led to the suggestion of a disruption of developmental modularity – or a functional overprint – in order to maintain

the larger modular organisation of the vertebral column as a whole (Chapter 5; Randau and Goswami 2017b).

Although there have been recent additions to the literature on the morphological, biomechanical and developmental changes to the vertebral column in mammals or across vertebrates in general (Hautier et al. 2010; Pierce et al. 2013; Buchholtz 2014; Böhmer et al. 2015; Head and Polly 2015; Molnar et al. 2015; Randau and Goswami 2017b), much is yet unknown on the evolution of the vertebral column and how patterns of trait integration or modularity may affect its response to selection (Goswami et al. 2014). Here we analyse patterns of shape covariation across the presacral vertebral column in order to quantify the modular organisation of the axial skeleton in felids. Specifically, we use three-dimensional geometric morphometrics to describe presacral vertebral shape and quantify intervertebral integration with pairwise comparisons of presacral vertebrae using phylogenetic two-block partial least square analysis (PLS). The results of the pairwise PLS analyses were used to test whether specific sets of vertebrae show higher magnitude of shape integration (i.e. greater covariation) within the set than with vertebral units outside of the set, therefore forming a 'module' (Terentjev 1931; Olson and Miller 1958; Goswami and Polly 2010c). The hypothesised intervertebral modules assessed with pairwise PLS results were drawn from the literature and are as follows (Fig. 6.1): 1) the 'traditional regions' hypothesis: Traditional

regional boundaries (i.e., cervical, thoracic and lumbar) in the felid vertebral column form discrete morphological modules (Narita and Kuratani 2005; De Iuliis and Pulerà 2006; Buchholtz 2007; Müller et al. 2010; Buchholtz 2014); 2) the 'cervicothoracic and lumbar modules' hypothesis: Two modules composed of multiple vertebrae that share a common allometric pattern (Randau et al. 2016b) can be found in the presacral axial skeleton: an anterior cervicothoracic module (where vertebrae show positive allometry related to centrum and neural spine dimensions) and a lumbar module module (with positive allometry of traits related to the neural spine lever arm) (Chapter 3; Randau et al. 2016b); 3) the 'thoracolumbar' hypothesis: Thoracic and lumbar vertebrae show high covariation (Raff 1996; Polly et al. 2001; Narita and Kuratani 2005; Buchholtz 2007; Müller et al. 2010); 4) the 'anticlinality' hypothesis: Vertebrae T10 to T12 compose an 'anticlinality module' (Chapter 3; Randau et al. 2016b); and 5) the 'developmental model disruption' hypothesis: Boundaries of modular organisation of the vertebral column match the key vertebral positions where the intravertebral developmental two-module (centrum and neural spine) model is not supported, specifically at the edges of the C3 – C5 cervical module, between cervicals and thoracics (i.e., at T1), the division of the vertebral column into pre- and postdiaphragmatic regions at T8, and at the last two presacral vertebrae L6 and L7 (Chapter 5; Randau and Goswami 2017b).

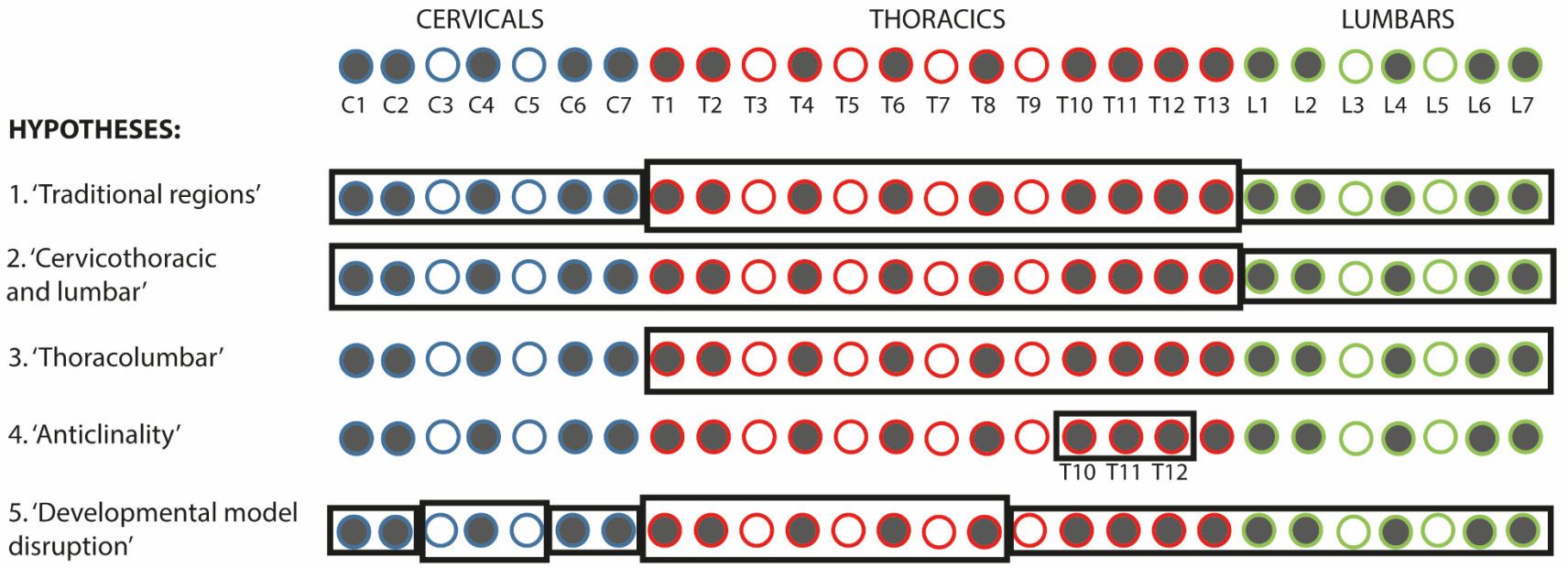

Fig. 6.1: Illustration of the five hypotheses tested here regarding modular patterns of shape covariation across the presacral vertebral column. Black rectangles illustrate sets of vertebrae which are hypothesized to show high integration among themselves and therefore to form a module. See text for detailed description of hypotheses. Hypothesis 1: Traditional regions. Hypothesis 2: Cervicothoracic and lumbar modules. Hypothesis 3: Thoracolumbar module. Hypothesis 4: Anticlinality model composed of vertebrae T10, T11 and T12. Hypothesis 5: Developmental model disruption. C, T, and L stand for cervicals (blue outline), thoracics (red outline), and lumbars (green outline), respectively. Filled circles describe landmarked vertebrae.

Finally, we further conducted separate analyses of intervertebral integration for the two intravertebral developmental modules (centrum and neural spine). Specifically, the same pairwise phylogenetic PLS analyses were conducted across the presacral vertebral column, but traits were limited to those from either the neural spine or the centrum (Chapter 5; Boyd 1976; Christ et al. 2007; Randau and Goswami 2017b). Following from our previous results showing the widespread developmental two-module model of intravertebral covariation, this latter analysis allows us to assess if the patter of intervertebral covariation across the vertebral column is the same for the whole vertebral morphology and for when only trait units regarding each of these modules are considered (Tables S6.1 and S6.2 for landmarks' identity, following Chapter 5; Randau and Goswami 2017b).

Material and Methods

An Immersion Microscribe G2X (Solution Technologies, Inc., Oella, Maryland) was used to collect three-dimensional (3D) landmarks on 19 out of the 27 felid presacral vertebrae. These 19 vertebrae comprised the atlas (C1), axis (C2), C4, C6, C7, T1, T2, T4, T6, T8, T10, T11, T12, T13, L1, L2, L4, L6, and L7 (where C stands for cervical, T for thoracic, and L for lumbar). Reasons for vertebrae selection have been detailed extensively in previous studies (Chapters 2 for

methodology description, and Chapters 3, 4 and 5 for discussion; Randau et al. 2016a; Randau et al. 2016b; Randau and Goswami 2017b); in short, the chosen vertebrae cover the observed range in presacral vertebral morphology and include vertebrae which compose the boundaries between traditional vertebral morphological regions (e.g., C7 and T1 forming the boundary between the cervical and thoracic regions).

Following the methodology outlined in Chapter 2 and in our previous study (Chapter 5; Randau and Goswami 2017b), different sets of landmarks were collected per specific vertebrae due to differences in vertebral morphology throughout the axial skeleton: 12 landmarks were gathered on C1 (atlas), 14 on C2 (axis), 18 on C4, 20 on C6, 16 on C7 – T10, 16 on T11, 17 on T12 – T13, 19 on L1 – L4, and 17 on L6 – L7 (Fig. 6.2. and see Table S5.1 and S5.2 for landmarks identity). The chosen landmarks have been analysed in Chapter 2 and in previous publications (Randau et al. 2016a; Randau and Goswami 2017b), and have been shown to accurately describe the main aspects of vertebral shape, both when whole vertebral morphology was considered and regarding smaller landmark-module sets within individual vertebra. Furthermore, shape analyses of this data showed that they were able to capture morphological changes correlated with ecological specialisation in felids (Chapter 5; Randau and Goswami 2017b). These landmarks were collected on 66 complete specimens of nine felid species (*Acinonyx jubatus*,

Felis catus, Leopardus pardalis, Leptailurus serval, Neofelis nebulosa, Panthera leo, Panthera pardus, Prionailurus bengalensis and *Puma concolor*; Table S6.3 for specimen numbers). The final dataset was therefore composed of 1254 individual vertebrae. The subset of nine species studied here include representatives of the ecological specialisations that have been described for Felidae (i.e., locomotion and prey size specialisations; Chapter 2; Ewer 1973; Carbone et al. 1999; Sunquist and Sunquist 2002; Meachen-Samuels and Van Valkenburgh 2009a, 2009b; MacDonald et al. 2010). Within this family, species vary in locomotor specialisation, including cursorial (e.g., *Acinonyx jubatus*), terrestrial (e.g., *Panthera leo*), scansorial (e.g., *Panthera pardus*) and arboreal (e.g., *Neofelis nebulosa*) species. With regards to specialisation in prey size, felids range from small prey specialists (<15kg; e.g., *Felis catus*) to large prey specialists (>25Kg; e.g., *Puma concolor*), with a few species being less specialised and killing prey depending more on availability (mixed prey size; e.g., *Leopardus pardalis*). In addition to ecological specialisation, the species chosen for this study also represent the range in body mass observed in extant members of the family (e.g., from ~3kg in the domestic cat, *Felis catus*, to over 200kg in the lion (*Panthera leo*) (Sunquist and Sunquist 2002; MacDonald et al. 2010).

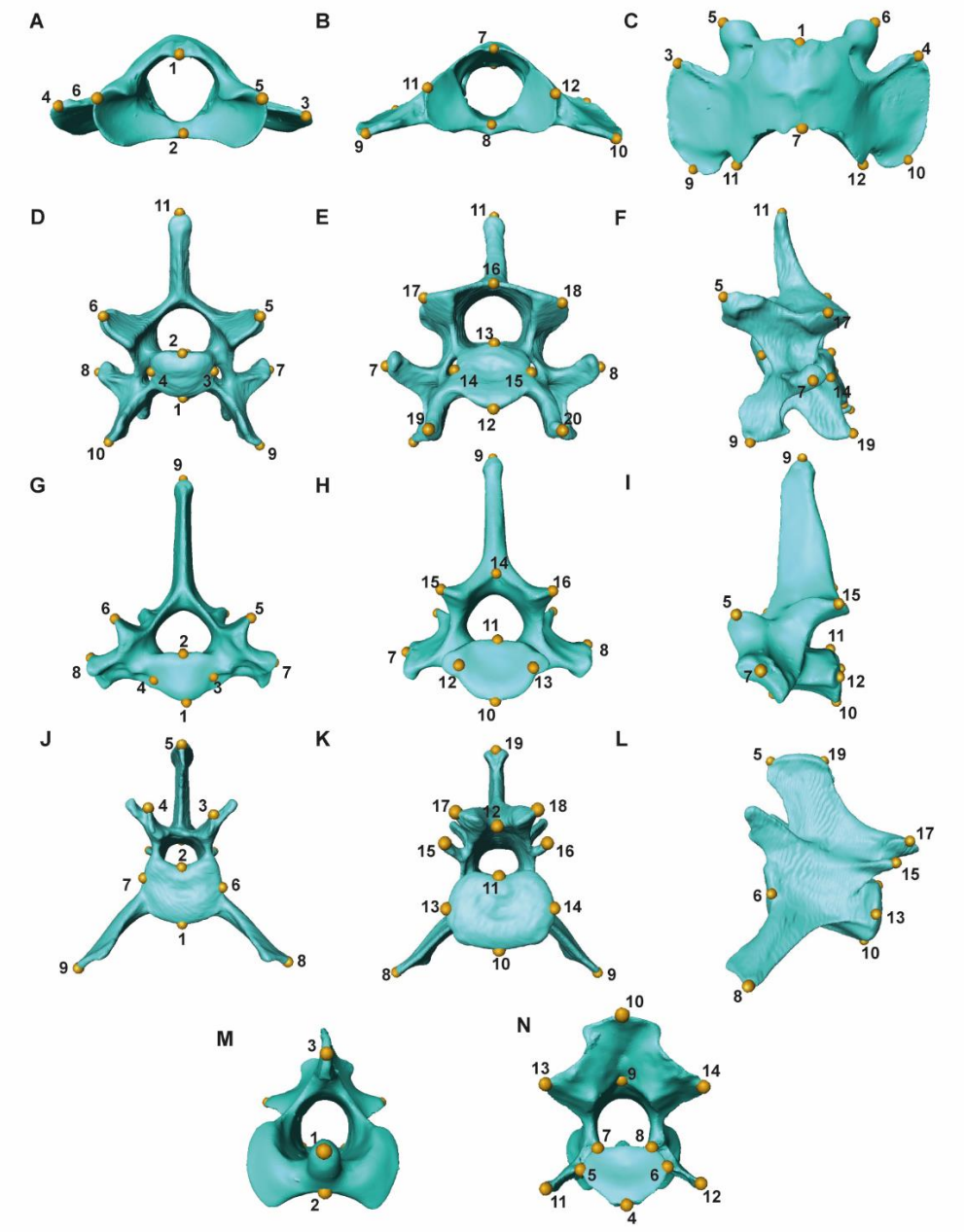

Fig. 6.2: Examples of the different vertebral morphologies across the presacral vertebral column of felids and their respective three-dimensional landmarks. Each of the vertebrae shown here is a representative of a unique shape or possesses the maximum number of landmarks per morphology (i.e. the unique C1 and C2, an example of the cervical morphology with C6, T1 demonstrating the thoracic morphology, and L1 showing the lumbar

morphology): (A-C) atlas (C1) in anterior, posterior and dorsal view; (D-F) C6 in anterior, posterior and lateral view; (G-I) (Cont.)

(Cont. (G-I) T1 in anterior, posterior and lateral view; (J-L) L1 in anterior, posterior and lateral view; and (M-N) axis (C2) in anterior and posterior view. Vertebral images are from CT scans of *Acinonyx jubatus* (Cheetah, USNM 520539). Vertebra-specific landmark descriptions can be found in Table S6.1.

Data analysis

Analyses were carried out in R version 3.2.3 (R Core Team 2015a), using the 'geomorph' (Adams and Otarola-Castillo 2013; Adams et al. 2015) package. Prior to subsequent analyses, the landmark data for each vertebral type (i.e., vertebrae grouped by vertebral position, e.g. C1, C2, C4, T1, etc.) was separately aligned with a Generalised Procrustes Superimposition (GPA) in order to remove effects of scale, translation and rotation. The stability of the covariance matrices for each vertebrae was assessed by bootstrapping each dataset 10,000 times and comparing the covariance matrices of the original and resampled dataset with random skewers analysis (Goswami and Polly 2010c; Melo et al. 2016). This analysis demonstrated that covariance matrix repeatability was high, ranging from 0.91 to 0.96 with a median of 0.94 and thus our sampling was sufficient for accurately estimating vertebral covariance matrices.

Vertebral shape covariation

The degree of morphological integration (i.e., shape covariation) per each possible pairwise combination between the vertebrae included here (e.g., C1 and C2, C1 and C4, C2 and C4 etc.) was measured using a two-block partial least square (PLS) analysis (Rohlf and Corti 2000; Bookstein et al. 2003). This analysis was performed while accounting for phylogenetic relatedness, and was quantified by following these steps: first, landmark data for each vertebral type (e.g., T10) was separated into single species sets (e.g., *Panthera leo* only), which were individually aligned with a GPA. Species means per each vertebral type were then calculated from these Procrustes coordinates. Finally, pairwise mean vertebral shape covariation was estimated with a phylogenetic PLS, under a Brownian motion model of evolution (Adams and Felice 2014). Phylogenetic relationships between the species studied here were calculated using a pruned version of the composite tree by Piras et al. (Piras et al. 2013). Statistical significance of each pairwise integration test was evaluated against a null distribution generated by repeating the phylogenetic PLS analysis after randomly permuting specimen rows for one vertebral dataset. Repeating this procedure with 5000 iterations generated the distribution against which the significance of the original results were compared.

There is some discussion on whether phylogeny should be corrected for when analysing patterns of integration, as removing this signal might conceal real genetically or developmentally driven modularity or integration (Polly et al. 2013). However, the phylogenetic PLS methodology used (Adams and Felice 2014) has been widely accepted (e.g., Kane and Higham 2015; Hu et al. 2016; Klaczko et al. 2016), and the application of this correction here reveals the major patterns of vertebral column organisation even in a highly conservative scenario.

The estimated degree of integration (i.e., covariation between pairs of vertebrae) and the statistical significance of each test (p-value; significance cut-off used a p-value < 0.05 threshold, but see below) were then compiled in matrices where sets of vertebrae showing significant shape covariation (i.e., modules) could be visualised.

Covariation across centrum versus *neural spine modules throughout the vertebral column*

A second phylogenetic PLS analysis was carried out using the Procrustes-aligned mean species coordinates for landmarks present in the centrum or neural spine modules only (see Table S5.2 for landmarks identity). Landmark assignment to these modules was based on developmental origins of vertebral

components in amniotes (Christ et al. 2007) and ossification centres in felids (Boyd 1976). Additionally, analysis of intravertebral morphological modularity across felids has shown that this model is supported in most presacral vertebrae across felids (Randau and Goswami 2017b).

Multiple comparisons and statistical significance

Because each individual vertebrae was involved in multiple comparisons, the significance test results (i.e., p-values) of each of the distinct PLS analyses were corrected using a Benjamini-Hochberg procedure with a false discovery rate at 0.05, a relatively strict value (Benjamini and Hochberg 1995). The Benjamini-Hochberg correction is a method for taking into account false positives (i.e., cases in which the raw p-value is below the chosen threshold, e.g., 0.05, purely due to chance) in multiple comparisons analyses. We chose to use this procedure instead of the more common Bonferroni correction due to the latter method's tendency to find a sizeable number of false negatives in analyses that include a large number of comparisons (e.g., a Bonferroni-corrected significance test for an analysis containing 171 comparisons, such as the one presented here, at an initial significance threshold of p-value < 0.05, would entail that only p-values < 0.0003 were to be considered significant) (Benjamini and Hochberg 1995). The way in which the Benjamini-Hochberg method classifies p-values according to their significance is by using a ranking system.

First, all raw p-values are ordered in a crescent manner (i.e., from smallest to largest) and ranked from i=1 (lowest) to m= the total number of tests. These ranked raw p-values are then compared to their 'Benjamini-Hochberg critical values, calculated as $(i/m)Q$, where Q is the chosen false discovery rate (0.05 here). The largest p-value which is still lower than their critical value plus all other lower raw p-values are classified as significant (Benjamini and Hochberg 1995; McDonald 2014). This method also calculates Benjamini-Hochberg'-corrected p-values for easier visualisation, which are displayed here along with the raw p-values.

Allometry and vertebral integration

As discussed in Chapter 2, allometry of vertebral shape was not corrected for prior to the analyses of intervertebral integration. Allometric shape changes (i.e., those directly driven by changes in body size) have been suggested to be a strong driver contributing towards morphological integration, particularly when analyses are performed between partitions within a single structure, because allometric effects may integrate a single structure uniformly (Klingenberg 2008; Goswami and Polly 2010c; Klingenberg and Marugán-Lobón 2013). However, our previous work on vertebral shape in the species studied here (Chapter 4; Randau et al. 2016a) has demonstrated that allometry varies across the presacral vertebral column, but only explain around 11% of

vertebral shape differences across felids (mean 11.1%, median 9.9%). Further, body mass evolution in felids has been shown to be highly dependent on phylogenetic relationships (Sunquist and Sunquist 2002; MacDonald et al. 2010; Cuff et al. 2015); therefore, correcting for size after having applied the phylogenetic correction performed here could potentially overcorrect and introduce error into our analyses. Finally, keeping in mind that the aim of this study was to investigate patterns of integration across the vertebral column, correcting for a factor that may be one of the constituents of such integration would potentially obscure real biological patterns of covariation between the vertebrae studied here.

Results

Vertebral shape covariation

Phylogenetic PLS analysis demonstrated that 108 out of the total 171 pairwise analyses were not significant (p-value > 0.05, Table 6.1 and Table S6.4), suggesting extensive modularity of the presacral vertebral column.. Nevertheless, the remaining 63 significant pairwise analyses allowed for identification of sets of vertebrae which presented particularly strong within-group covariation (i.e., PLS covariation > 0.90, p-value < 0.05). According to these results, six sets of highly covarying vertebrae were identified as follows:

1) C1 to T1; 2) C6 to T2; 3) T4 to T8; 4) T10 to T11; 5) T12 to L7; and 6) a set showing covariation between C1 to C7 (with the exception of C4) and T12 to L7, with the exception of the pairwise comparisons between C1 and the lumbars L4 and L6, and C6 and L7.

After Benjamini-Hochberg correction (multiple comparisons correction, see Material and methods; Tables 6.1 and S6.4), the number of covariation tests that were not significant increased to 113, leaving 58 significant results. Those tests that were rendered not significant after this correction were concentrated between the first cervicals (C1 – C4) and C7 and T1, C1 and the end-thoracics and lumbars, and some of the covariation results between the pre-diaphragmatic thoracics (i.e., thoracic vertebrae between T1 and T8). Thus, the overall pattern of intervertebral modularity was similar after correction for multiple comparisons.

Covariation across centrum versus *neural spine modules throughout the vertebral column*

Centrum: Results from the phylogenetic PLS on centrum-only landmarks supported modules largely similar to those found when whole vertebral morphology was analysed: 1) C1 – T2, with three exceptions in pairwise comparisons between C4 and T1, C6 and C7, and C6 and T1, formed a cervical and first thoracics set; and 2) T12 to L7 composed a set with very strong within module covariation (i.e., > 0.95; Tables 6.2 and S6.5). However, other vertebral

combinations were also apparent: 3) T6 - L6 vertebrae; 4) Between C1 – C4 and T8 – L4, with the exception of T11, which only presented significant shape covariation with C1 and C7 among the cervicals; and 5) C7 and every other vertebra included in this analyses, with the exception of C6.

Correction of this analysis' significance level with the Benjamini-Hochberg procedure reduced and rendered non-significant most pairwise comparisons between C1 – C6 and T12 – L4 but had little effect on most other modules (Tables 6.2 and S6.5).

Neural spine: There were fewer significant pairwise covariation results from the phylogenetic PLS on neural spine-only landmarks than from the centrum-only analysis (i.e., 76 *versus* 114 significant covariation results prior to correction for multiple comparisons, respectively; Tables 6.3 and S6.6). The significant pairwise tests on neural spine-only landmarks displayed four distinct modules: 1) between C1 and C7, with the exception of C4; 2) between T10 and T11; 3) between vertebrae in the T12 – L7 region; and 4) between the cervicals C1 – C7, with the exception of C4, and T12 – L7. Benjamini-Hochberg correction did not change these patterns and mainly reduced the covariations between the cervicals and the vertebrae in the T12 – L7 region, and other vertebral pairs in the thoracic region (Tables 6.3 and S6.6).

Table 6.1: Results of phylogenetic Partial Least Squares analysis of all landmarks. Above diagonal cells show the pairwise correlation values (i.e., degree of integration) between each pair of vertebrae, while below diagonal values display the correlation values with significance levels after Benjamini-Hochberg correction. Results in bold and in grey shaded cells show significant correlations and suggested modules, while results in italics and with white shaded cells are not significant (p-value > 0.05, Table S6.4).

	ATLAS	**AXIS**	**C4**	**C6**	**C7**	**T1**	**T2**	**T4**	**T6**	**T8**	**T10**	**T11**	**T12**	**T13**	**L1**	**L2**	**L4**	**L6**	**L7**
ATLAS		**0.978**	*0.899*	**0.936**	**0.902**	**0.899**	*0.859*	*0.864*	0.909	0.951	*0.818*	0.875	**0.915**	**0.883**	**0.89**	**0.885**	*0.848*	*0.871*	**0.903**
AXIS	**0.978**		**0.952**	**0.979**	**0.95**	**0.916**	*0.881*	*0.858*	*0.871*	0.943	0.914	0.91	**0.952**	**0.935**	**0.938**	**0.941**	**0.904**	**0.92**	**0.947**
C4	*0.899*	**0.952**		**0.988**	*0.892*	*0.878*	*0.887*	*0.861*	*0.82*	*0.87*	*0.737*	*0.71*	*0.835*	*0.884*	*0.903*	*0.892*	*0.869*	*0.864*	*0.878*
C6	**0.936**	**0.979**	**0.988**		**0.981**	**0.985**	**0.98**	*0.889*	*0.899*	*0.941*	*0.825*	*0.873*	**0.97**	**0.985**	**0.984**	**0.984**	**0.985**	**0.978**	*0.956*
C7	*0.902*	**0.95**	*0.892*	**0.981**		**0.915**	*0.871*	*0.812*	*0.85*	0.924	*0.783*	*0.762*	**0.966**	**0.983**	**0.957**	**0.962**	**0.964**	**0.971**	**0.977**
T1	*0.899*	*0.916*	*0.878*	**0.985**	*0.915*		0.96	*0.831*	*0.833*	*0.926*	0.963	0.95	*0.9*	*0.882*	*0.884*	*0.908*	*0.856*	*0.885*	0.931
T2	*0.859*	*0.881*	*0.887*	**0.98**	*0.871*	**0.96**		*0.805*	*0.833*	*0.911*	*0.821*	*0.833*	*0.756*	*0.789*	*0.797*	*0.781*	*0.772*	*0.786*	*0.855*
T4	*0.864*	*0.858*	*0.861*	*0.889*	*0.812*	**0.831**	*0.805*		**0.949**	**0.97**	*0.823*	0.904	*0.859*	*0.847*	*0.815*	*0.851*	*0.829*	*0.867*	*0.81*
T6	*0.909*	*0.871*	*0.82*	*0.899*	*0.85*	*0.833*	*0.833*	**0.949**		**0.959**	0.931	0.939	0.91	*0.888*	*0.841*	*0.859*	*0.83*	*0.847*	*0.803*
T8	**0.951**	**0.943**	*0.87*	*0.941*	0.924	*0.926*	*0.911*	**0.97**	*0.959*		*0.856*	*0.832*	0.955	*0.926*	*0.889*	*0.924*	*0.89*	*0.906*	*0.861*
T10	*0.818*	*0.914*	*0.737*	*0.825*	*0.783*	*0.963*	*0.821*	*0.823*	**0.931**	*0.856*		**0.953**	*0.782*	0.88	*0.672*	*0.656*	*0.699*	*0.792*	*0.825*
T11	*0.875*	**0.91**	*0.71*	*0.873*	*0.762*	0.95	*0.833*	*0.904*	**0.939**	*0.832*	**0.953**		*0.817*	*0.796*	*0.723*	*0.699*	*0.672*	*0.686*	*0.775*
T12	**0.915**	**0.952**	*0.835*	*0.97*	**0.966**	*0.9*	*0.756*	*0.859*	*0.91*	**0.955**	*0.782*	*0.817*		**0.962**	**0.9**	**0.93**	**0.92**	**0.95**	**0.927**
T13	*0.883*	**0.935**	*0.884*	**0.985**	**0.983**	*0.882*	*0.789*	*0.847*	*0.888*	*0.926*	0.88	*0.796*	**0.962**		**0.978**	**0.981**	**0.968**	**0.968**	**0.956**
L1	*0.89*	**0.938**	*0.903*	**0.984**	**0.957**	*0.884*	*0.797*	*0.815*	*0.841*	*0.889*	*0.672*	*0.723*	*0.9*	**0.978**		**0.979**	**0.937**	**0.927**	**0.936**
L2	*0.885*	**0.941**	*0.892*	**0.984**	**0.962**	*0.908*	*0.781*	*0.851*	*0.859*	*0.924*	*0.656*	*0.699*	**0.93**	**0.981**	**0.979**		**0.966**	**0.964**	**0.957**
L4	*0.848*	*0.904*	*0.869*	**0.985**	**0.964**	*0.856*	*0.772*	*0.829*	*0.83*	*0.89*	*0.699*	*0.672*	**0.92**	**0.968**	**0.937**	**0.966**		**0.992**	**0.97**
L6	*0.871*	**0.92**	*0.864*	**0.978**	**0.971**	*0.885*	*0.786*	*0.867*	*0.847*	*0.906*	*0.792*	*0.686*	**0.95**	**0.968**	**0.927**	**0.964**	**0.992**		**0.977**
L7	*0.903*	**0.947**	*0.878*	*0.956*	**0.977**	*0.931*	*0.855*	*0.81*	*0.803*	*0.861*	*0.825*	*0.775*	*0.927*	**0.956**	**0.936**	**0.957**	**0.97**	**0.977**	

Table 6.2: Results of phylogenetic Partial Least Squares analysis of landmarks concerning the '*centrum*' module. Above diagonal cells show the pairwise correlation values (i.e., degree of integration) between each pair of vertebrae, while below diagonal values display the correlation values with significance levels after Benjamini-Hochberg correction Results in bold and in grey shaded cells show significant correlations and suggested modules, while results in italics and with white shaded cells are not significant (p-value > 0.05, Table S6.5).

	ATLAS	**AXIS**	**C4**	**C6**	**C7**	**T1**	**T2**	**T4**	**T6**	**T8**	**T10**	**T11**	**T12**	**T13**	**L1**	**L2**	**L4**	**L6**	**L7**
ATLAS		**0.936**	**0.921**	**0.907**	**0.931**	**0.929**	**0.892**	*0.894*	*0.873*	**0.91**	**0.898**	**0.902**	**0.916**	**0.87**	**0.897**	**0.898**	*0.866*	*0.866*	*0.877*
AXIS	**0.936**		**0.925**	**0.886**	**0.954**	**0.967**	**0.821**	*0.858*	*0.832*	**0.9**	**0.843**	*0.821*	**0.833**	**0.823**	**0.924**	**0.898**	**0.865**	*0.818*	**0.849**
C4	**0.921**	**0.925**		**0.983**	**0.954**	*0.906*	**0.944**	*0.894*	*0.894*	**0.942**	**0.928**	*0.891*	**0.893**	**0.906**	**0.928**	**0.918**	**0.918**	*0.882*	0.854
C6	**0.907**	**0.886**	**0.983**		*0.901*	*0.85*	**0.948**	*0.887*	*0.883*	*0.922*	**0.944**	*0.896*	*0.855*	*0.873*	**0.945**	*0.904*	*0.924*	*0.908*	*0.907*
C7	**0.931**	**0.954**	**0.954**	*0.901*		**0.958**	**0.913**	**0.9**	**0.894**	**0.954**	**0.919**	**0.92**	**0.946**	**0.953**	**0.978**	**0.986**	**0.975**	**0.966**	**0.935**
T1	**0.929**	**0.967**	*0.906*	*0.85*	**0.958**		*0.913*	*0.898*	*0.916*	**0.941**	*0.862*	*0.891*	*0.874*	*0.877*	**0.934**	**0.933**	**0.922**	*0.904*	*0.897*
T2	0.892	**0.821**	**0.944**	*0.948*	**0.913**	*0.913*		*0.868*	*0.857*	**0.933**	*0.831*	*0.887*	*0.885*	*0.887*	*0.842*	*0.87*	*0.861*	*0.839*	*0.916*
T4	*0.894*	*0.858*	*0.894*	*0.887*	*0.9*	*0.898*	*0.868*		**0.941**	**0.975**	*0.887*	**0.906**	*0.873*	*0.881*	*0.884*	*0.9*	*0.898*	**0.942**	*0.858*
T6	*0.873*	*0.832*	*0.894*	*0.883*	*0.894*	*0.916*	*0.857*	**0.941**		**0.99**	**0.895**	**0.947**	**0.891**	**0.913**	**0.91**	**0.918**	***0.893***	**0.922**	*0.884*
T8	**0.91**	**0.9**	**0.942**	*0.922*	**0.954**	*0.941*	*0.933*	**0.975**	**0.99**		**0.917**	**0.947**	**0.914**	**0.934**	**0.938**	**0.95**	**0.942**	**0.964**	*0.896*
T10	**0.898**	*0.843*	**0.928**	**0.944**	**0.919**	*0.862*	*0.831*	*0.887*	*0.895*	*0.917*		**0.945**	**0.965**	**0.949**	**0.975**	**0.957**	**0.961**	**0.922**	**0.905**
T11	**0.902**	*0.821*	*0.891*	*0.896*	**0.92**	*0.891*	*0.887*	**0.906**	**0.947**	**0.947**	**0.945**		**0.966**	**0.968**	**0.963**	**0.958**	**0.948**	**0.953**	*0.912*
T12	**0.916**	*0.833*	*0.893*	*0.855*	**0.946**	*0.874*	*0.885*	*0.873*	**0.891**	*0.914*	**0.965**	**0.966**		**0.989**	**0.984**	**0.99**	**0.991**	**0.959**	**0.983**
T13	*0.87*	*0.823*	*0.906*	*0.873*	**0.953**	*0.877*	*0.887*	*0.881*	**0.913**	**0.934**	**0.949**	**0.968**	**0.989**		**0.992**	**0.991**	**0.987**	**0.971**	**0.938**
L1	*0.897*	**0.924**	**0.928**	**0.945**	**0.978**	**0.934**	*0.842*	*0.884*	**0.91**	**0.938**	**0.975**	**0.963**	**0.984**	**0.992**		**0.986**	**0.977**	**0.981**	**0.95**
L2	*0.898*	**0.898**	*0.918*	*0.904*	**0.986**	*0.933*	*0.87*	*0.9*	**0.918**	**0.95**	**0.957**	**0.958**	**0.99**	**0.991**	**0.986**		**0.996**	**0.989**	**0.944**
L4	*0.866*	**0.865**	*0.918*	*0.924*	**0.975**	*0.922*	*0.861*	*0.898*	*0.893*	**0.942**	**0.961**	**0.948**	**0.991**	**0.987**	**0.977**	**0.996**		**0.986**	**0.94**
L6	*0.866*	*0.818*	*0.882*	*0.908*	**0.966**	*0.904*	*0.839*	**0.942**	**0.922**	**0.964**	**0.922**	**0.953**	**0.959**	**0.971**	**0.981**	**0.989**	**0.986**		**0.942**
L7	*0.877*	**0.849**	0.854	*0.907*	**0.935**	*0.897*	*0.916*	*0.858*	*0.884*	*0.896*	**0.905**	*0.912*	**0.983**	**0.938**	**0.95**	**0.944**	**0.94**	**0.942**	

Table 6.3: Results of phylogenetic Partial Least Squares analysis of landmarks concerning the 'neural spine' module. Above diagonal cells show the pairwise correlation values (i.e., degree of integration) between each pair of vertebrae, while below diagonal values display the correlation values with significance levels after Benjamini-Hochberg correction Results in bold and in grey shaded cells show significant correlations and suggested modules, while results in italics and with white shaded cells are not significant (p-value > 0.05, Table S6.6).

	ATLAS	**AXIS**	**C4**	**C6**	**C7**	**T1**	**T2**	**T4**	**T6**	**T8**	**T10**	**T11**	**T12**	**T13**	**L1**	**L2**	**L4**	**L6**	**L7**
ATLAS		**0.973**	*0.811*	**0.952**	**0.908**	**0.883**	**0.849**	*0.778*	*0.795*	*0.77*	**0.809**	*0.778*	**0.882**	**0.878**	**0.87**	**0.87**	**0.833**	**0.859**	**0.936**
AXIS	**0.973**		**0.954**	**0.99**	**0.955**	*0.879*	*0.878*	*0.864*	*0.893*	*0.893*	**0.927**	**0.926**	**0.983**	**0.955**	**0.942**	**0.96**	**0.939**	**0.947**	**0.953**
C4	*0.811*	*0.954*		**0.977**	*0.856*	*0.836*	*0.845*	*0.853*	*0.813*	*0.795*	*0.701*	*0.616*	*0.784*	*0.862*	*0.87*	*0.857*	*0.828*	*0.811*	*0.865*
C6	**0.952**	**0.99**	**0.977**		**0.984**	**0.983**	**0.983**	*0.876*	*0.891*	*0.893*	*0.808*	*0.858*	**0.981**	**0.989**	**0.988**	**0.988**	**0.979**	**0.976**	**0.969**
C7	**0.908**	**0.955**	*0.856*	**0.984**		*0.901*	*0.843*	*0.759*	*0.82*	*0.798*	*0.84*	*0.717*	**0.964**	**0.971**	**0.944**	**0.953**	**0.96**	**0.966**	**0.96**
T1	**0.883**	*0.879*	*0.836*	**0.983**	*0.901*		**0.95**	*0.787*	*0.777*	*0.875*	**0.912**	**0.909**	**0.905**	*0.857*	*0.839*	*0.873*	*0.813*	*0.862*	**0.912**
T2	*0.849*	*0.878*	*0.845*	**0.983**	*0.843*	**0.95**		*0.784*	*0.854*	*0.87*	*0.81*	*0.802*	*0.759*	*0.774*	*0.767*	*0.743*	*0.747*	*0.768*	*0.836*
T4	*0.778*	*0.864*	*0.853*	*0.876*	*0.759*	*0.787*	*0.784*		**0.947**	**0.935**	*0.837*	**0.877**	*0.827*	*0.811*	*0.772*	*0.812*	*0.792*	*0.827*	*0.759*
T6	*0.795*	*0.893*	*0.813*	*0.891*	*0.82*	*0.777*	*0.854*	**0.947**		*0.912*	**0.91**	**0.94**	*0.886*	*0.84*	*0.792*	*0.818*	*0.802*	*0.813*	*0.768*
T8	*0.77*	*0.893*	*0.795*	*0.893*	*0.798*	*0.875*	*0.87*	*0.935*	*0.912*		*0.849*	*0.806*	*0.84*	*0.803*	*0.76*	*0.797*	*0.758*	*0.792*	*0.86*
T10	*0.809*	**0.927**	*0.701*	*0.808*	*0.84*	*0.912*	*0.81*	*0.837*	*0.91*	*0.849*		**0.936**	**0.893**	*0.728*	*0.576*	*0.542*	*0.6*	*0.561*	*0.615*
T11	*0.778*	**0.926**	*0.616*	*0.858*	*0.717*	*0.909*	*0.802*	*0.877*	**0.94**	*0.806*	**0.936**		*0.78*	**0.83**	*0.536*	*0.745*	*0.57*	*0.615*	*0.733*
T12	**0.882**	**0.983**	*0.784*	**0.981**	**0.964**	*0.905*	*0.759*	*0.827*	*0.886*	*0.84*	**0.893**	*0.78*		**0.948**	**0.903**	**0.928**	**0.916**	**0.942**	*0.904*
T13	**0.878**	**0.955**	*0.862*	**0.989**	**0.971**	*0.857*	*0.774*	*0.811*	*0.84*	*0.803*	*0.728*	*0.83*	**0.948**		**0.983**	**0.979**	**0.967**	**0.955**	**0.945**
L1	**0.87**	**0.942**	*0.87*	**0.988**	**0.944**	*0.839*	*0.767*	*0.772*	*0.792*	*0.76*	*0.576*	*0.536*	**0.903**	**0.983**		**0.976**	**0.929**	**0.914**	**0.927**
L2	**0.87**	**0.96**	*0.857*	**0.988**	**0.953**	*0.873*	*0.743*	*0.812*	*0.818*	*0.797*	*0.542*	*0.745*	**0.928**	**0.979**	**0.976**		**0.96**	**0.955**	**0.948**
L4	*0.833*	*0.939*	*0.828*	**0.979**	**0.96**	*0.813*	*0.747*	*0.792*	*0.802*	*0.758*	*0.6*	*0.57*	**0.916**	**0.967**	**0.929**	**0.96**		**0.99**	**0.963**
L6	*0.859*	**0.947**	*0.811*	**0.976**	**0.966**	*0.862*	*0.768*	*0.827*	*0.813*	*0.792*	*0.561*	*0.615*	**0.942**	**0.955**	**0.914**	**0.955**	**0.99**		**0.967**
L7	**0.936**	**0.953**	*0.865*	*0.969*	**0.96**	**0.912**	*0.836*	*0.759*	*0.768*	*0.86*	*0.615*	*0.733*	*0.904*	**0.945**	**0.927**	**0.948**	**0.963**	**0.967**	

Discussion

The results presented here provide new information on the structural organisation of the vertebral column in felids, and potentially mammals in general. In light of the results presented here, the 'traditional regions' hypothesis (i.e., 'the cervical, thoracic and lumbar regions in the felid vertebral column form discrete morphological modules') and the 'cervicothoracic and lumbar modules' hypothesis (i.e. 'two modules composed of multiple vertebrae that share common allometric patterns: an anterior cervicothoracic and a lumbar module') could be rejected or considered insufficiently explanatory. Although high covariation was found between vertebrae within each of these regions, those either did not include all or most vertebrae which compose the regions or, more commonly, sets of highly covarying vertebral shapes were inclusive of vertebrae beyond the traditional boundaries. Specifically, in all of the analyses performed, with the exception of the phylogenetic PLS on the neural-spine landmarks, covariation in the anterior portion of the axial skeleton included high pairwise covariation between cervicals and the first thoracics. Additionally, all cervicals analysed here, with the exception of C4, displayed high covariation with the last thoracics and lumbar vertebrae.

A distinct module composed of vertebrae in the cervicothoracic boundary (i.e., C6 – T2) was found. A developmental covariation had already been suggested

for these units based on the migration of cells from their somites bound to the forelimbs, which may additionally have been involved in the first evolutionary steps that contributed to the muscularisation of the diaphragm (Buchholtz et al. 2012). Due to the lack of vertebrae C3 and C5 in our dataset, it was not possible to test for higher covariation between those and C4, composing the suggested C3 – C5 developmental module in mammals (Buchholtz et al. 2012). Nevertheless, C4 presented very high correlations with both C2 and C6, indicating that a C3 – C5 set would likely not be distinguishable as a separate morphological module in the analyses presented here.

High covariation was found between the two last thoracics, T12 and T13, and the lumbars. These two last thoracic vertebrae indeed have morphological characteristics that resemble lumbar shape more than they do rest of the thoracics, such as a larger centrum, a cranially oriented neural spine and the presence of accessory processes (Chapter 4; Slijper 1946; De Iuliis and Pulerà 2006; Randau et al. 2016a). This result thus supports the 'thoracolumbar' modularity hypothesis (i.e., 'thoracic and lumbar vertebrae show high covariation'), although only with regards to these last thoracics. Additionally, when considering mammals in general, this T12 – L7 modularity could facilitate, or be driven by, the homeotic changes between the thoracic and lumbar regions which can promote vertebral column variation without

changes in overall vertebral count (Narita and Kuratani 2005; De Iuliis and Pulerà 2006; Buchholtz 2007; Müller et al. 2010; Buchholtz 2014).

We found strong support for the 'anticlinality' hypothesis (Chapter 3; Randau et al. 2016b), although this was only composed of vertebrae T10 and T11, and not T12. This group comprises a biomechanically important region of the axial skeleton for two main reasons. Firstly, T10 is the diaphragmatic vertebra, which marks the dorsocaudal attachment of this septum and is also the first of the thoracic vertebrae to present ribs which are vertebrochondral, commonly named 'false' or 'floating', instead of vertebrosternal ribs (i.e., vertebrochondral ribs attach to cartilages of another rib instead of directly to the sternum) (De Iuliis and Pulerà 2006). This release from the physical constraint of direct attachment allows for greater sagittal bending towards the posterior end of the vertebral column, particularly in the ribless lumbar region (Polly et al. 2001; Narita and Kuratani 2005; Buchholtz 2014; Jones 2015). Secondly, T11 is the anticlinal vertebra, with a much reduced and usually perpendicular neural spine, marking the change in neural spine orientation from a caudally inclined process prior to this vertebra to the cranially orientated process present in vertebrae T12 through L7 (Slijper 1946; De Iuliis and Pulerà 2006; Randau et al. 2016a; Randau et al. 2016b). This change in neural spine orientation is especially well defined in carnivorans (specifically in Canidae and Felidae) and, along with the observed increase in centrum

length, promotes greater motion and sagittal bending of the posterior region of the axial skeleton (Chapters 3 and 4; Slijper 1946; Randau et al. 2016a; Randau et al. 2016b).

Finally, the boundaries of the modules found here mostly supported the 'developmental model disruption' hypothesis, in which it was proposed that boundaries of intervertebral modules would reflect the positions of vertebrae that did not show significant intravertebral modularity in a previous study (Chapter 4; Randau and Goswami 2017b). The intravertebral developmental modularity model of two modules was not supported in vertebrae C4, T1, T8, L6 and L7 (Chapter 5; Randau and Goswami 2017b), and the results presented here show that most of the intervertebral modules follow the hypothesized boundaries or have vertebral boundaries that only slightly differ from those by one vertebra (Fig. 6.3). This result is best displayed in the mid-posterior region. Anterior to the suggested boundary at T10 between the prediaphragmatic and postdiaphragmatic vertebrae, the T1-T8, or mid-thoracics T4 – T8 composed a distinct set; while the postdiaphragmatic vertebrae were divided into two modules (T10 – T11, and T12 – L7) with very high within-module covariation. As discussed above, these postdiaphragmatic vertebrae undergo more pronounced bending due to the release from the physical constraints of the ribs and diaphragm (Slijper 1946; Randau et al. 2016a; Randau et al. 2016b). Accordingly, previous studies have

shown that the T10 – L7 region shows higher ecological signal in felids and that measurements from this region are best at separating species in a vertebral morphospace (Chapters 3 and 4; Randau et al. 2016a; Randau et al. 2016b). Furthermore, our previous study (Chapter 5) has shown that these vertebrae also displayed the greatest overall intravertebral integration and morphological variance, an observation which supports the hypothesis of high integration being able to facilitate increased levels of disparity, and therefore promoting morphological evolution on those preferred axes of variation (i.e., "lines of least resistance" hypothesis) (Schluter 1996a; Goswami et al. 2014; Randau and Goswami 2017b). Taken together, these results indicate that the postdiaphragmatic vertebrae T10 – L7 compose an evolutionary highly responsive region which is organised into two strongly covarying modules. This modularity may therefore be responsible for maintaining the organisation and relative independence of this region, while the high integration both within each module and within individual vertebrae may contribute to higher levels of shape disparification (and ecological specialisation) while retaining functionality.

In the anterior vertebral column, support for the 'developmental model disruption' hypothesis is less clear, as the first two cervicals were not supported as a separate module. However, C4, which did not support the two-module developmental model in our analysis of intravertebral

modularity (Chapter 5; Randau and Goswami 2017b), only displayed significant covariation with two of the other analysed vertebrae. Additionally, two well-supported modules were found either near or involving the suggested boundary between the last cervical and first thoracic: a module composed of C1 – T1, and another of C6 – T2. As discussed above, these vertebrae have been suggested to be highly constrained by development (Narita and Kuratani 2005; Buchholtz et al. 2012; Buchholtz 2014), and show significant phylogenetic signal, but no ecological signal, in shape across felids (Chapter 4; Randau et al. 2016a).

The analyses presented here revealed surprisingly strong covariation between the most anterior and most posterior presacral vertebrae (C1 – C7 and T12 – L7 in the phylogenetic analysis, Table 5.1). This result was unexpected as we had hypothesized higher covariation between more thoracic and lumbar vertebrae instead (Jenkins 1971; Buchholtz 2007). However, the origin of this pattern may lie in vertebral ossification timing. A study looking at ossification sequences in the domestic cat skeleton (Boyd 1976) reported that thoracic elements developed prior to both the cervical and lumbar regions. In this case, this shared later ossification of cervical and lumbar vertebral elements could relate to the observed covariation of these two regions. Additionally, a more recent study of vertebral ossification in 17 species of mammals (Hautier et al. 2010) (including one monotreme, six marsupials and ten placentals, but not

including any felids) has shown that, although neural arches ossify first and begin ossification in the first cervicals and first thoracics, these are followed by ossification in the other cervicals and lumbar regions. Subsequently, centra ossify first in the thoracic region and ossification spreads both cranially and caudally (Hautier et al. 2010). This progression of centra ossification in both directions could indeed cause a coincidence in ossification timing in cervicals and posterior T12 – L7. While this potential explanation for the pattern of covariation among these two regions is speculative, it could be tested with more detailed ossification sequence data from felids, vertebral modularity studies across mammals, and biomechanical analyses of the axial skeleton across felids and other mammals.

The results from the phylogenetic PLS on centrum or neural-spine-related coordinates also offer some support for this new hypothesis of integration between cervicals and T12-L7, tentatively due to ossification timing (Tables 6.2 and 6.3). There was a clear and strong association between the neural-spine landmarks of cervical vertebrae (with the exception of C4) and vertebrae in the T12 – L7 region. This covariation was slightly less consistent but still present in the analysis of the centrum-related landmarks, although in this case the atlas (C1), C6 also displayed fewer covariations with posterior vertebrae in addition to C4. Additionally, those posterior vertebrae with significant covariation were generally the more anterior ones, from T8 – L4, with the

exception of T11, reflecting the direction of centrum ossification. However, we would expect a stronger signal of this covariation in the centrum landmarks, rather than the neural spine landmarks, contrary to our results.

The separate centrum and neural-spine analyses also supported the other modules found in the PLS analyses of whole vertebrae. Results from centrum-only landmarks showed modularity of the vertebral column into an anterior cervicothoracic module from C1 – T2, with five pairwise exceptions between atlas (C1) and T2, C4 and T1, C6 and C7, C6 and T1, and C6 and T2. This analysis also showed stronger interaction between the thoracics and lumbars, with a strong T6 – L6 module, and among vertebrae in the T12 – L7 module. Neural-spine traits further supported this T12 – L7 module, as well as the C1 – C7 module (with C1 and C4, C2 and C4, and C4 and C7 as exceptions), and the anticlinality T10 – T11 module.

Here we have performed an empirical analysis of intervertebral integration and compared our results to previously suggested hypotheses of developmental and functional modularity across the presacral vertebral column. Our results demonstrate that modularity is prevalent in the axial skeleton of felids, but that modules do not necessarily agree with the traditional regions of cervical, thoracic and lumbar vertebrae. Instead, vertebral morphological modules reflect four main groupings which organise

the vertebral column according to either developmental constraints or function. Those regions have also been shown to differ considerably in their morphological disparity, phylogenetic signal, and ecological specialisation, and have been suggested to present opposing levels of evolvability. Additionally, the observed interaction between the cervicals and lumbars may reflect their shared ossification timing. Finally, the recovered modules supported the hypothesis that overall modularity of the vertebral column reflects the positions of the few vertebrae which show disruption of the intravertebral developmental two-module model. Specifically, the few vertebrae in which the developmental two-module model was not supported form the boundaries of the intervertebral modules found here

Although this study is limited to a subset of representatives from a single family, the similarities in the modular organisation found here to developmental patterns shared across mammals suggest that these results may reflect a common mammalian condition. Importantly, the modular organisation of the vertebral column demonstrated here highlights that both development and function are important factors shaping vertebral shape diversification. Therefore, it may be the trade-off between these influences that control the disparity observed in the axial skeleton across mammalian families.

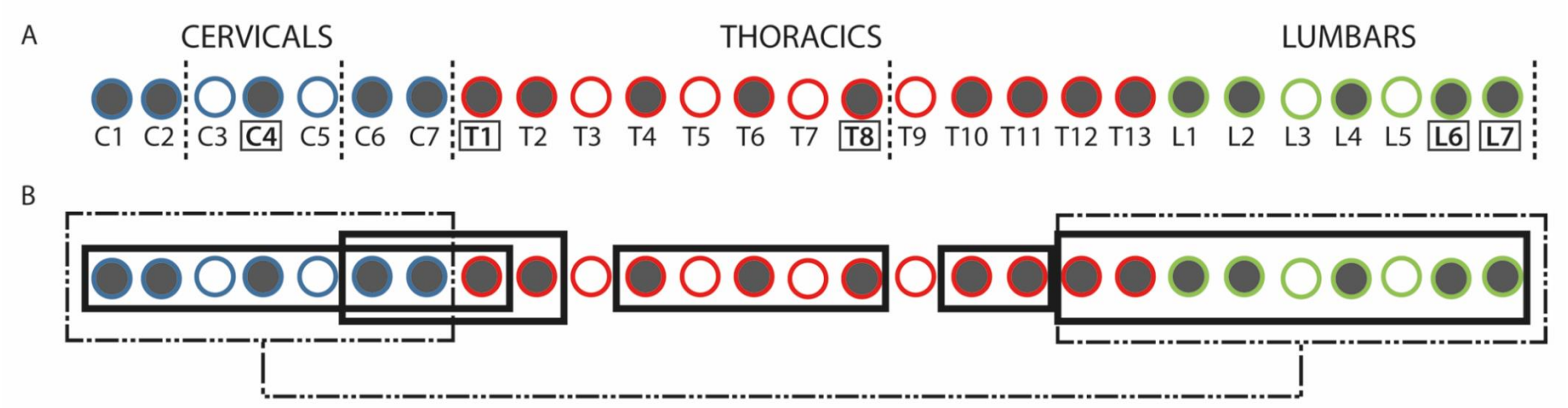

Fig. 6.3: Schematics of vertebral column modules based on pairwise correlations between vertebrae. A. Vertical dashed lines are hypothesized regional boundaries based on vertebrae showing disruption of the two-module model for intravertebral shape covariation (vertebrae C4, T1, T8, L6, and L7, Chapter 5; Randau and Goswami 2017b). B. Rectangular boxes showing suggested vertebral column modules. Dashed boxes and connecting line describe correlations between the cervicals and the T12 – L7 vertebrae. C, T, and L stand for cervicals (blue outline), thoracics (red outline), and lumbars (green outline), respectively. Grey-filled circles describe landmarked vertebrae.

Appendix 6.1

Table S6.1: Landmark number and description per vertebra.

VERTEBRA	LANDMARK	DESCRIPTION
ATLAS	1	Anterior mid-point of dorsal arch
	2	Anterior mid-point of ventral arch
	3	Anterior lateral-most tip of left transverse process
	4	Anterior lateral-most tip of right transverse process
	5	Dorso-anterior-most tip of left pre-zygapophysis
	6	Dorso-anterior-most tip of right pre-zygapophysis
	7	Posterior mid-point of dorsal arch
	8	Posterior mid-point of ventral arch
	9	Posterior lateral-most tip of left transverse process
	10	Posterior lateral-most tip of right transverse process
	11	Posterior-most tip of left post-zygapophysis
	12	Posterior-most tip of right post-zygapophysis
AXIS	1	Anterior-most point at tip of den
	2	Ventral mid-point at base of den
	3	Anterior-most point of neural spine
	4	Posterior ventral mid-point of centrum
	5	Posterior left lateral-most point of width of centrum
	6	Posterior right lateral-most point of width of centrum
	7	Posterior left dorso-lateral point of centrum
	8	Posterior right dorso-lateral point of centrum
	9	Posterior dorsal mid-point of the neural canal
	10	Dorsal posterior-most point at tip of neural spine
	11	Left lateral-most posterior tip of transverse process
	12	Right lateral-most posterior tip of transverse process
	13	Posterior-most dorsal point of left post-zygapophysis
	14	Posterior-most dorsal point of right post-zygapophysis
C4	1	Anterior ventral mid-point of centrum
	2	Anterior dorsal mid-point of centrum
	3	Anterior left lateral-most point of centrum
	4	Anterior left lateral-most point of centrum
	5	Anterior dorsal-most point of left pre-zygapophyses
	6	Anterior dorsal-most point of right pre-zygapophyses
	7	Anterior-most point of left lamina

	8	Anterior-most point of right lamina
	9	Dorsal-most point at tip of neural spine
	10	Posterior ventral mid-point of centrum
	11	Posterior dorsal mid-point of centrum
	12	Posterior Left lateral-most point of centrum
	13	Posterior right lateral-most point of centrum
	14	Posterior dorsal mid-point of the neural canal
	15	Posterior-most point of left post-zygapophyses
	16	Posterior-most point of right post-zygapophyses
	17	Lateral-most point of left transverse process
	18	Lateral-most point of right transverse process
C6	1	Anterior ventral mid-point of centrum
	2	Anterior dorsal mid-point of centrum
	3	Anterior left lateral-most point of centrum
	4	Anterior left lateral-most point of centrum
	5	Anterior dorsal-most point of left pre-zygapophyses
	6	Anterior dorsal-most point of right pre-zygapophyses
	7	Lateral-most point of left transverse process
	8	Lateral-most point of right transverse process
	9	Anterior-most point of left lamina
	10	Anterior-most point of right lamina
	11	Dorsal-most point at tip of neural spine
	12	Posterior ventral mid-point of centrum
	13	Posterior dorsal mid-point of centrum
	14	Posterior Left lateral-most point of centrum
	15	Posterior right lateral-most point of centrum
	16	Posterior dorsal mid-point of the neural canal
	17	Posterior-most point of left post-zygapophyses
	18	Posterior-most point of right post-zygapophyses
	19	Posterior-most point of left lamina
	20	Posterior-most point of right lamina
C7 - T10*	1	Anterior ventral mid-point of centrum
	2	Anterior dorsal mid-point of centrum
	3	Anterior left lateral-most point of centrum
	4	Anterior left lateral-most point of centrum
	5	Anterior dorsal-most point of left pre-zygapophysis
	6	Anterior dorsal-most point of right pre-zygapophysis
	7	Lateral-most point of left transverse process
	8	Lateral-most point of right transverse process
	9	Dorsal-most point at tip of neural spine
	10	Posterior ventral mid-point of centrum
	11	Posterior dorsal mid-point of centrum
	12	Posterior Left lateral-most point of centrum

	13	Posterior right lateral-most point of centrum
	14	Posterior dorsal mid-point of the neural canal
	15	Posterior-most point of left post-zygapophysis
	16	Posterior-most point of right post-zygapophysis
T11	1	Anterior ventral mid-point of centrum
	2	Anterior dorsal mid-point of centrum
	3	Anterior left lateral-most point of centrum
	4	Anterior left lateral-most point of centrum
	5	Anterior dorsal-most point of left pre-zygapophysis
	6	Anterior dorsal-most point of right pre-zygapophysis
	7	Posterior-most point of tip of left accessory process
	8	Posterior-most point of tip of right accessory process
	9	Dorsal-most point at tip of neural spine
	10	Posterior ventral mid-point of centrum
	11	Posterior dorsal mid-point of centrum
	12	Posterior Left lateral-most point of centrum
	13	Posterior right lateral-most point of centrum
	14	Posterior dorsal mid-point of the neural canal
	15	Posterior-most point of left post-zygapophysis
	16	Posterior-most point of right post-zygapophysis
T12 - T13	1	Anterior ventral mid-point of centrum
	2	Anterior dorsal mid-point of centrum
	3	Anterior left lateral-most point of centrum
	4	Anterior left lateral-most point of centrum
	5	Anterior dorsal-most point of left pre-zygapophyses
	6	Anterior dorsal-most point of right pre-zygapophyses
	7	Anterior Dorsal-most point at tip of neural spine
	8	Posterior Dorsal-most point at tip of neural spine
	9	Posterior ventral mid-point of centrum
	10	Posterior dorsal mid-point of centrum
	11	Posterior Left lateral-most point of centrum
	12	Posterior right lateral-most point of centrum
	13	Posterior dorsal mid-point of the neural canal
	14	Posterior-most point of left post-zygapophyses
	15	Posterior-most point of right post-zygapophyses
	16	Posterior-most point of tip of left accessory process
	17	Posterior-most point of tip of right accessory process
L1 - L4	1	Anterior ventral mid-point of centrum
	2	Anterior dorsal mid-point of centrum
	3	Anterior dorsal-most point of left pre-zygapophyses
	4	Anterior dorsal-most point of right pre-zygapophyses

	5	Dorsal anterior-most point at tip of neural spine
	6	Anterior left lateral-most point of centrum
	7	Anterior left lateral-most point of centrum
	8	Lateral-most point of left transverse process
	9	Lateral-most point of right transverse process
	10	Posterior ventral mid-point of centrum
	11	Posterior dorsal mid-point of centrum
	12	Posterior dorsal mid-point of the neural canal
	13	Posterior Left lateral-most point of centrum
	14	Posterior right lateral-most point of centrum
	15	Posterior-most point of tip of left accessory process
	16	Posterior-most point of tip of right accessory process
	17	Posterior-most point of left post-zygapophyses
	18	Posterior-most point of right post-zygapophyses
	19	Dorsal posterior-most point at tip of neural spine
L6 - L7	1	Anterior ventral mid-point of centrum
	2	Anterior dorsal mid-point of centrum
	3	Anterior dorsal-most point of left pre-zygapophyses
	4	Anterior dorsal-most point of right pre-zygapophyses
	5	Dorsal anterior-most point at tip of neural spine
	6	Anterior left lateral-most point of centrum
	7	Anterior left lateral-most point of centrum
	8	Lateral-most point of left transverse process
	9	Lateral-most point of right transverse process
	10	Posterior ventral mid-point of centrum
	11	Posterior dorsal mid-point of centrum
	12	Posterior dorsal mid-point of the neural canal
	13	Posterior Left lateral-most point of centrum
	14	Posterior right lateral-most point of centrum
	15	Posterior-most point of left post-zygapophyses
	16	Posterior-most point of right post-zygapophyses
	17	Dorsal posterior-most point at tip of neural spine

Table S6.2: Summary of landmarks composing each developmental module organisation of vertebral organisation, following Chapter 5 (Randau and Goswami 2017b).

	CENTRUM MODULE	NEURAL-SPINE MODULE
ATLAS	2; 8	1; 3 – 7; 9 - 12
AXIS **(3 MODULES)**	1, 2, 4 - 8	3; 9 – 14
C4	1 – 4; 10 – 13	5 – 9; 14 – 18
C6	1 – 4; 12 – 15	5 – 11; 16 – 20
C7 – T10	1 – 4; 10 – 13	5 – 9; 14 – 16
T11	1 – 4; 8 – 11	5 – 7; 12 – 16
T12 – T13	1 – 4; 9 – 12	5 – 8; 13 – 17
L1 – L4	1; 2; 6; 7; 10; 11; 13; 14	3 – 5; 8; 9; 12; 15 – 19
L6 – L7	1; 2; 6; 7; 10; 11; 13; 14	3 – 5; 8; 9; 12; 15 – 17

Table S6.3: Specimen number information per species for the individuals used in the analyses presented here. Museum abbreviations are as follows: NHM: Natural History Museum, London; MNHN: Muséum National d'Histoire Naturelle, Paris; MCZ: Harvard Museum of Natural History, Cambridge; AMNH: American Museum of Natural History, New York; FMNH: Museum of Natural History, Chicago; USNM: Smithsonian National Museum of Natural History, Washington D.C.

Species	**Specimen number**
Acinonyx jubatus	FMNH 127834
	FMNH 57826
	USNM 520539
	AMNH 119655
	AMNH 119657
	AMNH 119656
	AMNH 36426
Felis catus	USNM 396268
	USNM 396392
	USNM 397631
	USNM 398871
	USNM A21665
	NHM 1952 10 20 4
	NHM 1988 1
Leopardus pardalis	FMNH 93174
	FMNH 68895
	USNM 271094
	USNM A14182
	MNHN 1998 1866
	MNHN A3456
	AMNH 214744
	AMNH 248728
Leptailurus serval	FMNH 127843
	FMNH 44438
	FMNH 60491
	USNM 548666
	NHM 1855 6 30 2
	NHM 1845 9 25 23
	AMNH 34767
Neofelis nebulosa	FMNH 54304
	USNM 399291
	USNM 545387
	MNHN 1961 217
	MNHN 1980 16
	NHM 1854 6 14 2
	NHM 1965 1 18 1

	AMNH 35273
Panthera leo	FMNH 49340
	USNM 172677
	MCZ 9487
	AMNH 85147
Panthera pardus	USNM 15684
	USNM 303320
	MNHN 1892 1079
	MNHN A13045 1844
	MNHN 1898 100
	MNHN 1906 454
	MNHN 1945 70
	MNHN A7932
	MNHN BII 4
	MNHN CG1998 582
	AMNH 54462
Prionailurus bengalensis	FMNH 99363
	FMNH 121228
	USNM 317283
	NHM 1309b
	NHM 77 2896
	NHM 1979 2895
	NHM 1309b 1858
Puma concolor	FMNH 129339
	USNM A21528
	USNM 264166
	MNHN 1937 4
	AMNH 181997
	AMNH 90213
	AMNH 10259

Table S6.4: Above diagonal cells display the p-values for the pairwise correlation values from the phylogenetic PLS analysis of all landmarks' coordinates. Below diagonal values show the p-values after Benjamini-Hochberg correction. Results in bold and with grey shaded cells are significant (p-value < 0.05).

	ATLAS	AXIS	C4	C6	C7	T1	T2	T4	T6	T8	T10	T11	T12	T13	L1	L2	L4	L6	L7
ATLAS		**0.001**	*0.051*	**0.014**	**0.03**	**0.033**	*0.132*	*0.119*	**0.023**	**0.004**	*0.155*	**0.036**	**0.014**	**0.039**	**0.03**	**0.024**	*0.08*	*0.052*	**0.023**
AXIS	**0.01**		**0.005**	**0.002**	**0.004**	**0.018**	*0.083*	*0.213*	*0.109*	**0.011**	**0.024**	**0.015**	**0.004**	**0.008**	**0.003**	**0.004**	**0.023**	**0.013**	**0.003**
C4	*0.108*	**0.022**		**0.001**	*0.087*	*0.192*	*0.141*	*0.249*	*0.497*	*0.316*	*0.623*	*0.722*	*0.256*	*0.133*	*0.075*	*0.085*	*0.128*	*0.147*	*0.114*
C6	**0.042**	**0.016**	**0.01**		**0.004**	**0.005**	**0.014**	*0.757*	*0.644*	*0.401*	*0.687*	*0.468*	**0.025**	**0.005**	**0.004**	**0.006**	**0.005**	**0.012**	*0.079*
C7	*0.071*	**0.02**	*0.163*	**0.02**		*0.050**	*0.13*	*0.528*	*0.267*	**0.04**	*0.322*	*0.41*	**0.001**	**0.001**	**0.002**	**0.001**	**0.004**	**0.002**	**0.001**
T1	*0.077*	*0.051*	*0.266*	**0.022**	*0.107*		**0.03**	*0.464*	*0.47*	*0.097*	**0.008**	**0.012**	*0.081*	*0.2*	*0.175*	*0.108*	*0.256*	*0.126*	**0.036**
T2	*0.212*	*0.161*	*0.219*	**0.042**	*0.212*	**0.03**		*0.663*	*0.444*	*0.132*	*0.249*	*0.227*	*0.626*	*0.642*	*0.433*	*0.514*	*0.529*	*0.496*	*0.285*
T4	*0.201*	*0.289*	*0.315*	*0.757*	*0.559*	**0.041**	*0.675*		**0.013**	**0.008**	*0.17*	**0.02**	*0.136*	*0.247*	*0.223*	*0.148*	*0.193*	*0.118*	*0.388*
T6	*0.06*	*0.19*	*0.537*	*0.66*	*0.331*	*0.161*	*0.502*	**0.041**		**0.018**	**0.012**	**0.008**	**0.043**	*0.094*	*0.169*	*0.144*	*0.232*	*0.191*	*0.479*
T8	**0.02**	**0.041**	*0.649*	*0.466*	*0.088*	*0.273*	*0.212*	**0.03**	*0.051*		*0.23*	*0.33*	**0.013**	*0.099*	*0.171*	*0.082*	*0.141*	*0.102*	*0.396*
T10	*0.228*	*0.061*	*0.727*	*0.695*	*0.39*	*0.071*	*0.315*	*0.243*	**0.041**	*0.302*		**0.001**	*0.163*	**0.034**	*0.458*	*0.533*	*0.384*	*0.142*	*0.107*
T11	*0.081*	**0.044**	*0.319*	*0.518*	*0.473*	*0.518*	*0.301*	*0.055*	**0.03**	*0.397*	**0.01**		*0.084*	*0.153*	*0.236*	*0.391*	*0.518*	*0.436*	*0.219*
T12	**0.042**	**0.02**	*0.212*	*0.063*	**0.01**	*0.518*	*0.649*	*0.215*	*0.093*	**0.041**	*0.238*	*0.161*		**0.003**	**0.019**	**0.012**	**0.013**	**0.007**	**0.027**
T13	*0.087*	**0.03**	*0.386*	**0.022**	**0.01**	*0.178*	*0.66*	*0.315*	*0.175*	*0.18*	*0.078*	*0.227*	**0.01**		**0.001**	**0.001**	**0.002**	**0.003**	**0.006**
L1	*0.071*	**0.019**	*0.154*	**0.02**	**0.016**	*0.247*	*0.496*	*0.298*	*0.243*	*0.243*	*0.515*	*0.305*	**0.01**	**0.001**		**0.001**	**0.002**	**0.003**	**0.001**
L2	*0.061*	**0.02**	*0.161*	**0.026**	**0.01**	*0.19*	*0.553*	*0.222*	*0.22*	*0.161*	*0.56*	*0.461*	**0.016**	**0.001**	0.01		**0.001**	**0.001**	**0.001**
L4	*0.161*	*0.06*	*0.212*	**0.022**	**0.02**	*0.319*	*0.559*	*0.266*	*0.303*	*0.219*	*0.459*	*0.554*	**0.019**	**0.002**	0.016	0.01		**0.001**	**0.001**
L6	*0.108*	**0.041**	*0.222*	**0.041**	**0.016**	*0.211*	*0.537*	*0.201*	*0.266*	*0.183*	*0.219*	*0.497*	**0.026**	**0.003**	0.019	0.01	**0.01**		**0.001**
L7	*0.06*	**0.019**	*0.197*	0.161	**0.01**	*0.081*	*0.35*	*0.46*	*0.525*	*0.463*	*0.19*	*0.295*	0.067	**0.006**	0.01	0.01	**0.01**	**0.01**	

Table S6.5: Above diagonal cells display the p-values for the pairwise correlation values from the phylogenetic PLS analysis of centrum-only coordinates. Below diagonal values show the p-values after Benjamini-Hochberg correction. Results in bold and with grey shaded cells are significant (p-value < 0.05).

	ATLAS	AXIS	C4	C6	C7	T1	T2	T4	T6	T8	T10	T11	T12	T13	L1	L2	L4	L6	L7
ATLAS		**0.005**	**0.018**	**0.02**	**0.011**	**0.008**	**0.036**	*0.054*	*0.088*	**0.025**	**0.02**	**0.016**	**0.005**	**0.047**	**0.031**	**0.032**	*0.08*	*0.079*	*0.085*
AXIS	**0.019**		**0.008**	**0.019**	**0.001**	**0**	**0.012**	*0.055*	*0.072*	**0.019**	**0.03**	*0.067*	**0.029**	**0.048**	**0.005**	**0.01**	**0.019**	*0.07*	**0.05***
C4	**0.042**	**0.025**		**0.001**	**0.005**	*0.086*	**0.017**	*0.126*	*0.115*	**0.015**	**0.022**	*0.097*	**0.045**	**0.037**	**0.018**	**0.033**	**0.038**	*0.088*	*0.218*
C6	**0.042**	**0.042**	**0.006**		*0.161*	*0.468*	**0.032**	*0.322*	*0.327*	*0.125*	**0.024**	*0.188*	*0.24*	*0.214*	**0.018**	*0.133*	*0.073*	*0.089*	*0.121*
C7	**0.031**	**0.006**	**0.019**	*0.179*		**0.002**	**0.019**	**0.042**	**0.043**	**0.004**	**0.007**	**0.01**	**0.001**	**0.001**	**0**	**0**	**0**	**0**	**0.007**
T1	**0.025**	**0**	*0.109*	*0.468*	**0.01**		*0.059*	*0.148*	*0.072*	**0.027**	*0.199*	*0.095*	*0.121*	*0.128*	**0.025**	**0.038**	**0.05***	*0.084*	*0.126*
T2	*0.062*	**0.033**	**0.042**	*0.056*	**0.042**	*0.083*		*0.345*	*0.378*	**0.049**	*0.345*	*0.164*	*0.09*	*0.13*	*0.342*	*0.208*	*0.262*	*0.334*	*0.059*
T4	*0.079*	*0.079*	*0.146*	*0.336*	*0.07*	*0.167*	*0.349*		**0.015**	**0.001**	*0.055*	**0.048**	*0.054*	*0.069*	*0.089*	*0.065*	*0.054*	**0.012**	*0.197*
T6	*0.109*	*0.095*	*0.138*	*0.339*	*0.071*	*0.095*	*0.38*	**0.038**		**0**	**0.031**	**0.003**	**0.023**	**0.016**	**0.026**	**0.021**	**0.046**	**0.014**	*0.065*
T8	**0.048**	**0.042**	**0.038**	*0.146*	**0.018**	*0.051*	*0.075*	**0.006**	**0**		**0.048**	**0.011**	**0.046**	**0.02**	**0.025**	**0.013**	**0.019**	**0.005**	*0.155*
T10	**0.042**	*0.055*	**0.045**	**0.048**	**0.023**	*0.215*	*0.349*	*0.079*	*0.056*	*0.074*		**0.011**	**0.002**	**0.003**	**0.001**	**0.002**	**0.001**	**0.006**	**0.014**
T11	**0.04**	*0.092*	*0.117*	*0.206*	**0.03**	*0.115*	*0.181*	*0.074*	**0.014**	**0.031**	**0.031**		**0.002**	**0.001**	**0.004**	**0.006**	**0.01**	**0.008**	*0.07*
T12	**0.019**	*0.054*	*0.073*	*0.253*	**0.006**	*0.143*	*0.11*	*0.079*	**0.046**	*0.074*	**0.01**	**0.01**		**0**	**0**	**0**	**0**	**0.001**	**0.002**
T13	*0.074*	*0.074*	*0.063*	*0.229*	**0.006**	*0.147*	*0.148*	*0.094*	**0.04**	**0.042**	**0.014**	**0.006**	**0**		**0**	**0**	**0**	**0**	**0.004**
L1	*0.056*	**0.019**	**0.042**	**0.042**	**0**	**0.048**	*0.349*	*0.109*	**0.049**	**0.048**	**0.006**	**0.018**	**0**	**0**		**0**	**0.001**	**0**	**0.006**
L2	*0.056*	**0.03**	*0.058*	*0.151*	**0**	*0.064*	*0.224*	*0.09*	**0.044**	**0.035**	**0.01**	**0.021**	**0**	**0**	**0**		**0**	**0**	**0.005**
L4	*0.104*	**0.042**	*0.064*	*0.096*	**0**	*0.075*	*0.275*	*0.079*	*0.074*	**0.042**	**0.006**	**0.03**	**0**	**0**	**0.006**	**0**		**0**	**0.005**
L6	*0.103*	*0.094*	*0.109*	*0.109*	**0**	*0.108*	*0.344*	**0.033**	**0.037**	**0.019**	**0.021**	**0.025**	**0.006**	**0**	**0**	**0**	**0**		**0.022**
L7	*0.108*	*0.075*	*0.232*	*0.143*	**0.023**	*0.146*	*0.083*	*0.215*	*0.09*	*0.173*	**0.037**	*0.094*	**0.01**	**0.018**	**0.021**	**0.019**	**0.019**	**0.045**	

Table S6.6: Above diagonal cells display the p-values for the pairwise correlation values from the phylogenetic PLS analysis of neural spine-only coordinates. Below diagonal values show the p-values after Benjamini-Hochberg correction. Results in bold and with grey shaded cells are significant (p-value < 0.05).

	ATLAS	**AXIS**	**C4**	**C6**	**C7**	**T1**	**T2**	**T4**	**T6**	**T8**	**T10**	**T11**	**T12**	**T13**	**L1**	**L2**	**L4**	**L6**	**L7**
ATLAS		**0**	*0.122*	**0.003**	**0.005**	**0.016**	**0.046**	*0.2*	*0.11*	*0.312*	**0.031**	*0.051*	**0.012**	**0.014**	**0.005**	**0.005**	**0.019**	**0.021**	**0.003**
AXIS	**0**		**0.022**	**0**	**0.005**	*0.168*	*0.199*	*0.311*	*0.129*	*0.2*	**0.012**	**0.012**	**0**	**0.012**	**0.009**	**0.002**	**0.021**	**0.005**	**0.006**
C4	*0.234*	*0.057*		**0.003**	*0.192*	*0.325*	*0.332*	*0.319*	*0.453*	*0.733*	*0.63*	*0.852*	*0.467*	*0.2*	*0.102*	*0.133*	*0.204*	*0.301*	*0.15*
C6	**0.017**	**0**	**0.017**		**0.004**	**0.005**	**0.004**	*0.788*	*0.606*	*0.739*	*0.722*	*0.485*	**0.004**	**0.002**	**0.002**	**0.002**	**0.004**	**0.012**	**0.037**
C7	**0.019**	**0.019**	*0.332*	**0.018**		*0.057*	*0.279*	*0.788*	*0.376*	*0.68*	*0.122*	*0.555*	**0.003**	**0.001**	**0.003**	**0**	**0.003**	**0.001**	**0.004**
T1	**0.045**	*0.296*	*0.434*	**0.019**	*0.123*		**0.01**	*0.588*	*0.571*	*0.159*	**0.026**	**0.035**	**0.038**	*0.164*	*0.193*	*0.107*	*0.256*	*0.09*	**0.031**
T2	*0.105*	*0.332*	*0.437*	**0.018**	*0.401*	**0.034**		*0.723*	*0.279*	*0.3*	*0.246*	*0.278*	*0.631*	*0.628*	*0.439*	*0.585*	*0.552*	*0.533*	*0.329*
T4	*0.332*	*0.427*	*0.43*	*0.802*	*0.802*	*0.675*	*0.763*		**0.012**	**0.044**	*0.122*	**0.045**	*0.249*	*0.425*	*0.351*	*0.249*	*0.296*	*0.219*	*0.606*
T6	*0.224*	*0.243*	*0.561*	*0.682*	*0.483*	*0.664*	*0.401*	**0.035**		*0.114*	**0.019**	**0.004**	*0.076*	*0.266*	*0.318*	*0.249*	*0.278*	*0.284*	*0.65*
T8	*0.427*	*0.332*	*0.764*	*0.766*	*0.727*	*0.286*	*0.418*	*0.103*	*0.229*		*0.131*	*0.26*	*0.263*	*0.525*	*0.476*	*0.387*	*0.502*	*0.422*	*0.256*
T10	*0.077*	**0.035**	*0.692*	*0.763*	*0.234*	*0.066*	*0.391*	*0.234*	*0.052*	*0.243*		**0.001**	*0.012*	*0.346*	*0.655*	*0.814*	*0.604*	*0.847*	*0.731*
T11	*0.113*	**0.035**	*0.852*	*0.588*	*0.65*	*0.086*	*0.401*	*0.104*	**0.018**	*0.397*	**0.01**		*0.116*	**0.049**	*0.773*	*0.13*	*0.674*	*0.625*	*0.277*
T12	**0.035**	**0**	*0.575*	**0.018**	**0.017**	*0.09*	*0.692*	*0.391*	*0.162*	*0.398*	**0.035**	*0.231*		**0.001**	**0.016**	**0.007**	**0.012**	**0.007**	*0.055*
T13	**0.041**	**0.035**	*0.332*	**0.014**	**0.01**	*0.292*	*0.692*	*0.534*	*0.399*	*0.628*	*0.452*	*0.11*	**0.01**		**0**	**0**	**0.003**	**0.001**	**0.006**
L1	**0.019**	**0.031**	*0.213*	**0.014**	**0.017**	*0.332*	*0.548*	*0.455*	*0.43*	*0.581*	*0.709*	*0.796*	**0.045**	**0**		**0**	**0.002**	**0.004**	**0.002**
L2	**0.019**	**0.014**	*0.245*	**0.014**	**0**	*0.22*	*0.675*	*0.391*	*0.391*	*0.494*	*0.824*	*0.243*	**0.025**	**0**	**0**		**0**	**0**	**0.001**
L4	*0.052*	*0.055*	*0.335*	**0.018**	**0.018**	*0.394*	*0.65*	*0.418*	*0.401*	*0.605*	*0.682*	*0.725*	**0.035**	**0.017**	**0.014**	**0**		**0**	**0.001**
L6	*0.055*	**0.019**	*0.418*	**0.035**	**0.01**	*0.19*	*0.633*	*0.357*	*0.405*	*0.534*	*0.852*	*0.692*	**0.025**	**0.01**	**0.018**	**0**	**0**		**0.001**
L7	**0.017**	**0.022**	*0.273*	*0.089*	**0.018**	*0.077*	*0.436*	*0.682*	*0.708*	*0.394*	*0.764*	*0.401*	*0.121*	**0.022**	**0.014**	**0.01**	**0.01**	**0.01**	

Chapter 7: Shape covariation (or the lack thereof) between vertebrae and other skeletal traits in felids: the whole is not always greater than the sum of parts.

To be submitted to Evolution Letters.

Abstract

Within carnivorans, cats show comparatively little disparity in overall morphology, with species differing mainly in body size. However, detailed shape analyses of individual osteological structures, such as limb bones or the skull, have shown that felids display significant morphological differences that correlate with ecological and behavioural range observed in living species.

Recently, these shape analyses have been extended to the felid axial skeleton. Results demonstrate a functionally-partitioned vertebral column, with regions varying greatly in level of correlation between shape and ecology. Moreover, a clear distinction is evident between a phylogenetically-constrained neck region and a selection-responsive posterior spine.

Here, we test whether this regionalisation of function reflected in vertebral column shape is also translated into varying levels of phenotypic integration between this structure and most other skeletal elements. We accomplish this comparison by performing pairwise tests of integration between vertebral and other osteological units, quantified with 3D geometric morphometric data and analysed both with and without phylogenetic correction. To our knowledge, this is the first study to test for integration across a comprehensive sample of whole-skeleton elements.

Our results show that, prior to corrections, strong covariation is present between vertebrae across the vertebral column and all other elements, with the exception of the femur. However, most of these significant correlations disappear after correcting for phylogeny, which is a significant influence on cranial and limb morphology of felids and other carnivorans. Our results thus suggest that the vertebral column of cats displays relative independence from other skeletal elements and may represent several distinct evolutionary morphological modules.

Introduction

The relationship between form and function has been shown to be present in a widespread range of organismal traits, with several examples of correlated

changes in shape to promote adaptation to specific ecologies (e.g., Gonyea 1978; Lauder 1995; Moon 1999; Irschick 2002; Stayton 2006, 2008; McInnes et al. 2011; Ercoli et al. 2012; Hutchinson 2012). However, in a scenario where distinct organismal structures show covariation among themselves, independent adaptation of each structure to its optimal function may be hindered. Specifically, if selection drivers and/or directions are not the same in covarying traits, selection in one part may be obstructed by either opposing or stabilizing forces on the covarying others. Alternatively, a degree of independence may arise which allows for some decoupling between structures, and further independent change may follow. However simplified, these are the concepts on which the fields of integration (i.e., the overall covariation of traits) and modularity (i.e., the relative autonomy of integrated structures, which are termed modules, from other structures) have been based (Olson and Miller 1958).

This form-function relationship has been particularly well explored in studies of carnivoran evolution, potentially due to the charismatic status of most species in this mammalian order and consequent improved levels of ecological knowledge which facilitate these comparisons. Specifically, ecological and life history specialisations regarding a wide range of traits, from diet to locomotion to mating strategies (e.g., Gonyea 1978; Bertram and Biewener 1990; Antón and Galobart 1999; Antón et al. 2004; Holliday and Steppan 2004;

Van Valkenburgh 2007; Doube et al. 2009; Jones and Goswami 2010; Meachen-Samuels 2010; Salesa et al. 2010; Hudson et al. 2011; Zhang et al. 2012; Fabre et al. 2013a; Fabre et al. 2013b; Cuff et al. 2016a, 2016b; Randau et al. 2016b), have been shown to correlate with aspects of skeletal shape in living and fossil carnivorans. Within this order, the family of cat species (Felidae) shows little morphological disparity when only gross anatomy is considered, as most species differ mainly in body size and display a typical hypercarnivorous morphotype (Ewer 1973; Sunquist and Sunquist 2002; Holliday and Steppan 2004; Van Valkenburgh 2007; MacDonald et al. 2010). Rigorous shape analyses, however, have shown that cranial, dental and limb traits can successfully distinguish species that differ in ecology, particularly regarding either prey size or locomotor style (Gonyea 1978; Dayan et al. 1990; Meachen-Samuels and Van Valkenburgh 2009a, 2009b; Meachen-Samuels 2012). Nevertheless, limb and cranial shapes across Felidae have also been shown to be highly correlated with phylogeny (Meloro and O'Higgins 2011; Meloro and Slater 2012; Walmsley et al. 2012; Piras et al. 2013; Martín-Serra et al. 2014a).Recent work has shown that these ecologically-driven shape changes, although mostly concentrated in the cranium and limbs, are also present in vertebral morphology, although to a smaller and more regionalised degree. Specifically, it is at the posterior end of the vertebral column (i.e., T10 – L7 vertebrae) that vertebral shape correlates most significantly with either body mass, prey size choice (i.e., specialisation in small, mixed, and large prey), or

locomotor mode (i.e., cursorial, terrestrial, scansorial, and arboreal) (as discussed in Chapters 3 and 4; Randau et al. 2016a; Randau et al. 2016b), whilst vertebrae in the neck region are more conservative in shape. Even at this T10 – L7 region, the amount of vertebral shape variation across species is only explained by ecology to a relatively small degree (i.e., prey size and locomotor mode explained around 18% and 12% of the shape variance, respectively; Chapter 4, Randau et al. 2016a). In comparison, previous studies of felids have demonstrated that when using measurements of the skull and limbs it was possible to correctly discriminate between species' ecology at around 65% and 93% of the time, respectively (Meachen-Samuels and Van Valkenburgh 2009a, 2009b).

Furthermore, vertebral shape may be largely developmentally constrained across all regions of the axial skeleton, which would prevent more extensive changes in response to selection (Richardson and Chipman 2003; Asher et al. 2011; Losos 2011; Buchholtz 2012; Buchholtz et al. 2014; Galis et al. 2014). The mammalian vertebral column has been suggested to be under strong canalisation and developmental stability, which may explain its reduced variability with regards to vertebral count when compared to other vertebrate groups (Narita and Kuratani 2005; Müller et al. 2010; Buchholtz 2012; Buchholtz et al. 2012). Furthermore, we have demonstrated that a signal of developmental origin is present in most individual vertebral shape across

adult felids, with most vertebrae possessing two internal modules of high shape covariation which are reflective of developmental origin (Chapter 5; Randau and Goswami 2017b).

Taken together, the regionalised ecological signal in the vertebral column and the higher levels of shape adaptation in other skeletal elements raise the question of whether these ecologically-driven shape changes are correlated. Alternatively, differential influences on vertebral shape versus the rest of the skeleton may be reflected in the levels of integration and modularity among these elements. Here we test for shape covariation between presacral vertebrae and other skeletal elements, including the skull, girdles and limbs, in nine species of living cats in which the vertebral form and function relationship has already been explored (Chapters 3, 4, and 5; Randau et al. 2016a; Randau et al. 2016b; Randau and Goswami 2017b). Specifically, we assess whether vertebrae covary with other osteological structures within complex systems (e.g., individual bones within the forelimb) and whether vertebrae within the ecologically-informative T10 – L7 region show more frequent or higher correlations with other ecologically-informative skeletal elements. To perform this analysis, we use a powerful method developed specifically for assessing covariation among divergent datasets: the two-block Partial Least Squares (PLS) analysis analysis (Rohlf and Corti 2000; Bookstein et al. 2003).

As discussed in Chapter 2, PLS analyses find two independent axes which represent the greatest covariation between the pair of blocks, and are the standard methodology for testing for integration between two structures, whether different regions of a single element or entirely separate elements. Importantly, because PLS analyses do not take into consideration the variation within each of the structures, this methodology is appropriate for testing integration between highly different structures with distinct levels of complexity and divergent within-structure variation, or even between a set of landmark coordinates and a vector of categories concerning an ecological variable (Rohlf and Corti 2000; Bookstein et al. 2003; Goswami and Polly 2010c; Klingenberg 2013). As an example, Fabre et al. (2017) have recently tested the covariation between forelimb shape and two ecological variables regarding locomotion (i.e., scores for orientation and size of support) in strepsirrhine primates. Specifically, they characterised forelimb shape with a dataset of over 300 landmarks (i.e., total number of anatomical landmarks plus curve and surface semi-landmarks) per forelimb long bone, and each ecological variable had two scores (i.e., vertical and horizontal scores for support orientation, and small and large scores for support size). This example clearly highlights the appropriateness of PLS analyses in testing for covariation between blocks which differ greatly in dimensionality and variance structure, let alone shape.

Further, a common example in the literature concerning analyses of covariation between two structures in vertebrates is the test of covariation between skull and mandible (e.g., Monteiro et al. 2003; Bastir et al. 2005; Hautier et al. 2012; Cornette et al. 2013a; Adams and Felice 2014; Álvarez et al. 2015; Adams 2016). In this example, both PLS blocks are composed of a set of landmarks, but due to the contrasting levels of complexity between skull and dentary, these blocks greatly differ with regards to landmark number. Additionally, phylogenetic PLS analysis has been applied to the skull-mandible system to test for covariation between these structures among different species while still accounting for the phylogenetic relationships between them (e.g., Adams and Felice 2014). Both examples discussed here highlight the suitability of this technique to measure integration between blocks which vary greatly in dimensions, such as the osteological units analysed here (e.g., the atlas and the skull, with 12 and 38 landmarks each, respectively).

Material and Methods

Using an Immersion Microscribe G2X (Solution Technologies, Inc., Oella, Maryland), three-dimensional (hereafter, 3-D) landmarks were collected on 29 osteological elements throughout the skeleton of nine living felid species. Visits to seven international museums resulted in a dataset of 40 specimens

spanning these nine species, as even large collections hold a relatively small number of complete skeletons. Specimen number per species ranged from two in *Panthera leo* to eight in *Panthera pardus* (Table S7.1).

The skeletal elements included were: 19 presacral vertebrae (C1, C2, C4, C6, C7, T1, T2, T4, T6, T8, T10, T11, T12, T13, L1, L2, L4, L6, and L7), skull, dentary, scapula, forelimb long bones (i.e., humerus, radius and ulna), pelvis, hindlimb long bones (i.e., femur and tibia), and sacrum. Axial elements (i.e., vertebrae, skull, dentary, pelvis, and sacrum) were landmarked across the whole structure. All other bones were paired skeletal structures and were only landmarked on the left side of the skeleton (i.e., left scapula, humerus, radius, ulna, femur, and tibia). Due to the nature of museum specimens, most pelvis specimens were separated into halves, and therefore the left and right sides had to be landmarked, and hence analysed, separately. Vertebral selection was done per the reasoning discussed in Chapter 2, based on the results of a pilot study showing clustering of vertebrae in the morphospace, and vertebrae which were analysed in our previous studies (Chapters 3, 4 and 6; Randau et al. 2016a; Randau et al. 2016b; Randau and Goswami 2017b, 2017a).

Species analysed here included: cheetah (*Acinonyx jubatus*), puma (*Puma concolor*), lion (*Panthera leo*), leopard (*Panthera pardus*), clouded leopard (*Neofelis nebulosa*), serval (*Leptailurus serval*), leopard cat (*Prionailurus bengalensis*), ocelot (*Leopardus pardalis*), and domestic cat (*Felis catus*). As

discussed in the Introduction and Methodology chapters (Chapters 1 and 2), these species represent the ranges of body mass and ecological (locomotory and prey size specialisations) spectra observed across the extant species of the Felidae family (Table 7.1, and Table S7.1 for specimen numbers), with examples of cursorial to arboreal felids which specialise in small, mixed and large species (Sunquist and Sunquist 2002; Meachen-Samuels and Van Valkenburgh 2009a, 2009b; MacDonald et al. 2010). Landmark identities and numbers were object-specific, and varied from 12 (C1) to 17 (L6 and L7) in presacral vertebrae, and from nine (pelvis, on each side) to 38 (skull) in all other elements (Table S7.2, and Figs. 7.1 – 7.5 for illustration of landmarks' positions).

Table 7.1: Felid species included in the studies and information on their ecological categories. Ecological variables were collected from the literature (Sunquist and Sunquist 2002; Meachen-Samuels and Van Valkenburgh 2009a, 2009b; MacDonald et al. 2010).

Species	Common Name	Prey Size	Locomotion
Acinonyx jubatus	Cheetah	Large	Cursorial
Felis catus	Domestic cat	Small	Scansorial
Leopardus pardalis	Ocelot	Small	Arboreal
Leptailurus serval	Serval	Small	Terrestrial
Neofelis nebulosa	Clouded leopard	Mixed	Arboreal
Panthera leo	Lion	Large	Terrestrial
Panthera pardus	Leopard	Large	Scansorial
Prionailurus bengalensis	Leopard cat	Small	Scansorial
Puma concolor	Puma	Large	Scansorial

Testing matrix repeatability

The stability of the covariance matrices for the non-vertebral units tested here was assessed with a bootstrap analysis of each dataset over 10,000 times and using a random skewers analysis to compare the covariance matrices of the original and resampled datasets (Goswami and Polly 2010c; Melo et al. 2016). Results demonstrated that covariance matrix repeatability was high, with values ranging from 0.90 to 0.96 with a median and a mean of 0.94 (for results concerning the repeatability of the covariance matrices from vertebral datasets, see Chapter 6).

Data analyses

All analyses carried out here were performed in R version 3.3.1 (R Core Team 2016), using the 'geomorph' package (Adams and Otarola-Castillo 2013). Prior to all subsequent analyses, each skeletal component was individually aligned with a generalised Procrustes superimposition (GPA) in order to extract shape coordinates by removing the effects of rotation, scale and translation.

Covariation between each of the presacral vertebrae included here and the other skeletal components was measured pairwise with a two-block Partial Least Squares (hereafter, PLS) analysis, using the 'integration.test' function in 'geomorph'.

The PLS analyses performed here calculated the correlation coefficient as a measure of the covariation between each pairwise comparison, with significance level set at p-values equal or under 0.05.

In order to account for relatedness among the felid species in our sample, skeletal integration was also quantified with a phylogenetic Partial Least Squares analysis as discussed on Chapter 2, under a model of Brownian motion evolution (Adams and Felice 2014) and using a recent phylogeny of felids (Piras et al. 2013), which was pruned to include only the nine species studied here. Prior to phylogenetic PLS analysis, landmark data for each element was first separated into species sets (e.g., landmark data for skull specimens of ocelots) and aligned with a GPA. These species-specific Procrustes coordinates were then used to calculate the mean species shape per each bone, which was then analysed with the 'phylo.integration' function in 'geomorph'. Significance level was again set at p-values equal or under 0.05.

Multiple comparisons correction of the significance level

The analyses of integration performed here involved a large number of pairwise comparisons (i.e., 209 tests of integration between pairs of vertebra x other skeletal elements). As discussed in Chapter 2, in order to correct for an increased chance of false positives (i.e., finding a p-value < 0.05 purely due to

chance) due to this large number of comparisons, a Benjamini-Hochberg procedure (Benjamini and Hochberg 1995) was applied, with a false discovery rate at 0.05 (McDonald 2014), following the methodology outlined in the Methodology chapter (Chapter 2), and used in Chapter 6 (Randau and Goswami 2017a).

Allometry

Shape coordinates for vertebral and other skeletal traits were not directly corrected for allometry prior to the integration analyses, following the discussion in Chapter 2. Importantly, due to the high correlation of body size and evolutionary relatedness in Felidae, further correction after applying a phylogenetic PLS would likely introduce error (also, see below for discussion of comparison of results of general and phylogenetic PLS analyses).

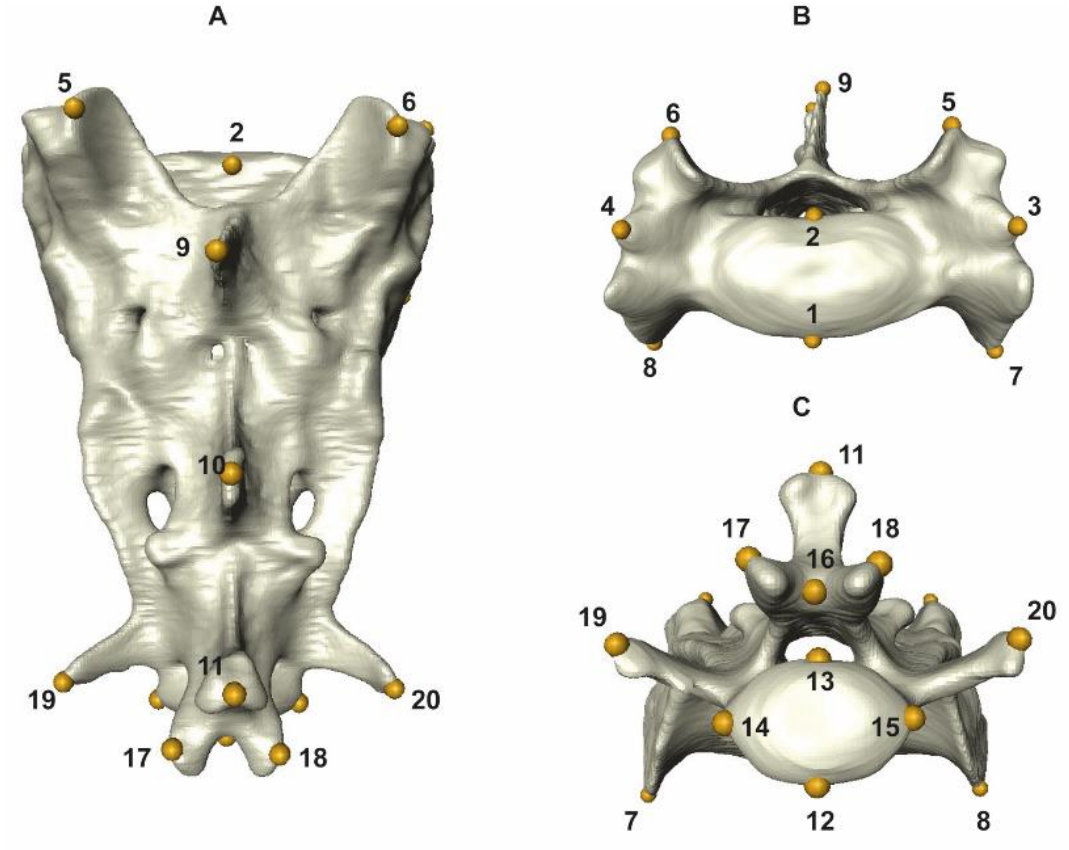

Fig. 7.1 Three-dimensional reconstruction of the sacrum of a cheetah (*Acinonyx* jubatus, USNM520539) in dorsal (A), anterior (B), and posterior (C) views, showing position of three-dimension landmarks. Analysed landmarks were collected directly from osteological specimens. For the list of all landmarks and their description, see Table S7.2.

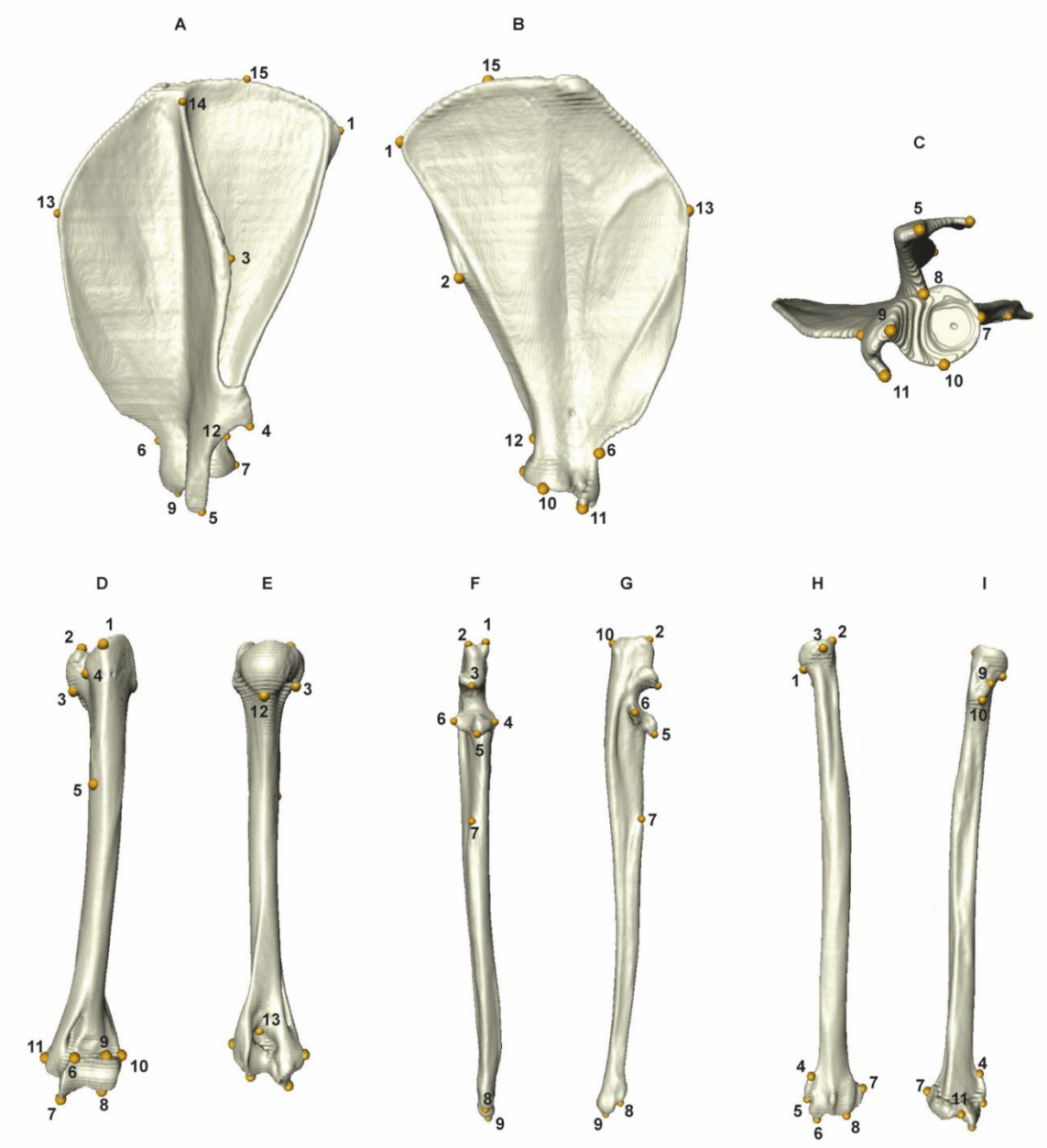

Fig. 7.2 Three-dimensional reconstruction of the elements of the pectoral girdle (scapula) and forelimb with their respective landmarks. The scapula is shown in lateral (A), medial (B), and ventral (C) views. The humerus (D and E), the ulna (F and G) and the radius (H and I) are shown in anterior (D, F and H) and posterior (E, G and I) views. Elements are not to scale. The scapula and humerus represent elements of a serval (*Leptailurus serval*, NHM 133), while the ulna and radius are reconstructions of domestic cat (*Felis catus*, RVC21) bones. For the list of all landmarks and their description, see Table S7.2.

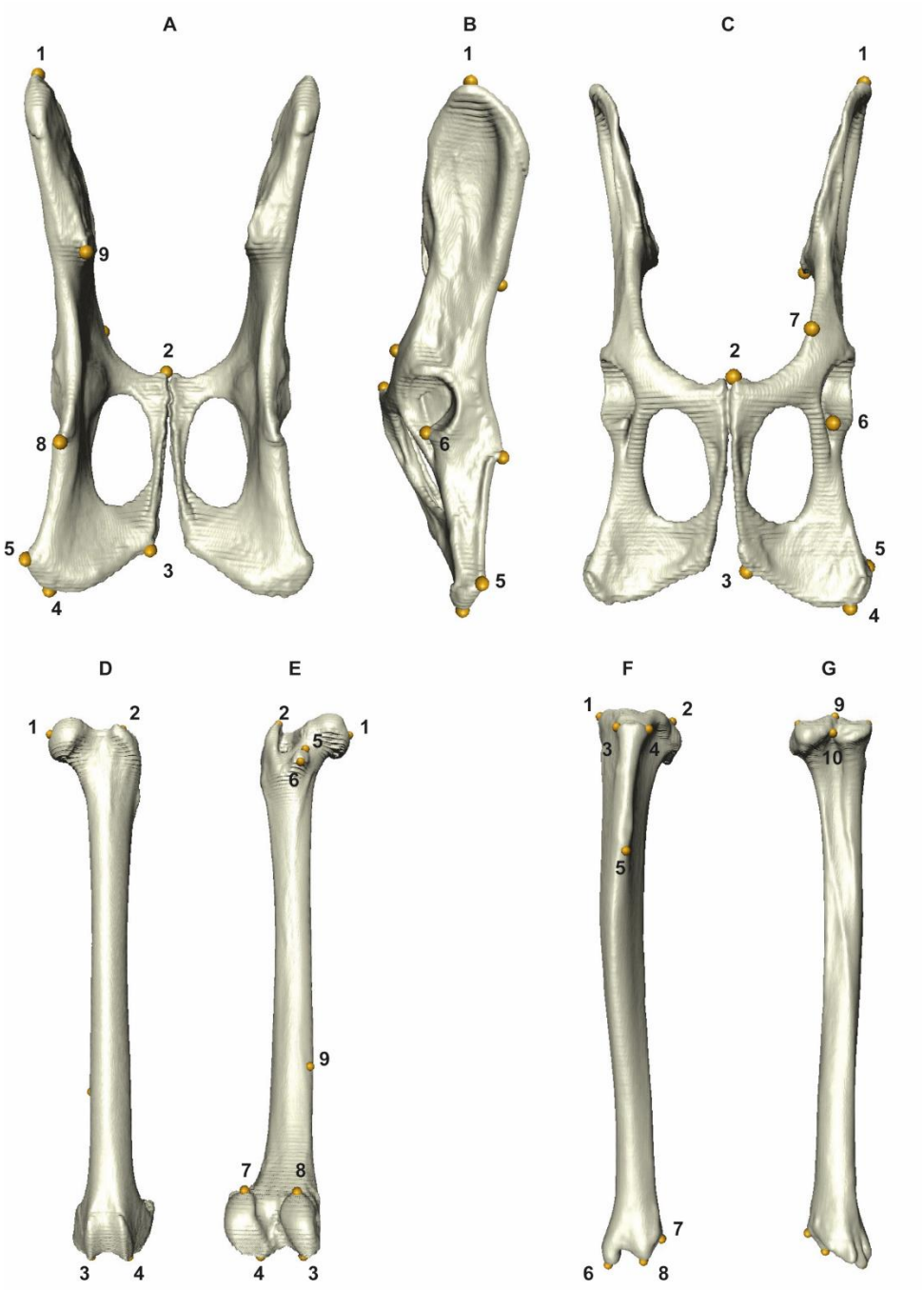

Fig. 7.3 Three-dimensional reconstruction of the elements of the pelvic girdle and hindlimb of a serval (*Leptailurus serval*, NHM 133) with their respective landmarks. The pelvis is shown in dorsal (A), lateral (B), and ventral (C) views. The femur (D and E), and the tibia (F and G) are shown in anterior (D and F) and posterior (E and G, and I) views. Elements are not to scale. The pelvis and femur represent elements of a serval (*Leptailurus serval*, NHM 133), while the tibia belongs to a domestic cat (*Felis catus*, RVC21). For the list of all landmarks and their description, see Table S7.2.

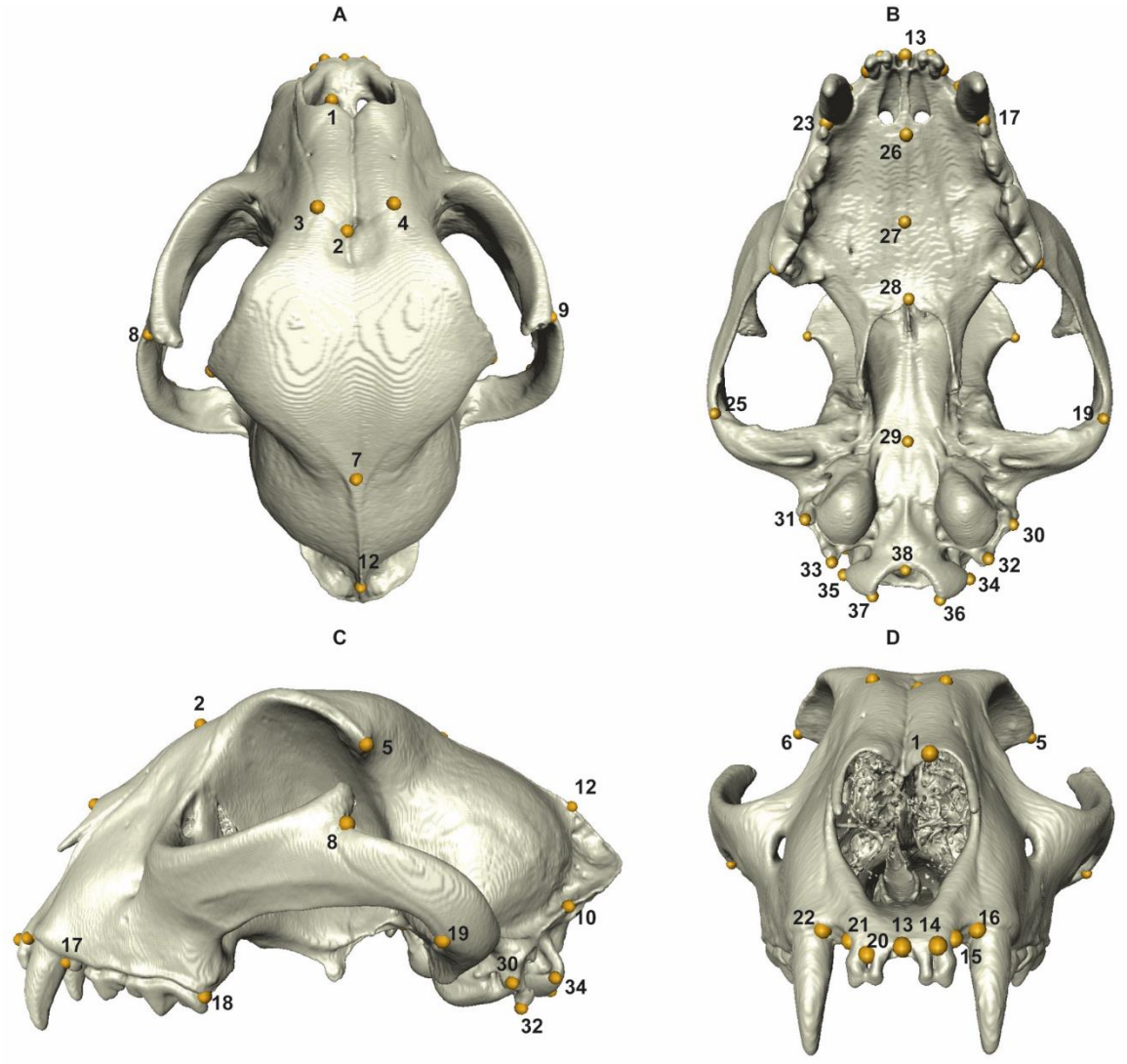

Fig. 7.4 Three-dimensional reconstruction of the skull of a cheetah (*Acinonyx* jubatus, USNM520539) showing the three-dimensional landmarks which were collected in dorsal (A), ventral (B), lateral (C) and frontal (D) views. For the list of all landmarks and their description, see Table S7.2.

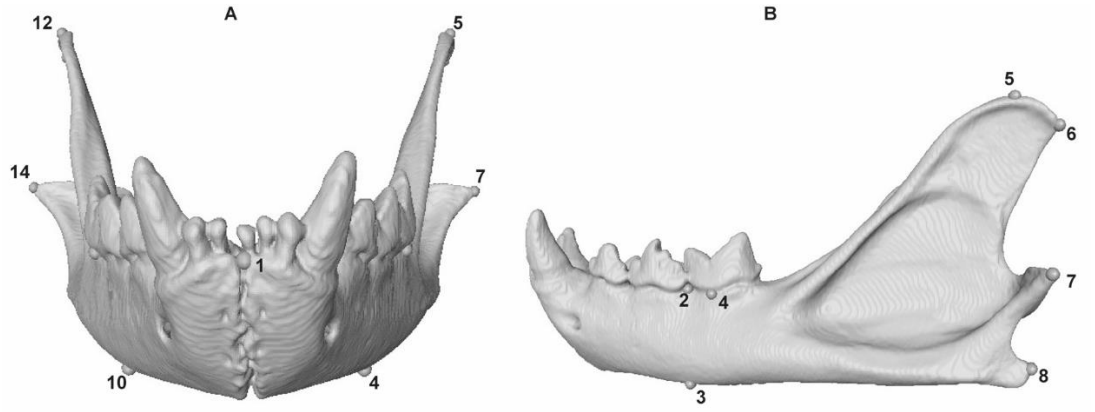

Fig. 7.4 Three-dimensional reconstruction of the dentary of a cheetah (*Acinonyx* jubatus, USNM520539) showing the three-dimensional landmarks which were collected in frontal (A) and lateral (B) views. For the list of all landmarks and their description, see Table S7.2.

Results

Skeletal shape covariation

Without considering the effects of phylogeny, 198 of the 209 pairwise comparisons between vertebrae and other skeletal elements were significant (p-value < 0.05; Tables 7.2 and 7.3). Ten of the 11 results which were not significant involved the femur and various vertebrae, and the eleventh non-significant result involved the C4 and the scapula. Across the significant results, 169 out of 198 showed high to very high integration (i.e., PLS correlations between 0.704 and 0.921) between vertebrae and the rest of the skeleton. Benjamini-Hochberg correction rendered only one additional result non-significant: the integration between L4 and the sacrum (Table 7.2).

Phylogenetic correction

In contrast to the uncorrected analyses, only 97 out of the 209 pairwise tests were significant when analysed with phylogenetic PLS (Tables 7.4 and 7.5). As before, all of the significant results displayed very high correlations, with coefficients ranging between 0.829 and 0.985. However, correcting for multiple comparisons removed most of the significant results, leaving only 15 pairwise integration tests still significant after it (Table 7.4). Out of these 15 significant correlations, 11 involved vertebrae T10 to L2 versus four in the cervical region, while none was found involving the C7 – T8 vertebrae.

Discussion

Modularity is a prevailing characteristic of the vertebral column in felids (Chapters 5 and 6; Randau et al. 2016a; Randau and Goswami 2017a, 2017b), and most likely of mammals in general (Buchholtz 2007; Buchholtz et al. 2012). In fact, modular organisation is ubiquitous across multiple levels of structures in the skeleton of organisms, observed across functionally linked elements (e.g., modular organisation within entire limbs, Schmidt and Fischer 2009; Fabre et al. 2014b; or across the vertebral column, Chapter 6, Randau and Goswami 2017a) and within different components of individual elements

Table 7.2: Results from the PLS analysis showing correlation levels in each pairwise comparison between vertebrae and other skeletal traits. Italics demark results which were not significant (p-value > 0.05), and asterisk (*) marks the tests which were not significant after Benjamini-Hochberg correction. The letters 'L' and 'R' after Pelvis denote either the left or right side of this structure, respectively.

	SKULL	DENTARY	SCAPULA	HUMERUS	ULNA	RADIUS	SACRUM	PELVIS L	PELVIS R	FEMUR	TIBIA
ATLAS	0.871	0.85	0.738	0.842	0.797	0.806	0.748	0.833	0.824	*0.58**	0.855
AXIS	0.913	0.888	0.818	0.891	0.776	0.839	0.864	0.917	0.919	*0.55**	0.898
C4	0.855	0.8	*0.643**	0.834	0.816	0.833	0.818	0.782	0.787	0.665	0.845
C6	0.853	0.811	0.733	0.877	0.801	0.859	0.847	0.85	0.856	0.722	0.857
C7	0.872	0.791	0.778	0.822	0.772	0.768	0.827	0.814	0.823	0.673	0.83
T1	0.835	0.758	0.744	0.752	0.719	0.738	0.782	0.801	0.815	0.688	0.791
T2	0.803	0.796	0.69	0.772	0.763	0.805	0.704	0.796	0.804	0.76	0.818
T4	0.783	0.831	0.738	0.827	0.683	0.765	0.751	0.781	0.787	*0.514**	0.809
T6	0.772	0.811	0.749	0.849	0.773	0.856	0.78	0.729	0.715	*0.529**	0.843
T8	0.722	0.762	0.678	0.769	0.751	0.776	0.768	0.736	0.726	*0.5**	0.767
T10	0.727	0.696	0.684	0.833	0.773	0.822	0.697	0.716	0.668	*0.433**	0.803
T11	0.787	0.712	0.67	0.838	0.78	0.783	0.72	0.695	0.655	0.77	0.844
T12	0.854	0.735	0.741	0.761	0.815	0.671	0.71	0.78	0.795	*0.556**	0.795
T13	0.896	0.756	0.764	0.78	0.848	0.771	0.782	0.857	0.849	0.657	0.753
L1	0.851	0.716	0.732	0.681	0.781	0.689	0.75	0.885	0.863	*0.515**	0.767
L2	0.884	0.732	0.783	0.798	0.825	0.734	0.76	0.921	0.892	*0.538**	0.733
L4	0.869	0.711	0.793	0.68	0.817	0.791	0.647*	0.831	0.807	*0.524**	0.673
L6	0.873	0.766	0.765	0.717	0.747	0.619	0.76	0.775	0.784	0.73	0.72
L7	0.797	0.645	0.684	0.566	0.575	0.543	0.697	0.767	0.779	0.611	0.543

Table 7.3: P-values from the PLS analysis showing correlation levels in each pairwise comparison between vertebrae and other skeletal traits. Italics demarks results which were not significant (p-value > 0.05), and asterisk (*) marks the tests which were not significant after Benjamini-Hochberg correction. Letters 'L' and 'R' as above.

	SKULL	DENTARY	SCAPULA	HUMERUS	ULNA	RADIUS	SACRUM	PELVIS L	PELVIS R	FEMUR	TIBIA
ATLAS	0.001	0.001	0.001	0.001	0.001	0.001	0.002	0.001	0.001	*0.069**	0.001
AXIS	0.001	0.001	0.001	0.001	0.001	0.001	0.001	0.001	0.001	*0.129**	0.001
C4	0.001	0.001	*0.067**	0.001	0.001	0.001	0.001	0.002	0.002	0.003	0.001
C6	0.001	0.001	0.019	0.001	0.001	0.001	0.001	0.001	0.001	0.003	0.001
C7	0.001	0.001	0.001	0.001	0.001	0.001	0.001	0.001	0.001	0.003	0.001
T1	0.001	0.001	0.005	0.001	0.001	0.002	0.002	0.001	0.001	0.004	0.001
T2	0.001	0.001	0.012	0.001	0.001	0.001	0.024	0.001	0.001	0.001	0.001
T4	0.001	0.001	0.003	0.001	0.006	0.001	0.002	0.001	0.001	*0.333**	0.001
T6	0.001	0.001	0.002	0.001	0.001	0.001	0.002	0.001	0.001	*0.172**	0.001
T8	0.003	0.001	0.036	0.001	0.001	0.001	0.005	0.001	0.001	*0.392**	0.001
T10	0.001	0.001	0.001	0.001	0.001	0.001	0.002	0.001	0.002	*0.139**	0.001
T11	0.001	0.001	0.002	0.001	0.001	0.001	0.003	0.002	0.005	0.001	0.001
T12	0.001	0.002	0.005	0.001	0.001	0.004	0.01	0.001	0.001	*0.121**	0.001
T13	0.001	0.001	0.001	0.001	0.001	0.001	0.001	0.001	0.001	0.011	0.001
L1	0.001	0.001	0.001	0.001	0.001	0.001	0.001	0.001	0.001	*0.08**	0.001
L2	0.001	0.001	0.001	0.001	0.001	0.001	0.001	0.001	0.001	*0.062**	0.001
L4	0.001	0.001	0.001	0.002	0.001	0.001	0.05*	0.001	0.001	*0.087**	0.002
L6	0.001	0.001	0.001	0.001	0.001	0.005	0.003	0.001	0.001	0.001	0.001
L7	0.001	0.002	0.001	0.028	0.01	0.017	0.009	0.001	0.001	0.001	0.021

Table 7.4: Results from the phylogenetic PLS analysis showing correlation levels in each pairwise comparison between vertebrae and other skeletal traits under a model of Brownian motion. Italics demarks results which were not significant (p-value > 0.05), and bold formatting marks the tests which remained significant after Benjamini-Hochberg correction. Letters 'L' and 'R' as above.

	SKULL	DENTARY	SCAPULA	HUMERUS	ULNA	RADIUS	SACRUM	PELVIS L	PELVIS R	FEMUR	TIBIA
ATLAS	*0.903*	**0.941**	*0.876*	*0.859*	*0.846*	*0.859*	*0.887*	0.927	0.943	*0.744*	0.898
AXIS	*0.901*	0.934	0.924	0.935	*0.881*	0.886	*0.863*	**0.965**	**0.979**	*0.766*	0.926
C4	*0.735*	0.918	0.952	*0.812*	0.916	*0.843*	*0.888*	*0.907*	0.919	*0.741*	*0.807*
C6	*0.941*	*0.923*	*0.954*	*0.93*	**0.985**	*0.901*	*0.961*	0.977	0.978	*0.94*	*0.94*
C7	0.963	0.915	0.935	0.915	**0.94**	*0.737*	*0.867*	0.946	0.94	0.929	0.91
T1	*0.831*	*0.851*	*0.875*	0.943	*0.83*	0.925	*0.827*	0.916	0.927	*0.807*	*0.838*
T2	*0.843*	0.91	*0.839*	*0.813*	*0.731*	*0.818*	*0.883*	*0.811*	*0.846*	0.915	*0.854*
T4	*0.695*	0.908	0.932	*0.836*	*0.866*	*0.845*	*0.761*	*0.854*	*0.873*	*0.678*	*0.814*
T6	*0.814*	0.947	0.92	0.945	*0.866*	0.912	*0.837*	*0.87*	*0.878*	*0.814*	0.929
T8	*0.931*	0.947	*0.87*	*0.873*	*0.895*	*0.896*	*0.892*	*0.919*	*0.927*	*0.832*	*0.874*
T10	*0.699*	*0.811*	0.891	**0.958**	*0.803*	0.898	*0.798*	0.932	0.917	0.928	0.863
T11	*0.681*	*0.826*	0.912	**0.968**	0.943	*0.832*	*0.89*	*0.757*	*0.717*	*0.646*	0.93
T12	*0.895*	0.888	0.93	*0.878*	0.92	*0.845*	*0.866*	0.914	0.909	*0.846*	**0.937**
T13	*0.902*	0.902	0.933	*0.879*	**0.964**	*0.752*	*0.859*	**0.966**	0.952	0.869	0.881
L1	*0.848*	0.896	0.937	0.888	**0.941**	*0.724*	*0.821*	**0.977**	**0.963**	*0.823*	*0.805*
L2	*0.857*	0.902	0.939	*0.852*	0.93	*0.695*	*0.799*	**0.983**	**0.969**	*0.788*	*0.805*
L4	*0.873*	0.901	0.943	0.894	0.934	*0.697*	*0.79*	0.935	0.926	0.829	*0.814*
L6	0.886	0.901	0.929	*0.869*	0.925	*0.671*	*0.805*	0.941	0.938	0.856	*0.851*
L7	0.955	0.939	0.939	*0.892*	0.939	*0.688*	*0.9*	0.964	0.952	0.935	*0.87*

Table 7.5: P-values from the phylogenetic PLS analysis showing correlation levels in each pairwise comparison between vertebrae and other skeletal traits under a model of Brownian motion. Italics demark results which were not significant (p-value > 0.05), and bold formatting marks the tests which remained significant after Benjamini-Hochberg correction. Letters 'L' and 'R' as above.

	SKULL	DENTARY	SCAPULA	HUMERUS	ULNA	RADIUS	SACRUM	PELVIS L	PELVIS R	FEMUR	TIBIA
ATLAS	*0.08*	**0.005**	*0.137*	*0.138*	*0.104*	*0.07*	*0.27*	0.019	0.01	*0.382*	0.043
AXIS	*0.087*	0.013	0.049	0.016	*0.078*	0.036	*0.461*	**0.001**	**0.001**	*0.357*	0.008
C4	*0.76*	0.028	0.012	*0.345*	0.03	*0.103*	*0.219*	*0.055*	0.036	*0.444*	*0.297*
C6	*0.258*	*0.239*	*0.154*	*0.19*	**0.002**	*0.182*	*0.178*	0.009	0.008	*0.092*	*0.106*
C7	0.01	0.022	0.03	0.041	0.016	*0.366*	*0.384*	0.005	0.016	0.018	0.02
T1	*0.433*	*0.211*	*0.204*	0.02	*0.229*	0.017	*0.664*	0.034	0.022	*0.313*	*0.276*
T2	*0.278*	0.028	*0.315*	*0.342*	*0.494*	*0.162*	*0.33*	*0.284*	*0.156*	0.017	*0.131*
T4	*0.79*	*0.023*	0.022	*0.172*	*0.071*	*0.076*	*0.858*	*0.107*	*0.08*	*0.517*	*0.134*
T6	*0.445*	0.004	0.045	0.007	*0.069*	0.017	*0.667*	*0.092*	*0.091*	*0.159*	0.012
T8	*0.084*	0.028	*0.352*	*0.248*	*0.097*	*0.054*	*0.503*	*0.063*	*0.05*	*0.252*	*0.187*
T10	*0.476*	*0.093*	0.047	**0.003**	*0.081*	0.007	*0.501*	0.008	0.017	0.007	0.015
T11	*0.56*	*0.099*	0.022	**0.002**	**0.002**	*0.052*	*0.14*	*0.238*	*0.437*	*0.401*	0.009
T12	*0.06*	0.038	0.02	*0.066*	0.021	*0.076*	*0.284*	0.022	0.028	*0.083*	**0.002**
T13	*0.053*	0.023	0.03	*0.064*	**0.003**	*0.236*	*0.331*	**0.002**	0.008	0.037	0.039
L1	*0.111*	0.023	0.021	0.044	**0.002**	*0.143*	*0.417*	**0.001**	**0.002**	*0.052*	*0.091*
L2	*0.074*	0.016	0.022	*0.065*	0.009	*0.202*	*0.498*	**0.001**	**0.001**	*0.076*	*0.074*
L4	*0.06*	0.009	0.02	0.047	0.013	*0.18*	*0.535*	0.007	0.017	0.045	*0.069*
L6	0.044	0.015	0.031	*0.064*	0.019	*0.415*	*0.535*	0.01	0.015	0.048	*0.056*
L7	0.015	0.006	0.035	*0.103*	0.027	*0.597*	*0.355*	0.01	0.011	0.015	*0.082*

(e.g., withing the skull, Goswami 2006a; Goswami and Polly 2010b; within humeral shape, Arias-Martorell et al. 2014; or within vertebrae, Chapter 5, Randau and Goswami 2017b). It may therefore be hypothesised that modularity is a universal characteristic of complex traits and may be expected to exist at even higher levels of organisation within organisms, such as between the vertebral column and the limbs or the skull.

Noticeably, as discussed in the previous chapter (Chapter 6; Randau and Goswami 2017a), the observed patterns of trait organisation are dependent on the level of analyses performed, as a hierarchical order has been demonstrated for the modular arrangement of biological traits: e.g., the mammalian skull has been demonstrated to be organised into multiple small partitions representing functional groups (Cheverud 1982, 1995; Goswami 2006a; Goswami and Finarelli 2016) which are defined within two larger blocks, inclusive of a higher number of bones each, that are observable when the focus of the analysis changes to a 'face' versus 'neurocranium' level (Drake and Klingenberg 2010). Similarly, a hierarchical organisation seems present in the presacral vertebral column of felids with the aforementioned two blocks within most individual vertebrae (Chapter 5; Randau and Goswami 2017b), which are themselves partitioned between five larger modules across the spine, each including multiple vertebrae (Chapter 6; Randau and Goswami 2017a). The results presented here strongly suggest a third level of

organisation in which the vertebral column as a whole structure is considered a separate module within the complete skeletal system of felids. Importantly, in light of the results shown throughout this thesis, particularly in the last two chapters (Chapters 5 and 6; Randau and Goswami 2017b, 2017a), it becomes clear that these distinct levels of organisation are driven by either development and function, with each of these sources of covariation playing a more significant role in shape disparification at different levels (e.g., the functional overprint of the developmental two-module model of intravertebral covariation discussed in Chapter 5; Randau and Goswami 2017b).

Studies of the vertebral column have shown that its function and organisation vary widely through time and across taxa. Large shifts in vertebral form and function have been observed in the shift from axial-driven to appendicular-focused locomotion, in the change to a parasagittal limb posture in mammals, and in the appearance of a muscularised diaphragm, which both affected locomotion and potentially constrained vertebral count (Buchholtz and Stepien 2009; Schilling 2011; Buchholtz et al. 2012). Additionally, the increase in regionalisation in the evolution of the mammalian axial skeleton has long been suggested to allow compartmentalisation of function across the vertebral series (Slijper 1946). Therefore, the mammalian vertebral column has been hypothesised to have experienced increases in complexity through time, even

whilst being highly constrained throughout development (Buchholtz 2012, 2014).

This change in complexity and organisation in traits is central to the theory of modularity, by which higher independence between certain sets of traits may evolve to break constraints due to pleiotropy and canalisation, thus allowing further individual trait responses to selection (Cheverud 1996; Wagner 1996; Schlosser and Wagner 2004; Goswami and Polly 2010b). Further, whereas modularity may facilitate independent traits to undergo specific and more extensive changes, high levels of integration within modules or across overall structures have been suggested to also promote greater shape disparification if the main axis of variation agrees with the direction of selection (Schluter 1996a; Goswami et al. 2014). This has been empirically observed in the vertebral column of felids, with vertebrae which have the highest levels of overall integration also displaying the greatest disparity (Chapter 5; Randau and Goswami 2017b). On the other hand, integration across traits which are part of a functional unit is necessary to maintain coordination of shape changes across traits and preserve operative biomechanical systems, which means shape disparification of individual traits may be constrained by the integration across the system (Olson and Miller 1958). In carnivorans, high integration across functional units has been demonstrated in the forelimb of musteloids, with high covariation between bones forming and allowing the

rotation of the lower arm (i.e., ulna and radius), and the bones forming the elbow joint (i.e., humerus and ulna, and ulna and radius), which is the key articulation allowing a plethora of behaviours (Fabre et al. 2014b). Similarly, a recent study on the appendicular skeleton of terrestrial carnivorans (Martín-Serra et al. 2015) demonstrated that species which have a specialised cursorial mode of locomotion have higher covariation patterns across their limbs than non-cursorial taxa, and suggested that functional specialisation is correlated with an increase in integration.

Within the mammalian family of cats (Felidae), our recent work has shown a clear partitioning of the vertebral column into regions showing ecological specialisation and higher morphological disparity across species and regions with higher phylogenetic conservativeness (Chapter 4, Randau et al. 2016a). We further identified a great degree of independence across these regions (Chapter 6, Randau and Goswami 2017a). Specifically, ecology was shown to be correlated more strongly with vertebral shape in the posterior region (i.e., from the diaphragmatic T10 to the last lumbar L7), which also displayed the highest levels of intravertebral integration (Randau and Goswami 2017b), but not anteriorly (Chapters 3 and 4, Randau et al. 2016a; Randau et al. 2016b). These contrasting signals suggested a link between responsiveness to selection and a release from phylogenetic constraints or functional constraints associated with the diaphragm and thus anterior to the T10 – L7 axial region.

This lack of uniformity in function was reflected in the sets of discrete morphological modules found across the vertebral column (Chapter 6; Randau and Goswami 2017a), again corroborating with the hypothesis that increased modularity allows morphological change and adaptation to circumvent ancestral constraints.

Despite this significant ecological signal in the posterior vertebral column of felids, a comparative stronger ecological signal has been observed in other skeletal traits, such as the skull, mandible, and limbs (Dayan et al. 1990; Van Valkenburgh 2007; Meachen-Samuels and Van Valkenburgh 2009a, 2009b; Meachen-Samuels 2012; Fabre et al. 2013b; Meloro et al. 2013; Samuels et al. 2013). This correlation between ecology and shape in other elements has, however, also been demonstrated to be highly dependent on phylogeny and body mass. After correcting for the influence of size and taxonomic relatedness on shape, the ecological signal across much of the skeleton in felids was usually largely reduced or removed (Meloro and O'Higgins 2011; Meloro and Slater 2012; Walmsley et al. 2012; Piras et al. 2013; Martín-Serra et al. 2014a). Body size has been suggested to be one of the main influences on musculo-skeletal shape in felids (Doube et al. 2009; Cuff et al. 2015; Cuff et al. 2016a, 2016b), but this trait too is heavily influenced by phylogenetic relationships among cats, with large species concentrated almost singularly in

the genus *Panthera* (Sunquist and Sunquist 2002; Johnson et al. 2006; MacDonald et al. 2010; Cuff et al. 2015).

In this study, few correlations between the shapes of vertebrae and other skeletal traits were significant after correction for phylogeny and multiple comparisons. Among the results which were significant after all corrections, most (13 out of 15) involved forelimb elements (i.e., humerus and ulna) or the pelvic girdle. Although admittedly still in small numbers, most (11 out of 15) of these significant results involved vertebrae within the more ecologically disparate T10 – L7 region, with the remaining four observed in the cervical region. Interestingly, results from both the analyses with and without phylogenetic correction showed little significant covariation between vertebral and femoral shapes. Although the femur was represented by relatively few landmarks, these results are unlikely to be due to a mere lack of shape characterisation, as the same or even smaller landmark numbers were used in other traits (ten in the ulna, and nine on each side of the pelvis). However, these landmark numbers are comparable to or greater than the number of landmarks or measurements in other studies of limb integration and morphology (e.g., Meachen-Samuels and Van Valkenburgh 2009b; Walmsley et al. 2012; Samuels et al. 2013; Fabre et al. 2014b; Martín-Serra et al. 2014a, 2014b; Martín-Serra et al. 2015). Moreover, a previous study reported increased effect of body size on femoral proportions in felids (Schmidt and

Fischer 2009), which might contribute to its dissociation from vertebral morphology. However, this observation requires further study with a larger sample size in order to isolate other possible conflating factors. Generally, therefore, there is a consensus in the literature that both ecological signal and levels of integration across the appendicular and cranial skeletons of carnivorans are decreased or completely wiped out when phylogeny (or phylogenetically structured traits, such as body size) is taken into account (Goswami 2006b; Walmsley et al. 2012; Fabre et al. 2013a; Martín-Serra et al. 2014b; Martín-Serra et al. 2015).

The clear contrast between the strong influences of phylogeny and (strongly phylogenetically-structured) body mass on the shape of the cranium, limbs, and anterior vertebrae in felids (Chapter 4; Randau et al. 2016a) may explain the large effect of phylogenetic correction on our results. Once phylogenetic effects are considered, the apparently strong shape covariation across the felid skeleton disappears almost entirely, suggesting that phylogeny, and with it body mass, may be the main forces shaping felid osteological morphology and skeletal integration in general.

In Chapter 6, I identified strong integration within five vertebral modules across the presacral column, which were supported even after phylogenetic relationships were considered (Randau and Goswami 2017a). Taken together, the high integration within vertebral modules and the lack of correlation

between those and other skeletal elements suggest that the vertebral column may be an independently evolving structure, relative to the other parts of the skeleton, and its integration may be driven largely by different factors than that of other elements, specifically constrained by development as opposed to being responsive to ecology. Notably, the relatively widespread uniformity in presacral vertebral count across mammals, and even more so within Felidae (all cats present 27 presacral vertebrae) suggests that the mammalian presacral column is under strong developmental constraint (Galis 1999; Narita and Kuratani 2005; Wellik 2007; Buchholtz and Stepien 2009; Hautier et al. 2010; Müller et al. 2010; Asher et al. 2011; Varela-Lasheras et al. 2011; Buchholtz et al. 2012; Fleming et al. 2015). In support of this hypothesis, we have previously confirmed that felid presacral vertebral shape is structured largely according to the developmental origins of vertebral components (i.e., '*centrum*' versus '*neural-spine*' related) (Chapter 5, Randau and Goswami 2017b), demonstrating that development is also a strong constraint on changes in vertebral shape and not only in number. Although this conclusion may seem contradictory to the idea of diverse and regionalised vertebral shape in mammals evolving in response to meristic constrains (i.e., constraints on numbers), it may actually be the developmental signalling across the vertebrae that allows for greater shape disparity in areas of greatest integration (as observed in the T10 – L7 region) (Chapters 5 and 6; Randau and Goswami 2017b, 2017a).

Together, these observations support the inference that the lack of strong integration between the vertebral column and the rest of the skeleton is due to the different factors influencing the shape of each of these regions. Whilst studies of cranial and appendicular elements show that there is a strong correlation between shape and ecological specialisation, although this is strongly phylogenetically structured, developmental origin and processes may more highly influence and shape vertebral morphology.

Appendix 7.1

Table S7.1: Species and museum collection numbers for the specimens included in this study. Museum collection abbreviations are as follows: NHM: Natural History Museum, London; MNHN: Muséum National d'Histoire Naturelle, Paris; MCZ: Harvard Museum of Natural History, Cambridge; AMNH: American Museum of Natural History, New York; FMNH: Museum of Natural History, Chicago; USNM: Smithsonian National Museum of Natural History, Washington D.C.

Species	Specimen number
Acinonyx jubatus	FMNH127834
	AMNH119655
	AMNH119656
	AMNH119657
Felis catus	NHM 1952 10 20 4
	USNM 396268
	USNM 397631
Leptailurus serval	FMNH 127843
	FMNH 44438
	FMNH 60491
	NHM 1845 9 25 23
Leopardus pardalis	AMNH 214744
	AMNH 248728
	MNHN 1998 1866
	MNHN A3456
	USNM 271094
Neofelis nebulosa	FMNH 54304
	MNHN 1961 217
	NHM 1965 1 18 1
	USNM 545387
Panthera leo	AMNH 85147
	MCZ 9487
Panthera pardus	AMNH 54462
	MNHN 1892 1079
	MNHN 1945 70
	MNHN A13045 1844
	MNHN A7932
	MNHN BII 4
	USNM 15684
	USNM 303320
Prionailurus bengalensis	FMNH 99363
	NHM 1309b 1858
	NHM 1979 2895

	USNM 317283
Puma concolor	AMNH10259
	AMNH90213
	FMNH129339
	MNHN1937 4
	USNM A21528
	USNM264166

Table S7.2: Landmark anatomical descriptions per vertebra and other skeletal traits.

Atlas

1 Anterior mid-point of dorsal arch
2 Anterior mid-point of ventral arch
3 Anterior lateral-most tip of left transverse process
4 Anterior lateral-most tip of right transverse process
5 Dorso-anterior-most tip of left pre-zygapophysis
6 Dorso-anterior-most tip of right pre-zygapophysis
7 Posterior mid-point of dorsal arch
8 Posterior mid-point of ventral arch
9 Posterior lateral-most tip of left transverse process
10 Posterior lateral-most tip of right transverse process
11 Posterior-most tip of left post-zygapophysis
12 Posterior-most tip of right post-zygapophysis

Axis

1 Anterior-most point at tip of den
2 Ventral mid-point at base of den
3 Anterior-most point of neural spine
4 Posterior ventral mid-point of centrum
5 Posterior left lateral-most point of width of centrum
6 Posterior right lateral-most point of width of centrum
7 Posterior left dorso-lateral point of centrum
8 Posterior right dorso-lateral point of centrum
9 Posterior dorsal mid-point of the neural canal
10 Dorsal posterior-most point at tip of neural spine
11 Left lateral-most posterior tip of transverse process
12 Right lateral-most posterior tip of transverse process
13 Posterior-most dorsal point of left post-zygapophysis
14 Posterior-most dorsal point of right post-zygapophysis
1 Anterior ventral mid-point of centrum
2 Anterior dorsal mid-point of centrum
3 Anterior left lateral-most point of centrum
4 Anterior left lateral-most point of centrum

5 Anterior dorsal-most point of left pre-zygapophyses
6 Anterior dorsal-most point of right pre-zygapophyses
7 Anterior-most point of left lamina
8 Anterior-most point of right lamina
9 Dorsal-most point at tip of neural spine
10 Posterior ventral mid-point of centrum
11 Posterior dorsal mid-point of centrum
12 Posterior Left lateral-most point of centrum
13 Posterior right lateral-most point of centrum
14 Posterior dorsal mid-point of the neural canal
15 Posterior-most point of left post-zygapophyses
16 Posterior-most point of right post-zygapophyses
17 Lateral-most point of left transverse process
18 Lateral-most point of right transverse process

C6

1 Anterior ventral mid-point of centrum
2 Anterior dorsal mid-point of centrum
3 Anterior left lateral-most point of centrum
4 Anterior left lateral-most point of centrum
5 Anterior dorsal-most point of left pre-zygapophyses
6 Anterior dorsal-most point of right pre-zygapophyses
7 Lateral-most point of left transverse process
8 Lateral-most point of right transverse process
9 Anterior-most point of left lamina
10 Anterior-most point of right lamina
11 Dorsal-most point at tip of neural spine
12 Posterior ventral mid-point of centrum
13 Posterior dorsal mid-point of centrum
14 Posterior Left lateral-most point of centrum
15 Posterior right lateral-most point of centrum
16 Posterior dorsal mid-point of the neural canal
17 Posterior-most point of left post-zygapophyses
18 Posterior-most point of right post-zygapophyses
19 Posterior-most point of left lamina
20 Posterior-most point of right lamina

C7 - T10

1 Anterior ventral mid-point of centrum
2 Anterior dorsal mid-point of centrum
3 Anterior left lateral-most point of centrum
4 Anterior left lateral-most point of centrum
5 Anterior dorsal-most point of left pre-zygapophysis
6 Anterior dorsal-most point of right pre-zygapophysis
7 Lateral-most point of left transverse process
8 Lateral-most point of right transverse process

9 Dorsal-most point at tip of neural spine
10 Posterior ventral mid-point of centrum
11 Posterior dorsal mid-point of centrum
12 Posterior Left lateral-most point of centrum
13 Posterior right lateral-most point of centrum
14 Posterior dorsal mid-point of the neural canal
15 Posterior-most point of left post-zygapophysis
16 Posterior-most point of right post-zygapophysis

T11

1 Anterior ventral mid-point of centrum
2 Anterior dorsal mid-point of centrum
3 Anterior left lateral-most point of centrum
4 Anterior left lateral-most point of centrum
5 Anterior dorsal-most point of left pre-zygapophysis
6 Anterior dorsal-most point of right pre-zygapophysis
7 Posterior-most point of tip of left accessory process
8 Posterior-most point of tip of right accessory process
9 Dorsal-most point at tip of neural spine
10 Posterior ventral mid-point of centrum
11 Posterior dorsal mid-point of centrum
12 Posterior Left lateral-most point of centrum
13 Posterior right lateral-most point of centrum
14 Posterior dorsal mid-point of the neural canal
15 Posterior-most point of left post-zygapophysis
16 Posterior-most point of right post-zygapophysis

T12 - T13

1 Anterior ventral mid-point of centrum
2 Anterior dorsal mid-point of centrum
3 Anterior left lateral-most point of centrum
4 Anterior left lateral-most point of centrum
5 Anterior dorsal-most point of left pre-zygapophyses
6 Anterior dorsal-most point of right pre-zygapophyses
7 Anterior Dorsal-most point at tip of neural spine
8 Posterior Dorsal-most point at tip of neural spine
9 Posterior ventral mid-point of centrum
10 Posterior dorsal mid-point of centrum
11 Posterior Left lateral-most point of centrum
12 Posterior right lateral-most point of centrum
13 Posterior dorsal mid-point of the neural canal
14 Posterior-most point of left post-zygapophyses
15 Posterior-most point of right post-zygapophyses
16 Posterior-most point of tip of left accessory process
17 Posterior-most point of tip of right accessory process

L1 - L4

1 Anterior ventral mid-point of centrum
2 Anterior dorsal mid-point of centrum
3 Anterior dorsal-most point of left pre-zygapophyses
4 Anterior dorsal-most point of right pre-zygapophyses
5 Dorsal anterior-most point at tip of neural spine
6 Anterior left lateral-most point of centrum
7 Anterior left lateral-most point of centrum
8 Lateral-most point of left transverse process
9 Lateral-most point of right transverse process
10 Posterior ventral mid-point of centrum
11 Posterior dorsal mid-point of centrum
12 Posterior dorsal mid-point of the neural canal
13 Posterior Left lateral-most point of centrum
14 Posterior right lateral-most point of centrum
15 Posterior-most point of tip of left accessory process
16 Posterior-most point of tip of right accessory process
17 Posterior-most point of left post-zygapophyses
18 Posterior-most point of right post-zygapophyses
19 Dorsal posterior-most point at tip of neural spine

L6 - L7

1 Anterior ventral mid-point of centrum
2 Anterior dorsal mid-point of centrum
3 Anterior dorsal-most point of left pre-zygapophyses
4 Anterior dorsal-most point of right pre-zygapophyses
5 Dorsal anterior-most point at tip of neural spine
6 Anterior left lateral-most point of centrum
7 Anterior left lateral-most point of centrum
8 Lateral-most point of left transverse process
9 Lateral-most point of right transverse process
10 Posterior ventral mid-point of centrum
11 Posterior dorsal mid-point of centrum
12 Posterior dorsal mid-point of the neural canal
13 Posterior Left lateral-most point of centrum
14 Posterior right lateral-most point of centrum
15 Posterior-most point of left post-zygapophyses
16 Posterior-most point of right post-zygapophyses
17 Dorsal posterior-most point at tip of neural spine

Sacrum

1 Anterior ventral mid-point of centrum
2 Anterior dorsal mid-point of centrum
3 Anterior lateral-most point of left articular surface with pelvis
4 Anterior lateral-most point of right articular surface with pelvis
5 Anterior dorsal-most point of left pre-zygapophyses

6 Anterior dorsal-most point of right pre-zygapophyses
7 Anterior ventral-most point of left articular surface with pelvis
8 Anterior ventral-most point of right articular surface with pelvis
9 Dorsal-most point at tip of first neural spine
10 Dorsal-most point at tip of second neural spine
11 Dorsal-most point at tip of third neural spine
12 Posterior ventral mid-point of centrum
13 Posterior dorsal mid-point of centrum
14 Posterior Left lateral-most point of centrum
15 Posterior right lateral-most point of centrum
16 Posterior dorsal mid-point of the neural canal
17 Posterior-most point of left post-zygapophyses
18 Posterior-most point of right post-zygapophyses
19 Lateral-most point of left transverse process
20 Lateral-most point of right transverse process

Scapula

1 Most dorsal point of the posterior border
2 Ventral boundary of the teres major process
3 Posterior-most lateral mid-point of the scapular spine
4 Distal tip of the acromion process
5 Most posterior point of the metacromion
6 Point of maximum curvature at the posterior border of the neck
7 Most posterior point of the border of the glenoid fossa
8 Midpoint of the lateral border of the glenoid fossa (point of max curvature from lateral view)
9 Most proximal (anterior) point of the border of the glenoid fossa at the anterior side
10 Medial-most mid-point of the glenoid fossa
11 Medial-most tip point of the coracoid process
12 Point of maximum curvature at the anterior border of the neck
13 Anterior-most point of the anterior border
14 Dorsal-most point of the scapular spine
15 Dorsal-most mid-point of proximal facet

Pelvis (Each side)

1 Anterior-most (maximum cranial) projection of the iliac wing
2 Anterior-most (maximum cranial) point of the pelvic symphysis
3 Posterior-most (maximum caudal) point of the pelvic symphysis
4 Ventral projection of the ischial tuberosity
5 Dorsal projection of the ischial tuberosity
6 Acetabular notch
7 Iliopectineal eminence
8 Dorsal-most point of spine of ischium
9 Posterior-most (maximum caudal) projection of the articular surface for sacrum

Humerus

1 Anterior-most point of the greater tuberosity
2 Anterior-most point of the lesser tuberosity
3 Proximal-most ventral point of the lesser tuberosity
4 Proximal-most point of the pectoral ridge
5 Junction point of pectoral ridge and deltoid ridge
6 Proximal-most point of the trochlea
7 Distal-most point of the trochlear ridge
8 Distal-most point on the capitulum
9 Proximal-most point of the capitulum at the anterior side
10 Lateral-most point of the lateral epicondyle
11 Medial-most point of the medial epicondyle
12 Distal-most point of the humeral head
13 Proximal-most point at the dorsal border of the olecranon fossa

Ulna

1 Proximo-anterior-most medial point of the edge of the olecranon process
2 Proximo-anterior-most lateral point of the edge of the olecranon process
3 Distal-most point of the superior edge of the trochear notch
4 Latero-distal-most point of the coronoid process in anterior view
5 Distal-most point of the radial notch in anterior view
6 Lateral-most point of the radial notch in anterior view
7 Antero-lateral tip of the interosseous crest of ulna
8 Distal-most point of articular facet with radius
9 Distal-most point of the tip of the styloid process
10 Proximo-posterior-most point of the edge of the olecranon process

Radius

1 Proximo-medial-most point of the head
2 Proximo-latero-most point of the fovea
3 Proximo-antero-most point of the fovea
4 Proximo-dorso-most point of the styloid process
5 Medial-most point of the styloid process
6 Distal-most point of the styloid process
7 Distal-most point of facet with ulna
8 Lateral-most mid-point of articular facet with ulna
9 Dorso-medial point of the bicipital tuberosity
10 Ventral point of the bicipital tuberosity
11 Proximo-dorsal point of articular surface

Femur

1 Proximo-medial-most point of the head
2 Proximo-most point of the greater trochanter
3 Distal-most medial edge point of the patellar trochlear

4 Distal-most lateral edge point of the patellar trochlear
5 Medial projection of the proximal diaphysis
6 Lateral projection of the proximal diaphysis
7 Proximal-most point on superior part of the lateral condyle
8 Proximal-most point on superior part of the medial condyle
9 Distal-most point of the linea aspera

Tibia

1 Proximal-most point on the medial edge of the medial condyle
2 Proximal-most point on the lateral edge of the lateral condyle
3 Proximal-most medial end of the tibial tuberosity
4 Proximal-most lateral end of the tibial tuberosity
5 Distal-most end of the margo cranialis (crista tibiae)
6 Distal-most tip of the medial malleolus
7 Lateral-most point of the fibula facet
8 Distal-most point of the trochlea tali
9 Proximal-most point in the intercondyloid area
10 Distal-most point of the intercondyloid area/Proximal-most point of the popliteal notch

Skull

1 Anterior-most left tip of nasal
2 Anterior mid-point (left) of frontal
3 Left suture between nasal-maxilla-frontal
4 Right suture between nasal-maxilla-frontal
5 Lateral-most point of left post-orbital process
6 Lateral-most point of right post-orbital process
7 Middle point of suture between frontal and parietal bones
8 Left lateral superior-most point of suture between zygomatic and squamosal
9 Right lateral superior-most point of suture between zygomatic and squamosal
10 Left lateral/superior-most suture between parietal/occipital/squamosal
11 Right lateral/superior-most suture between parietal/occipital/squamosal
12 Middle point of suture between parietal and interparietal bones
13 Anterior-most left tip of premaxilla
14 Anterior-most point of alveolar length of left I3
15 Posterior-most point of alveolar length left of I3
16 Anterior-most point of alveolar length of left Upper C
17 Posterior-most point of alveolar length of left of Upper C
18 Latero-posterior-most point of end of left P4's alveolus
19 Posterior-most point of left zygomatic
20 Anterior-most point of alveolar length of right I3
21 Posterior-most point of alveolar length right of I3
22 Anterior-most point of alveolar length of right Upper C
23 Posterior-most point of alveolar length of right of Upper C

24 Latero-posterior-most point of end of right P4's alveolus
25 Posterior-most point of right zygomatic
26 Anterior-mid point of maxilla suture
27 Posterior-mid point of maxilla suture
28 Posterior-mid point of palatine suture
29 Posterior-mid point of presphenoid
30 Left lateral-most ventral point of the mastoid process
31 Right lateral-most ventral point of the mastoid process
32 Posterior-most point of left jugular process
33 Posterior-most point of right jugular process
34 Left lateral-most point of occipital condylar breath
35 Right lateral-most point of occipital condylar breath
36 Left posterior-most point of occipital condyle forming border of foramen magnum
37 Right posterior-most point of occipital condyle forming border of foramen magnum
38 Posterior-most middle point of basioccipital (ventral limit of foramen)

Dentary

1 Dorsal-most anterior middle point
2 Dorsal-most point of left jaw depth at p4/m1 junction
3 Ventral-most point of left jaw depth at p4/m1 junction
4 Lateral middle point of left m1 alveolus (line from between paraconid and protoconid)
5 Dorsal-most tip of left coronoid process (lateral view)
6 Posterior-most point of left coronoid process
7 Lateral-most tip of left condyloid process
8 Dorso-posterior-most tip of left angular process
9 Dorsal-most point of right jaw depth at p4/m1 junction (Middle point between p4-m1)
10 Ventral-most point of right jaw depth at p4/m1 junction
11 Lateral middle point of right m1 alveolus (line from between paraconid and protoconid)
12 Dorsal-most tip of right coronoid process (lateral view)
13 Posterior-most point of right coronoid process
14 Lateral-most tip of right condyloid process
15 Dorso-posterior-most tip of right angular process

Chapter 8: Conclusions

To evolutionary biologists, the study of organismal shape in a comparative context is key to the understanding of species interactions with both biotic and abiotic factors, ultimately grounding the concept of adaptation (Rose and Lauder 1996; Schluter 1996b). However, the evolution of shape does not only rely on selection, and it is also dependent upon and driven by the innate characteristics of the phenotype, namely, on how free morphologies are to respond to pressures and change (Olson and Miller 1958). A central property governing shape evolution is the covariation pattern within and across traits (i.e., integration and modularity), which has been shown to greatly influence morphological changes, and to both promote and constrain disparity (Chapter 5; Schluter 1996a; Hansen and Houle 2008; Marroig et al. 2009; Goswami et al. 2014; Randau and Goswami 2017b). Moreover, these integration and modularity patterns have themselves been hypothesized to change over time and across clades, and can therefore govern shape evolution (Wagner and Altenberg 1996; Badyaev et al. 2005; Clune et al. 2013; Goswami et al. 2014; Goswami et al. 2015).

The evolution of a vertebral column has greatly expanded the morpho-functional space of body axes, and its presence is the defining trait of one of the major animal groups (i.e., Vertebrata) (Barthez 1798; Slijper 1946; Koob and

Long 2000; Kardong 2005). This key innovation has been shown to be the permissive factor for the extensive range of locomotory and feeding behaviours observed across vertebrate clades, and specifically in mammals, the vertebral column has been shown to have a critical role from body support to respiration (Slijper 1946; Pridmore 1992; Gál 1993b; Shapiro 1995; Long et al. 1997; Long et al. 2002; Argot 2003; Kardong 2005; Shapiro et al. 2005; Shapiro 2007; Pierce et al. 2011). However, the study of the vertebral column is surprisingly still restricted in number and scope with comparison to other structures, such as the appendicular and cranial systems (see Chapters 1 and 7).

The work discussed throughout this thesis delineated the evolutionary drivers and constraints that shape vertebral disparity in the mammalian carnivoran family Felidae (cats). Specifically, I have explored how the shape of the vertebral column of living species of felids is influenced by the distinct ecologies and body masses observed across the family, and how patterns of within and across vertebral covariation governs the regionalisation of shape and function. Throughout, I have applied a variety of approaches, with both linear and geometric morphometric data, to test hypotheses of biomechanical, ecological, developmental and phylogenetic influences and constraints on vertebral form. Additionally, I quantified the levels of covariation across presacral vertebrae, and between presacral vertebrate and other skeletal

elements, such as the skull and limbs, and identified morphological modules which may promote evolutionary responsiveness to selection. Here I summarise the results of each of the above-mentioned approaches and discuss how these results integrate to provide a comprehensive understanding of the evolution of the vertebral column in cats.

Regionalisation of the ecological signal

The results of the pilot study demonstrated that there is considerable overlap of vertebral units in the morphospace, and separation of vertebral shape types into five clusters: C4, C3 – C6 (with the exception of C4), C7, the thoracic vertebrae, and the lumbar vertebrae. This initial exploration showed that it was possible to focus the 3D analyses on a restricted sample of 19 out the total 27 presacral vertebrae, and therefore allow for greater sample sizes per vertebral type and species. This overlap of morphospace occupation and signal was consistently recovered in the subsequent analyses with both linear data on all presacral vertebrae, and three-dimensional landmarks collected on the chosen 19 vertebrae.

Regarding the study of vertebral morphology and its relationship with function, there was an overall similarity between the results from the linear (Chapter 3; Randau et al. 2016b) and three-dimensional (3D) landmark-based

(Chapter 4; Randau et al. 2016a) approaches. With both datasets and corresponding analytical approaches, a signal of correlation between species' ecology and vertebral shape was recovered. However, there was clear evidence that this signal is heterogeneously distributed and, importantly, higher in the posterior region of the axial skeleton. Nevertheless, the resolution of the results differed between datasets, and as expected (see Chapters 1 and 2), with the increased resolution and power of the 3D dataset and geometric morphometric analyses, these results were much more detailed, specifically regarding the variation of the strength of the ecological signal across the spine, the shape differences between prey size and locomotory specialists, and the influences of both phylogeny and body size on vertebral shape.

Although both approaches showed a significant correlation between vertebral morphology and modes of locomotion in the lumbar region, analyses of linear data were unable to discriminate shape changes amongst the prey size groups. This lack of resolution was also present when analysing individual components of linear shape (e.g., centrum width) across the locomotor groups, again suggesting that geometric shape analyses are best at identifying cryptic differences among groups with significant overall morphological similarity, such as felid species (Ewer 1973; Leyhausen 1979; Sunquist and Sunquist 2002; MacDonald et al. 2010).

The increased analytical power of geometric morphometric analyses was able to reveal a clear dichotomy in drivers of vertebral shape change across the vertebral column: whilst vertebrae in the anterior-most region exhibited significant phylogenetic signal and were conservative in shape across ecological categories, vertebrae in the posterior region, specifically vertebrae in the T10 – L7 region, displayed the highest ecological signal. These results suggest that either differential selection acts on these vertebral sections, or that this T10 – L7 region possesses more respondability towards selection forces (Hansen and Houle 2008).

With the 3D dataset, I also presented in Chapter 4 a novel application of the Phenotypic Trajectory Analysis (PTA; Adams and Collyer 2007, 2009; Collyer and Adams 2013), which allowed me to overcome the longstanding issue of analysing a complex structure composed of discrete units, such as the axial skeleton. When applied to the T10 – L7 region, this methodology further confirmed the patterns of vertebral shape variation observed across felid ecomorphs. Moreover, this multidimensional quantitative approach provided a clear example of how one aspect of vertebral shape (i.e., centrum length) may have played a central role in the evolution of cursoriality in felids: with longer vertebrae which also display overall less shortening from L1 to L7 than other species, cheetahs may be able to produce intensified sagittal bending

and therefore increase stride length (Hildebrand 1959; Long et al. 1997; Koob and Long 2000; Pierce et al. 2011).

Allometry in vertebral morphology

Specifically regarding the linear results, I have shown that increases in body mass were linked to stabilisation of the anterior axial skeleton, but that its effects on the lumbar vertebrae could generate passive stability by correlated enlargement of the epaxial musculature. However, this allometric scaling of the neural spine lever arm could also result in increased active ability for sagittal flexion. Hence, differential changes driven by body mass alone suggested distinct function across the anteroposterior length of the vertebral column.

Both linear and 3D analyses of vertebral scaling with distinct measures of size informed that shape changes which are size-driven show great regionalisation, and differ in identity and intensity across the vertebral column. Importantly, the results discussed in Chapter 4 demonstrate that allometry has its highest effect in the posterior T10 – L7 region, but that its effect on shape is still considerably low (i.e., with a mean of 11.1% and a median 9.9% of shape variation explained by its allometric relationship with size).

Caveats

The results presented throughout this thesis regarding ecological specialisation driving changes in vertebral shape concern analyses at the evolutionary scale (i.e., across species, rather than within species). These comparisons across species allow for the study of macroevolutionary patterns and trends (Klingenberg and Marugán-Lobón 2013), and their wider scope allow for inferences to be made about the evolution of the vertebral column in other groups which possess similar vertebral development (i.e., potentially all other placental mammals) (Narita and Kuratani 2005; Müller et al. 2010; Buchholtz 2012; Buchholtz et al. 2012; Buchholtz 2014).

Although the nature of three-dimensional landmarks and their increased dimensionality allows for a more refined and improved extraction and quantification of biological information, the increased dependency of geometric morphometric techniques on larger samples sizes commanded that prioritisation of larger samples sizes per species were collected, with a necessary restriction to the number of species selected. This focus on increasing specimen numbers within species meant that only 25% of the living species of felids were covered in this thesis. However, as discussed in Chapters 1 and 2, careful consideration was put into selecting species which would accurately represent the extant diversity in Felidae by selecting species which covered the full breadth of ecological, size and phylogenetic ranges

recorded in the literature, and for which the visited museums held the largest numbers of specimens. As discussed in Chapter 2, a plethora of techniques were applied in order to deal with reduced sample sizes without detriment to the analyses, and to account for the taxonomic structure of the species included.

A related caveat regarding specimen number concerns the sample size of individual species and the availability of information such as specimens' sex. It was not possible to test if males and females differ in the amount of vertebral shape changes explained by the factors analysed here. Further analyses focusing on a more restricted species sample, with contrasting levels of sociality per species (e.g., lions versus ocelots; Sunquist and Sunquist 2002; MacDonald et al. 2010), would be beneficial to test the effects that sexual dimorphism may have on vertebral shape.

Integration and modularity in vertebral shape

The analyses of vertebral morphology, with scaling results showing series of consecutive vertebrae displaying the same set of allometric measurements, and the heterogeneity of phylogenetic and ecological signal, provided initial indication of the morphological regionalisation of the axial skeleton.

Additionally, these results denoted that the regionalisation of shape in the axial skeleton may not map precisely onto traditional vertebral regions.

Confirming the presence of modularity and assessing the patterns of integration within the axial skeleton is of great importance as these factors have been shown to greatly affect the evolution of traits by either promoting or constraining trait changes in response to selection (Cheverud 1996; Hansen and Houle 2008; Marroig et al. 2009; Klingenberg and Marugán-Lobón 2013; Sears et al. 2013; Goswami et al. 2014).

Throughout Chapters 5 to 7, I applied a combination of analyses to test for covariation within vertebrae, between vertebrae across the axial skeleton, and between vertebrae and other skeletal components. I also assessed the relationship between magnitudes of vertebral integration and disparity both within and across species.

Intravertebral covariation

For the tests of intravertebral modularity patterns based on development (Chapter 5; Randau and Goswami 2017b), two methodologies were compared. As discussed in Chapter 2, comparison of these techniques was performed due to the recent implementation of the covariance ratio (Adams 2016) as a measure of modularity replacing the popular RV coefficient (Escoufier 1973;

Klingenberg 2009). The covariance ratio has been shown to be more robust to changes in specimen and landmark sample sizes and to have a higher statistical power than the RV coefficient. Nevertheless, the results of both analyses were very consistent throughout.

With these analyses, I demonstrated that the developmental two-module model (i.e., '*centrum*' and '*neural spine*') is widespread in the presacral vertebrae of adult felids (Chapter 4; Randau and Goswami 2017b). I have also shown that the few occasions in which this developmental pattern of covariation was disrupted occurred at the boundaries of larger, multi-vertebrae modules across the vertebral column. Hence, these results led me to suggest that this widespread developmental intravertebral patterning can be overprinted by function and in order to preserve larger (i.e., multi-vertebrae) modular organisation.

A caveat to these analyses was that allometry was not corrected for prior to testing for intravertebral modularity per the reasons discussed on Chapter 2. Nevertheless, although allometry has been suggested to be a driver of integration, its effects are likely to affect whole structures (i.e., the entire vertebra) uniformly (Klingenberg 2008; Goswami and Polly 2010c; Klingenberg and Marugán-Lobón 2013). Therefore, rather than promoting the partition of shape covariation, any allometric effects left in the shape data

would likely not have contributed to the modularity patterns found in these results.

The results from the analyses of intravertebral trait integration and disparity showed that the T10 – L7 region presented the highest values of morphological integration and disparity. This observation provided empirical support to the hypothesis that phenotypic integration may promote morphological variance on the preferred axes of variation (Schluter 1996a; Goswami et al. 2014), and, taken together with the significant ecological signal observed at this region, it strongly supports the hypothesis that this posterior region may display the highest evolutionary respondability to selection (Hansen and Houle 2008; Randau et al. 2016a).

Intervertebral covariation

The analyses of integration across vertebrae (Chapter 6; Randau and Goswami 2017a) demonstrated the prevalence of multi-vertebral modules in the vertebral column and provided strong support to the hypothesis that vertebrae at the boundaries of such modules display disruption of their internal pattern of developmental covariation (Chapter 5; Randau and Goswami 2017b). Secondly, these intervertebral integration results also showed that the T10 – L7 vertebrae are organised into two evolutionary independent modules: the anticlinal T10 – T11 module, and the posterior

thoracics and lumbar module (T12 – L7). Rather than supporting the traditional vertebral regions of the axial skeleton, the results presented here suggest that developmental constraint and biomechanical function, along with instances of shared ossification timing, are the main drivers of vertebral shape integration in felids. Since the developmental patterns observed in felids are shared across mammals (Hautier et al. 2010; Müller et al. 2010; Buchholtz 2012; Buchholtz et al. 2012; Buchholtz 2014), these results may reflect a general mammalian condition.

A limitation to this analysis of intervertebral integration was that not all of the 27 presacral vertebrae were included, and therefore, pairwise tests of vertebral covariation were not exhaustive. Nevertheless, for most of the eight vertebrae which were excluded from this analysis it was possible to make strong inferences on their module identity. For example, cervical vertebrae C3 – C5 have been suggested to form a mid-cervical module due to the commitment of migratory muscle precursor cells from their somites to the diaphragm (Buchholtz et al. 2012), but vertebrae C3 and C5 were not included in this analysis. Nevertheless, the covariation patterns between C4 and many other vertebrae, including strong covariations with vertebrae in the C1 – T1 module suggest that an isolated C3 – C5 module would not have been recovered. Instead, the strong covariations found in the pairwise comparisons among

vertebrae C1 – T1, including C4, suggest that both C3 and C5 would be equally integrated within this anterior module.

Along with C3 and C5, four of the other six excluded vertebrae were included into modules which showed covariation spanning multiple units. As an example, L3 and L5 were included in the T12 – L7 module which showed very high covariation among all pairwise comparisons, including adjacent vertebrae, such as T12, T13 and L1, or between vertebrae at the extremes of the modules, such as between T12 or T13 and L6 or L7. Therefore, this strongly suggests that such vertebrae are included in the proposed modules.

Only two out of the eight excluded vertebrae (i.e., T3 and T9) are situated at the margins of proposed modules, and hence, their covariation patterns could not be inferred with the same level of confidence. Two modules were found surrounding each of these vertebrae: C6 – T2 and T4 – T8 surround T3, whereas T4 – T8 and T10 – T11 surround T9. Considering the very strong correlation between T10 and T11, lack of correlation between these vertebrae and any other units, and their identities as the diaphragmatic and anticlinal vertebrae, it is likely that T9 would have been included in the T4 – T8 module. T3 would also likely fall within the T4 to T8, as C6 – T2 is a proposed module which concerns the transition between cervicals to thoracics, and muscularisation of the forelimb (Buchholtz 2014). Nevertheless, these

hypotheses should the empirically tested on a complete presacral sample for confirmation, perhaps for a single, well-sampled species.

Covariation across the skeleton

The strength of developmental control of vertebral morphology may have also been the driving force in largely dissociating the evolution of the vertebral column from covariation with the other skeletal elements, such as the limbs and cranium. This dissociation may have allowed a significant degree of independence between these traits for changes in response to selection. This may explain the large discrepancy between the influences that ecological variables, such as locomotor or prey size group, have in vertebral shape versus their observed correlations in the shape of the cranial and appendicular elements. In short, I have shown that these variables have their highest levels of correlation with shape at the T10 – L7 vertebral region, but that even at this region they only explain between 12% and 18% of total vertebral shape variation. This is in contrast with the observations that ecology is highly correlated with the shape of the skull and limbs in felids and explains between 65% and 93% of the variation of these structures across species (Meachen-Samuels and Van Valkenburgh 2009a, 2009b), although this ecological signal is still highly phylogenetically structured (Goswami 2006b; Meachen-Samuels and Van Valkenburgh 2009a, 2009b; Walmsley et al. 2012; Fabre et al. 2013a; Martín-Serra et al. 2014b; Martín-Serra et al. 2015). In my last data chapter

(Chapter 7), I have shown that vertebrae present many fewer and weaker correlations with skull, girdle and limb elements compared to the intervertebral integration discussed in Chapter 6 (Randau and Goswami 2017a). Both phylogenetic relatedness and (phylogenetically driven) body size effects seem to be the main integrating factors coordinating covariation between the axial, including cranial, and appendicular skeletons. Once these factors are taken into account, the prevalent modularity in organismal organisation in felids is made obvious. Thus, I suggest that it was this dissociation which allowed for further functional specialisation of the cranium and limbs of felids while the vertebral column remains largely constrained by its developmental patterning.

Taken together, the results concerning modular organisation of units from individual vertebrae to intervertebral relationships and across the skeleton reveal great complexity in trait evolution. Specifically, these results suggest a hierarchy of covariation patterns which changes according to the level of analyses: whereas individual elements possess their own overall integration, and may present modularity which is determined by differential developmental origins, when the level of analyses is either zoomed out or zoomed in to include consecutively more traits or divide traits into parts, further relationships are uncovered (West-Eberhard 2003; Wagner et al. 2007). This is true for example in analyses of complex structures such as the skull,

which is an overall highly integrated trait (Goswami et al. 2015), and also greatly covaries with the mandible (Adams 2016), but has been shown to display distinct levels of modularity: 1. Two partitions: face and neurocranium (Drake and Klingenberg 2010; Klingenberg and Marugán-Lobón 2013); or 2. Each of the two skull partitions possessing functional sub-divisions which drive covariation into six blocks (Cheverud 1982, 1995; Goswami 2006a; Goswami and Finarelli 2016). Therefore, similar complexity in patterns of covariation has been demonstrated here regarding the vertebral column (Fig. 8.1): from an evolutionary independent structure when whole-skeletal analyses are performed (Chapter 7), to being organised into six modules across the vertebral column (Chapter 6; Randau and Goswami 2017a), and finally presenting a two-module structure when individual vertebrae are considered (Chapter 5; Randau and Goswami 2017b). This heterogeneity in covariation patterns may reflect, or indeed allow biological organisation, and indicate both constrains (e.g., evolutionary history and development) and the product of selection (e.g., functional modules) (Raff 1996; Wagner and Altenberg 1996; West-Eberhard 2003; Wagner et al. 2007).

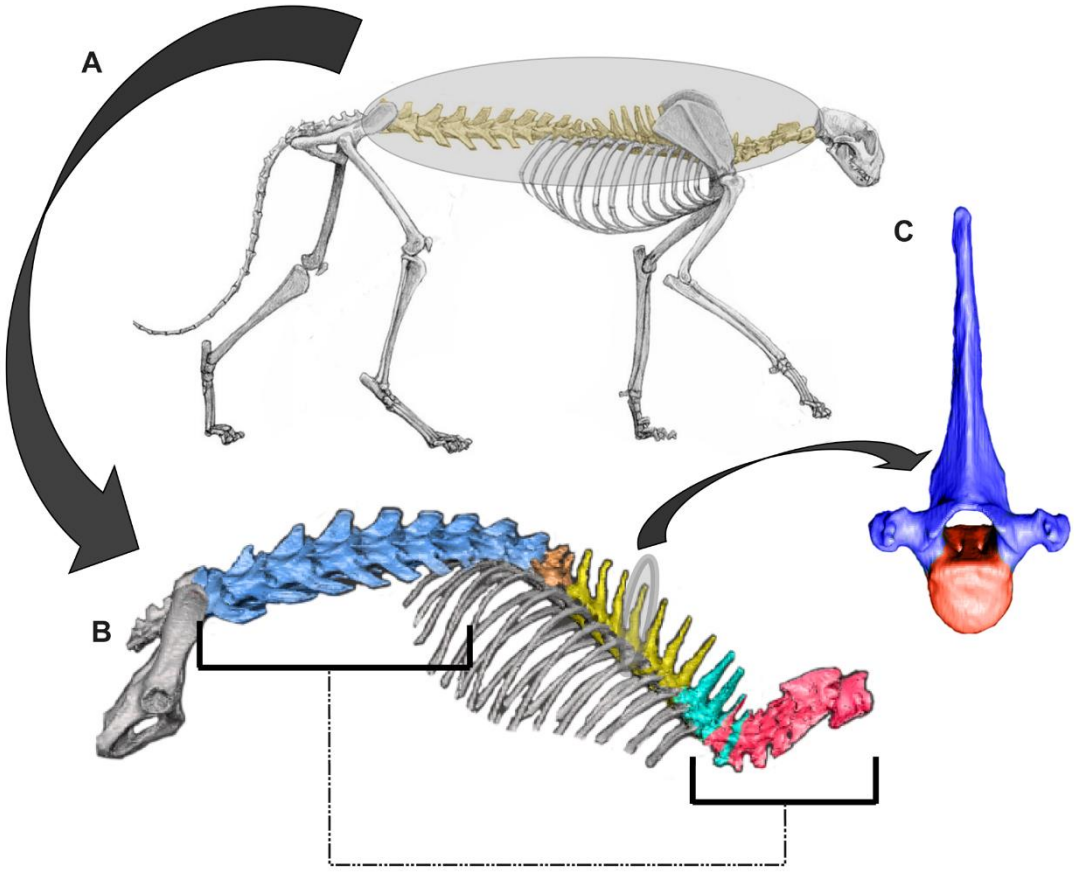

Fig. 8.1: The hierarchical structure of modularity in the presacral vertebral column of felids. A. The skeleton of a cheetah (*Acinonyx* jubatus) showing the presacral vertebral column, marked in yellow and circled, as an evolutionary module, independent from the rest of the skeleton. B. Within the vertebral column (here, a domestic cat specimen, *Felis catus*), five main intervertebral modules are suggested and coloured accordingly: C1 – C7 (in pink); T3 – T9 (in yellow); an overlapping C6 – T2 (in cyan), T10 – T11 (in brown) and T12 – L7 (in blue). Additionally, a module comprised of the cervicals (C1 – C7) and the lumbars (L1 – L7) is displayed by the black lines. C. When the analysis is zoomed in to focus on individual vertebrae, most presacral vertebrae show shape covariation partitioned into two intravertebral modules, the centrum (in red) and the neural spine (in dark blue). Source: 'A' was modified from the Chasing Sabretooths blog: https://chasingsabretooths.wordpress.com/2016/12/16/sprint-of-the-giant-cheetah/.

Here I have presented a thorough analysis of the evolution of the vertebral column in felids. I have applied an array of methods to deal with two kinds of data (linear and three-dimensional), and techniques which account for the appropriateness of the data to each of the analyses. Both the studied trait (i.e., the vertebral column), and the scope of the work (from analyses of individual vertebrae to patterns observed across the vertebral column, and whole skeleton) discussed here represent a significant expansion of current work on phenotypic modularity and integration and lay new ground for further research.

Future Directions

1. **How do these patterns of trait covariation and ecological signal heterogeneity compare to other mammalian clades?**

Regarding the results of integration and modularity both within and across vertebrae, and between the axial skeleton and elements of the cranial and appendicular systems, there is strong indication that the conclusions I have discussed here may be applied to other mammalian families. This hypothesis is based on the shared developmental constraints acting on the vertebral column which are ancestral to the living families (Narita and Kuratani 2005; Müller et al. 2010; Buchholtz et al. 2012). Nevertheless, although relatively

minor, some variation does occur in some of these clades (Asher et al. 2011). Therefore, further investigation of the morphological change of vertebral shape and its drivers in other mammalian clades, both within Carnivora and from other more distantly related orders, is required. Specifically, some of the questions that should be addressed in future research include, but are not restricted to:

1. *Do clades with greater ecological disparity also present the highest correlation values between those factors and vertebral shape in the postdiaphragmatic region?*

2. *Consequently, is the cervical column of all mammals not only very constrained in terms of numbers, but also as phylogenetically conservative in shape, as in felids?*

3. *Are the patterns of trait covariation shown here, across all comparison levels, shared across Mammalia?*

4. *In clades in which meristic changes have been observed both across and within species, are these changes concentrated within specific modules, such as at the last T12 – L7 vertebral set?*

2. **Ontogenetic *versus* evolutionary patterns of trait covariation:**

As highlighted above, patterns of trait covariation may change throughout organismal development and growth (Zelditch and Carmichael 1989; Goswami et al. 2012; Goswami et al. 2014; Goswami et al. 2016). It is therefore interesting to consider that the patterns of intervertebral correlations observed for the adult specimens studied here may differ from the pattern at different stages of development. Although specimens from early ontogenetic stages might be difficult to acquire for non-model species, such specimens are readily available for the domestic cat (*Felis catus*) at museum collections and veterinary universities. Indeed, there already is work underway to start investigating this question. As part of a collaborating team, which includes researchers at three research institutions (University College London, UK, The Royal Veterinary College, UK, and Harvard University, USA), I have already started to secure multiple domestic cat specimens at early ontogenetic stages.

3. **Reconstructing the ecology of key fossil taxa:**

Finally, the correlation between vertebral morphology and ecological categories observed in living felids may be used to reconstruct the ecology of fossil felids based on similarities of vertebral shape across the column. Specifically, within Felidae there are key fossil taxa for which extensive material, including complete vertebral columns, has been found, but whose ecological characteristics, namely regarding locomotion, are yet unknown,

such as sabre-toothed species (e.g., *Smilodon fatalis*) and the American cheetah (*Miracinonyx trumani*) (Van Valkenburgh et al. 1990; Turner and Antón 1996; Barnett et al. 2005). By comparing the axial skeletal morphology of such species, specifically at the T10 – L7 region, to the variation of living taxa through the use of the Phenotypic Trajectory Analysis (PTA) methodology, we may be able to further improve reconstruction of their ecologies and, hence, characterisation of fossil faunas. As part of contributions to conference presentations (i.e., poster symposium at the 74th Annual Meeting for the Society of Vertebrate Palaeontology in Dallas, USA, and oral presentation at the 11th International Congress of Vertebrae Morphology in Maryland, USA), I have conducted preliminary analyses of a complete vertebral column of an American cheetah fossil specimen. Comparisons to the morphology observed in living cats, with use of PTA, demonstrated that, when the whole vertebral column was analysed, this fossil was most similar to the living puma (*Puma concolor*, a scansorial felid). However, regional analysis focusing on the T10 – L7 region showed that, at this region of the vertebral column where locomotor signal has its highest influence on shape, the fossil morphology was different from the puma's and in fact indistinguishable from the posterior vertebral column of modern cheetahs. These results agreed with previous observations that the American cheetah is phylogenetically more closely related to pumas than to modern cheetahs (Barnett et al. 2005), but that it shows morphological adaptations in the limbs and skull which are congruent with a more cursorial

mode of locomotion (Van Valkenburgh et al. 1990) and thus perhaps convergent with the specializations in extant cheetahs.

Additionally, fossil felid species have achieved much larger body masses than the range observed in living species (Turner and Antón 1996; Piras et al. 2013; Randau et al. 2013; Cuff et al. 2015; Cuff et al. 2017). Including these species in allometric analyses could clarify if the scaling relationships observed for the studied living species also apply at such higher body mass values.

This work has shed further and new light into the drivers and constraints of mammalian vertebral column evolution with a focus on the cat family. This thesis therefore begins to clarify the interplay between form and function, and the constraints which delimit the available vertebral morphospace, onto which shape can change and accommodate functional specialisation. As defined by the philosopher John Locke (1689), this 'under-labouring research' lays new ground with empirical observations, in a relatively understudied structure and provides an important step forward in our understanding of the structure that represents one of the most important innovations in animal evolution.

Reference list:

Adams, D. C. (2014a). A generalized K statistic for estimating phylogenetic signal from shape and other high-dimensional multivariate data. *Systematic Biology, 63*(5), 685-697.

Adams, D. C. (2014b). A method for assessing phylogenetic least squares models for shape and other high-dimensional multivariate data. *Evolution, 68*(9), 2675-2688.

Adams, D. C. (2016). Evaluating modularity in morphometric data: challenges with the RV coefficient and a new test measure. *Methods in Ecology and Evolution, 7*(5), 565-572.

Adams, D. C., & Collyer, M. L. (2007). Analysis of character divergence along environmental gradients and other covariates. *Evolution, 61*(3), 510-515.

Adams, D. C., & Collyer, M. L. (2009). A general framework for the analysis of phenotypic trajectories in evolutionary studies. *Evolution, 63*(5), 1143-1154.

Adams, D. C., & Collyer, M. L. (2015). Permutation tests for phylogenetic comparative analyses of high-dimensional shape data: what you shuffle matters. *Evolution and Development, 69*(3), 823-829.

Adams, D. C., Collyer, M. L., & Sherrat, E. (2015). geomorph: Software for geometric morphometric analyses. R package version 2.1.x. (2.1.x ed.).

Adams, D. C., & Felice, R. N. (2014). Assessing trait covariation and morphological integration on phylogenies using evolutionary covariance matrices. *PLoS One, 9*(4), e94335.

Adams, D. C., & Nistri, A. (2010). Ontogenetic convergence and evolution of foot morphology in European cave salamanders (Family: Plethodontidae). *BMC Evol Biol, 10*, 216-227.

Adams, D. C., & Otarola-Castillo, E. (2013). geomorph: an R package for the collection and analysis of geometric morphometric shape data. *Methods in Ecology and Evolution, 4*, 393-399.

Adams, D. C., Rohlf, F. J., & Slice, D. E. (2004). Geometric morphometrics: Ten years of progress following the 'revolution'. *Italian Journal of Zoology, 71*(1), 5-16.

Adams, D. C., Rohlf, F. J., & Slice, D. E. (2013). A field comes of age: geometric morphometrics in the 21st century. *Hystrix, 24*(1), 1-10.

Alvarez, A., Ercoli, M. D., & Prevosti, F. J. (2013). Locomotion in some small to medium-sized mammals: a geometric morphometric analysis of the penultimate lumbar vertebra, pelvis and hindlimbs. *Zoology (Jena), 116*(6), 356-371.

Álvarez, A., Perez, S. I., & Verzi, D. H. (2015). The Role of Evolutionary Integration in the Morphological Evolution of the Skull of Caviomorph Rodents (Rodentia: Hystricomorpha). *Evolutionary Biology, 42*(3), 312-327.

Anderson, M. J. (2001a). A new method for non-parametric multivariate analysis of variance. *Austral Ecology, 26*(1), 32-46.

Anderson, M. J. (2001b). Permutation tests for univariate or multivariate analysis of variance and regression. *Canadian Journal of Fisheries and Aquatic Sciences, 58*(3), 626-639.

Andersson, K., & Werdelin, L. (2003). The evolution of cursorial carnivores in the Tertiary: implications of elbow-joint morphology. *Proceedings of Royal Society of London B, 270 Suppl 2*, S163-165.

Antón, M., & Galobart, A. (1999). Neck function and predatory behavior in the scimitar toothed cat Homotherium latidens. *Journal of Vertebrate Paleontology, 19*(4), 771-784.

Antón, M., Salesa, M. J., Pastor, J. F., Sánchez, I. M., Fraile, S., & Morales, J. (2004). Implications of the mastoid anatomy of larger extant felids for the evolution and predatory behaviour of sabretoothed cats (Mammalia, Carnivora, Felidae). *Zoological Journal of the Linnean Society, 140*, 15.

Argot, C. (2003). Functional-adaptive anatomy of the axial skeleton of some extant marsupials and the paleobiology of the paleocene marsupials Mayulestes ferox and Pucadelphys andinus. *J Morphol, 255*(3), 279-300.

Arias-Martorell, J., Potau, J. M., Bello-Hellegouarch, G., & Perez-Perez, A. (2014). Brief communication: Developmental versus functional three-dimensional geometric morphometric-based modularity of the human proximal humerus. *Am J Phys Anthropol, 154*(3), 459-465.

Armbruster, W. S., Pelabon, C., Bolstad, G. H., & Hansen, T. F. (2014). Integrated phenotypes: understanding trait covariation in plants and animals. *Philosophical Transactions of the Royal Society London B, 369*(1649), 20130245.

Arnold, P., Forterre, F., Lang, J., & Fischer, M. S. (2016). Morphological disparity, conservatism, and integration in the canine lower cervical spine: Insights into mammalian neck function and regionalization. *Mammalian Biology, 81*(2), 153-162.

Arthur, W. (1997). *The origin of animal body plans: a study in evolutionary developmental biology*. Cambridge: Cambridge University Press.

Arthur, W. (2002). The emerging conceptual framework of evolutionary developmental biology. *Nature, 415*, 757-764.

Asher, R. J., Lin, K. H., Kardjilov, N., & Hautier, L. (2011). Variability and constraint in the mammalian vertebral column. *J Evol Biol, 24*(5), 1080-1090.

Badyaev, A. V. (2010). The beak of the other finch: coevolution of genetic covariance structure and developmental modularity during adaptive evolution. *Philosophical Transactions of the Royal Society London B, 365*(1543), 1111-1126.

Badyaev, A. V., & Foresman, K. R. (2004). Evolution of morphological integration. I. Functional units channel stress-induced variation in shrew mandibles. *Am Nat, 163*(6), 868-879.

Badyaev, A. V., Foresman, K. R., & Young, R. L. (2005). Evolution of morphological integration: Developmental accommodation of stress-induced variation. *Am Nat, 166*(3), 382-295.

Barnett, R., Barnes, I., Phillips, M. J., Martin, L. D., Harington, C. R., Leonard, J. A., et al. (2005). Evolution of the extinct sabretooths and the american cheetahlike cat. *Current Biology, 15*(15), R589-R590.

Barthez, P. J. (1798). *Nouvelle méchanique des mouvements de l'homme et des animaux.* Paris: A Carcassonne, de l'imprimerie de Pierre Polère.

Bastir, M., Rosas, A., & Sheets, H. D. (2005). The morphological integration of the hominoid skull: A Partial Least Aquares and PC analysis with implications for European middle pleistocene mandibular variation. In D. E. Slice (Ed.), *Modern morphometrics in physical anthropology* (pp. 265-284). New York: Kluwer Academic/Plenum Publishers.

Bell, E., Andres, B., & Goswami, A. (2011). Integration and dissociation of limb elements in flying vertebrates: a comparison of pterosaurs, birds and bats. *J Evol Biol, 24*(12), 2586-2599.

Benjamini, Y., & Hochberg, Y. (1995). Controlling the false discovery rate: A practical and powerful approach to multiple testing. *Journal of the Royal Statistical Society. Series B (Methodological), 57*(1), 289-300.

Bennett, V. C., & Goswami, A. (2011). Does developmental strategy drive limb integration in marsupials and monotremes? *Mammalian Biology, 76*(1), 79-83.

Benoit, M. H. (2010). What's the difference? A multiphasic allometric analysis of fossil and living lions. In A. Goswami, & A. Friscia (Eds.), *Carnivoran evolution: New views on phylogeny, form and function* (pp. 165-188). Cambridge: Cambridge University Press.

Bertram, J. E., & Biewener, A. A. (1990). Differential scaling of the long bones in the terrestrial carnivora and other mammals. *J Morphol, 204*(2), 157-169.

Biewener, A. A. (1989). Scaling body support in mammals: limb posture and muscle mechanics. *Science, 245*(4913), 45-48.

Biewener, A. A. (2005). Biomechanical consequences of scaling. *Journal of Experimental Biology, 208*(9), 1665-1676.

Blomberg, S. P., Garland, T., & Ives, A. R. (2003). Testing for Phylogenetic Signal in Comparative Data: Behavioral Traits Are More Labile. *Evolution, 57*(4), 717.

Böhmer, C., Rauhut, O. W., & Wörheide, G. (2015). Correlation between Hox code and vertebral morphology in archosaurs. *Proceedings of the Royal Society B, 282*(1810).

Bolker, J. A. (2000). Modularity in development and why it matters to evo-devo. *American Zoologist, 40*(5), 770-776.

Bookstein, F. L. (1991). *Morphometric tools for landmark data: geometry and biology*. New York, USA: Cambridge University Press.

Bookstein, F. L. (2015). Integration, Disintegration, and Self-Similarity: Characterizing the Scales of Shape Variation in Landmark Data. *Evolutionary Biology, 42*(4), 395-426.

Bookstein, F. L., Gunz, P., Mitterœcker, P., Prossinger, H., Schæfer, K., & Seidler, H. (2003). Cranial integration in Homo: singular warps analysis of the midsagittal plane in ontogeny and evolution. *Journal of Human Evolution, 44*(2), 167-187.

Boszczyk, B. M., Boszczyk, A. A., & Putz, R. (2001). Comparative and functional anatomy of the mammalian lumbar spine. *Anatomical Records, 264*, 157–168.

Boyd, J. S. (1976). Studies on the appearance of the centres of ossification of the axial skeleton in the feline fœtus. *Anatomia, Histologia, Embryologia, 5*(3), 193-292.

Breit, S., & Künzel, W. (2004). A morphometric investigation on breed-specific features affecting sagittal rotational and lateral bending mobility in the canine cervical spine (C3-C7). *Anatomia, Histologia, Embryologia, 33*(4), 244-250.

Buchholtz, E. A. (2001a). Swimming styles in Jurassic ichthyosaurs. *Journal of Vertebrate Paleontology, 21*, 61-73.

Buchholtz, E. A. (2001b). Vertebral osteology and swimming style in living and fossil whales (Order: Cetacea). *Journal of Zoology, 253*, 175-190.

Buchholtz, E. A. (2007). Modular evolution of the Cetacean vertebral column. *Evolution and Development, 9*(3), 278-289.

Buchholtz, E. A. (2012). Flexibility and constraint: patterning the axial skeleton in mammals. In R. J. Asher, & J. Müller (Eds.), *From clone to bone: The synergy of morphological and molecular tools in palaeobiology* (pp. 230-256). Cambridge: Cambridge University Press.

Buchholtz, E. A. (2014). Crossing the frontier: a hypothesis for the origins of meristic constraint in mammalian axial patterning. *Zoology (Jena), 117*(1), 64-69.

Buchholtz, E. A., Bailin, H. G., Laves, S. A., Yang, J. T., Chan, M. Y., & Drozd, L. E. (2012). Fixed cervical count and the origin of the mammalian diaphragm. *Evolution and Development, 14*(5), 399-411.

Buchholtz, E. A., & Stepien, C. C. (2009). Anatomical transformation in mammals: developmental origin of aberrant cervical anatomy in tree sloths. *Evolution and Development, 11*(1), 69-79.

Buchholtz, E. A., Wayrynen, K. L., & Lin, I. W. (2014). Breaking constraint: axial patterning in *Trichechus* (Mammalia: Sirenia). *Evolution and Development, 16*(6), 382-393.

Burke, A. C., Nelson, C. E., Morgan, B. A., & Tabin, C. (1995). *Hox* genes and the evolution of vertebrate axial morphology. *Development, 121*, 4333-4346.
Carbone, C., Mace, G. M., Roberts, S. C., & Macdonald, D. W. (1999). Energetic constaints on the diet of terrestrial carnivores. *Nature, 402*, 286-288.
Carbone, C., Teacher, A., & Rowcliffe, J. M. (2007). The costs of carnivory. *PLoS Biol, 5*(2), e22.
Cardini, A., & Loy, A. (2013). On growth and form in the "computer area": from geometric to biological morphometrics. *Hystrix, 24*(1), 1-5.
Cardini, A., & Polly, P. D. (2013). Larger mammals have longer faces because of size-related constraints on skull form. *Nat Commun, 4*, 2458.
Carlson, H., Halbertsma, J., & Zomlefer, M. (1979). Control of the Trunk during Walking in the Cat. *Acta Physiologica Scandinavica, 105*(2), 251-253.
Carroll, S. B., Grenier, J. K., & Weatherbee, S. D. (2001). *From DNA to diversity.* Malden, MA: Blackwell Science.
Chatzigianni, A., & Halazonetis, D. J. (2009). Geometric morphometric evaluation of cervical vertebrae shape and its relationship to skeletal maturation. *American Journal of Orthodontics and Dentofacial Orthopedics, 136*(4), 481.e481-481.e489.
Chen, X., Milne, N., & O'Higgins, P. (2005). Morphological variation of the thoracolumbar vertebrae in Macropodidae and its functional relevance. *J Morphol, 266*(2), 167-181.
Cheverud, J. M. (1982). Phenotypic, genetic, and environmental morphologicalintegration in the cranium. *Evolution, 36*(3), 499-516.
Cheverud, J. M. (1995). Morphological integration in the saddle-back tamarin (*Saguinus fuscicollis*) cranium. *American Naturalist, 145*(1), 63-89.
Cheverud, J. M. (1996). Developmental integration and the evolution of pleiotropy. *American Zoologist, 36*, 44-50.
Cheverud, J. M., Wagner, G. P., & Dow, M. M. (1989). Methods for the comparative analysis of variation patterns. *Systematic Zoology, 38*(3), 201-213.
Christ, B., Huang, R., & Scaal, M. (2007). Amniote somite derivatives. *Developmental Dynamics, 236*(9), 2382-2396.
Christ, B., Huang, R., & Wilting, J. (2000). The development of the avian vertebral column. *Anatomy and embryology, 202*(3), 179-194.
Clune, J., Mouret, J. B., & Lipson, H. (2013). The evolutionary origins of modularity. *Proceedings of the Royal Society B - Biological Sciences, 280*(1755), 20122863.
Collyer, M. L., & Adams, D. C. (2013). Phenotypic trajectory analysis: comparison of shape change patterns in evolution and ecology. *Hystrix, 24*(1), 75–83.
Collyer, M. L., Sekora, D. J., & Adams, D. C. (2015). A method for analysis of phenotypic change for phenotypes described by high-dimensional data. *Heredity (Edinb)*.
Cornette, R., Baylac, M., Souter, T., & Herrel, A. (2013a). Does shape co-variation between the skull and the mandible have functional consequences? A 3D approach for a 3D problem. *J Anat, 223*(4), 329-336.
Cornette, R., Baylac, M., Souter, T., & Herrel, A. (2013b). Does shape covariation between the skull and the mandible have functional consequences? A 3D approach for a 3D problem. *J Anat, 223*(4), 329-336.
Cuff, A. R., Goswami, A., & Hutchinson, J. R. (2017). Reconstruction of the musculoskeletal system in an extinct lion. *Palaeontologia Electronica, 20.2.23A*, 1-25.
Cuff, A. R., Randau, M., Head, J. J., Hutchinson, J. R., Pierce, S. E., & Goswami, A. (2015). Big cat, small cat: Reconstructing body size evolution in living and extinct Felidae. *J Evol Biol, 28*(8), 1516-1525.

Cuff, A. R., Sparkes, E. L., Randau, M., Pierce, S. E., Kitchener, A. C., Goswami, A., et al. (2016a). The scaling of postcranial muscles in cats (Felidae) I: forelimb, cervical, and thoracic muscles. *J Anat, 229*(1), 128-141.

Cuff, A. R., Sparkes, E. L., Randau, M., Pierce, S. E., Kitchener, A. C., Goswami, A., et al. (2016b). The scaling of postcranial muscles in cats (Felidae) II: hindlimb and lumbosacral muscles. *J Anat, 229*(1), 142-152.

Davies, T. J., Meiri, S., Barraclough, T. G., & Gittleman, J. L. (2007). Species co-existence and character divergence across carnivores. *Ecol Lett, 10*(2), 146-152.

Day, L. M., & Jayne, B. C. (2007). Interspecific scaling of the morphology and posture of the limbs during the locomotion of cats (Felidae). *Journal of Experimental Biology, 210*(4), 642-654.

Dayan, T., Simberloff, D., Tchernov, E., & Yom-Tov, Y. (1990). Feline Canines: Community-Wide Character Displacement Among the Small Cats of Israel. *Am Nat, 136*(1), 39-60.

De Iuliis, G., & Pulerà, D. (2006). The cat. In *The dissection of vertebrates: a laboratory manual* (1st Edition ed., pp. 131-226). Burlington, MA: Academic Press.

Dickinson, M. H. (2000). How Animals Move: An Integrative View. *Science, 288*(5463), 100-106.

Doube, M., Wiktorowicz-Conroy, A., Christiansen, P., Hutchinson, J. R., & Shefelbine, S. (2009). Three-dimensional geometric analysis of felid limb bone allometry. *PLoS One, 4*(3), e4742.

Drake, A. G., & Klingenberg, C. P. (2010). Large-scale diversification of skull shape in domestic dogs: disparity and modularity. *Am Nat, 175*(3), 289-301.

Driscoll, C. A., Menotti-Raymond, M., Roca, A. L., Hupe, K., Johnson, W. E., Geffen, E., et al. (2007). The Near Eastern origin of cat domestication. *Science, 317*(5837), 519-523.

Dumont, M., Wall, C. E., Botton-Divet, L., Goswami, A., Peigne, S., & Fabre, A. C. (2015). Do functional demands associated with locomotor habitat, diet, and activity pattern drive skull shape evolution in musteloid carnivorans? *Biological Journal of the Linnean Society, 117*(4), 858-878.

Ercoli, M. D., Prevosti, F. J., & ÁLvarez, A. (2012). Form and function within a phylogenetic framework: locomotory habits of extant predators and some Miocene Sparassodonta (Metatheria). *Zoological Journal of the Linnean Society, 165*(1), 224-251.

Escoufier, Y. (1973). Le traitement des variables vectorielles. *Biometrics, 29*(4), 751-760.

Ewer, R. F. (1973). *The Carnivores*: Cornell University Press.

Fabre, A. C., Cornette, R., Huyghe, K., Andrade, D. V., & Herrel, A. (2014a). Linear versus geometric morphometric approaches for the analysis of head shape dimorphism in lizards. *J Morphol, 275*(9), 1016-1026.

Fabre, A. C., Cornette, R., Peigne, S., & Goswami, A. (2013a). Influence of body mass on the shape of forelimb in musteloid carnivorans. *Biological Journal of the Linnean Society, 110*(1), 91-103.

Fabre, A. C., Cornette, R., Slater, G., Argot, C., Peigne, S., Goswami, A., et al. (2013b). Getting a grip on the evolution of grasping in musteloid carnivorans: a three-dimensional analysis of forelimb shape. *J Evol Biol, 26*(7), 1521-1535.

Fabre, A. C., Goswami, A., Peigné, S., & Cornette, R. (2014b). Morphological integration in the forelimb of musteloid carnivorans. *J Anat, 225*(1), 19-30.

Fabre, A. C., Marigó, J., Granatosky, M. C., & Schmitt, D. (2017). Functional associations between support use and forelimb shape in strepsirrhines and their relevance to inferring locomotor behavior in early primates. *Journal of Human Evolution, 108*, 11-30.

Felsenstein, J. (1985). Phylogenies and the comparative method. *Am Nat, 125*(1), 1-15.

Figueirido, B., Serrano-Alarcon, F. J., Slater, G. J., & Palmqvist, P. (2010). Shape at the cross-roads: homoplasy and history in the evolution of the carnivoran skull towards herbivory. *J Evol Biol, 23*(12), 2579-2594.

Finch, M., & Freedman, L. (1986). Functional-morphology of the vertebral column of *Thylacoleo carnifex* Owen (Thylacoleonidae, Marsupialia). *Australian Journal of Zoology, 34*, 1-16.

Fleming, A., Kishida, M. G., Kimmel, C. B., & Keynes, R. J. (2015). Building the backbone: the development and evolution of vertebral patterning. *Development, 142*(10), 1733-1744.

Foth, C., Brusatte, S. L., & Butler, R. J. (2012). Do different disparity proxies converge on a common signal? Insights from the cranial morphometrics and evolutionary history of Pterosauria (Diapsida: Archosauria). *J Evol Biol, 25*(5), 904-915.

Fruciano, C. (2016). Measurement error in geometric morphometrics. *Development, Genes and Evolution, 226*(3), 139-158.

Fruciano, C., Franchini, P., & Meyer, A. (2013). Resampling-based approaches to study variation in morphological modularity. *PLoS One, 8*(7), e69376.

Gál, J. M. (1993a). Mammalian spinal biomechanics II. Intervertebral lesion experiments and mechanisms of bending resistance. *Journal of Experimental Biology, 174*, 281-297.

Gál, J. M. (1993b). Mammalian spinal biomechanics. I. Static and dynamic mechanical properties of intact intervertebral joints. *Journal of Experimental Biology, 174*, 247-280.

Galis, F. (1999). Why do almost all mammals have seven cervical vertebrae? Developmental constraints, Hox genes and cancer. *Journal of Experimental Biology, 285*, 19-26.

Galis, F., Carrier, D. R., van Alphen, J., van der Mije, S. D., Van Dooren, T. J., Metz, J. A., et al. (2014). Fast running restricts evolutionary change of the vertebral column in mammals. *Proceedings of the National Academy of Science USA, 111*(31), 11401-11406.

Garland, T., Jr., Dickerman, A. W., Janis, C. M., & Jones, J. A. (1993). Phylogenetic Analysis of Covariance by Computer Simulation. *Systematic Biology, 42*(3), 265-292.

German, A., & Hill, J. (2006). *Data analysis using regression and multilevel/hierarchical models (Analytical methods for social research)* (1st ed.). New York: Cambridge University Press.

Gittleman, J. L., & Van Valkenburgh, B. (1997). Sexual dimorphism in the canines and skulls of carnivores: effects of size, phylogeny, and behavioural ecology. *Journal of Zoology, 242*(1), 97-117.

Gómez-Robles, A., & Polly, P. D. (2012). Morphological integration in the hominin dentition: Evolutionary, developmental, and functional factors. *Evolution, 66*(4), 1024-1043.

Gonyea, W. J. (1976). Adaptive differences in the body proportions of large felids. *Acta Anatomica (Basel), 96*, 81-96.

Gonyea, W. J. (1978). Functional implications of felid forelimb anatomy. *Acta Anatomica (Basel), 102*(2), 111-121.

Goodall, C. R. (1991). Procrustes methods in the statistical analysis of shape. *Journal of the Royal Statistical Society B, 53*, 285-339.

Goswami, A. (2006a). Cranial modularity shifts during mammalian evolution. *Am Nat, 168*(2), 270-280.

Goswami, A. (2006b). Morphological integration in the carnivoran skull. *Evolution, 60*(1), 15.

Goswami, A., Binder, W. J., Meachen, J., & O'Keefe, F. R. (2015). The fossil record of phenotypic integration and modularity: A deep-time perspective on developmental and evolutionary dynamics. *PNAS, 112*(16), 4891-4896.

Goswami, A., & Finarelli, J. A. (2016). EMMLi: a maximum likelihood apprach to the analysis of modularity. *Evolution, 70*(7), 1622-1637.

Goswami, A., Milne, N., & Wroe, S. (2010). Biting through constraints: cranial morphology, disparity and convergence across living and fossil carnivorous mammals. *Proceedings of the Royal Society B, 278*(1713), 1831-1839.

Goswami, A., & Polly, P. D. (2010a). The influence of character correlations of phylogenetic analyses: a case study of the carnivoran cranium. In A. Goswami, & A. Friscia (Eds.), *Carnivoran evolution: New views on phylogeny, form, and function.* (pp. 141-164). Cambridge: Cambridge University Press.

Goswami, A., & Polly, P. D. (2010b). The influence of modularity on cranial morphological disparity in Carnivora and Primates (Mammalia). *PLoS One, 5*(3), e9517.

Goswami, A., & Polly, P. D. (2010c). Methods of studying morphological integration and modularity. In J. Alroy, & G. Hunt (Eds.), *Quantitative methods in paleobiology* (Vol. 16, pp. 213-243). Cambridge, UK: Paleontological Society Special Publications.

Goswami, A., Polly, P. D., Mock, O. B., & Sanchez-Villagra, M. R. (2012). Shape, variance and integration during craniogenesis: contrasting marsupial and placental mammals. *J Evol Biol, 25*(5), 862-872.

Goswami, A., Randau, M., Polly, P. D., Weisbecker, V., Bennett, C. V., Hautier, L., et al. (2016). Do Developmental Constraints and High Integration Limit the Evolution of the Marsupial Oral Apparatus? *Integr Comp Biol, 56*(3), 404-415.

Goswami, A., Smaers, J. B., Soligo, C., & Polly, P. D. (2014). The macroevolutionary consequences of phenotypic integration: from development to deep time. *Philosophical transactions of the Royal Society B, 369*(1649), 1-15.

Goswami, A., Weisbecker, V., & Sanchez-Villagra, M. R. (2009). Developmental modularity and the marsupial-placental dichotomy. *Journal of Experimental Zoology (Molecular and Developmental Evolution), 312B*(3), 186-195.

Gould, S. J. (1966). Allometry and size in ontogeny and phylogeny. *Biological Reviews, 41*, 587-640.

Graf, W., De Waele, C., & Vidal, P. P. (1995). Functional anatomy of the head-neck movement system of quadrupedal and bipedal mammals. *J Anat, 186*(1), 55-74.

Gray, H., Standring, S., Ellis, H., & Berkovitz, B. (2005). *Gray's Anatomy: The Anatomical Basis of Clinical Practice.* (39th ed.). Edinburgh: Churchill Livingstone: Elsevier.

Guinard, G., & Marchand, D. (2010). Modularity and Complete Natural Homeoses in Cervical Vertebrae of Extant and Extinct Penguins (Aves: Sphenisciformes). *Evolutionary Biology, 37*(4), 210-226.

Gunz, P., Mitteroœcker, P., Neubauer, S., Weber, G. W., & Bookstein, F. L. (2009). Principles for the virtual reconstruction of hominin crania. *Journal of Human Evolution, 57*, 48-62.

Hall, B. K. (1977). Chondrogenesis of the somitic mesoderm. *Advances in anatomy, embryology, and cell biology, 53*(4), 3-47.

Hallgrímsson, B., Jamniczky, H., Young, N. M., Rolian, C., Parsons, T. E., Boughner, J. C., et al. (2009). Deciphering the Palimpsest: Studying the Relationship Between Morphological Integration and Phenotypic Covariation. *Evolutionary Biology, 36*(4), 355-376.

Hallgrímsson, B., Willmore, K., & Hall, B. K. (2002). Canalization, developmental stability, and morphological integration in primate limbs. *Am J Phys Anthropol, 119*(S35), 131-158.

Halpert, A. P., Jenkins, F. A., Jr., & Franks, H. (1987). Structure and scaling of the lumbar vertebrae in African bovids (Mammalia, Artiodactyla). *Journal of Zoology, 211*(2), 239-258.

Hammer, Ø., Harper, D. A. T., & Ryan, P. D. (2001). PAST: Paleontological statistics software package for education and data analysis. *Palaeontologia Electronica, 4*(1-9), 9.
Hansen, T. F., & Houle, D. (2008). Measuring and comparing evolvability and constraint in multivariate characters. *J Evol Biol, 21*(5), 1201-1219.
Harmon, L., Weir, J., Brock, C., Glor, R., Challenger, W., Hunt, G., et al. (2014). Analysis of evolutionary diversification. (2.0.6 ed., pp. Methods for fitting macroevolutionary models to phylogenetic trees.).
Harris, E. F., & Smith, R. N. (2009). Accounting for measurement error: A critical but often overlooked process. *Archives of Oral Biology, 54*(1), S107-S117.
Hautier, L., Lebrun, R., & Cox, P. G. (2012). Patterns of covariation in the masticatory apparatus of hystricognathous rodents: implications for evolution and diversification. *J Morphol, 273*(12), 1319-1337.
Hautier, L., Weisbecker, V., Sanchez-Villagra, M. R., Goswami, A., & Asher, R. J. (2010). Skeletal development in sloths and the evolution of mammalian vertebral patterning. *PNAS, 107*(44), 18903-18908.
Head, J. J., & Polly, P. D. (2015). Evolution of the snake body form reveals homoplasy in amniote Hox gene function. *Nature, 520*(7545), 86-89.
Herrel, A., McBrayer, L. D., & Larson, P. M. (2007). Functional basis for intersexual differences in bite force in the lizard *Anolis carolinensis*. *Biological Journal of the Linnean Society, 91*(1), 111-119.
Hildebrand, M. (1959). Motions of the running cheetah and horse. *Journal of Mammalogy, 40*(4), 481-495.
Holliday, J. A., & Steppan, S. J. (2004). Evolution of hypercarnivory: the effect of specialization on morphological and taxonomic diversity. *Paleobiology, 30*(1), 108-128.
Hu, Y., Ghigliotti, L., Vacchi, M., Pisano, E., Detrich, H. W., 3rd, & Albertson, R. C. (2016). Evolution in an extreme environment: developmental biases and phenotypic integration in the adaptive radiation of antarctic notothenioids. *BMC Evol Biol, 16*(1), 142-153.
Hua, S. (2003). Locomotion in marine mesosuchians (Crocodylia): the contribution of the 'locomotion profiles'. *Neues jahrbuch für geologie und palaontologie abhandlungen, 227*, 139-152.
Hudson, P. E., Corr, S. A., Payne-Davis, R. C., Clancy, S. N., Lane, E., & Wilson, A. M. (2011). Functional anatomy of the cheetah (Acinonyx jubatus) forelimb. *J Anat, 218*(4), 375-385.
Hunter, L. (2005). *Cats of Africa: Behavior, Ecology and Conservation.* Baltimore: The Johns Hopkins University Press.
Husson, F., Josse, J., Le, S., & Mazet, J. (2016). Multivariate exploratory data analysis and data mining. R package version 1.31.5. (1.31.5 ed., pp. Exploratory data analysis methods such as principal component methods and clustering.).
Hutchinson, J. R. (2012). On the inference of function from structure using biomechanical modelling and simulation of extinct organisms. *Biol Lett, 8*(1), 115-118.
Ilin, A., & Raiko, T. (2010). Practical approaches to principal component analysis in the presence of missing values. *Journal of Machine Learning Research, 11*, 1957-2000.
Ireland, C. R. (2010). *Experimental Statistics for Agriculture and Horticulture.* (Vol. 352). Cambridge, MA: CABI Publishing.
Irschick, D. J. (2002). Evolutionary approaches for studying functional morphology: examples from studies of performance capacity. *Integrative Comparative Biology, 42*(2), 278-290.
Jenkins, F. A. (1974). *Primate locomotion*. New York ; London: Academic Press.

Jenkins, F. A., Jr. (1971). *The postcranial skeleton of African cynodonts: problems in the early evolution of the mammalian postcranial skeleton.* (Vol. 36, Bulletin of the Peabody museum of natural history). New Haven, Connecticut: Yale University.

Johnson, D. R., McAndrew, T. J., & Oguz, O. (1999). Shape differences in the cervical and upper thoracic vertebrae in rats (*Rattus norvegicus*) and bats (*Pteropus poiocephalus*): can we see shape patterns derived from position in column and species membership? *J Anat, 194*(2), 249-253.

Johnson, W. E., Eizirik, E., Pecon-Slattery, J., Murphy, W. J., Antunes, A., Teeling, E., et al. (2006). The late Miocene radiation of modern Felidae: a genetic assessment. *Science, 311*(5757), 73-77.

Johnson, W. E., & O'Brien, S. J. (1997). Phylogenetic reconstruction of the Felidae using 16S rRNA and NADH-5 mitochondrial genes. *Journal of Molecular Evolution, 44*(Supplement 1), S98-S116.

Jones, K. E. (2015). Evolutionary allometry of the thoracolumbar centra in felids and bovids. *J Morphol, 276*(7), 818-831.

Jones, K. E., & German, R. Z. (2014). Ontogenetic allometry in the thoracolumbar spine of mammal species with differing gait use. *Evolution and Development, 16*(2), 110-120.

Jones, K. E., & Goswami, A. (2010). Morphometric analysis of cranial morphology in pinnipeds (Mammalia, Carnivora): convergence, ecology, ontogeny, and dimorphism. In A. Goswami, & A. Friscia (Eds.), *Carnivoran Evolution: New Views on Phylogeny, Form anfd Function* (pp. 342-373): Cambridge University Press.

Jones, K. E., & Pierce, S. E. (2015). Axial allometry in a neutrally buoyant environment: Effects of the terrestrial-aquatic transition on vertebral scaling. *J Evol Biol, 29*(3), 594-601.

Kaliontzopoulou, A., Carretero, M. A., & Llorente, G. A. (2007). Multivariate and geometric morphometrics in the analysis of sexual dimorphism variation in *Podarcis* lizards. *J Morphol, 268*(2), 152-165.

Kane, E. A., & Higham, T. E. (2015). Complex systems are more than the sum of their parts: Using integration to understand performance, biomechanics, and diversity. *Integr Comp Biol, 55*(1), 146-165.

Kardong, K. V. (2005). *Vertebrates: Comparative anatomy, function, evolution.* New York: McGraw-Hill Higher Education.

Kitchener, A. C. (1991). *The Natural History of the Wild Cats.* London: A&C Black.

Klaczko, J., Sherrat, E., & Setz, E. Z. F. (2016). Are diet preferences associated to skulls shape diversification in xenodontine snakes? *PLoS One, 11*(2), e0148375.

Klingenberg, C. P. (2003). Developmental instability as a research tool: using patterns of fluctuating asymmetry to infer the developmental origins of morphological integration. In M. Polak (Ed.), *Developmental instability: causes and consequences.* (pp. 427–442). New York: Oxford University Press.

Klingenberg, C. P. (2005). Developmental constraints, modules and evolvability. In B. Hallgrimsson, & B. K. Hall (Eds.), *Variation* (pp. 219-247). San Diego: Academic Press.

Klingenberg, C. P. (2008). Morphological Integration and Developmental Modularity. *Annual Review of Ecology, Evolution, and Systematics, 39*(1), 115-132.

Klingenberg, C. P. (2009). Morphometric integration and modularity in configurations of landmarks: tools for evaluating a priori hypotheses. *Evolution and Development, 11*(4), 405-421.

Klingenberg, C. P. (2010). Evolution and development of shape: integrating quantitative approaches. *Nature Reviews Genetics, 11*(9), 623-635.

Klingenberg, C. P. (2013). Cranial integration and modularity: insights into evolution and development from morphometric data. *Hystrix, 24*(1), 43-58.
Klingenberg, C. P., & Marugán-Lobón, J. (2013). Evolutionary Covariation in Geometric Morphometric Data: Analyzing Integration, Modularity, and Allometry in a Phylogenetic Context. *Systematic Biology, 62*(4), 591–610.
Klingenberg, C. P., Mebus, K., & Auffray, J. C. (2003). Developmental integration in a complex morphological structure: how distinct are the modules in the mouse mandible? *Evolution and Development, 5*(5), 522-531.
Koob, T. J., & Long, J. H. (2000). The vertebrate body axis: Evolution and mechanical function. *American Zoologist, 40*(1), 1-18.
Laffont, R., Renvoisé, E., Navarro, N., Alibert, P., & Montuire, S. (2009). Morphological modularity and assessment of developmental processes within the vole dental row (Microtus arvalis, Arvicolinae, Rodentia). *Evolution and Development, 11*(3), 302-311.
Lauder, G. V. (1995). On the inference of function from structure. In J. J. Thomason (Ed.), *Functional anatomy of vertebrates: an evolutionary perspective.* (pp. 11 - 18). Cambridge: Cambridge University Press.
Lazić, M. M., Carretero, M. A., Crnobrnja-Isailović, J., & Kaliontzopoulou, A. (2015). Effects of environmental disturbance on phenotypic variation: an integrated assessment of canalization, developmental stability, modularity, and allometry in lizard head shape. *Am Nat, 185*(1), 44-58.
Leyhausen, P. (1979). *Cat behavior: the predatory and social behavior of domestic and wild cats.*: New York, NY: Garland. STMP Press.
Locke, J. (1689). *An essay concerning human understanding* (1st ed.). London: Thomas Basset.
Long, J. H., Adcock, B., & Root, R. G. (2002). Force transmission via axial tendons in undulating fish: a dynamic analysis. *Comparative Biochemistry and Physiology Part A: Molecular & Integrative Physiology, 133*(4), 911-929.
Long, J. H., Pabst, D. A., Shepherd, W. R., & McLellan, W. A. (1997). Locomotor design of dolphin vertebral columns: bending mechanics and morphology of Delphinus delphis. *Journal of Experimental Biology, 200*, 65-81.
Losos, J. B. (2011). Convergence, adaptation, and constraint. *Evolution, 65*(7), 1827-1840.
MacDonald, D., Macdonald, D. W., & Loveridge, A. J. (2010). *The Biology and Conservation of Wild Felids*: Oxford University Press.
Macpherson, J. M., & Fung, J. (1998). Activity of thoracic and lumbar epaxial extensors during postural responses in the cat. *Experimental Brain Research, 119*(3), 315-323.
Macpherson, J. M., & Ye, Y. (1998). The cat vertebral column: stance configuration and range of motion. *Experimental Brain Research, 119*(3), 324-332.
Maddison, W. P., & Maddison, D. R. (2014). Mesquite: a modular system for evolutionary analysis. (3.01 ed.).
Manfreda, E., Mitterœcker, P., Bookstein, F. L., & Schæfer, K. (2006). Functional morphology of the first cervical vertebra in humans and nonhuman primates. *The Anatomical Record, 289B*(5), 184-194.
Mao, X., & Ryan, T. (2013). Generalized Least Square in comparative Phylogenetics. (0.0-1 ed., pp. Based on the Generalized Least Square model for comparative Phylogenetics.).
Mardia, K. V., Kent, J. T., & Bibby, J. M. (1979). *Multivariate analysis* (1st ed.). London: Academic PRess.
Marroig, G., Shirai, L. T., Porto, A., de Oliveira, F. B., & De Conto, V. (2009). The evolution of modularity in the mammalian skull II: Evolutionary consequences. *Evolutionary Biology, 36*(1), 136-148.

Martín-Serra, A., Figueirido, B., & Palmqvist, P. (2014a). A three-dimensional analysis of morphological evolution and locomotor performance of the carnivoran forelimb. *PLoS One, 9*(1), e85574.

Martín-Serra, A., Figueirido, B., & Palmqvist, P. (2014b). A three-dimensional analysis of the morphological evolution and locomotor behaviour of the carnivoran hind limb. *BMC Evol Biol, 14*(129), 1-13.

Martín-Serra, A., Figueirido, B., Perez-Claros, J. A., & Palmqvist, P. (2015). Patterns of morphological integration in the appendicular skeleton of mammalian carnivores. *Evolution, 69*(2), 321-340.

Martins, E. P., & Hansen, T. F. (1996). The statistical analysis of interspecific data: a review and evaluation of comparative methods. In E. P. Martins (Ed.), *Phylogenies and the comparative method in animal behavior.* (pp. 22-75). Oxford: Oxford University Press.

Martins, E. P., & Hansen, T. F. (1997). Phylogenies and the comparative method: a general approach to incorporating phylogenetic information into the analysis of interspecific data. *Am Nat, 149*, 646-667.

Marugán-Lobón, J., & Buscalioni, Á. D. (2006). Avian skull morphological evolution: exploring exo- and endocranial covariation with two-block partial least squares. *Zoology (Jena), 109*(3), 217-230.

Mattern, M. Y., & McLennan, D. A. (2000). Phylogeny and speciation of felids. *Cladistics, 16*(2), 232-253.

McDonald, J. H. (2014). *Handbook of biological statistics* (3rd ed.). Baltimore, Maryland: Sparky House Publishing.

McInnes, L., Baker, W. J., Barraclough, T. G., Dasmahapatra, K. K., Goswami, A., Harmon, L. J., et al. (2011). Integrating ecology into macroevolutionary research. *Biol Lett, 7*(5), 644-646.

Meachen-Samuels, J. A. (2010). Comparative Scaling of Humeral Cross-Sections of Felids and Canids Using Radiographic Images. *Journal of Mammalian Evolution, 17*(3), 193-209.

Meachen-Samuels, J. A. (2012). Morphological convergence of the prey-killing arsenal of sabertooth predators. *Paleobiology, 38*(1), 1-14.

Meachen-Samuels, J. A., & Van Valkenburgh, B. (2009a). Craniodental indicators of prey size preference in the Felidae. *Biological Journal of the Linnean Society, 96*(4), 784-799.

Meachen-Samuels, J. A., & Van Valkenburgh, B. (2009b). Forelimb indicators of prey-size preference in the Felidae. *J Morphol, 270*(6), 729-744.

Meachen-Samuels, J. A., & Van Valkenburgh, B. (2010). Radiographs reveal exceptional forelimb strength in the sabertooth cat, Smilodon fatalis. *PLoS One, 5*(7), e11412.

Meachen, J. A., O'Keefe, F. R., & Sadleir, R. W. (2014). Evolution in the sabre-tooth cat,*Smilodon fatalis*, in response to Pleistocene climate change. *J Evol Biol, 27*(4), 714-723.

Melo, D., Garcia, G., Hubbe, A., Assis, A. P., & Marroig, G. (2016). EvolQR: An R package for evolutionary quantitative genetics. *F1000Research, 4*(925), 1-25.

Meloro, C., Elton, S., Louys, J., Bishop, L. C., & Ditchfield, P. (2013). Cats in the forest: predicting habitat adaptations from humerus morphometry in extant and fossil Felidae (Carnivora). *Paleobiology, 39*(3), 323-344.

Meloro, C., & O'Higgins, P. (2011). Ecological Adaptations of Mandibular Form in Fissiped Carnivora. *Journal of Mammalian Evolution, 18*(3), 185-200.

Meloro, C., & Slater, G. J. (2012). Covariation in the skull modules of cats: the challenge of growing saber-like canines. *Journal of Vertebrate Paleontology, 32*(3), 677-685.

Mitteroecker, P., & Gunz, P. (2009). Advances in Geometric Morphometrics. *Evolutionary Biology, 36*(2), 235-247.

Mitteroecker, P., Gunz, P., Windhager, S., & Schæfer, K. (2013). A brief review of shape, form, and allometry in geometric morphometrics, with applications to human facial morphology. *Hystrix, 21*(1), 59-66.

Molnar, J. L., Pierce, S. E., Bhullar, B.-A. S., Turner, A. H., & Hutchinson, J. R. (2015). Morphological and functional changes in the vertebal column with increasing aquactic adaptation in crocodylomorphs. *Royal Society Open Science, 2*, 1-22.

Molnar, J. L., Pierce, S. E., & Hutchinson, J. R. (2014). An experimental and morphometric test of the relationship between vertebral morphology and joint stiffness in Nile crocodiles (*Crocodylus niloticus*). *Journal of Experimental Biology, 217*, 758-768.

Monteiro, L. R. (2013). Morphometrics and the comparative method: studying the evolution of biological shape. *Hystrix, 24*(1), 25-32.

Monteiro, L. R., Duarte, L. C., & dos Reis, S. F. (2003). Environmental correlates of geographical variation in skull and mandible shape of the punaré rat *Thrichomys apereoides* (Rodentia: Echimyidae). *Journal of Zoology, 261*, 47-57.

Moon, B. R. (1999). Testing an inference of function from structure: snake vertebrae do the twist. *J Morphol, 241*(3), 217-225.

Müller, J., Scheyer, T. M., Head, J. J., Barrett, P. M., Werneburg, I., Ericson, P. G., et al. (2010). Homeotic effects, somitogenesis and the evolution of vertebral numbers in recent and fossil amniotes. *Proceedings of the National Academy of Science USA, 107*(5), 2118–2123.

Narita, Y., & Kuratani, S. (2005). Evolution of the vertebral formulae in mammals: a perspective on developmental constraints. *Journal of Experimental Zoology Part B: Molecular and Developmental Evolution, 304*(2), 91-106.

Nogueira, M. R., Peracchi, A. L., & Monteiro, L. R. (2009). Morphological correlates of bite force and diet in the skull and mandible of phyllostomid bats. *Functional Ecology, 23*(4), 715-723.

Nowak, R. M. (1999). *Mammals of the world* (Sixth ed., Vol. II). Baltimore and London: The John Hopkins University Press.

Nyakatura, J. A., & Fischer, M. S. (2010). Functional morphology and three-dimensional kinematics of the thoraco-lumbar region of the spine of the two-toed sloth. *Journal of Experimental Biology, 213*, 4278-4290.

Nyakatura, K., & Bininda-Emonds, O. R. (2012). Updating the evolutionary history of Carnivora (Mammalia): a new species-level supertree complete with divergence time estimates. *BMC Biol, 10*, 12-34.

O'Higgins, P., Cobb, S. N., Fitton, L. C., Gröning, F., Phillips, R., Liu, J., et al. (2010). Combining geometric morphometrics and functional simulation: an emerging toolkit for virtual functional analyses. *J Anat, 218*(1), 3-15.

Olson, E. C., & Miller, R. L. (1958). *Morphological Integration*. Chicago: University of Chicago Press.

Paradis, E., Claude, J., & Strimmer, K. (2004). APE: analyses of phylogenetics and evolution in R language. *Bioinformatics, 20*, 289-290.

Pavlicev, M., Cheverud, J. M., & Wagner, G. P. (2009). Measuring Morphological Integration Using Eigenvalue Variance. *Evolutionary Biology, 36*(1), 157-170.

Pecon-Slattery, J., Pearks Wilkerson, A. J., Murphy, W. J., & O'Brien, S. J. (2004). Phylogenetic assessment of introns and SINEs within the Y chromosome using the cat family felidae as a species tree. *Molecular Biology and Evolution, 21*(12), 2299-2309.

Peigné, S. (1999). *Proailurus*, l'un des plus anciens Felidae (Carnivora) d'Eurasie: systématique et évolution. *Bulletin de la Société d'Histoire Naturelle de Toulouse., 135*, 125-134.

Pierce, S. E., Ahlberg, P. E., Hutchinson, J. R., Molnar, J. L., Sanchez, S., Tafforeau, P., et al. (2013). Vertebral architecture in the earliest stem tetrapods. *Nature, 494*(7436), 226-229.

Pierce, S. E., Angielczyk, K. D., & Rayfield, E. J. (2008). Patterns of morphospace occupation and mechanical performance in extant crocodilian skulls: a combined geometric morphometric and finite element modeling approach. *J Morphol, 269*(7), 840-864.

Pierce, S. E., Angielczyk, K. D., & Rayfield, E. J. (2009). Shape and mechanics in thalattosuchian (Crocodylomorpha) skulls: implications for feeding behaviour and niche partitioning. *J Anat, 215*(5), 555-576.

Pierce, S. E., Clack, J. A., & Hutchinson, J. R. (2011). Comparative axial morphology in pinnipeds and its correlation with aquatic locomotory behaviour. *J Anat, 219*(4), 502-514.

Piras, P., Maiorino, L., Teresi, L., Meloro, C., Lucci, F., Kotsakis, T., et al. (2013). Bite of the cats: Relationships between functional integration and mechanical performance as revealed by mandible geometry. *Systematic Biology, 62*(6), 878–900.

Polly, P. D., Head, J. J., & Cohn, M. J. (2001). Testing modularity and dissociation: The evolution of regional proportions in snakes. In M. L. Zelditch (Ed.), *Beyond heterochrony: The evolution of development* (1st ed., pp. 392). United States of America: Wiley-Blackwell.

Polly, P. D., Lawing, A. M., Fabre, A. C., & Goswami, A. (2013). Phylogenetic principal components analysis and geometric morphometrics. *Hystrix, 24*(1), 33-41.

Porto, A., De Oliveira, F. B., Shirai, L. T., De Conto, V., & Marroig, G. (2009). The evolution of modularity in the mammalian skull I: morphological integration patterns and magnitudes. *Evolutionary Biology, 36*, 118-135.

Pratchett, T. (1991). *Reaper man*. London, UK: Transworld Publishers.

Pridmore, P. A. (1992). Trunk Movements during Locomotion in the Marsupial Monodelphis-Domestica (Didelphidae). *J Morphol, 211*(2), 137-146.

R Core Team (2015a). R: A language and environment for statistical computing. (3.2.3 ed.). Vienna, Austria: R Foundation for Statistical Computing.

R Core Team (2015b). R: A language and environment for statistical computing. (3.1.3 ed.). Vienna, Austria: R Foundation for Statistical Computing.

R Core Team (2016). R: A language and environment for statistical computing. (3.3.1 ed.). Vienna, Austria: R Foundation for Statistical Computing.

Raff, R. A. (1996). *The shape of life*. Chicago: The University of Chicago Press.

Raff, R. A., & Sly, B. J. (2000). Modularity and dissociation in the evolution of gene expression territories in development. *Evolution and Development, 2*(2), 102-113.

Randau, M., Carbone, C., & Turvey, S. T. (2013). Canine evolution in sabretoothed carnivores: Natural selection or sexual selection? *PLoS One, 8*(8), e72868.

Randau, M., Cuff, A. R., Hutchinson, J. R., Pierce, S. E., & Goswami, A. (2016a). Regional differentiation of felid vertebral column evolution: a study of 3D shape trajectories. *Organisms Diversity and Evolution, 17*(1), 305-319.

Randau, M., & Goswami, A. (2017a). Morphological modularity in the vertebral column of Felidae (Mammalia, Carnivora). *BMC Evol Biol, 17*, 133-144.

Randau, M., & Goswami, A. (2017b). Unravelling intravertebral integration, modularity and disparity in Felidae (Mammalia). *Evolution and Development, 19*, 85-95.

Randau, M., Goswami, A., Hutchinson, J. R., Cuff, A. R., & Pierce, S. E. (2016b). Cryptic complexity in felid vertebral evolution: shape differentiation and allometry of the axial skeleton. *Zoological Journal of the Linnean Society, 178*(1), 183-202.

Revell, L. J. (2009). Size-correction and principal components for interspecific comparative studies. *Evolution, 63*(12), 3258-3268.
Richardson, M. K., & Chipman, A. D. (2003). Developmental constraints in a comparative framework: A test case using variations in phalanx number during amniote evolution. *Journal of Experimental Zoology (Mol Dev Evol), 296B*, 8-22.
Rohlf, F. J. (1999). Shape statistics: Procrustes superimpositions and tangent spaces. *Journal of Classification, 16*, 197-223.
Rohlf, F. J., & Corti, M. (2000). Use of two-block partial least-squares to study covariation in shape. *Systematic Biology, 49*(4), 740-753.
Rohlf, F. J., & Slice, D. E. (1990). Extensions of the Procrustes method for the optimal superimposition of landmarks. *Systematic Biology, 39*(1), 40-59.
Rose, M. R., & Lauder, G. V. (1996). *Adaptation*. London: Academic Press.
Rudwick, M. J. S. (2005). Denizens of a former world. In M. J. S. Rudwick (Ed.), *Bursting the limits of time: The reconstruction of geohistory in the age of revolution* (pp. 349-416). Chicago: The University of Chicago Press.
Salesa, M. J., Anton, M., Turner, A., & Morales, J. (2010). Functional anatomy of the forelimb in Promegantereon* ogygia (Felidae, Machairodontinae, Smilodontini) from the late miocene of spain and the origins of the sabre-toothed felid model. *J Anat, 216*(3), 381-396.
Samuels, J. X., Meachen, J. A., & Sakai, S. A. (2013). Postcranial morphology and the locomotor habits of living and extinct carnivorans. *J Morphol, 274*(2), 121-146.
Schaller, G. B. (1972). *The serengeti lion: A study of predator prey relationships*. Chicago: University of Chicago Press.
Schilling, N. (2011). Evolution of the axial system in craniates: morphology and function of the perivertebral musculature. *Frontiers in Zoology, 8*(4), 1-19.
Schilling, N., & Long, J. H., Jr. (2014). Axial systems and their actuation: new twists on the ancient body of craniates. *Zoology (Jena), 117*(1), 1-6.
Schlager, S. (2016). Morpho. (2.4.1.1 ed., pp. A toolbox for Morphometric calculations. Including sliding operations for Semilandmarks, importing, exporting and manipulating of 3D-surface meshes and semi-automated placement of surface landmarks.).
Schlosser, G., & Wagner, G. P. (2004). *Modularity in development and evolution*. Chicago: University of Chicago Press.
Schluter, D. (1996a). Adaptive radiation along genetic lines of least resistance. *Evolution, 50*(5), 1766-1774.
Schluter, D. (1996b). Ecological causes of adaptive radiation. *Am Nat, 148*, S40-S64.
Schmidt, M., & Fischer, M. S. (2009). Morphological integration in mammalian limb proportions: dissociation between function and development. *Evolution, 63*(3), 749-766.
Sears, K. E., Bianchi, C., Powers, L., & Beck, A. L. (2013). Integration of the mammalian shoulder girdle within populations and over evolutionary time. *J Evol Biol, 26*(7), 1536-1548.
Sears, K. E., Goswami, A., Flynn, J. J., & Niswander, L. A. (2007). The correlated evolution of *Runx2* tandem repeats, transcriptional activity, and facial length in Carnivora. *Evolution and Development, 9*(6), 555-565.
Shapiro, L. J. (1995). Functional morphology of indrid lumbar vertebrae. *Am J Phys Anthropol, 98*(3), 323-342.
Shapiro, L. J. (2007). Morphological and functional differentiation in the lumbar spine of lorisids and galagids. *Am J Primatol, 69*(1), 86-102.

Shapiro, L. J., Seiffert, C. V., Godfrey, L. R., Jungers, W. L., Simons, E. L., & Randria, G. F. (2005). Morphometric analysis of lumbar vertebrae in extinct Malagasy strepsirrhines. *Am J Phys Anthropol, 128*(4), 823-839.

Sheets, H. D., & Zelditch, M. L. (2013). Studying ontogenetic trajectories using resampling methods and landmark data. *Hystrix, 24*(1), 67 -73.

Simes, R. J. (1986). An improved Bonferroni procedure for multiple tests of significance. *Biometrika, 73*(3), 751-754.

Slater, G. J., & Van Valkenburgh, B. (2008). Long in the tooth: evolution of sabertooth cat cranial shape. *Paleobiology, 34*(3), 403-419.

Slater, G. J., & Van Valkenburgh, B. (2009). Allometry and performance: the evolution of skull form and function in felids. *J Evol Biol, 22*(11), 2278-2287.

Slijper, E. J. (1946). *Comparative biologic-anatomical investigations on the vertebral column and spinal musculature of mammals.* (Verhandelingen der Koninklijke Nederlandsche Akademie van Wetenschappen, Afdeeling Natuurkunde): North-Holland Pub, Amsterdam.

Smeathers, J. E. (1981). *A mechanical analysis of the mammalian lumbar spine.* Thesis dissertation., University of Reading,

Smit, T. H. (2002). The use of a quadruped as an in vivo model for the study of the spine - biomechanical considerations. *European Spine Journal, 11*(2), 137-144.

Sokal, R. R., & Rohlf, F. J. (2009). *Introduction to biostatistics* (2nd ed.). Mineola, New York, USA: Dover Publications.

Stayton, C. T. (2005). Morphological evolution of the lizard skull: a geometric morphometrics survey. *J Morphol, 263*(1), 47-59.

Stayton, C. T. (2006). Testing hypotheses of convergence with multivariate data: morphological and functional convergence among herbivorous lizards. *Evolution, 60*(4), 824-841.

Stayton, C. T. (2008). Is convergence surprising? An examination of the frequency of convergence in simulated datasets. *J Theor Biol, 252*(1), 1-14.

Sunquist, M., & Sunquist, F. (2002). *Wild Cats of the World*. Chicago and London: University of Chicago Press.

Terentjev, P. V. (1931). Biometrische Untersuchungen über die Morpho-Logischen Merkmale von *Rana ridibunda* Pall: (Amphibia, Salientia). *Biometrika, 23*(1/2), 23-51.

Tseng, Z. J., Wang, X., Slater, G. J., Takeuchi, G. T., Li, Q., Liu, J., et al. (2014). Himalayan fossils of the oldest known pantherine establish ancient origin of big cats. *Proceedings of the Royal Society B - Biological Sciences, 281*(1774), 20132686.

Turner, A., & Antón, M. (1996). *The big cats and their fossil relatives: an illustrated guide to their evolution and natural history*. New York: Columbia University Press.

Van Valkenburgh, B. (2007). Déjà vu: the evolution of feeding morphologies in the Carnivora. *Integrative Comparative Biology, 47*(1), 147-163.

Van Valkenburgh, B., Grady, F., & Kurtén, B. (1990). The Plio-Pleistocene Cheetah-Like Cat Miracinonyx inexpectatus of North America. *Journal of Vertebrate Paleontology, 10*(4), 434-454.

Varela-Lasheras, I., Bakker, A. J., van der Mije, S. D., Metz, J. A., van Alphen, J., & Galis, F. (2011). Breaking evolutionary and pleiotropic constraints in mammals: On sloths, manatees and homeotic mutations. *Evodevo, 2*, 11-35.

Vidal, P. P., Graf, W., & Berthoz, A. (1986). The orientation of the cervical vertebral column in unrestrained awake animals. I. Resting position. *Experimental Brain Research, 61*(3), 549-559.

Waddington, C. H. (1942). Canalization of development and the inheritance of acquired characters. *Nature, 150*, 563-565.

Wagner, G. P. (1984). On the eigenvalue distribution of genetic and phenotypic dispersion matrices: Evidence for a nonrandom organization for quantitative character variation. *Journal of Mathematical Biology, 21*, 77-95.
Wagner, G. P. (1996). Homologues, natural kinds and the evolution of modularity. *American Zoologist, 36*, 36-43.
Wagner, G. P., & Altenberg, L. (1996). Complex adaptation and the evolution of evolvability. *Evolution, 50*, 967-976.
Wagner, G. P., Pavlicev, M., & Cheverud, J. M. (2007). The road to modularity. *Nature Reviews Genetics, 8*, 921-931.
Walmsley, A., Elton, S., Louys, J., Bishop, L. C., & Meloro, C. (2012). Humeral epiphyseal shape in the felidae: the influence of phylogeny, allometry, and locomotion. *J Morphol, 273*(12), 1424-1438.
Ward, A. B., & Mehta, R. S. (2014). Differential occupation of axial morphospace. *Zoology (Jena), 117*(1), 70-76.
Warton, D. I., Duursma, R. A., Falster, D. S., & Taskinen, S. (2012). smatr 3 - an R package for estimation and inference about allometric lines. *Methods in Ecology and Evolution, 3*(2), 257-259.
Warton, D. I., Wright, I. J., Falster, D. S., & Westoby, M. (2006). Bivariate line-fitting methods of allometry. *Biology Reviews, 81*(2), 259-291.
Wayne, R. K. (1986). Cranial morphology of domestic and wild canids: The influence of development onmorphological change. *Evolution, 40*(2), 243-261.
Wellik, D. M. (2007). Hox patterning of the vertebrate axial skeleton. *Developmental Dynamics, 236*(9), 2454-2463.
Werneburg, I. (2015). Neck motion in turtles and its relation to the shape of the temporal skull region. *Comptes Rendus de l'Académie des Sciences Series IIA Earth and Planetary Science, 14*(6-7), 527-548.
Werneburg, I., Wilson, L. A., Parr, W. C., & Joyce, W. G. (2015). Evolution of neck vertebral shape and neck retraction at the transition to modern turtles: an integrated geometric morphometric approach. *Systematic Biology, 64*(2), 187-204.
West-Eberhard, M. J. (1989). Phenotypic plasticity and the origins of diversity. *Annual Review of Ecology and Systematics, 20*, 249-278.
West-Eberhard, M. J. (2003). *Developmental plasticity and evolution*. Oxford: Oxford University Press.
Winslow, J. B. (1732). *Exposition anatomique de la structure du corps humain.*

(Vol. IV). Paris: Guillaumz Desprez, Imprimeur & Libraire ordinaire du Roi.
Wozencraft, W. C. (2005). Order carnivora. In D. E. Wilson, & D. M. Reeder (Eds.), *Mammal species of the world* (3rd ed., pp. 532–548). Baltimore, MD.: Johns Hopkins University Press.
Wroe, S., Chamoli, U., Parr, W. C., Clausen, P., Ridgely, R., & Witmer, L. (2013). Comparative Biomechanical Modeling of Metatherian and Placental Saber-Tooths: A Different Kind of Bite for an Extreme Pouched Predator. *PLoS One, 8*(6), 1-9.
Young, R. L., & Badyaev, A. V. (2006). Evolutionary persistence of phenotypic integration: Influence of developmental and functional relationships on complex trait evolution. *Evolution, 60*(6), 1291-1299.
Young, S. P., & Goldman, E. A. (1946). *The puma: mysterious American cat*. New York: Dover Publications, Inc.
Zelditch, M. L., & Carmichael, A. C. (1989). Growth and intensity of integration through postnatal growth in the skull of *Sigmodon fulviventer*. *Journal of Mammalogy, 70*, 477-484.

Zelditch, M. L., Swiderski, D. L., Sheets, H. D., & Fink, W. L. (2012). *Geometric morphometrics for biologists: a primer.* (2nd Edition ed.). Amsterdam: Elsevier/Academic Press.

Zelditch, M. L., Wood, A. R., & Swiderski, D. L. (2009). Building developmental integration into functional systems: function-induced integration of mandibular shape. *Evolutionary Biology, 36*, 71-87.

Zhang, K. Y., Wiktorowicz-Conroy, A., Hutchinson, J. R., Doube, M., Klosowski, M., Shefelbine, S. J., et al. (2012). 3D Morphometric and posture study of felid scapulae using statistical shape modelling. *PLoS One, 7*(4), 771-784.